Design strategy structural concrete in 3D

focusing on uniform force results and sequential analysis

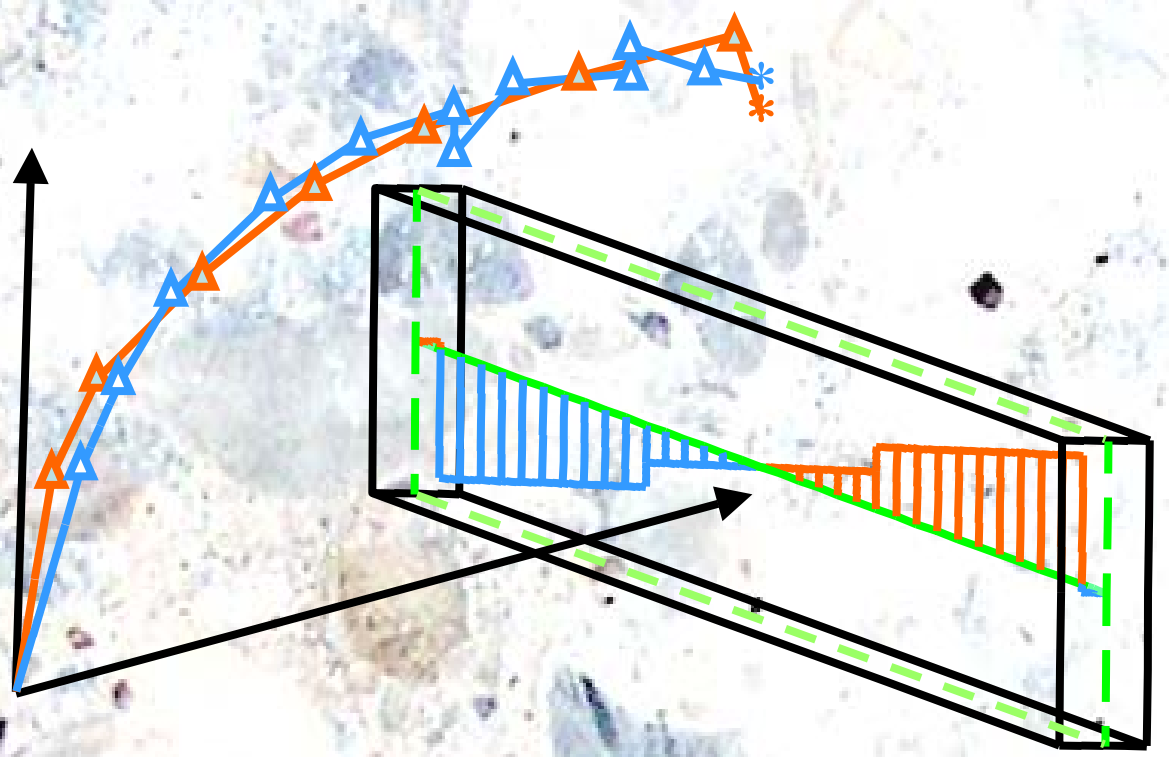

Ane de Boer

Design strategy structural concrete in 3D
focusing on uniform force results and sequential analysis

Proefschrift

ter verkrijging van de graad van doctor
aan de Technische Universiteit Delft
op gezag van de Rector Magnificus prof.ir. K.C.A.M. Luyben,
voorzitter van het College van Promoties,
in het openbaar te verdedigen op maandag 8 februari 2010 om 12.30 uur

door

Ane DE BOER

civiel ingenieur
geboren te Warga

Dit proefschrift is goedgekeurd door de promotoren:

Prof.dr.ir. J. Blaauwendraad

en

Prof.dr.ir. J.C. Walraven

Samenstelling promotiecommissie:

Rector Magnificus	Voorzitter
Prof.dr.ir. J. Blaauwendraad	Technische Universiteit Delft, promotor
Prof.dr.ir. J.C. Walraven	Technische Universiteit Delft, promotor
Dr.ir. C. van der Veen	Technische Universiteit Delft, copromotor
Prof.dr. J. Vantomme	Koninklijke Militaire School, Brussel
Prof.dr.ir. D.A. Hordijk	Technische Universiteit Eindhoven
Prof.dr.ir. B. de Vries	Technische Universiteit Eindhoven
Prof.dr.ir. J.G. Rots	Technische Universiteit Delft

Published and distributed by:

Ane de Boer
Email: anedeboer@hetnet.nl

ISBN 978-90-9025077-9

Printed by Sieca Repro, Delft, The Netherlands

SUMMARY

Introduction (chapter 1)
In analysis software models the infrastructural constructions are often reduced to geometrical linear and surface models (plane stress and shell models). The selection of a model much depends on the speed of the analysis process and the total processing time. The increased computer power has boosted the visualisation of pre-designs since the end of the nineties. The multi-disciplinary nature of a (pre-)design has also placed more focus on the Building Information Model (BIM). This concept may be regarded as a continuation of the product models of the eighties.

Modelling of structures (chapter 2)
Our aim is to (re)use the geometrical data from the visualisation software, presented as solid models, in the design software. We also want other (even non-technical) disciplines to gain an insight into the structural designs. This makes the use of solid models in the analysis software obvious, especially in the case of structural concrete designs that have more volume if compared to steel designs. In steel we express thickness in millimetres, whereas in concrete these quickly become centimetres.
As far as overall processing time is concerned, the analysis of solid models (total analysis time including time for input and output) is no longer a problem for the current computers. However, the analysis software generally does not connect with the structural design in concrete, especially when it comes to calculating the amount of reinforcement. After all, solid models present the stresses, strains and deflections as the result of an analysis, whereas the calculation of the amount of reinforcement is based on forces and moments.

Transparent results for the differences in analysis models (chapters 3, 4 and 5)
In the first part of this PhD research we have developed a procedure to obtain forces and moments from the solid models. The forces and moments are calculated and presented on reference lines or reference planes by integrating stresses along heights or widths of a section. These reference lines and reference planes may be compared to the ‘old’ system lines or system planes of the linear and surface models. This means that there is full transparency(uniformity) in the results regarding the possible analysis models. The same procedure is suitable for geometrical orthotropic models such as structures. In the past the box structures in the analysis process were mostly calculated using orthotropic surface models due to the desired reduction of the overall processing time of the analysis itself. The results of the 3D geometrical surface models and reference planes in this study may be compared to the results based on the ‘old’ orthotropic analysis models.
At the result level the analysis models are now transparent. The course of stresses and/or strains has now been made more clear. This especially applies to structural areas that cannot be related directly to pure bending, but which are still disturbed areas. This is therefore an important step towards improved acceptance of solid models in structural design. The speed of the computer and the developments in the field of internal equation solutions in analysis software have produced so much gain in time in recent years that the overall processing time has become minimal. Although the analysis time of a solid model will still remain longer than with other models, the time required to schematise a structure has been reduced. The schematisations are necessary in linear and surface models, while still leading to a number of limitations for the result. The improved clarity and the possible checks on the design mean that the quality of the analysis model has strongly improved. This may lead to a reduction of the overall failure cost in construction, estimated to amount to 7-12% of the total building sum.

Sequential analysis (chapter 6)
The second part of this PhD research deals with the consistent checking of a (pre-)design. In practice, the checks on the designs of concrete structures are done on the basis of regulations, including safety factors. Earlier, there was only a single general structural safety factor, but this has now been split up into partial safety factors for both the material and the load. In concrete structures the checks mainly take place in various cross sections. When checking the cross section, the designer can start from cracked concrete, but not when determining the course of the forces of the entire structure. This is not consistent. A crack pattern leads to a redistribution of forces, and by allowing a crack pattern to a limited extent and by using partial safety factors, the safety of the entire structure is still guaranteed. The fully non-linear analyses that include the integral crack pattern may then be applied to demonstrate the safety. The regulations indicate how such a check should take place, but this is not an accepted procedure in current engineering practice. It is also not mandatory. A fully non-linear analysis of a structure is time-consuming, and is considered to be a highly specialist analysis. Also, it is not guaranteed in advance that it leads to the saving of costs. Perhaps this non-linear analysis process should be used for the assessment of the integral life cycle cost rather just the building cost.

The assessment of safety and risk has become increasingly important in the design of a structure. That is why it is desirable in the analysis to assess the actual stresses in steel and concrete during the serviceability limit state of a structure in connection with the chance that it will occur. The eventual cracked state must be analysed using a non-linear analysis up to the serviceability limit state. This still causes practical problems. Although the crack pattern is still limited in this state, it may interfere to the extent that the non-linear process does not reach this desired load level through the instability of the software. This is often caused by the redistribution of forces or stresses. To obtain a stable analysis process we have developed a calculating method that will supply a robust redistribution of forces and moments. This method also serves to check the ultimate limit state of a structure. This defines the aim of the second part of this PhD research. We have selected a quasi non-linear method, consisting of a series of linear elastic calculations. We call this a *sequential analysis*. The solution routine should remain robust throughout the crack pattern, allowing redistribution by the crack pattern. Through iterative reduction of the material properties (stiffness and tensile strength) of concrete within an always robust linear analysis, this method can be used for an entire structure. The total processing time can be estimated after one iteration. Up to the level of the ultimate limit state a maximum of 60 iterations is needed, 4 iterations per load increment. This has reduced the processing time from days to hours.

Verification and validation of sequential method (chapters 7, 8 and 9)
The sequential method has been tested against three experiments conducted in Toronto, Canada, that were also subjected to a fully non-linear analysis. The results are equal for both the experiments and the fully non-linear analysis. The crack widths can be determined directly from the analyses and be compared to the admissible values. Sensitivity assessments in analyses of the same experiments indicate how the partial safety factors are influenced.

Sensitivity analyses (chapter 10)
The real results from this analysis form the basis of a safety assessment through partial safety factors or a probabilistic analysis, resulting in the probability of a fault or failure. If the design does not comply with the required level, it can be adjusted.
In this manner the design chain has been closed in the sense that a check has taken place on the basis of consistent results in a closed analysis process. The assumption is that through a regulation specific aspects are covered by partial safety factors. This assumption has gained more ground as a result of this research. Also, the integral method offers possibilities for optimisations in the design of concrete structures. This closed analysis process has created the possibility to start an automated design process. The acceptance of the new process is also in line with the present focus on integral design costs based on life cycle, environment and durability.
Apart from the design of new structures, the tool developed here is also very suitable for the assessment of the condition of existing structures. Important in this respect are changes in the material properties or in the load. On the basis of the archived geometry and the reinforcement that is present we can now quickly assess the influence on the safety factors.

SAMENVATTING

Introductie (hoofdstuk 1)
Infrastructurele constructies worden bij het gebruik van analysesoftware veelal geschematiseerd tot geometrische lijn- en vlakmodellen (schijf- en schaalmodellen). Bij de modelkeuze speelt de snelheid van het analyseproces en de totale doorlooptijd een grote rol. Met de toegenomen kracht van de computer is het visualiseren van voorontwerpen eind jaren ’90 opgekomen. Door het multidisciplinaire karakter van een (voor)ontwerp krijgt het “Building Information Model” (B.I.M) meer aandacht. Dit concept kan gezien worden als een voortzetting van de productmodellen in de jaren ’80.

Modellering constructies (hoofdstuk 2)
We willen de geometrische data uit de visualisatiesoftware, gepresenteerd als volumemodellen, in de ontwerpsoftware (her)gebruiken. Ook willen we andere (ook niet-technische) disciplines inzicht geven in de constructieve ontwerpen. Dan ligt het gebruik van volumemodellen in de analysesoftware voor de hand, zeker als het gaat om constructieve betonontwerpen, die ten opzichte van de staalontwerpen volumineuzer van aard zijn. Bij staal drukken we diktes uit in millimeters, terwijl bij beton eerder sprake is van centimeters.
De analyse van volumemodellen is qua doorlooptijd (totale analysetijd inclusief tijd voor invoer en uitvoer) met de huidige computers geen probleem meer. De analysesoftware sluit in zijn algemene vorm echter niet aan op het constructieontwerp in beton, zeker niet voor het berekenen van de hoeveelheden wapening. Immers,volumemodellen voeren spanningen, rekken en verplaatsingen uit als resultaat van een analyse, terwijl het berekenen van de hoeveelheid wapening geschiedt op basis van krachten en momenten.

Transparante resultaten voor verschillen analysemodellen (hoofdstuk 3, 4 en 5)
In het eerste deel van dit promotieonderzoek hebben we een procedure ontwikkeld om vanuit de volumemodellen krachten en momenten als resultaat te krijgen. Door middel van integratie van spanningen over hoogtes of breedtes van een snede worden de krachten en momenten op referentielijnen of referentievlakken berekend en weergegeven. Deze referentielijnen of referentievlakken zijn vergelijkbaar met de “oude” systeemlijnen of systeemvlakken bij de lijn- en vlakmodellen. Hiermee is een volledige transparantie in resultaten bereikt ten aanzien van de mogelijke analysemodellen. Dezelfde procedure is bruikbaar voor geometrische orthotrope modellen, zoals kokerconstructies. In het verleden zijn kokerconstructies in het analyseproces veelal berekend met orthotrope vlakmodellen vanwege de gewenste reductie in de totale doorlooptijd van de analyse. De resultaten van de in deze studie verkregen 3D geometrische vlakmodellen en referentievlakken kunnen vergeleken worden met de resultaten gebaseerd op de “oude” orthotrope analysemodellen.
Op resultaatniveau zijn de analysemodellen nu transparant. Het verloop van spanningen en/of rekken is hiermee inzichtelijker geworden. Dit geldt zeker ten aanzien van constructiegebieden die niet direct gerelateerd kunnen worden aan zuivere buiging, maar gestoorde gebieden zijn. Hiermee is een belangrijke stap gezet tot een betere acceptatie van volumemodellen bij het ontwerpen van constructies. De snelheid van de computer en de ontwikkeling van het oplossen van de interne vergelijkingen binnen de analysesoftware leveren de laatste jaren zoveel tijdwinst, dat de doorlooptijd minimaal is geworden. Weliswaar zal de analysetijd van een volumemodel nog steeds groter blijven dan van de overige modellen, maar de benodigde schematisatietijd voor een constructie is wel gereduceerd. Bij lijn- en vlakmodellen zijn deze schematisaties noodzakelijk en deze leveren de nodige beperkingen op ten aanzien van het resultaat. Door de grotere

inzichtelijkheid van en mogelijke controles op het ontwerp is de kwaliteit van het analysemodel sterk verbeterd. Wellicht kunnen de totale faalkosten, die in de bouw geschat worden op 7-12% van de bouwsom, hiermee verminderd worden.

Sequentiële analyse (hoofdstuk 6)
Het tweede deel van het promotieonderzoek gaat over het op consistente wijze controleren van een (voor)ontwerp. Controles op ontwerpen van betonconstructies gebeuren in de praktijk op basis van voorschriften, waarin veiligheidsfactoren zijn opgenomen. Vroeger was er sprake van één algemene constructie veiligheidsfactor, tegenwoordig is deze opgesplitst in partiele veiligheidsfactoren voor materiaal en belasting. Voor betonconstructies vindt de controle vooral plaats in diverse doorsneden. Bij de doorsnedecontrole mag de constructeur uitgaan van gescheurd beton, maar niet bij het bepalen van het krachtenverloop van de totale constructie. Dat is niet consistent. Scheurvorming geeft herverdeling van krachten en via het beperkt toelaten van scheurvorming en het gebruik van partiele veiligheidsfactoren wordt de veiligheid van de totale constructie toch gewaarborgd. Via volledige niet-lineaire analyses waarin scheurvorming integraal meegenomen wordt, kan de veiligheid wel worden aangetoond. De voorschriften geven aan hoe een dergelijke controle zou moeten gebeuren, het is echter niet een geaccepteerde procedure binnen de huidige ingenieurspraktijk en is ook niet verplicht. Een volledige niet-lineaire analyse van een constructie is tijdrovend en wordt gezien als een zeer specialistische analyse. Ook staat niet op voorhand vast dat het tot besparingen kan leiden. Wellicht zou bij het beschouwen van integrale levensduurkosten in plaats van enkel de bouwkosten, dit niet-lineaire analyseproces meer ingezet kunnen worden.

Het beschouwen van veiligheid en risico's speelt steeds meer een rol bij het ontwerp van een constructie. Daarom is het gewenst de werkelijke spanningen in staal en beton bij een analyse in de bruikbaarheidsgrenstoestand van een constructie te beschouwen in samenhang met de kans van optreden. De eventueel gescheurde toestand moet geanalyseerd worden met een niet-lineaire analyse tot de bruikbaarheidsgrenstoestand. In de praktijk levert dat nog problemen op. Weliswaar is de scheurvorming in deze toestand nog gering, het kan echter wel zo storend zijn, dat het niet-lineaire proces softwaretechnisch door instabiliteit niet dit gewenste belastingniveau haalt. Dat komt vaak door de herverdeling van krachten of spanningen. Om een stabiel analyseproces te krijgen, hebben we een methode ontwikkeld, die rekentechnisch voor een robuuste herverdeling van krachten en momenten zorgt. Met deze methode kan ook de controle van de uiterste grenstoestand van een constructie worden uitgevoerd. Hiermee is het doel van het tweede deel van dit promotieonderzoek gedefinieerd. We hebben gekozen voor een quasi niet-lineaire methode die bestaat uit een reeks van lineair-elastische berekeningen. We noemen dit een *sequentiële analyse*. De oplosroutine moet onder scheurvorming robuust blijven, terwijl herverdeling door scheurvorming mag plaatsvinden. Via een iteratieve reductie van de materiaaleigenschappen (stijfheid en treksterkte) van beton binnen een altijd robuuste lineaire analyse kan deze methode voor een volledige constructie gebruikt worden. De totale doorlooptijd is in te schatten na één iteratie. Tot het niveau van de uiterste grenstoestand zijn maximaal zestig iteraties nodig, vier iteraties per belastingincrement. De doorlooptijd is hiermee teruggebracht van dagen naar uren.

Verificatie en validatie sequentiële methode (hoofdstuk 7, 8 en 9)
De sequentiële methode is getoetst aan de hand van drie experimenten in Toronto, Canada, waarvan eveneens een volledige niet-lineaire analyse is uitgevoerd. De resultaten zijn gelijkwaardig, zowel voor de experimenten als volledige niet-lineaire analyse.
De scheurwijdtes kunnen rechtstreeks bepaald worden uit de analyses en vergeleken worden met toelaatbare waarden. Gevoeligheidsbeschouwingen bij analyses van dezelfde experimenten geven aan hoe de partiële veiligheidsfactoren worden beïnvloed.

Gevoeligheidsanalyses (hoofdstuk 10)
De werkelijke resultaten uit deze analyse zijn de basis voor een veiligheidsbeschouwing via partiële veiligheidsfactoren of een probabilistische analyse, met als resultaat een kans van optreden van een tekortkoming of falen. Mocht het ontwerp het gewenste niveau niet halen dan kan het aangepast worden.
De ontwerpketen is hiermee gesloten in de zin dat er een controle heeft plaats gevonden op basis van consistente resultaten in een gesloten analyseproces. Via een voorschrift denkt men bepaalde aspecten af te dekken met partiële veiligheidsfactoren. Die veronderstelling is door het onderzoek in dit promotieproject harder gemaakt. Tevens biedt de integrale methode mogelijkheden om te komen tot optimalisaties binnen het ontwerpen van betonconstructies. Met dit gesloten analyseproces is de mogelijkheid geschapen, om een geautomatiseerd ontwerpproces op te starten. Acceptatie van het nieuwe proces sluit ook aan bij de huidige aandacht voor integrale ontwerpkosten op basis van levensduur, milieu en duurzaamheid.
Behalve voor het ontwerpen van nieuwe constructies is het ontwikkelde gereedschap goed te gebruiken voor het beoordelen van de conditie van bestaande bouw. Hierbij zijn wijzingen in materiaaleigenschappen of belasting van belang. Op basis van de gearchiveerde geometrie en aanwezige wapening kunnen we op een snelle manier de invloed op de veiligheidsfactoren beschouwen.

ACKNOWLEDGEMENTS

The research presented in this thesis has been carried out at the Faculty of Civil Engineering and Geosciences of Delft University of Technology.

First of all I would like to thank the Civil Engineering Division of the Ministry of Transport, Public Works and Water Management. Special thanks go to the former head of the Building Research department Hans Jongedijk for giving me the space and the support in carrying out this research and my recent head of the Civil Engineering department Martien op't Hof for the support on the finishing touch of this research. In this way I like to thank many colleagues inside as well as outside the department and division that supported me in this PhD period.

Secondly I would like to thank Cor van der Veen of the Faculty of Civil Engineering of Delft University of Technology for his very fruitful cooperation. Together with Prof. Joost Walraven and Prof. Johan Blaauwendraad I got after critical appraisals nice hints for improvements, which leads after several discussions to a nice piece of work.

More in the private environment I like to express my gratitude to my family and friends of work & sport. They kept me on the way of doing research, which could be explained also in words outside the research environment.

Further, I appreciate very much the contribution of Koen Donker van Heel for his job to make a correct English language version of this thesis.

Finally, I have to thank my wife Ans Wichers for the many outdoor activities during this rather long period of research work, to keep the research motivation in the right direction.

Ane de Boer
Arnhem, December 2009

KEYWORDS

Concrete structures, civil engineering, finite element method, serviceability limit state, crack width, ultimate limit state, judging condition concrete structure, building information model

ABBREVIATIONS

BIM - Building Information Model
CAD - Computer Aided Design
D - Dimensional, in 1D, 2D, 2½D and 3D
ESPRIT - European Strategic Programme for Research and Development of Information Technology
FE - Finite Element
FEA - Finite Element Analysis
GEM - Generic Engineering analysis Model, ESPRIT project 8894
IFC - International Foundation Classes
IGES - Initial Graphics Exchange Specifications
ISO - International Organisation for Standardisation
R&D - Research and Development
RVU - Representative Volume Unit
SLS - Service Limit State
SPM - Stringer-Panel Model
STEP - STandard for the Exchange of Product model data
STM - Strut and Tie Model
ULS - Ultimate Limit State

NOTATIONS

Roman upper case symbols

E_{28} – Young's modulus of 28 day aged concrete
E_s – Young's modulus reinforcement steel
F – nodal force
G_F – fracture energy
G_{F0} – basic fracture energy
M_y, M_z – bending moment
M_x – torsional moment
N_x – normal force
Q_y, Q_z – shear force
R_y – reaction force nodal support
W_{zmax}, W_{zmin} – section modulus

Roman lower case symbols

b – width cross section
c – coverage longitudinal reinforcement
$c(\kappa)$ – cohesion as a function of the internal state variable κ
d – effective depth
dx, dy, dz – displacements
du_x, du_y, du_z – translation increments
eg – dead weight
f_t – tension strength
f_c, f_{cc} – compression strength
f_{cm} – mean compression strength

f_{cm0} – basic compression strength
$f_{ct,eff}$ – average concrete tensile stress (f_{ct}) at the expected moment of first crack pattern
g – gravity
h – height cross section
h – crack bandwidth fracture energy
h_{eff} – minimum of 2.5×(h-d) or (h-x_e)/3 or h/2
k_1 – coefficient (=0.8) for bars with a high bond behaviour
k_2 – strain distribution coefficient =0.5 for bending and 1.0 for pure tension
k_3 – 3.4
k_4 – 0.425
k_t – short term loading
m_{xx}, m_{yy}, m_{xy} – distributed moments
n_{xx}, n_{yy}, n_{xy} – in plane forces
q – uniform distributed load
q_{xz}, q_{yz} – distributed forces
$s_{r,max}$ – the maximum crack width
w_k – the maximum crack width
x, y, z – Cartesian coordinates or axes
x_e – height compression zone concrete

Greek symbols

α_e – relation E_s/E_c
ε_{xx}, ε_{yy}, ε_{zz} – normal strain components
ε_{sm} – mean strain of the reinforcement bar
ε_{cm} – mean concrete strain between the cracks
ε_{nn} – normal strain
γ_{xy}, γ_{yz}, γ_{zx} – shear strain components
θ – dilatancy angle
ρ – density material
ρ – reinforcement ratio related to the whole concrete cross section
$\rho_{s,eff}$ – relation $A_s/(b \times h_{eff})$
σ_1, σ_2, σ_3 – principal stress
σ_{nn} – normal stress
σ_s – stress tension reinforcement
σ_{xx}, σ_{yy}, σzz – normal stress components
σ_{xy}, σ_{yz}, σ_{zx} – shear stress components
ϕ – angle of the internal friction
ϕ_{eq} – equivalent diameter

TABLE OF CONTENTS

1 INTRODUCTION

1.1 Actual practice of the use of FE models for the design of concrete structures

It is almost impossible to image a design engineer these days without a computer and the software to match. Compared to earlier days, the increasing speed of the computer also enables the design engineer to approach the design problem at ever higher levels.
It is common practice to describe the geometry of a structure in a way that is as simple as possible. This is also known as the simulation or modelling of a structure. The simplest method is the 1D geometry model, in which the longitudinal axis of the geometry also describes the longitudinal axis of the 1D calculation model. This is then linked to a cross section, thus achieving the full description of the entire geometry of the structure. If the cross section varies along the length, this cross section may be entered in a variable way. This approach still applies to beams, hence the name beam models instead of 1D geometry models. The use of 1D calculation models is generally the quickest way to analyse a structure.
If the designer requires a description of the length and width of the geometry, this geometry may be described using a 2D or 2½D surface model. In 2D the length and height of the geometry of the structure are described, linking the thickness of the structural components to the model elements. In 2½D the length and width of the geometry of a structure are described. The height of the various structural components is then linked to the model elements to describe the entire structure. For solid slabs or bridge decks this is an accepted description. In view of the extension of the geometry description to two directions, this calculation method takes slightly more time, but stays within accepted limits.
Naturally, the entire geometry of the infrastructural construction is built up in three directions, whereas the calculation model is mostly based on a 2½D surface model. If a total solid model of the geometry of an infrastructural structure in three directions is required, however, this becomes a full 3D model consisting of solid elements. This describes the geometry of a structure in all three directions. No further simulation is possible regarding the geometry of the structure. Given the extension with one direction compared to the 2½D surface model the calculation time required is slightly higher, but still acceptable in terms of modelling and overall calculation time.
Apart from the increasing speed of the computer, other determining factors in the design process are the speed of saving on the internal discs, the disc capacity and the size of the software arrays. At present, both the disc capacity and the size of the software arrays are sufficient. The speed of the computers themselves and the speed of saving material to the disc have strongly increased in recent years, but still could be improved upon.
In short, both 1D and 2D may count on a high level of acceptance within the design environment. However, apart from the geometry description the type of analysis is also important in the overall processing time of a design. The usual analysis of the entire structure is a linear static analysis, meaning that there is a linear relation between the stresses and strains that occur in the material under load. Static means that the design does not include a calculation over time. The total processing time of a design, including time for modelling, analysis and interpretation, may be termed acceptable for 1D and 2½D models. The full 3D models are still seen as unacceptable models, because of their limited output on behalf of the design as well as the unacceptable longer calculation time.
However, at present the full 3D models of concrete structures no longer require a long processing time spanning hours or days, giving the design engineer extra opportunities for

a better understanding of the stresses and/or strains that occur. A geometry model at a higher level offers a more correct stress image than lower geometry models such as 1D, 2D and 2½D, due to the limited prior assumptions. The total design time may be reduced by a geometry transfer from the predesign process, the architectural or other (design) environments, depending on the aim and the status of the design. This improves quality, because no data will be missed or forgotten.
The 3D geometry description of a structure may then also be used in other disciplines, e.g. the archiving of damage that has occurred during management and maintenance inspections by inspectors without a technical background. People no longer need specific knowledge to understand the geometry model described, because the 3D approach is in full sync with reality. It will then be easy to add the locations of the damage and the deterioration processes to the 3D structure kept in a database. The saved 3D geometry model in question may also be used for an adaptation of a structure, such as the use of a hard shoulder as a driving lane, or the extension of a viaduct with an additional driving lane. Any discipline may, each in its own way, benefit from the saved 3D geometry model. It allows a visually realistic presentation, meaning that it enables better interpretation by both technicians and non-technicians, which may be important, for instance, when discussing the building of new roads during public enquiry procedures.
Any shape in the structure devised by the architect may be included by the design engineer in the geometry description. This will help to reduce the friction that sometimes occurs when people are confronted with architectural high-brow forms and shapes. The design engineer then only needs to fully concentrate on the analysis and the interpretation of the results of the analysis. These results will have to be checked against the prevailing building regulations to achieve a safe structure. It stands to reason that if the geometry of a structure is described according to the most realistic method, the results of the analysis will also reflect the most realistic image. This will give more meaning to ‘thinking in safe structures’. More precise obtained stresses and/or strains lead to more precise safety indices for a (sub)structure. Up till now, the safety of a structure is formulated in partial safety factors regarding material and load. Perhaps in the future a safety index of a (sub)structure will become mandatory, in which the corresponding loads and materials will each receive their own ratio in the index.
In special cases non-linear, dynamic or non-linear dynamic analyses are performed next to the linear static analysis, in order to achieve a better simulation of the behaviour of a structure. Even though most materials behave in a non-linear manner these additional analyses are not included into the design process of a concrete structure.
The acceptance of non-linear analyses in the current design practice is still very low, and is still seen as extremely time-consuming. However, owing to the increasing calculation power of the computer as well as recent cases of damage to structures, this view is beginning to change. Furthermore, the non-linear analysis of a structure is mostly little robust and a highly specialist endeavour.
For this reason, a non-linear analysis is exclusively used to check complex structures. There are only few specialists in this domain. Also, the regulations do not describe the manner in which a structure is to be checked, a handicap that doesn’t stimulate the use of non-linear analysis. Optimisation of the design of a structure using a linear static analysis is not really rewarded, let alone the optimal use of material. This type of analysis could be used in the 3D domain, albeit that the processing time must still be expressed in days, and this does not promote its acceptance in design practice.

1.2 **Design of concrete structures**

When it comes to the use of material, the optimal design of a concrete structure consists of the design with the right balance in the application of concrete and reinforcement, possibly supplemented by prestressed reinforcement. Other aspects such as the building process, the speed of building, the building inconvenience, the sustainability or economic building also play a role. This all has to take place within the existing frameworks of the current rules and regulations. The prevailing regulations define the partial safety factors that delineate the design room. This presupposes that the design of the structure is sufficiently safe.
Using a linear static analysis of the design (no crack formation in the concrete and no yielding of the reinforcement) the specific force variation of the structure is analysed. The relevant cross sections, selected on the basis of the calculated force variation in a linear static analysis, are optimised in a non-linear iteratively method. The force distribution is dependent on these changes in stiffness. This already indicates that the variation of stiffness quantities of the cross section may lead to changes in other cross sections. There is no direct mutual coupling between the various cross sections. Once more, apart from concrete and reinforcement, use is also made of prestressed reinforcement, the optimisation process becomes more difficult. However, in view of the actual presence of (partial) safety factors in designing structures, there is no reason to assume that designing is done incorrectly.
The analysis process is set up in such a way that iteration is possibly halted sooner, because designing for the optimal result is left almost unrewarded. If precision is deemed sufficient, this is often a reason to stop the process of analysis. But if the mutual effects of the cross sections on each other are included in the design process, this will allow an investigation of an analysis model that is more complete.
The regulations prescribe a check of the design regarding the serviceability limit state and the ultimate limit state. A check based on a non-linear analysis is not necessary, but may become a future possibility in view of the development of computer technology, both in hardware and software. Especially the automated check by a computer of the service state of the structure may become mandatory in the future, because the non-linear effect will be small up to and including this state. A redistribution of forces as a result of crack formation in the concrete will in that case be automatically accounted for the model. This will also enable a check of the crack width through any conceivable load history.
The check of a full 3D analysis model through a complete non-linear analysis is still not part of standard design practice, albeit that the approach by De Jong of Delft University of Technology [Jong2002] may mean that the possible future lies near the probable future or desirable future. In his study three types of research are mentioned, research directly aimed at practice, research for the near future and research aiming somewhere over the horizon of the future. Examples of this latter type of research are the developments of the PC and telephony during the past 40 years. In concrete technology itself one may think of higher strength concrete or the development of fibre-reinforced concrete. This is illustrated by figure 1.1.
First, the linear static analysis through a 3D solid model will have to be accepted or made mandatory, for the non-linear variant to get a chance at all. However, the 3D solid model may be earmarked as the most complete model. It completes the abovementioned option of an integral view of all cross sections in the design. In short, it does have potency.

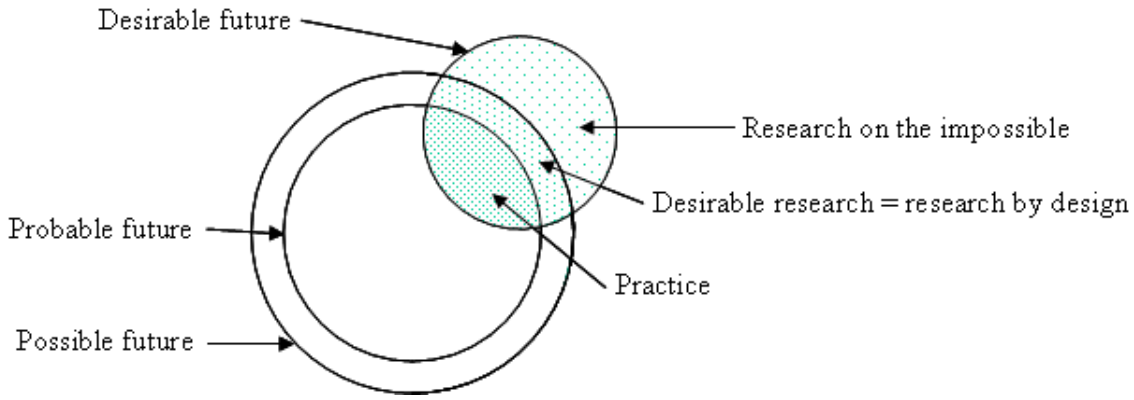

Figure 1.1 Approach to research and practice

The appearance and acceptance of a 3D analysis model will considerably shorten the modelling time required for a structure, viz. to reduce the design to a linear or surface model. At that moment the transfer of the geometry of the structure from the software used during the predesign process is one on one. One could still enter geometrical modifications at this point, but this is not the most likely option.
A second geometry set-up on behalf of the analyst is no longer necessary with this geometry transfer, because the quality of the correct geometry data of the structure is guaranteed.
The interpretation of results following the reduction to a linear or surface model is in the case of a 3D solid model no longer applicable.
The 3D solid model simultaneously offers the possibility to apply loads to a specific surface of the entire structure. With a linear model the point of application of the load is mostly a single point or a section of the line. With a surface model the load may also be, as is already suggested by the name, applied at a corresponding surface or part of a surface. For ease of modelling the applied loads are mostly linked to a point serving as the point of application.
The result of the approach where the point of application of the load is a single point leads to extreme maximum and minimum values at the same time at or around this point of application. These maximum and minimum values in turn lead to debates about averaging the extreme values at these specific points. At a deeper level one finds the type of contact surface between the surface of application of the structure and the corresponding load surface. This contact surface does not have to be connected one on one with the corresponding surface of application, which in turn may influence the results on and around the surface of application. For the time being, this is not taken into account in the construction analyses. It is rather an aspect that is included into the analyses to simulate laboratory tests of structural components. One example is the use of load-bearing plates during laboratory experiments [VanVliet2000].
Just like the loads the supports are mostly modelled as nodal supports in the design process, because this is also the easiest procedure in the modelling process. The abovementioned application identities under loads on points and surfaces also play a role when modelling and interpreting supports. Unambiguousness when handling areas of concentration like load and support surfaces leads to more focus on modelling these areas in order to enable the correct force variation in the design process and, in turn, include it into the calculation model.

Still, it will remain possible to apply both loads and supports to a nodal point in 3D solid models, to stimulate the transition to 3D solid models. This does, however, often require a closer interpretation of results to enable a correct estimation of extreme maximum and minimum values at these points.

1.3 The role and state of the art of research aspects

Looking back at the past 25 years of research on the modelling of concrete structures, the following aspects may be distinguished from each other:
- Modelling aspects
- Material models of concrete structures
- Integration of software packages

1.3.1 Modelling aspects

The model lay-out of a concrete structure is often still based on a 1D geometry model. Although in recent years there has been a considerable increase in the use of the 2½D geometry model instead of the 1D model, the designer still shows a preference for the use of the 1D geometry model because of its simplicity and speed. With deep beams, walls and floors they tend to opt for a surface model, whereas with floors or solid slabs, tilting at <80 degrees or >110 degrees if seen from above, one should always select a surface lay-out. This is necessary to correctly account for all force components when designing the reinforcement.
For concrete and reinforcing steel primarily an isotropic material is assumed. However, in design practice the reinforcement is exclusively designed on the basis of the linear static results of the various load cases. With non-linear analyses non-linear material parameters are added on behalf of crack formation in the concrete as well as the plasticity of both steel (for flowing) and concrete (crushing). Reinforcing bars in structures therefore have to be added as 1D elements in the case of non-linear analyses.
Looking at the analysis process of the concrete models developed one may conclude that research in the field of solving equations has led to considerable progress. The solution possibilities have shifted from direct to iterative, that have for the past 10 years and especially in full 3D models shown an acceleration in the processing time of the analysis process with minimal factors 20. In essence, this means that full 3D models for structures are possible on a simple desktop PC.

1.3.2 Material models for the analysis of concrete structures

First a distinction may be made in micro, meso and macro concrete models. The micro concrete model provides an insight at grain structure level of the concrete. This is in fact a model that is limited to the laboratory, representing a specific **R**epresentative **V**olume **U**nit (henceforth RVU). This takes place at both the 2D and 3D levels. The components of concrete reach a size of 0.5×10^{-3} m according to Van Mier [vanMier1997].
In the ideal case the relations established in this model, e.g. between stresses and strains, should be used as input in meso and macro concrete models. However, unfortunately one still has to rely on assumptions on this scale in order to arrive at the current calculation rules for meso and macro concrete models. It will be clear that it is not possible to model and analyse an entire concrete structure in this manner, due to the size of a structure.

Research at the meso level also means setting up an RVU model, the fineness having been increased by one order. In this case the concrete is divided into aggregate, cement and possible pores. The mutual interaction between the various materials is also included. The various components differ in size from 0.5×10^{-3} m to 0.5×10^{-1} m.
It is clear that this allows the analysis of small (up to 1 m, see the experiments by Vliet [Vliet2000] concrete structures. The inclusion of reinforcement often does not take place in this type of model, and if it does, this will be in a second instance, when the influence of the reinforcement on such small units needs to be investigated. Finally, there is the macro level for structures, where the dimensions will exceed 0.5×10^{-1} m.
Much research has taken place in the field of crack formation during the past 25 years. Much attention has been devoted to especially the material models in the 1D and 2D environment. Ever since the introduction of the smeared crack concept [Rots1998] in structural elements some progress was made within the confines of the current regulations, but crack formation as a subject of its own does not have an operational environment in today's design. The checking for crack widths is often still done manually. Looking at two important regulations, the internationally well-known MC90 [Model Code 1990] and the Dutch Code VBC95 [Voorschriften Beton Constructies 1995], the conclusion is that these do contain a number of articles relating to checking procedures. However, since these tests have not been included into the calculation software in a way that may be called unambiguous, the designer still has to interpret the results from his analysis far too much. Also, the designer is not really being rewarded if he uses the available checking options.
A large number of crack models has been developed since 1980, but a generally applicable numerical material model still hasn't been found. Nielsen [Nielsen1984 and Nielsen1999] has made much progress through the plasticity of concrete, aimed at the ultimate limit state of a structure. Feenstra [Feenstra1993] also included plasticity into the crack models to render these more stable in case of the drop in the load mentioned earlier.
The current research field is now also looking at environmental influences that should help to generalise the crack models developed up till now. This includes influences such as humidity and temperature on the development of concrete from the so-called 'green' phase to the hardening phase and subsequently to the hardened phase. In this case the 'damage' phenomenon is rather popular, whereas in fact it is a way to rewrite the scenario with a view to crack formation and the plasticity of the concrete material.
The problem in the design process is mainly the robustness of the analysis process. Especially the crack formation of concrete can cause quite a lot of problems in a non-linear analysis. When a starting crack propagated further if the load increases, a sudden drop in the load may occur after a redistribution of the stresses in the direction of abutting concrete or reinforcement parts. In the calculation the cracks can in principle rotate in any direction as the result of increasing, decreasing and then once again increasing the load. The so-called 'snap-backs' in a load-deformation diagram form the subject of many studies. The 'locking' or bifurcation of specific points in a structure also occur, which does not help to promote the acceptance of nonlinear methods of analysis in the design environment. The dependency on the element distribution within a structure does play a role as well, as does the bandwidth of the cracked area.
In order to avoid the problems with the non-linear analysis process, in various papers dealing with brickwork Beranek [Beranek1994] stated that by using sequential linear static analyses it was also possible to analyse concrete structures this way. The method is based on a 3D failure surface.
However, in 1994 the possibilities for 3D analysis were not really sufficient, meaning that they were deemed impossible to carry out using the computers of that era. The total processing time of such an analysis would take days, if not weeks. One of the limitations

in this period was that this 3D failure surface was exclusively linked to brittle cracking behaviour and not to the present standard post-cracking behaviour of concrete. These softening branches for concrete are the result of experimental research in various laboratories worldwide. Well-known models have been proposed by Popovics [Popovics1973], Reinhardt [Reinhard1984], Cornelissen [Cornelissen1986] and Hordijk [Hordijk1991].
Both the processing time and the post-cracking behaviour of concrete formed the most probable cause for this method not having been developed further by the software developers of the time. The consequence, however, is that this method has not been incorporated into a generally applicable software package. It also meant this method was not made available to the market. Rots [Rots2002, Rots2006], who succeeded Beranek at Delft University of Technology/Architecture, has rekindled the fire in recent years. Together with Invernizzi from Turin and Belletti from Parma he is now looking for ways to apply this method to brickwork structures.
In various publications Rots demonstrated that the method is valid in specific cases, but there is still a long way to go to convince other researchers. Also, a number of specific options is still missing, even though these are already robust and accepted in the realm of the non-linear specialists. Despite all this, this is a development that bodes well for the future.

1.3.3 Integration of software packages

Also the integration of modelling environments is the subject of rapid development. At present, the sketch made by an architect can already be translated into a 3D geometry environment through an automated process. In the eighties the first steps were taken to set up a central database for a structure through product modelling. In the nineties an agreement was reached on the global STEP protocol [STEP-API-214] for the exchange of geometry data between software packages. The European Esprit project was one of the examples in this field with publications from Böhms1995 and Böhms1997.
The efficiency in using FE models for development of products in the machinery industry is described by Juvet and Kenis in Juvet2001.
An important role has been played by the aircraft manufacturer Boeing, taking the issue to a more general level. The successor of the STEP protocol is the **I**nternational **F**oundation **C**lasses protocol [IFC] or **B**uilding **I**nformation **M**odel (BIM) concept. This concept is used around the globe and is being further developed for application in any discipline that is even remotely linked to building of any kind, see fig 2.1. As far as recent European publications are concerned, mention must be made of the publications from Germany, where McFarlan2006, Holzhauer2006 and Richter2006 demonstrated the general interaction in papers written for building in wood and steel. CUR2006 is a report from the project COINS in the Netherlands, where an object approach is supported.

Figure 1.2 The IFC process

As a matter of fact, the automotive, aircraft and space industries will of course remain leading in the field. These sectors also feature most R&D funding, a situation that was recently corroborated by the EU R&D Scoreboard [EU Website, 2005 report]. The leading 3 enterprises in R&D in Europe are automotive companies. The first construction firm follows only at position 57, showing an R&D investment of 5% of the enterprise heading the list. The second construction firm is found at position 130 with an R&D investment of 2%. Outside Europe the first builder occupies position 160 with likewise 5% R&D investment compared to number 1, the second builder being at 227 with 3% R&D investment. In short, in this respect another industry will be leading, albeit that the concrete structure industry should be able to benefit from these changes in the design domain. Various software packages already include an IFC entry and exit of sorts, so with a little extra research in concrete structures this may result in a more integrated approach to the design process.

Recently, Autocad supplier Autodesk announced its intentions to invest in 3D models. ADOBE used the 2006 ICT Building Fare in Utrecht, the Netherlands, to state that their PDF format allows the representation of 3D designs. The software suppliers in the concrete structure sector are also talking about 3D CAD and visualisation. However, in the latter case their vision is still made up of 3D geometry structures, viz. the basis is still formed by lines and planes. An analysis based on 3D solid models is not the issue here yet, but 3D modelling in a modelling environment is already possible. One good example is the Tekla package from Finland [Tekla2006].

An IFC-based link allows the generation of a linear or surface model on behalf of an analysis package. Taking the analysis in the direction of a 3D solid model is not operational yet, but is something that is expected by developers in the foreseeable future. Undoubtedly, it is technically possible on the basis of the abovementioned IFC format. This will serve to design a reinforcement through a reinforcement analysis programme based on the analysed force variations. Up to now the amount of reinforcement is calculated on the basis of the results from linear or surface models. In a paper, Foster and Marti [Foster2003] have described a procedure that enables the calculation of reinforcement from solid models. A follow-up to this was included into the FIB Guideline 2008 [FIB2008], where this concept has been taken further. Parallel to this follow-up Hoogenboom and DeBoer had also a publication in Heron [Hoogenboom2008]. However, this procedure has not yet been implemented in a lot of software packages.

Also, from the point of view of geometry the IFC format does not distinguish between reinforcement components that have their own identity, in the sense that stirrups and bars do not have an own identity yet as opposed to the identity of the structural components of the concrete. It seems obvious to provide both the reinforcing net and reinforcing bars with their own identities. In the future these reinforcement identities may then also be

exported to an analysis package, e.g. to be entered as a reinforcement table on behalf of an inspection of a structure through a non-linear analysis. This will require more research as well as an additional implementation.
The prestress, being a load on the reinforcing bar, will therefore still have to be set up as an extension within the overall IFC implementation.
In hybrid structures that include concrete, some adaptations must also be included into the description. In this respect, attention must be paid to the interfaces between the concrete and other materials. These are of a minimal thickness or are provided with dowels. Joining surfaces will require their own identity. For instance, with steel-concrete decks the dowels that fix the concrete to the steel or composite beams will need to have a special identity to enable the designer to explicitly include the dowel behaviour into the design analysis.

1.4 Objectives and scope of this study

The aim of this study is twofold. The point of departure is that in the future 3D solid models will increasingly be used in the design practice, because of the high integration factor of software packages to streamline the design process.
The first aim of this research will be to generate the results from full 3D models needed to allow the calculation of the amounts of reinforcement. This is a specific area of attention that will not be addressed by any other industry, only the concrete industry is stakeholder.
In this way the results are uniform over all types of FE models, the output is transparent over 1D, 2D and 3D. By using full 3D models the design practice will also be better able to link up with the architectural models, and this will promote the collaboration between designers and architects.
Also, a 3D solid model allows people not schooled in technical matters to get a good impression of the design already in the design phase, because the design is no longer presented through frontal 2D drawings, but become 'real' 3D objects, including see-through spaces, etc.
The second aim of this research is the introduction of an automated method in the design process to enable the check-optimisation-iteration based on a series of linked linear static analyses of the concrete structure. This series of linked linear static analyses will then replace the fully non-linear analysis. The "Beranek method" mentioned earlier will be applied to full 3D models including a softening branch for concrete under tensile stress. In the future this method will serve to perform a fast check during the design process on the serviceability limit state and the ultimate limit state of a structure.
A check on the serviceability limit state is made possible by a series of succeeding linear static analyses. The check on the limit state will also use a series of linked non-linear analyses, only making use of the robust aspects of the non-linear analysis.
In this manner, the design process has become a closed dimensioning process, allowing optimisation in an integrated way. The existing methods for reinforcement design based on the linear static analysis will for the time being be maintained. At this point only a check on and a possible optimisation of the definitive design can take place. This will help to improve the balancing of the design of a structure within the fully automated cycle of design, analysis, checking and optimisation.
It will be clear that the second aim of this research is the main aim, relegating the research aim mentioned first to the second place. However, in view of the importance of the first research aim in relation to 3D modelling of structures and the impact on the current design process, this will have to be worked out in detail first. Only then we can proceed to the main research aim. This has also fixed the table of contents.

1.5 Schedule of chapters

Chapter 2 will address the specific parts of the design of a concrete structure that are of importance and need to be recorded for the benefit of an archive in the analysis models that are currently used.
Chapter 3 will deal with the first research aim, to obtain results from a 3D solid model in such a way that reinforcement analysis programmes and checking programmes will require no adaptations. These results will henceforth be referred to as composed results, because these are not the usual results that may be generated as an output result of a 3D solid model. In this way the current design environment of a concrete structure will remain intact in a manner that is as flexible as possible.

Chapter 4 will present the various options for composed results from solid, shell and plane stress models and diagrams using an analysed example.
Chapter 5 deals with the evaluation of the composed results and the added value for the engineering practice.
Chapter 6 will address the theory of the main aim of this research, the second aim. First, the sequential linear static analysis will be explained, to be followed by an explanation how to deal with the plasticity of reinforcement and concrete.
Chapter 7 contains a survey of experiments such as the ones carried out in the Toronto laboratory, which were published in a large number of scientific papers.
Chapter 8 will deal with the results of the fully non-linear analyses of the three selected experiments.
Chapter 9 contains the results of the same experiments, this time analysed with the use of the sequential method proposed here.
Chapter 10 will evaluate this approach, once again listing the advantages and disadvantages involved, and also addressing the corresponding advantages of the use of full 3D models, as observed to this date. Some sensitivities aspects of the approach will be discussed more in detail.
Finally, chapter 11 will list the conclusions of this research report.

2 MODELLING CONCRETE STRUCTURES AND THE FINITE ELEMENT METHOD

2.1 Introduction

In design practice the modelling of concrete structures still mainly takes place on the basis of input data. These input data are obtained by studying a predesign that offers all the global measurements and dimensions. Following this, a new design model is made, the calculation model. This process is shown in the diagram in figure 2.1.

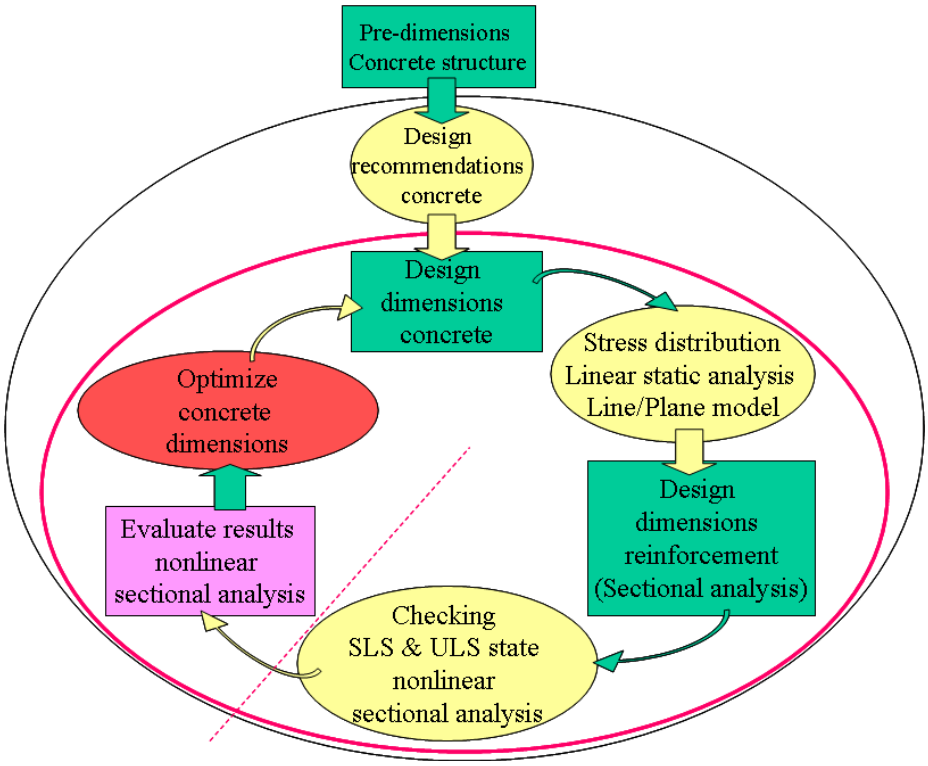

Figure 2.1 Current design process of a concrete structure

The first box at the top of figure 2.1 indicates the global dimensions of the concrete structure resulting from the first analyses of the sketch design made by the architect. The architect may have used rules of thumb, meaning that this part of the process falls outside the analysis of the design. This explains the use of the black and red ovals for the design environment.
The global analyses of the structure and the cross section then serve to determine the global dimensions of the concrete structure.
After this, a linear static analysis based on a linear or surface model may be used to determine the force variables in the structure. Following this procedure, the dimensions of the reinforcement that will be required are established at cross section level.
These specific cross sections are then used to check against the relevant rules and regulations. The cross sections of the structure selected by the designer are checked for their serviceability limit state and the ultimate limit state. If crack formation occurs and is allowed in the structure this effectively means that there is a redistribution of forces at the cross sectional level, and in a direct sense also at the level of the entire structure, provided

the cross section behaviour is directly linked to the behaviour of the structure on a whole model description.
A direct check of the selected dimensions at both the cross sectional level as well as of the level of the structure is possible by performing a fully non-linear analysis. A fully non-linear analysis of the entire structure would fit at this spot within the design process. However, the non-linear analysis is not yet accepted in this environment as a tool to perform this check within the design process.
At the point where the check takes place the design process of a structure usually comes to a halt. This is indicated in figure 2.1 by the red dotted line.
Following this procedure, it is possible to initiate an optimisation iteration through an evaluation of these results, leading to adaptations of the concrete dimensions. The entire process will start anew and anew until the optimal design has been achieved. However, this part of the optimisation process is often left out of the procedure. Once the checks are satisfactory the design process is mostly terminated. Measured over time, the effort is often not rewarded, meaning that in this sense no optimisation occurs.
The check through a non-linear analysis is done only highly sporadically, in fact, only if more depth is required regarding a specific force variation as the result of crack formation or upsetting of the concrete or yielding of the steel. Also, the non-linear analysis is not seen as robust. As far as the design process for concrete structures is concerned, the optimisation based on non-linear results is still far away. This concludes the description of figure 2.1.
To achieve full control over the design process of a concrete structure the first requirement will be to set up a full calculation model that does not rely on model schematisations. With the solid model this is the case. The reinforcement quantities may then be calculated through the composed results from the solid model, based on the usual cross section analyses and using the current calculation software packages. Following this, the serviceability limit state and the ultimate limit state of the structure may be checked against the current rules and regulations using a series of linked linear static analyses. When performing a check on the ultimate limit state use will be partly made of the robust components of the fully non-linear analysis of a structure. The results may then be evaluated, possibly leading to adaptations to both the concrete and reinforcement quantities and dimensions.
After this, the entire calculation process may start again, including the check on both states of the structure. This process is depicted in figure 2.2.
Compared to figure 2.1 the non-linear checking process will no longer take place at the cross section level, but in an integrated manner along the entire calculation model. The evaluation will also address the entire calculation model. The redistribution of forces as a result of crack formation or plasticity therefore takes place in the entire model.
The shift towards a full 3D model and robust checks on both limit states of the structure lead to a closed design process. This entire calculation process therefore lends itself well to process automation. Apart from this, when there is a change in e.g. the calculation of the reinforcement dimensions on the basis of solid models or when a reliability index analysis is added, this process may be extended in a simple manner.
When making use of geometry data from the software of the sketch design made by the architect, these geometry data are translated into a 3D geometry model of the structure. This may be done in an unambiguous manner, meaning that in the design process further use may be made of one and the same geometry for the structure that is to be designed. This improves the quality of the design data that have to be transferred to other parties. In due time there will be a one on one link on the basis of the IFC results between the sketch design of the architect and the design process of the analyst.

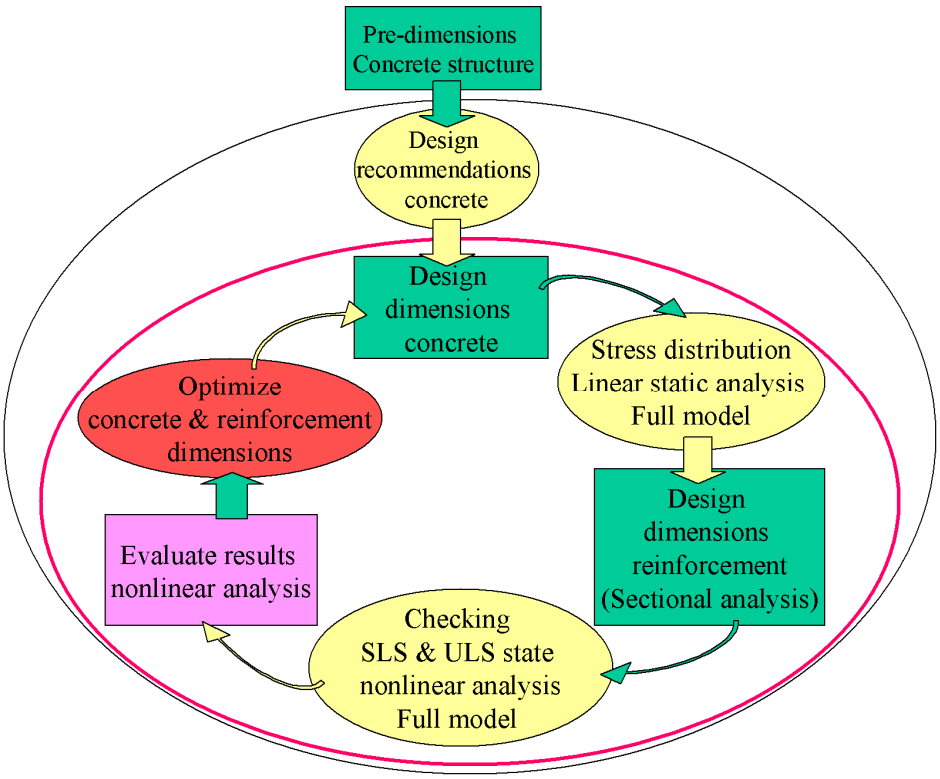

Figure 2.2 Diagram of the future design process

When using a **C**omputer **A**ided **D**esign (CAD) code in the predesign process of a structure, the relevant geometry data from this CAD environment may be transformed directly to the analysis environment. Already, the CAD environment also offers the possibility to set up structures in a 3D geometry. A CAD environment often contains more tools designed for user-friendliness, helping to create a 3D geometry. The integration of CAD with analysis packages for 3D solid models is relatively straightforward at this level, because in this case there is only a need for modifications concerning the connections of the various structural components. With full 3D geometries these are one on one. Modifications are in order, however, with 2D and 1D models, e.g. when a connection has to be made between a column (1D geometry) and a floor (2D geometry). In this case the column will have to be extended by half of the floor thickness to achieve a connection in a combined 1D-2D model. If this transformation cannot take place, the structure will be entered geometrically by hand or with the use of a preprocessor that is linked to the analysis package. The various ways to enter data are shown in figure 2.3.

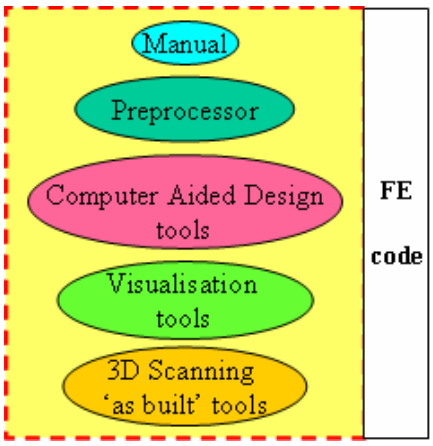

Figure 2.3 Ways to enter a FE model

In the future, the entering of an FE model will increasingly less be done by hand or through a preprocessor. This will more and more often be done using a CAD sketch/design package, a visualisation package or a 3D scanning package and is discussed in 2002 [DeBoer2002]. The CAD sketch/design package is already rather popular and accepted in the design environment, whereas the visualisation package is increasingly being used in presentations of structures for people without any technical knowledge. This package allows them to inspect the design from any conceivable angle (from the inside or outside of the structure).
It is probable that in due time a sketch/design package will generate the most input for the analysis package, because this is where all design disciplines can store their geometrical data in a database, varying from concrete, steel, concrete steel, composites, installations, electricity to ventilation. In fact, this will only stimulate people to carry out an analysis on the basis of the 3D solid model, which will help the process of acceptance.
The checks on the geometry and especially the coinciding or crossing geometries (e.g. of reinforcements or installation piping) may be carried out in advance in the software package used to set up the geometry of the structure. These checks will therefore improve the quality of the design stage of the structure. Users can already indicate in the modelling package which geometrical components of a structure will have to be entered into the analysis package. This means the flexibility of the design stage has been improved vis-à-vis the analysis, whereas it is still possible to gain an overview of the entire structure. At present, the modelling packages are mostly linked to analysis packages based on the beam model. In the future this will have to be extended towards the surface and solid models, ultimately leading to the use of the 3D solid model.
Depending on the type of analysis model that has to be selected, the geometry is entered. After this, the material parameters, supports and loads are added to the various geometrically entered components, so that the analysis process may start. This analysis process is a linear static analysis from which one may then calculate the amounts of reinforcement. For each selected cross section the designer can perform a check at cross section level on the amount of reinforcement through a non-linear analysis. As far as calculation is concerned, no direct link has been made between the various cross sections. There are, however, calculation packages that have established a link between the 1D geometry model approach and a cross section package. In this respect mention must be made of Bentz [Bentz2000] with Response2000 and Roelfstra [Roelfstra2005] with ALP2000. This renders this approach comparable to the 1D geometry approach, in which the 1D element used is also split up into various zones along the height.

2.2 Geometry

It is possible to view the geometry of an entire structure if an analysis has to be made, but the geometry is mostly reduced till the structural parts belonging to the load-bearing capacity analysis. In its simplest form this will often be a rectangular cross section linked to a system line. With a variable cross section along the system line one may then opt for a linear second or third degree curve for the variation in the cross section, likewise linked to the system line, which is then itself also laid out as a second or third degree curve. This has to do with the variation of the neutral line with variable cross sections.
In surface modelling these aspects play a role as well, but they don't in solid models, because these models are able to describe the full geometry. The added value may be found in the fact that no reduction of the geometry occurs, meaning that the 'as built' or 'as designed' geometry is rendered in full. It is, however, possible to leave out

components to support an analysis, because these components do not really affect the analysis, such as consoles needed to support lamp posts. These consoles are not vital to the load-bearing capacity, but they are when the amounts of concrete and reinforcement and/or bill of materials are concerned.
As described above, within the BIM or the IFC concepts, apart from the usual geometry also the geometry of the accessories of a structure, such as wiring and cabling, lamp posts, crash barriers, railings, etc. will be added. It is e.g. also possible to split up a prestressing cable into the original prestressing cable, anchorages, couplings, plates and wedges. At the end of the design process this will generate a complete bill of materials that describes all components of the structure at the lowest possible level.

2.3 Material

The number of different concrete materials in a single structure will often be limited to one to three types of concrete (prefab concrete and two types of concrete poured into the construction), as well as two types of steel (reinforcement steel and prestressing steel). Depending on the type of the structure, material for soil(layers), supports and joints may be added to the calculation model. Depending on the type of analysis non-linear material properties will have to be added to the various materials. This addition of material properties is necessary in case an automated optimisation iteration has to be done.
In the BIM concept the solid models will also include the types of material of the details and accessories. This is a considerable extension, albeit that they may be excluded from the analysis through indexing, so that the analysis process is not taxed further. The details may also be included as a higher submodel. This prevents construction analyses that e.g. include bolts and anchoring bars.
If the BIM concept also entails the state of affairs during the life cycle of the structure, the time-dependent material parameters will also have to be included. This means that the material part will be heavier compared to the lower model types according to the original design concept. However, this approach is required in the current design contracts, including management and maintenance of a structure.

2.4 Supports

In the present design concept supports are rendered as dots or lines. In some cases in the surface model the surface of the support is actually included, but this is still an exception. With solid models, it seems reasonable to model the support as such. It has its own geometry and its own type(s) of material.
This also applies to the BIM concept for solid models. When the database containing the geometry and topology of the structure is extended, the time-dependent affairs during the life cycle of the object will also be entered into the database. This may be useful for the status of the object, including the entered findings during periodic inspections.

2.5 Load cases

Just like the supports, the loads are mostly included into the analysis model as a nodal load or linear load. In surface models the loads are surface loads, whereas in solid models all types of loads apply. Because there are various elements along the height of the

structure, this latter model type allows the exact inclusion of the gradient temperature load, unlike the other models. After all, the temperature gradient is generally important along the first 30 cm of a concrete structural component, measured from the surface. With beam or shell models the hypothesis that the cross section remains perpendicular to the longitudinal axis of the line element makes it difficult for this temperature gradient to apply to the first 30 cm. When using zones or layers for the height of the beam or shell element, for this load one may select an upper layer with a thickness of 30 cm. The temperature load may then apply to this layer. If the designer cannot provide a layered beam or shell element, the temperature load will have to be split up. Splitting the temperature load up into a uniform and a gradient component along the full height of the structure allows this simulation to take place. This simulation is described in “Concrete structures under temperature- and shrinkage deformation”[Breugel1996].
However, this temperature gradient is important, because it increasingly more often turns out that damage to a structure is the result of temperature loads. A good example of the effect of temperature gradients is the collapse of the airport terminal in Paris (2005).
For the BIM concept there is no change regarding loads or points of application, lines or surfaces.

2.6 Modelling types

2.6.1. Beam model

A beam model follows from a schematisation of a structure with beam elements. For the model this means the various components of the structure will be presented as lines that allow the linking of specific data such as geometry, material, load and support.

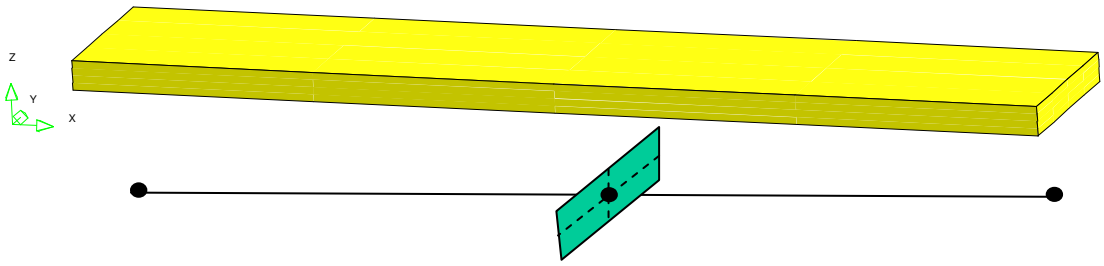

Figure 2.4 Schematisation to beam model

Figure 2.4 shows a beam with a rectangular cross section, that is schematically presented as a linear element (the black line) that is linked to the rectangular cross section (the green plane).
The schematisation to a linear element means that the plane of the cross section always remains perpendicular to the axis of the beam, also in a deformed state. As a result, the strains along the height of the beam are also distributed in a linear manner. If the cross section has a random shape, the cross section may be divided into zones. From the point of view of calculation, this makes the cross section slightly heavier, but in view of the simplicity of such a model this does not unduly affect the calculation time. Use may also be made of the simplest linear element, the line element. In this case only the surface and the moments of inertia of the cross section will have to be entered. However, this latter type does not allow numerical integration along the height or width of the cross section of the beam. In short, this type of element is not suitable for the non-linear analysis test. By

contrast, the zoned line elements can be numerically integrated along the height and width of the cross section.
The material properties may then be linked to the elements of a linear model.
The loads are limited to nodal or linear loads, possible varying along the length of the line in question. The temperature gradient load along a limited height of the cross section may be simulated as a uniform and a gradient load along the full height of the line element, as was shown in a publication by Breugel and others [Breugel1996]. The so-called own temperatures (temperatures that are the result of heating and cooling of concrete after pouring) are not included because of the low impact. These have therefore been neglected.
The support is mostly a dot or, in its most extended form, a section of a line.

2.6.2 Plane stress model

If the designer exclusively wants to analyse a beam or a wall, this will mostly be done using a plane stress model. When the computer capacity was still limited, this type of model was also used for advanced non-linear structure analyses, such as the cable-stayed bridge Heusden analysis by Klerks [Klerks1989]. Good examples of plane stress models for high beams etc. are the high wall beams of Braam, Asin and Hoogenboom [Braam1990, Asin1999, Hoogenboom1998].
In this case the cross section is projected onto a vertical plane, allowing the full modelling of the variation in the height of the structure. This means the thickness of the structure is linked to the corresponding vertical projection plane. This way, the assumption that is linked to the beam model, viz. that the cross section remains the level where the deformation of the beam occurs, is avoided. It is, however, important that the thickness is small compared to the other cross sectional dimensions. The load distribution along the height of the structure obtains a free form, but still depends on the thickness.

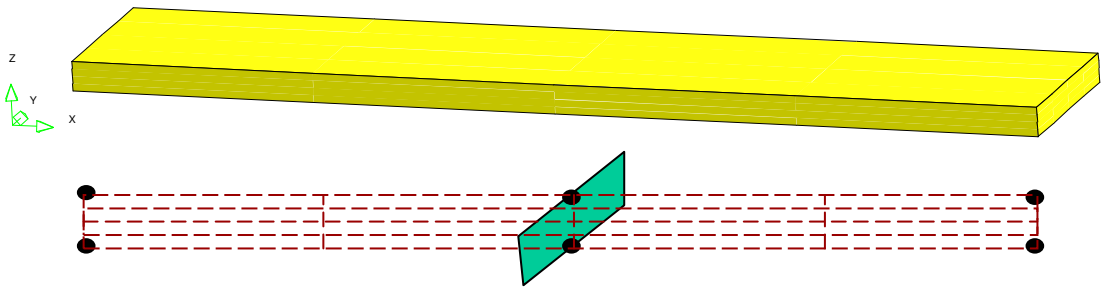

Figure 2.5 Schematisation to plane stress model

Figure 2.5 shows the plane of the vertical projection of the rectangular component of the structure, whereas the linked green rectangular box indicates the thickness of the beam along the height of the beam.
In general, the Finite Element Method allows users to enter a variable third dimension component. This third dimension component is mostly lacking with this type of model, which is why only one structural component can be entered at the same time in the xz plane (the vertically projected plane). One way to avoid this inconvenience is to use a surface model based on shell elements.
The material properties may then be linked to the shell elements of the plane stress model.
The loads are to be entered as a nodal and/or linear or surface load. The linear load and the surface load therefore apply to the full width of the model, which could be seen as a limitation of this type of model, but in view of the low frequency of its occurrence this limitation is non-existent. Other than with the beam model this type of model allows the

exact inclusion of the temperature gradient load. This may be seen as an advantage, because it enables the analysis of damage caused by temperature loads. Naturally, this model does not include a width effect.
As with the linear models the supports may be included as a dot or as a section of a line.

2.6.3 Plate bending, flat shell and curved shell model

The surface model as a shell model describes the geometry of a structure projected onto a horizontal plane. This reduces the height to a thickness linked to the corresponding plane, that may or may not show variations along the length and width. The strains along the height of the structure vary in a linear manner. A plate bending model does not include the forces in the plane, other than the schematisation to a flat shell model, which does include these forces. In this case the strains are viewed sequential for pure plate behaviour and for plane stress behaviour, in accordance with the plane stress model. This type of model can only be used for flat thin structures, similar to the flat shell models. However, the curved shell models can also handle curved structures such as the walls of tanks, the skins of ships and orthotropic steel bridge decks. Layered shell models are also applied, e.g. with overlaying steel bridge decks using higher strength concrete or asphalt concrete. If a thicker structure is in play, the solid model is preferred. Both types include the forces in the plane.
This type of model allows the full description of the crosswise direction of the structure, which is good for the transverse force application.

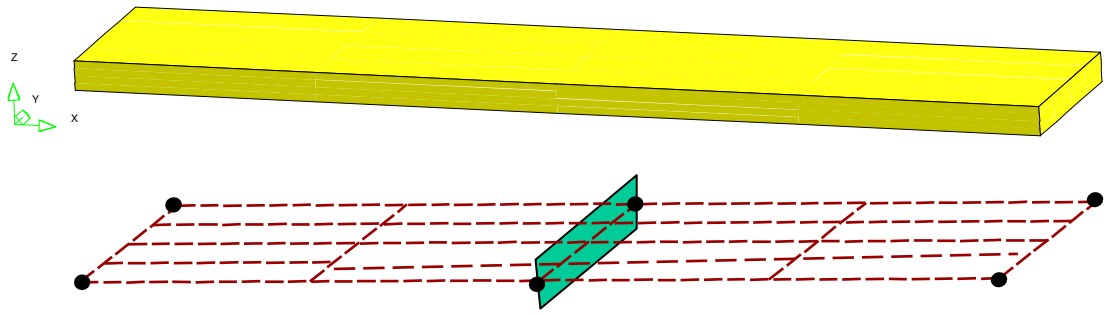

Figure 2.6 Schematisation to plate bending, flat shell or curved shell model

Figure 2.6 shows the horizontal projection of the structural component, whereas the corresponding height is rendered as a green plane along the width of the structural component.
The material properties may be linked to the shell elements of the shell model.
The load shows a limitation as far as the temperature gradient load is concerned, albeit that it can be simulated with the use of the publication by Breugel and others [Breugel1996], for which see the remarks made with the beam model. The advantage of the crosswise direction is that in this direction the load may be distributed and/or concentrated at a specific area, more or less like the various driving lanes of a plate viaduct each having its own traffic load.
With flat shell and curved shell models the forces in the plane are considered, allowing the inclusion of a prestressing load. This is similar to the beam models. With plate bending models the prestressing load has to be entered as the equivalent distributed load (balanced vertical load) perpendicular to the solid slab, which is not fully exact, but has been generally accepted.

The supports of the solid slab may be included into the model as dots and/or little surfaces. This surface model also allows skew structures as seen from above. This is essential for skew crossings of waterways or roads. Up to a point it is possible to schematise the structure to a beam model (if the structure is not too skew). However, once the angle is smaller than 80 degrees or larger than 100 degrees is advisable or mandatory to schematise the structure as a surface model, see the regulations for the design of concrete engineering structures [ROBK6] and the master's theses written by Otaredian [Otaredian1993] and van Vulpen [Vulpen2002].

2.6.4 Solid model

As implied by the name, the solid model provides a full description of the structure. It is up to the analyst to decide whether this description should really show all the details. In most cases only the really necessary elements are included, because there is still no central database similar to the BIM concept.

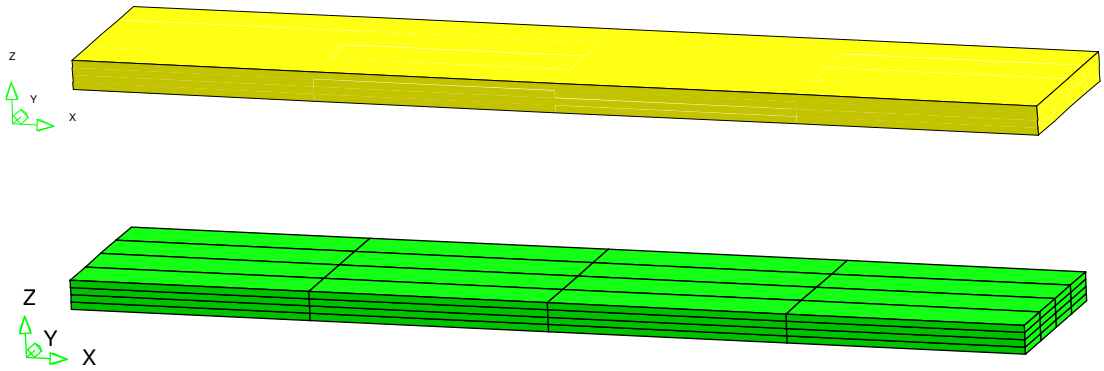

Figure 2.7 Schematisation to solid model

Figure 2.7 shows the schematisation of a structural component to a solid model. There is no longer an artificial link between heights and widths, because the full geometry of the structural component can now be described using the available solid elements in a general Finite Element Package.
Naturally, the material can be entered in full, including all loads. From the point of view of simplicity the supports will still be included as points. However, just like with the plate bending, flat shell and curved shell models there is no reason not to include surfaces as planes of application of the load, or even own solid elements with their own underlying components such as corresponding material properties.

2.7 Calculating the required reinforcement from 1D and 2D results

The 1D beam model analysis presents the designer with the following results: normal force N_x, transverse force Q_y and bending moment M_z.
With a selected coverage, depending on the environmental class etc. as mentioned in the prevailing regulations, the required reinforcement may be calculated per cross section using the internal lever arm and through force and moment balance. This applies to both the upper and lower reinforcement.

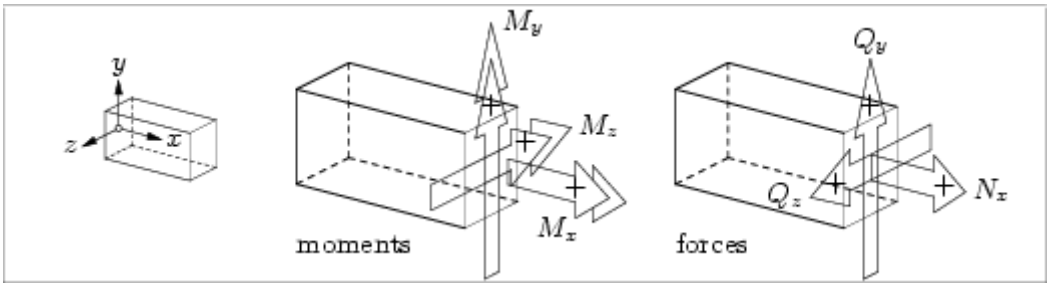

Figure 2.8 Notation of forces + indices 1D linear element

In the same manner, the transverse force Q_y produces a nominal shear stress per cross section, that should according to the present regulations also remain below a specific limit, linked to the quality of the concrete. This enables a calculation of the required stirrup reinforcement. A check based on a non-linear analysis is not usual in current design practice.

In principle, the plane stress model only provides strains, stresses and displacements. On this basis and with the help of the articles by Gupta [Gupta1986], Marti [Marti1991], Lourenco [Lourenco1993], Foster [Foster2003] and the publication of the FIB rapport 45 [FIB2008] it is possible to calculate the required amount of reinforcement.

Following this procedure, a number of iteration phases based on a non-linear analysis will serve to determine the amount of additional reinforcement. At the same time, the reinforcement will be checked.

The SpanCad [SpanCad1999] product is a 'special' among the Finite Element Packages. It is positioned somewhere between the framework analogy (Strut-and-Tie Method; STM) and the Finite Element Method, the basis being AutoCAD 2D. In the nineties Hoogenboom (Delft University), mentored by Blaauwendraad [Blaauwendraad1994], turned this into a product suitable for design practice [Hoogenboom1993, Hoogenboom1998].

Since the SpanCad type model is mostly used for special structures (consoles and high wall beams, the inclusion of a non-linear analysis has been more or less accepted in the present design practice. The calculation process is robust, showing little to no 'snap-back' behaviour.

The plate bending, flat shell and curved shell models result in distributed moments (kNm/m) and distributed forces (kN/m). This allows one to determine the required amount of reinforcement, even strip by strip. In this case a distinction has to be made between the shares as a result of the moment and the normal force. The way to calculate these shares has been put forward in a number of publications [Lourenco1995, Braam1993]. Based on these publications, in 2004 Palacio for his master's thesis [Palacio2004] under Lourenco set up a user interface surrounding the shares of normal forces and moments from solid slabs.

A method that is still in the research stage is the yield line or yield field theory by e.g. Nielsen [Nielsen1991], Denton [Denton2001] and Kennedy & Goodchild [Kennedy2003]. This method is still not generally accepted.

With a solid slab it is not customary to apply stirrups, because this will cost to much time when building a structure. Still, there must be a check on the transverse force. To bend the upper and lower layers of reinforcement upwards or downwards may help to cover the transverse force. The height of the structure, the coverage and the positioning of the reinforcing layers do play an important role, because reinforcement now has to be dimensioned in two directions.

Up to the present, the solid models do not include a direct output in terms of bending moments and forces that help to determine the reinforcement. The direct output is limited to strains, stresses and displacements. However, in 2003 Foster published a paper [Foster2003] indicating how to calculate the reinforcement directly from the stresses of a solid element. This has not been implemented yet in any Finite Element Package available on the market.

2.8 The use of the non-linear analysis to check the calculated reinforcement

As was seen in section 2.7, in the present design process the reinforcement is, in fact, only checked with the plane stress model. Even a non-linear analysis of a beam to optimise the reinforcement and/or concrete cross sections cannot count on sufficient reward in the design process. Such a non-linear analysis takes a number of hours and can certainly not be called robust.
A non-linear analysis is only included into the overall analysis or the design process in case of damage or complex geometrical designs. Furthermore, when new construction techniques are in play, sometimes use is made of the non-linear analysis. It is also used to reinforce or repair structures or to formulate recommendations, modifications or new guidelines.
However, a beam model lends itself very well to a non-linear analysis. Breakdown criteria resulting from the current regulations may be applied one on one as stopping criteria in the present Finite Element Packages. The interpretation of exceeding a specific stopping criterion in one or more locations of a structure is in that case still the responsibility of the designer. After all, even if an exact value is exceeded, this remains a value!
As far as the shell models and certainly the solid models are concerned, a non-linear analysis still has a long way to go in regular design practice. Examples are a box girder viaduct with CUR [CUR1994] and a skew solid slab with TNO-RWS [TNO1996]. In 2000 TNO carried out another extensive research that included a non-linear analysis of a skew box girder viaduct [TNO2000]. In this case the bridge deck and the various webs and bottom flanges of the different boxes were set up as a spatial shell model. In essence, however, this is still a 2½D geometry model.
In view of the present prestress and reinforcement this non-linear analysis required a processing time of about two months, whereas the check on the force behaviour of the viaduct and the reinforcement was found to be very difficult vis-à-vis the usual design formulas.

2.9 Expected results

In view of the fact that the focus of the analysis process will increasingly be on 3D geometry, the design process of the future will have to become verifiable, meaning better manageable.
An analysis method able to use the geometrical data from the predesign process and also allows a faster and robust processing time should meet with a high level of acceptance. Its layout should be such that new developments, like designing the reinforcement from solid models, should be able to replace the existing method with ease.
Also, through visualisations of specific results the 3D models will improve the insight into the force transfer and the redistribution of the force transfer after crack formation in a structure.

Apart from this, a 3D model is accessible to technicians and non-technicians alike, and this will stimulate communication about the building of structures.
In view of the above, there are ample reasons for further research, as will be clarified in the next chapters.

3 THEORY ON COMPOSING RESULTS TO LOWER MODEL TYPE RESULTS

3.1 Introduction

If one intends to transform the results of a 2D, 2½D or 3D geometry model to a 1D or 2½D geometry model, it seems obvious to opt for one single uniform approach. Since all models provide strains and stresses as a primary output option, the choice rather quickly becomes to use either of these two possibilities, strains or stresses.

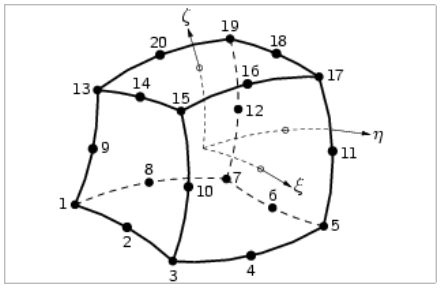

Figure 3.1 20-node solid element with displacement components

Figure 3.1 shows a 20-node solid element, in which each node has 3 nodal displacements in accordance with the displacement method. This results in 60 degrees of freedom per element. The 3 nodal displacements may be presented in the vector notation below:

$$u_e = \begin{pmatrix} u_x \\ u_y \\ u_z \end{pmatrix}$$

Naturally, apart from the 20-node solid element most libraries of the Finite Element Packages available on the market also contain a triangular and pyramid variant (figure 3.2).

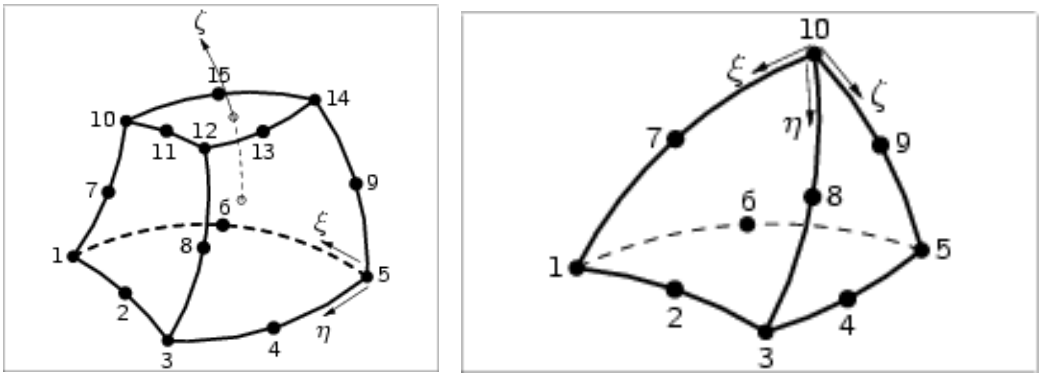

Figure 3.2 15-node and 10-node solid element

In principle, these two types of solid elements allow the set-up of any geometry model of a structure. The displacement increments have been defined, as is shown in figure 3.3 below.

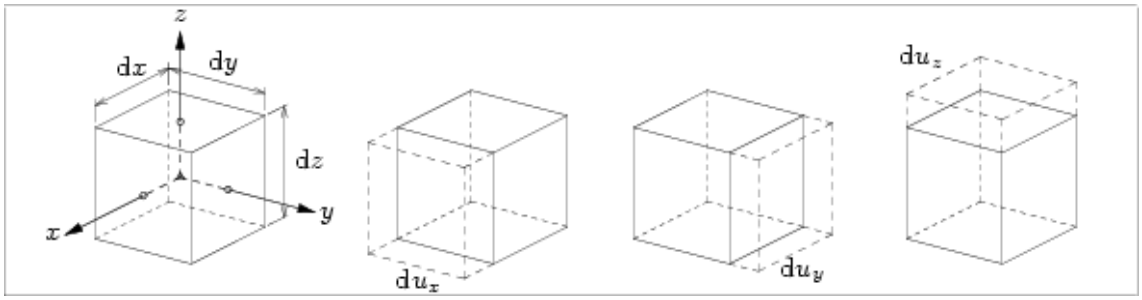

Figure 3.3 Definition of displacement increments

The corresponding strain equations for the solid elements are:

$$\varepsilon_{xx} = \frac{\partial u_x}{\partial x} \quad \varepsilon_{yy} = \frac{\partial u_y}{\partial y} \quad \varepsilon_{zz} = \frac{\partial u_z}{\partial z}$$

$$\gamma_{xy} = \frac{\partial u_x}{\partial y} + \frac{\partial u_y}{\partial x} \quad \gamma_{yz} = \frac{\partial u_y}{\partial z} + \frac{\partial u_z}{\partial y} \quad \gamma_{zx} = \frac{\partial u_z}{\partial x} + \frac{\partial u_x}{\partial z}$$

Since the amounts of reinforcement are calculated from the forces and moments of a beam model and/or shell model using the linear static analysis, the stresses are obviously the best candidates.

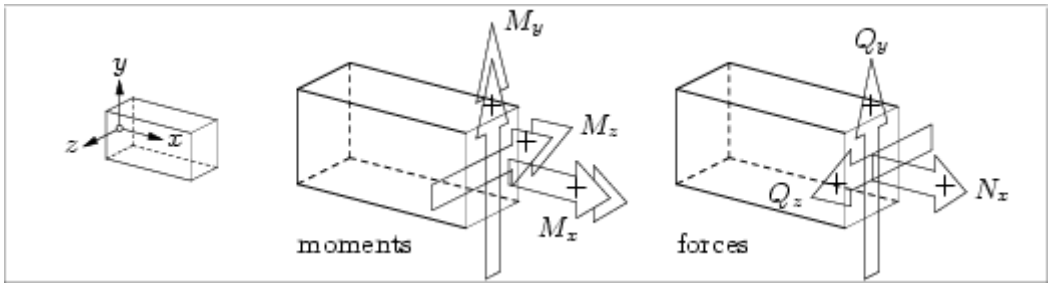

Figure 3.4 Force and moment components to determine the amount of reinforcement from a 3D beam element

The components customary in 3D are shown in figure 3.4, 3 forces in the 3 principal directions and 3 moments likewise in the 3 principal directions. The index x, y, or z indicates the direction of the force or moment component. The drawing convention for bending is that a positive bending moment applies to a positive stress in the positive area ($+M_z$ is aimed at the –z-direction). The same applies to the torsion moment M_x, where $+\sigma_{zx}$ is valid for the +y-direction.
In order to arrive from a plane stress model to results at beam model level, the stresses are integrated throughout the surface of the cross section. This results in the normal force N_x, and the same procedure applies to the transverse force Q_y. The bending moment M_z, however, also requires multiplication with the lever arm. In this manner the 3 composed result components from a plane stress model have been determined and reduced to results

at beam model level, thus allowing the calculation of the reinforcement of the plane stress model with the regular formulations.
This approach forms the basis for composing the composed output towards a lower model type output. In this case composed output is defined as an output that cannot be generated directly from a Finite Element Package available on the market today. It can, however, be produced through additional processing within or outside the package.
Similar component types may be rendered for the plate bending, flat shell and curved shell models, but these are distributed forces (kN/m) and distributed moments (kNm/m), in other words components per stretching unity of length, hence the designation with a small *q* and *m* and the double indices.
The first index indicates the normal direction of the element plane on which the component is exerting an influence, and the second indicates the direction in which the component exerts an influence. This means that with a positive moment a positive stress occurs in the positive z-direction of the element and that for the positive transverse force a positive shear stress takes place.
Apart from the force and the moment, this type of element also involves a shear force, viz. forces in the element plane. These are indexed in the same way as the distributed moments.

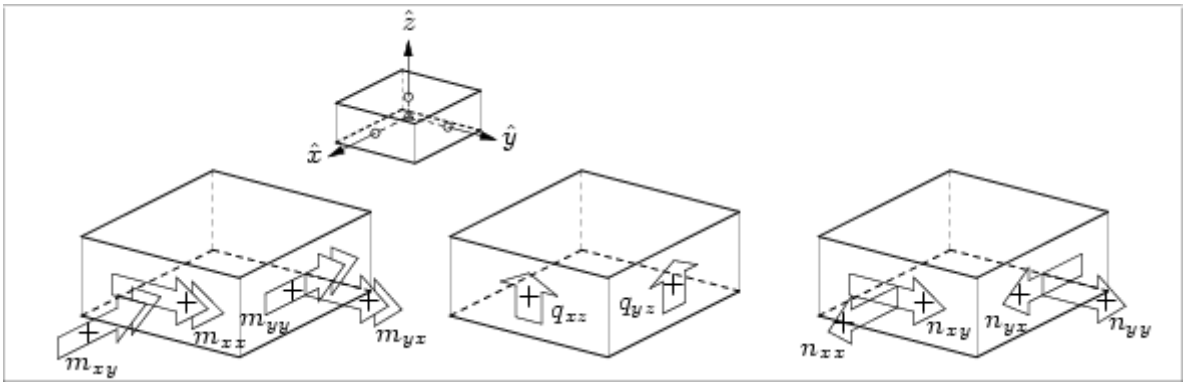

Figure 3.5 Force and moment components for the determination of the amounts of reinforcement from a 2½D shell element

Naturally, a plate element does not involve membrane components, because these have not been incorporated into the formulation of the plate element.
The stress components of the solid element look thus:

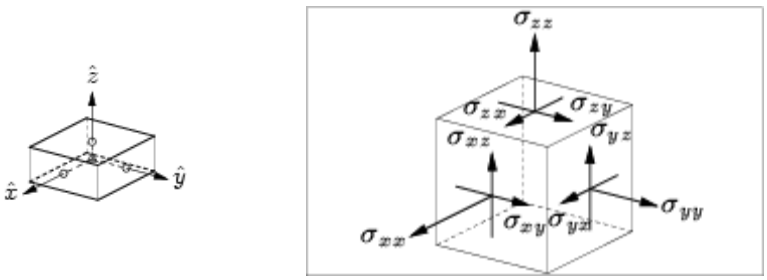

Figure 3.6 Stress components of solid element

Figure 3.6 features the usual 3 stress components per principal direction x, y or z for each plane of application. The first index indicates to which plane the component applies, the second index provides the direction of the component.

3.2 Back-substitution of stresses to generalised moments and forces at the 1D geometry level

In the beam theory (1D) the hypothesis that a cross section is always level and perpendicular to the longitudinal axis of the element has brought about a linear variation of the stresses along the height of the structure. This hypothesis not only makes the summation along the height and width of a cross section easier, it is also unambiguous along the cross section. In a geometry model other than the 1D model this height or width is not unambiguous, meaning that these may be linked to limitations.
The first limitation is that the corresponding elements along a height or width are required to be positioned on a line or a plane. To this end, the normal axis on the reference line or reference plane is selected. The normal axis on the reference line or reference plane on which the composed output is to be projected determines which elements contribute to the composed output of the line or plane in question.
It is of course possible to assign a numerical tolerance to the normal axis in order to allow some flexibility to model formation. In a way, this is not a disadvantage, because the designer was already used to structured element distributions with the beam and shell models. Free element distributions with pyramid elements occur more often recently. These distributions have no consequences for linear static analyses, albeit that the effect of this application with non-linear analyses is not sufficiently clear yet.
When extending the structured element distributions to optimisations based on non-linearity, in due time the need will occur to locally refine the element distribution. On the basis of the results, the existing element distribution will be refined. Naturally, in this case the choice is made for an unstructured element distribution.
This approach also takes into consideration the interoperability of the various models. In models that contain many elements, meaning that the total calculation time may get out of hand, the structural component that is to be investigated is modelled as a solid model, whereas the remaining part is laid out as a beam or shell model. The connection of these different models also takes place in accordance with the normal axis on a plane, as is shown in figure 3.7.

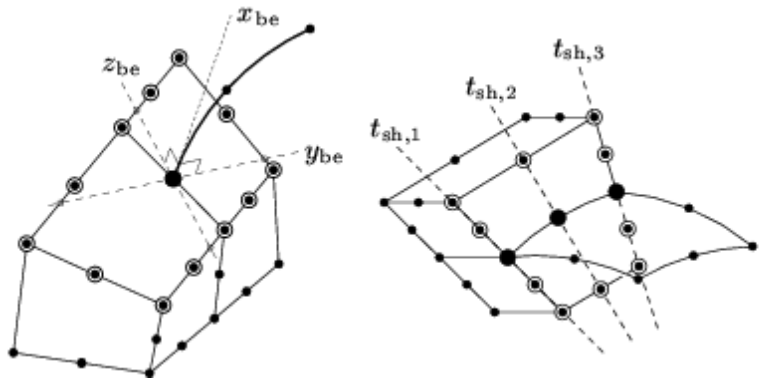

Figure 3.7 Connection of beam and shell models to solid model

Figure 3.7 shows the connection between the black-filled nodes in both submodels. The nodes that are connected to these are shown as encircled nodes, whereas the other nodes of the elements in question are drawn as a single dot.
In the left drawing in figure 3.7 the normal direction x_{be} is shown using the axes y_{be} and z_{be}. The connected nodes do not have to be positioned on one of these axes, albeit that they must be in the plane covered by these axes. In the right drawing the connected nodes

are exactly on the normal axes of the 3 nodes that provide the connection of the shell model to the solid model. It is very well possible that the various model components connect in an eccentric manner. This is shown in figure 3.8.

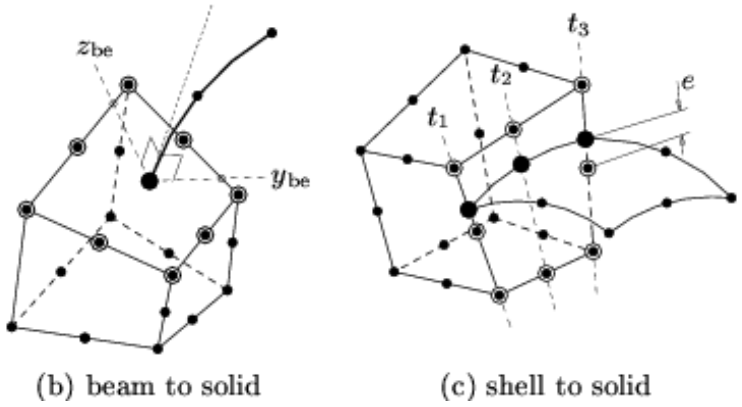

Figure 3.8 Eccentric connection of beam and shell model with solid model

Figure 3.8 shows the nodes in the same manner as figure 3.7, but it is obvious that with an eccentric connection the mutual eccentricity of the nodes comes from the coordinate components of these nodes. This automatically also means that use is made of the structured element distribution.

3.3 From solid model results to 2½D and 1D model results

In order to carry out the integration of the stress components along the height of a structure when producing composed results from the direct results of a solid element model, use may be made of a 2½D reference plane with 2½D reference elements.
With the 20-node solid elements this will be a quadrangular reference element. With a solid element that has a triangle as a base this will be a triangular reference element. Both reference elements will, just like the solid elements, be isoparametric regarding their formulation, meaning that curved shapes in the geometry do not have to be a problem when setting up the geometry of the structure.
Figure 3.9. shows a quadrangular reference plane, set up in a solid model.

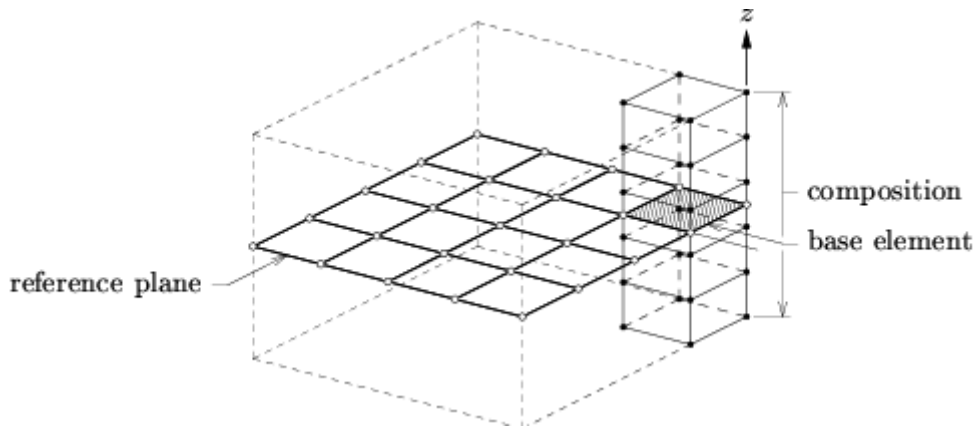

Figure 3.9 Solid model with quad-rectangular reference plane

No material or geometry is therefore assigned to the reference plane. Using the normal axis on the reference plane, the corresponding solid elements are assigned internally. It is possible to make use of a prior selection of elements in order to accelerate the search process of assigning solid elements. If the geometrical shapes are highly irregular a prior selection is desirable, if not necessary. After all, the normal axis of e.g. a reference plane of exclusively the bridge deck of a viaduct could cross the volume of the supporting beam. A contribution by the elements in the supporting beam is unwanted when analysing the amount of reinforcement of the bridge deck, meaning that in this case a prior selection is desirable.
It will be clear that when composing the stresses of a solid model to a triangular reference plane, this may be presented in the same manner. In this case it is equally possible to indicate during the prior selection along which solid elements integration should take place. This is done to accelerate the integration process, but also to control the process itself in view of the quality of the results.
The same applies to the composition of stresses of a solid model to a reference line.

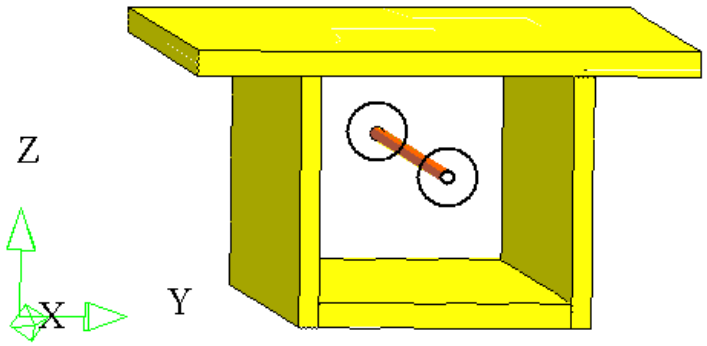

Figure 3.10 Composition of solid model to 1D reference line

Figure 3.10 shows that the integration does not exclusively occur in one direction, but in both directions. The small circles at the ends of the reference line represent the normal planes of the reference line. The solid elements, the results of which have to be included into the integration process, should fall within these.
It is obvious that there is a need for a prior selection of solid elements along which integration must take place to produce the results of the reference line.

3.4 From shell model results to 2½D and 1D model results

It is perhaps not so obvious with a 3D geometry consisting of shell elements to be able to compose the shell element results to a 2½D reference plane. However, the use of shell elements in a large number of structures in daily practice have assured its place in this section. This approach lends itself well to describing the 3D structure of a construction, albeit that it may be seen as the modified form of a full 3D approach. Within this approach they will remain 2½D elements. When computer capacity was still low (before 1985) it was normal practice to reduce an orthotropic geometry of a structure to an orthotropic plate and/or shell model. The composing possibilities with these models have even been extended, because this type of model is still very popular due to its unambiguousness.
For the input of an orthotropic solid slab model this means that for both directions in the plane of the plate and/or shell models two different geometry quantities have to be given.

This is mostly differentiated into parts for bending, membrane functioning and shear. In the case of bending there are five quantities, viz. the bending inertia around the x- and y-axes (i_{xx} and i_{yy}), the interaction inertia (i_{nu}) and both corresponding torsion inertias (i_{xy} and i_{yx}). For the description of the membrane functioning there are four quantities, to wit the shear surfaces in the x- and y-directions, the torsion surface and the corresponding interaction surface. The shear quantity is split up into a surface for shear in the X-Y and X-Z planes. This clearly shows that for the x- and y-directions different quantities may be given that generally apply for quantities in one direction. The connected input quantities with the indices nu, xy and yz are often cause for much debate, because they have to be defined differently for each Finite Element Package. Or in any case they have to be entered differently in an indirect manner; all the more reason to include the composing option for these types of geometries into this observation. When e.g. modelling a single-cell box it is possible to use shell elements for each plane from which the box is built up. Figure 3.11 shows a deck, two edge planes and a lower flange. The composition of the results to a single 2½D reference plane then produces the results that originally were the usual results of a model that was set up as an orthotropic plate or shell model.

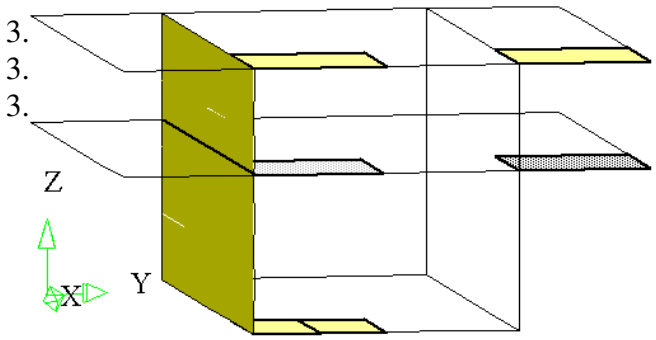

Figure 3.11 Composition of 3D geometry shell model to 2½D reference model

Figure 3.11 shows that the results of the overhang of the single-cell box cross section are projected onto the quadrangular reference plane below. For the middle section the figure shows that the results of the reference plane are built up from a summation of 1 element from the upper flange of the upper plane and two elements from the lower flange of the lower plane of the box. It is obvious that if the reference plane is built up around the web of a box cross section, the results of this web are also incorporated into the results of the reference plane in question. Also, the selection option of shell elements that are to be included for processing the results may be a great advantage.
The same shell model results may also be transferred to a reference line through the same composition method as used with the solid model.

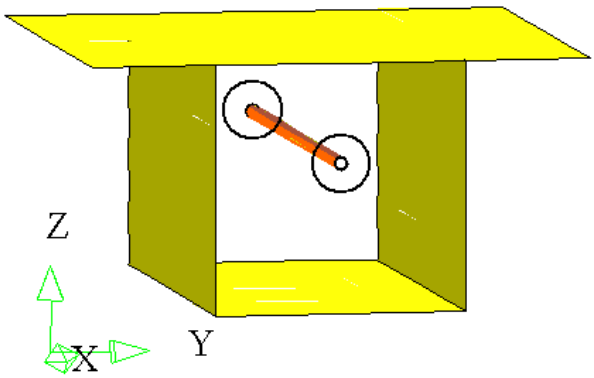

Figure 3.12 Composition of 2½D shell model to 1D reference line

Figure 3.12 shows a 2-node reference line with its two corresponding normal planes, that should contain the corresponding 2½D shell elements. The variant for this 2-node reference line element is a 3-node reference line element that naturally belongs to the matching 8-node shell elements.

3.5 From plane stress model results to 1D model results

The shell models are 2D surface models that have been laid out in the X-Y plane in most Finite Element Packages. This means the reference is limited to a reference line. Also, in this case the normal axis of the reference line is limited to the normal axis in the plane of the shell model.

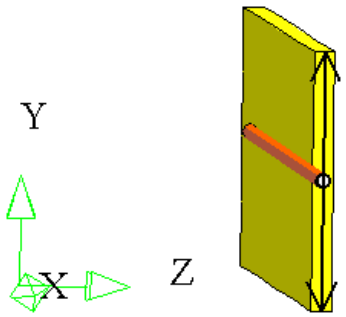

Figure 3.13 Composition of 2D model to 1D reference line

Figure 3.13 shows the reference line with the two directions of the normal axis, containing the results of the elements that have to be integrated.

3.6 Achieved results of the composed results

The aim of this chapter is to provide more transparency between the results of higher model and lower model types. To this effect a possibility was sketched to compose the stress of full 3D models into forces and moments. The output of results from different type of models can be compared directly.
Also, the stress of 3D structural models built from shell elements can be composed into results at shell and beam level. Finally, the stresses of a level stress model can be composed into results at beam level.

4 EXAMPLES OF COMPOSED RESULTS

4.1 Introduction

In order to validate the method described in Chapter 3, two examples will be presented in this chapter, in order to achieve the correct composed output.
The first example concerns a 1D beam with a rectangular cross section. This beam will be modelled in the various manners described above. This will be followed by a presentation of the composed output that is important for a later stage of the design process, when it comes to the dimensioning of the reinforcement.
The second example concerns a box girder, the composed output of which will be shown as if it were an orthotropic solid slab.

4.2 Example 1D beam with rectangular cross sections

4.2.1. General dimensions of beam

The beam with rectangular cross section will first be modelled as a solid model. It is a statically determined beam on two supports with a total length of 15 m, a width of 250 mm and a height of 800 mm.
The beam is made of concrete, and has an elasticity modulus E_{28} of 35,000 N/mm^2 and a Poisson ratio of 0.15. The specific density ρ for reinforced concrete is 2,500 kg/m^3. The gravitational acceleration is 9.81 m/sec^2.
The load on the beam consists of the dead weight load of the beam and two nodal loads. The dead weight load of the beam is entered as an uniform distributed load
q_{eg}=0.25×0.8×2,500×9.81 = 4,905 N/m.
Each nodal load is 8,000N, applying to the beam at 5 m from the end of the upper side of the beam. Both supports are positioned at 0.5 m from the ends of the beam.

4.2.2 Mechanical scheme of beam

The mechanical scheme is shown in figure 4.1.

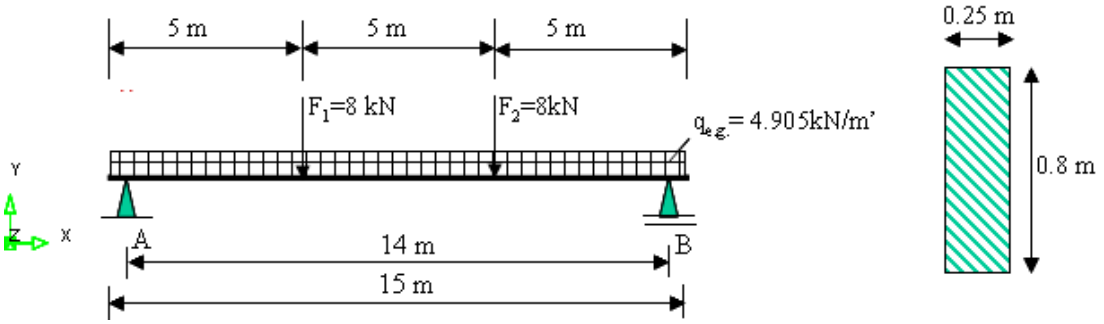

Figure 4.1 Mechanical scheme of beam

4.2.3 Analytical results

The reaction force Q_y at the location of the support is:

R_y $= F + 0.5 \times g \times q \times 15.0$
$= 8{,}000 + 0.5 \times 4{,}905 \times 15.0$
$= 44{,}787$ N

The corresponding action effect to the right of the left support amounts to:

Q_y $= F + 7.0 \times g \times q$
$= 8{,}000 + 7.0 \times 4{,}905$
$= 42{,}335$ N

The matching maximum shear stress at the vertical cross section of the left support is:

σ_{xy} $= 1.5 \times Q_y / A_x$
$= 1.5 \times 42{,}335 / (0.8 \times 0.25)$
$= 0.31751 \times 10^6$ N/m^2

The bending moment M_z at the middle of the span of the beam is:

M_z $= 0.5 \times g \times q \times 7.5^2 + F \times 2.5 - R_y \times 7.0$
$= 137{,}953.1 + 20{,}000 - 313{,}509$
$= 155{,}555.9$ Nm

The matching absolute normal stress in the extreme fibre in the middle of the span of the beam amounts to:

σ_{xx} $= M / W$
$= 155{,}555.9 / (0.166 \times 0.25 \times 0.8^2)$
$= 5{,}833$E+6 N/m^2

The deformations and stresses are a first indication whether the results from the various models truly match. After all, these results are the primary or direct results of all various types of models.

4.2.4 Beam model with solid elements

The main dimensions of the beam built with solid elements are shown in figure 4.2.

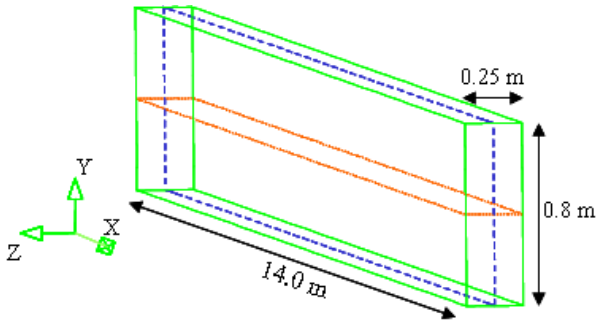

Figure 4.2 Geometry of beam element model

The view in figure 4.2 shows the enclosing lines of the model. In reality the beam is divided into two elements along the width, four elements along the height and 18 elements along the length. The width, height and length dimensions of the basic element are then $200 \times 250 \times 875$ mm^3. This leads to a ratio of 1:4 to 1:5 for the width:height and height:length ratio which is acceptable for a beam analysis. The material properties mentioned in section 4.2.1 are linked to the solid elements. The dead weight load is linked

to all solid elements as an uniform distributed solid load along the negative y-direction. The nodal loads are included as linear loads along the width of the beam, and applying to the upper edge of the beam.

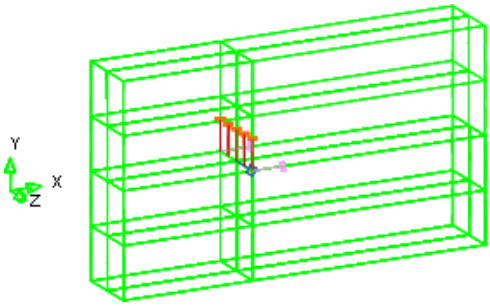

Figure 4.3 Detail of solid model containing supports in the middle plane

The supports are rendered as vertical stripes in figure 4.3. With a 3D model the supports are in three directions, which is also the case in this simple model. The location of the supports is in accordance with the location in the 1D geometry model. The red lines show the vertical supports that may be seen as a linear support over the full width of the beam. These are located in the horizontally positioned middle plane of the beam. The purple support lines show the supports in the longitudinal direction of the beam. In this case two points suffice to keep the beam numerically stable in the x-direction. The blue support line is 1 of the 2 supports that keep the beam numerically stable in the z-direction. These are located in the vertically oriented middle plane of the beam. In reality the supports are positioned at the lower side of the beam. However, for the comparison of this model with the results of the various other models the supports have for the time being been positioned in the heart of the beam. In beam and shell models this goes without saying, hence this assumption. Both reference planes in figure 4.2 are shown with blue dashes (vertical plane) and red dots (horizontal plane). These planes allow the projection of the generalised results for the vertical plane equal to the plane stress model (e.g. n_{xx}, …) and for the horizontal plane equal to the shell model (e.g. m_{xx}, ….).

4.2.5 Composed results for plane stress model from analysis of solid model

Contour plots and diagrams will be used to present the various results for the beam, modelled as a solid model. In view of the fact that the various stresses at the different reference planes are integrated along the height or width, the stresses have to be checked first against the results of the analysis. The load used here is the load combination of the own weight load and the nodal load, both having a load factor 1.0.

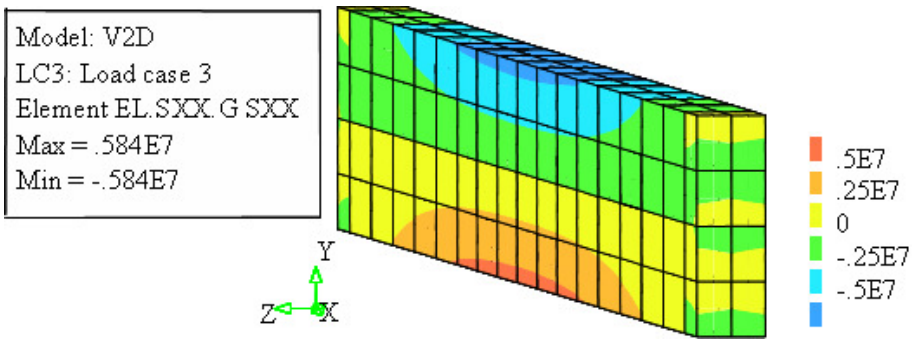

Figure 4.4 Stresses in the solid model at nodal level

The legend of figure 4.4 indicates, that the maximum stress in the solid model equals to 0.584×10^7. In section 4.2.3. the analytical calculation was 0.5833×10^7. This is a discrepancy of 0.12%, which is negligibly small, and a good reason to view the composed output results.

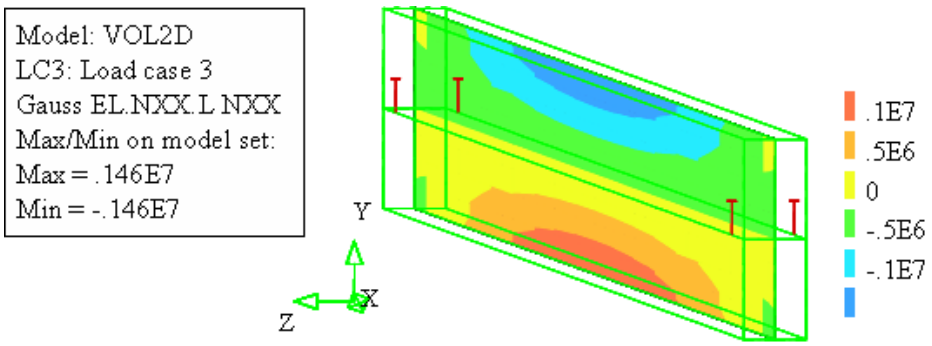

Figure 4.5 Shear force n_{xx} projected on vertically oriented reference plane

The figure clearly shows the neutral line and the bending character of the load on the beam. The integration of the stresses projected onto the vertical plane lead to the shear forces n_{xx}, n_{xy} and n_{yy}, in accordance with a plane stress model.
The absolute value 0.146×10^7 of the shear force n_{xx}, seen in the legend of figure 4.5, matches the analytical value and equals the product of the width of the beam (= 0.25 m) times the maximum stress in the middle of the beam in the upper fibre (0.58×10^7). This maximum stress corresponds well with the analytical result. In other words, the integration went well. This is a discrepancy of 0.12%, which is negligibly small. Figure 4.6 shows the shear force n_{xy}.

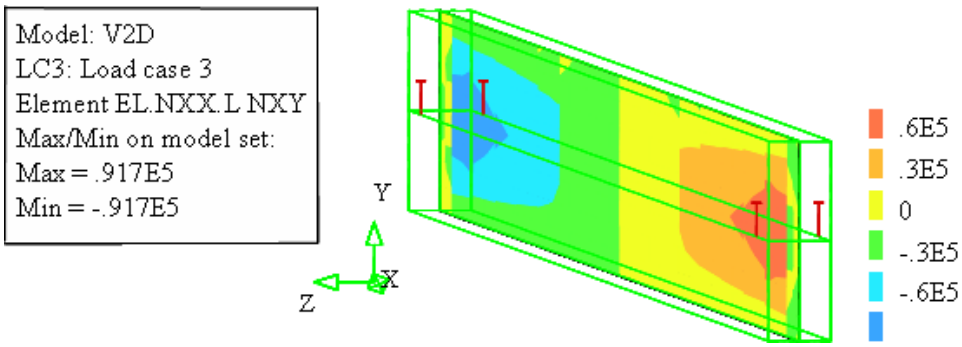

Figure 4.6 Shear force n_{xy} projected on vertically oriented reference plane

The maximum and minimum areas in figure 4.6 surrounding the support are remarkable, which is in line with the theory of the transverse force, which from an absolute point of view has to be maximal at the supports.
In the middle of the beam the vertical section marks the transition from negative values to positive values of the shear forces, viewing in the positive global x-direction. This is also, in accordance with the beam theory, the turning point of the transverse force with this load on this beam. The absolute maximum value of n_{xy} is 0.917×10^5 N at the support.
With a beam width of .25 m the absolute maximum shear stress σ_{xy} may be calculated, being

$$\sigma_{xy} = 0.917\times10^5 / 0.25 = 0.3668\times10^6 \text{ N/m}^2.$$

Compared to the analytical value there is a discrepancy of
$(0.3668\times10^6 - 0.3175\times10^6) / 0.3175\times10^6 = 15.5\%$.

The maximum calculated value from the solid model of the shear stress, $\sigma_{xy} = 0.365\times10^6$ N, and this is again in good harmony with the value calculated from the shear force n_{xy}.

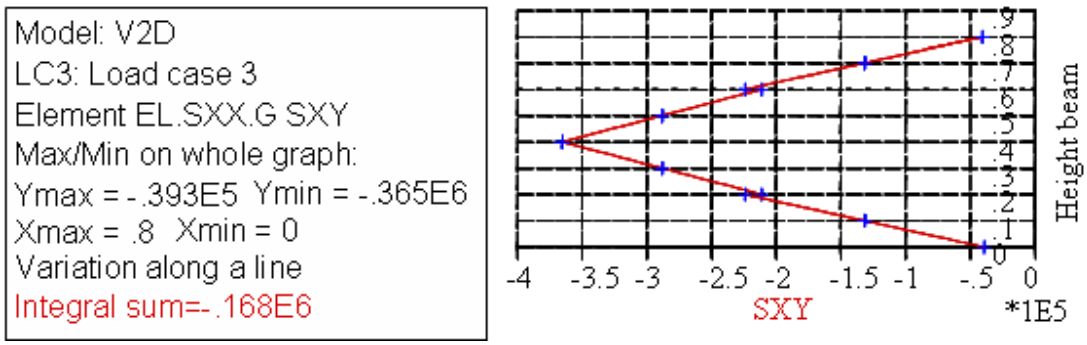

Figure 4.7 Shear stress σ_{xy} at the support along height of beam

The summation of the shear stresses along the height of the beam produces an average shear stress at the right section of $\sigma_{xy\text{-mean-FE}} = 0.21\times10^6$ N/m^2. The analytical solution generates an average shear stress at the same right side of $\sigma_{xy\text{-mean}} = 0.2117\times10^6$ N/m^2. Again, the difference is minimal.
A variation in element distributions along the height and length of the beam produces an unambiguous image for the value of the average shear stress, but there is a considerable difference between the maximum and minimum values. With 4 elements along the height, however, figure 4.7 shows almost no differences in the values for σ_{xy} at the transition of one element to the next. Since the reinforcement is calculated on the basis of the averages in the regulations, this is at this moment no reason for much concern. It does, however, require sufficient attention when interpreting analysis results.

4.2.6 Composed results for solid slab model from analysis of solid model

Looking at the composed results m_{xx}, m_{yy}, m_{xy}, q_{xy} and q_{xz} equal to the shell model, projected onto the horizontal plane, figure 4.8 will show the distributed moment m_{xx}, projected onto the horizontal oriented reference plane.

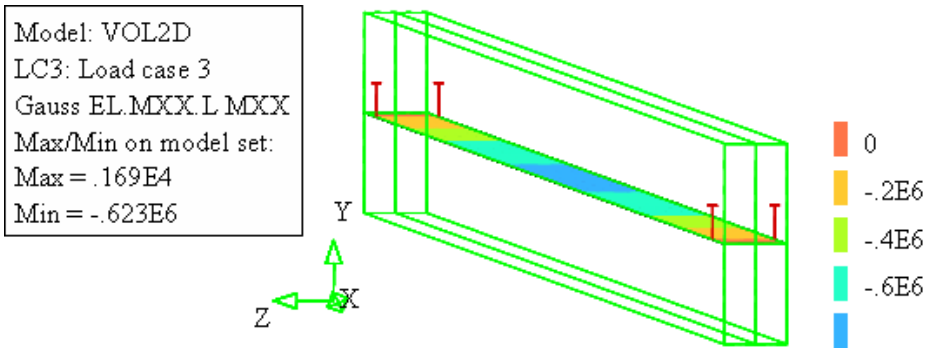

Figure 4.8 Distributed moments m_{xx} projected onto the horizontal oriented reference plane

The figure presents a distributed moment m_{xx}. The moment distribution along the length of the beam shows that at the support line there is a small moment with a value $m_{xx} = 0.169\times10^4$ N/m^2. This value is caused by the 0.5 m overhang. Also, the moment variation along the width of the beam is constant, which is equally correct. With a minimum value -0.623×10^6 N/m (see legend figure 4.8) in the middle of the beam, which is correct in view of the load (own weight and 2 nodal loads). The distribution of the distributed moment m_{xx} along the width of the beam is shown in figure 4.9.

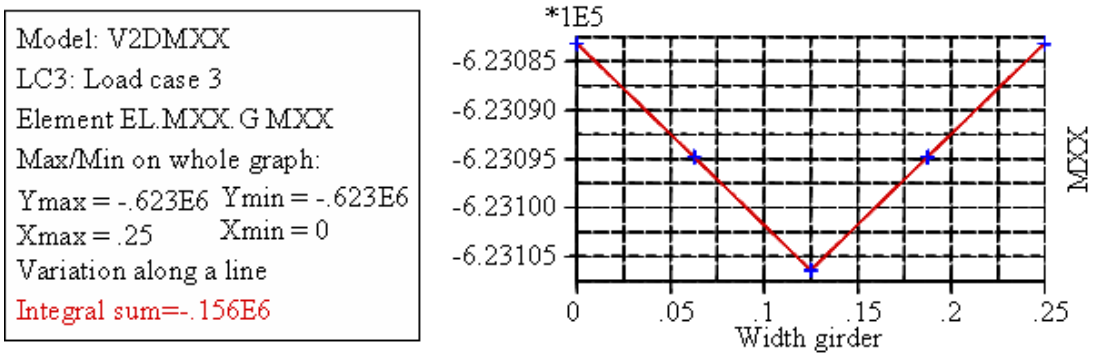

Figure 4.9 Distributed moments m_{xx} projected onto the horizontal reference plane in the middle of the beam along the width of the beam

If the various values surrounding the $m_{xx} = -0.623\times10^6$ Nm/m' are integrated along the beam width of 0.25 m, this produces the value 0.156×10^6 Nm for the bending moment M_z. The legend of figure 4.9 gives the same value 0.156×10^6 Nm. The analytical value calculated in section 4.2.3, namely $M_z = 155{,}555.9$ Nm matches this value very well.
Apart from the moment, the distributed transverse force q_{xy} is also important. This is shown in figure 4.10.

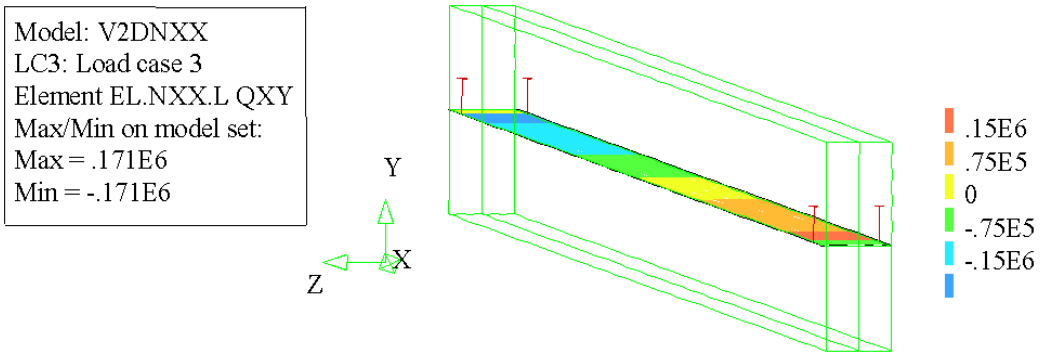

Figure 4.10 Distributed transverse force q_{xy} projected onto the horizontal reference plane

As with the shear force n_{xy} the turning point from negative to positive, seen in a positive global x-direction, is positioned in the middle of the beam. The absolute minimum and maximum are equal in value.
Also, the transverse force 42,335N (0.467×dead weight + 1.0×nodal load) should be large. Here as well the values of the distributed transverse force can be integrated along the beam width. Figure 4.11 shows the integrated result of the right section at the left support of the beam.

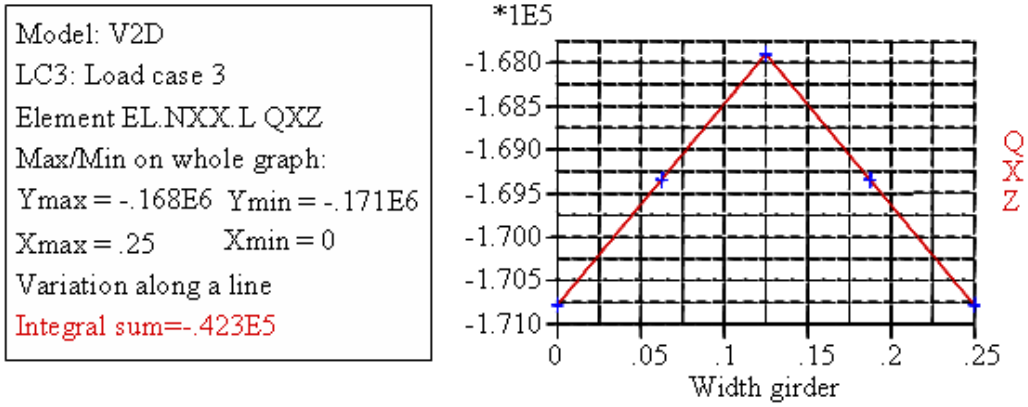

Figure 4.11 Distributed transverse force q_{xy} projected onto the horizontal reference plane of the right section at the left support and along the beam width

The integration of the distributed force q_{xy} along the beam width produces a value for the transverse force of 42,300 N (see legend figure 4.11). If one accounts for the rounding, this is the same value.

4.2.7 Composed results for beam model from analysis of solid model

Apart from the presentation of composed results in the vertical and horizontal reference plane, the results may also be presented on a reference line. The first result to be presented is the bending moment M_z.

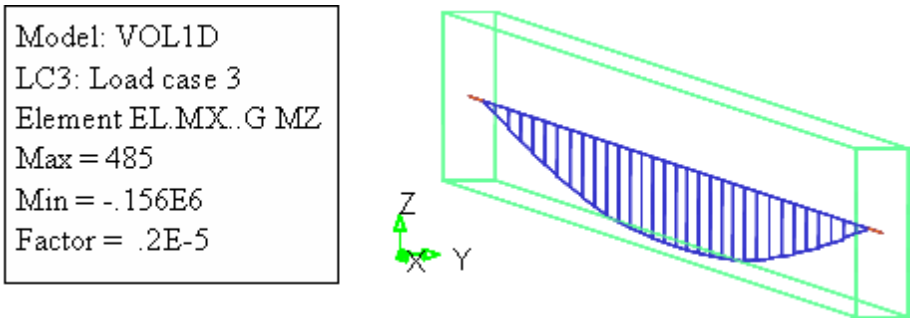

Figure 4.12 Bending moment M_z on the reference line in the solid model

The main shape shown in figure 4.12 is a parabolic curve that matches the results of an own weight load. The value of the bending moment M_z in the middle of the beam for the own weight load + the nodal loads is 155,555.9 Nm according to section 4.2.3. The minimal value of M_z is -0.156×10^6 Nm (see legend figure 4.12), which is the same.
A second composed result projected on a reference line is the transverse force of a solid model. The transverse force is shown in the next figure, also within the confines of the solid model itself.

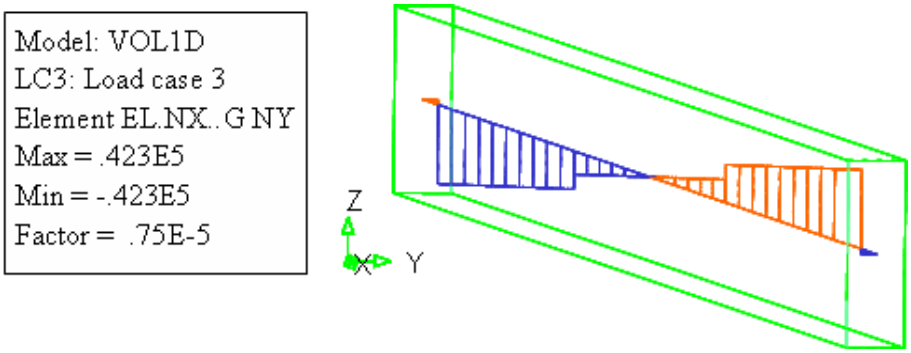

Figure 4.13 Transverse force Q_y on the reference line in the solid model

The diagram clearly shows the surges at the position of the nodal loads. The absolute value at the left support 0.423×10^5 matches the analytically calculated value of 4.2.3, namely 42,335.0 N.

4.3 Results for beam model from analysis of 2D plane stress model

The direct results from the plane stress model are the stresses and strains, displacements and shear forces. The composed results of a plane stress model are a bending moment M_z and a transverse force Q_y. The same beam will be used as in the solid model in order to be able to present the required composed results.
In this plane stress model, other than with the solid model a linear reference line element will be used. This means the results will also be linear, running along the length of a single referential element of the beam.

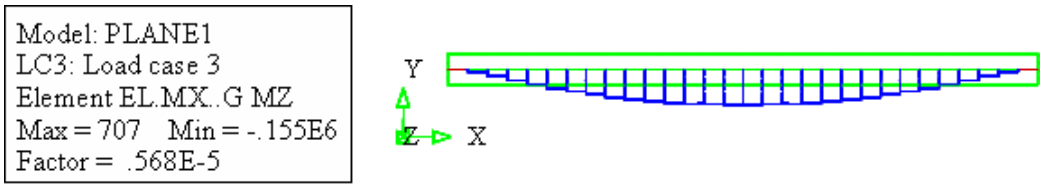

Figure 4.14 Bending moment M_z rendering of plane stress model

The bending moment M_z generated from the level stress model has a minimal value of -0.155×10^6, whereas for reasons of comparison the solid model in figure 4.12 has a minimal value of 0.156×10^6. This matches well.

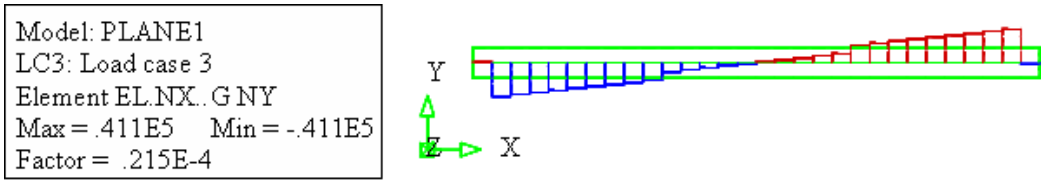

Figure 4.15 Transverse force Q_y rendering of plane stress model

With the plane stress model, the transverse force Q_y has an absolute value of 0.411×10^5, whereas the analytical value is 0.423×10^5. This difference of 2.9% is acceptable. Given the linear approach using linear plane elements in the plane stress model this difference

may be explained. Extrapolation of the location directly to the right of the left support gives a minimal Q_y value of 0.423×10^5. It is advised to use quadratic elements here as well, both in the model and for the reference lines or reference planes.

4.4 3D shell model results projected onto a reference plane

Up till now the study focused on the projection of results of solid models, projected onto reference planes and reference lines. However, in thin-walled structures such as boxes, use is often made of plate/plane or shell elements. The last example in this series therefore addresses a configuration of shell planes in the infrastructure sector.
This is a single-cell box girder, similar to the ones that are mainly used for abutments with large spans. In current design practice these abutments are designed on the basis of beam models. Since these are often spans with a length of 60 metres, a width of 18 metres and a height of four metres, these bridge decks are prestressed both lengthwise and crosswise.
If the prestressing process of such beams is to be viewed in a correct way, a plate/plane or shell model is highly desirable. If these results then have to be fed back into a solid slab or beam model the projection of the results of a shell model or a solid model onto a reference plane or reference line may help. This section will show the projection of the results on a reference plane.
The thicknesses of the concrete components are: deck thickness is 250 mm, lower flange thickness is 300 mm and web thickness is 225 mm. The beam (box girder) is shown in figure 4.16.

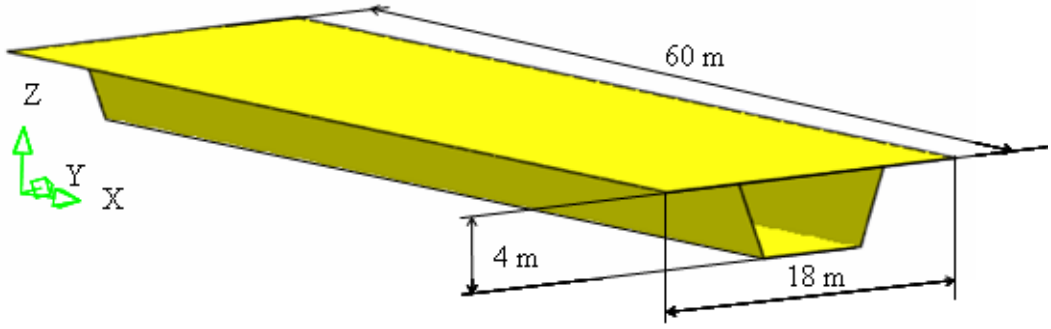

Figure 4.16 Single-cell box girder

Figure 4.17 shows the indicated thicknesses of the different planes of the box girder.

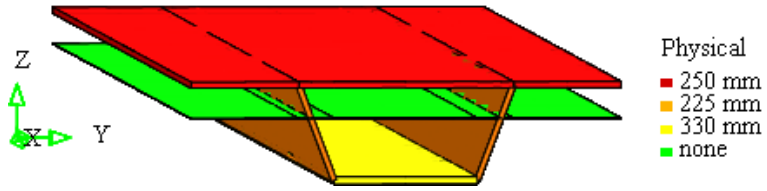

Figure 4.17 Thicknesses of structural components in box girder

The Young's modulus of the concrete is 35,000 N/mm^2 and the Poisson ratio is 0.15. The beam is under load of four nodal loads that apply to the section line between deck and web at 18 m from the end.

The vertical supports are positioned at the beginning and at the end of the section line between the lower flange and the web. This is shown in figure 4.18.

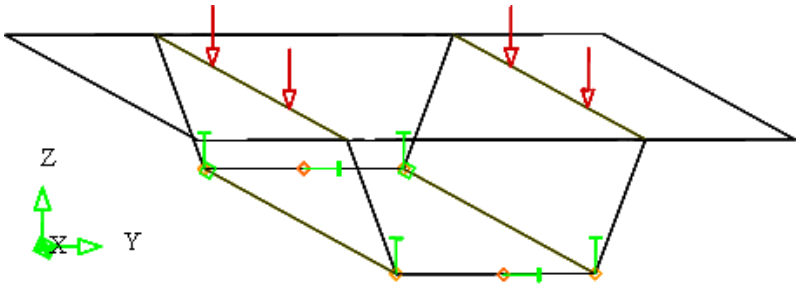

Figure 4.18 Overview of load and support in box girder

Due to the 3D geometry of the structure supports are also needed in the global x- and y-direction. The supports in the x-direction are at the beginning of the box cross section at the two corner points of the lower flange. The support in the y-direction takes place at the middle of the lower flange at the beginning of the box girder. This will keep the box cross section statically determined. Due to the slanting webs one and the same element distribution is used for both the box and the reference plane. This is shown in more detail in figure 4.19-20.

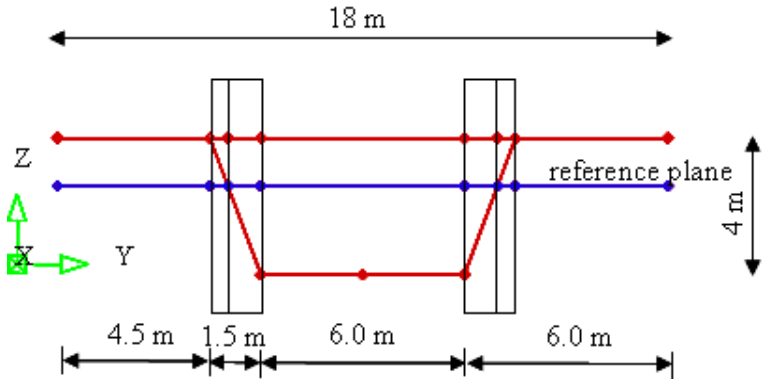

Figure 4.19 Box cross section including reference plane

The 4 rectangles mark the most difficult areas of the projection of the results onto the reference plane. The reference plane may be in the horizontal plane, but the webs of the box cross section are not.
It is advisable to bring the subdistribution on the main lines of the number of elements in the upper plane and the webs in harmony with the subdistribution of the elements in this horizontal reference plane. Figure 4.20 gives a better impression of this situation.

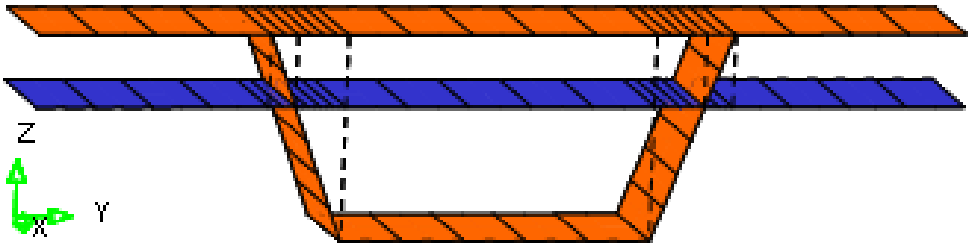

Figure 4.20 Distribution of the elements of a slice of the box cross section and corresponding reference plane

It is clearly visible that both overhangs in the upper flange of the box each contain 4 elements. The webs have 6 elements along the height, whereas the lower flange has 5 elements. In this case, the part of the upper flange in between the webs also contains 5 elements, with 6 smaller elements on each side.
The reference plane (shown in blue) has the same element distribution as the upper flange of the box cross section. For the elements in the upper flange the main pattern 4-6-5-6-4 has been maintained, but this could also have been 4-2-5-2-5.
Along the length of the entire box there are 22 elements.
The position of the reference plane in altitude vis-à-vis the box cross section is not really important in this case. Naturally, the altitude position does influence the value of the results projected onto the reference plane, but the normal axis direction is at this moment still the most important, to ensure that each reference element receives its own belonging elements for the projection of the results. On the basis of a first analysis it is relatively easy to adjust the height of the reference plane, resulting from the analysis results on the height of the box. This may e.g. be presented through the results of n_{xx} along the height of the web of the box cross section.

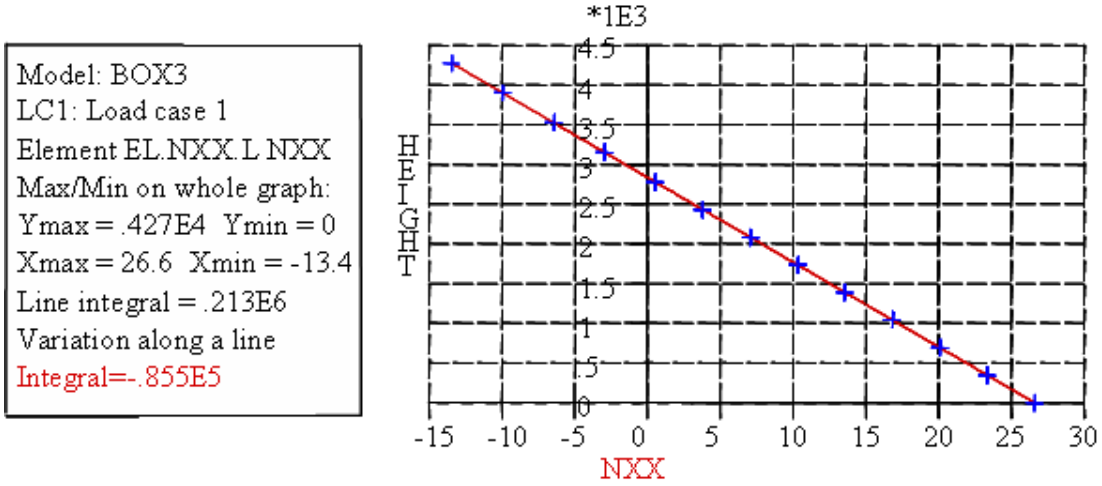

Figure 4.21 Shear force n_{xx} along the height of the web

The diagram shows that there is no element node result marked with a '+' that coincides with a n_{xx} value 0. This means the reference plane does not coincide with the geometrical centre of gravity of the entire box cross section. In the first instance, the reference plane was at 1,400 mm below the deck. The value of n_{xx} is -13.4 N/mm at the deck side, and 26.6 N/mm at the lower side at the lower flange. Seen from an absolute point of view, the difference in n_{xx} at the upper and lower fibre of the web is 40.0 N/mm. With a height of 4,000 mm and an upper fibre shear force of 13.4 N/mm, this means the reference plane would have to be situated at 1,340 mm below the upper fibre if this shear force is to be 0.0 at that position. For this reason the reference plane will have to shift another 60 mm in the global positive z-direction. This results in a normal force in the box cross section, and taking into account the belonging cross sections, that equals zero. This could also have been calculated in advance using a cross section programme! The ultimate moment field result on the reference plane with the adjusted position is shown in figure 4.22.
The distribution of the distributed bending moment M_z in figure 4.22 may be symmetrical, but it is not very handsome. The image between the webs shows a different image of the moment distribution than for both overhangs.

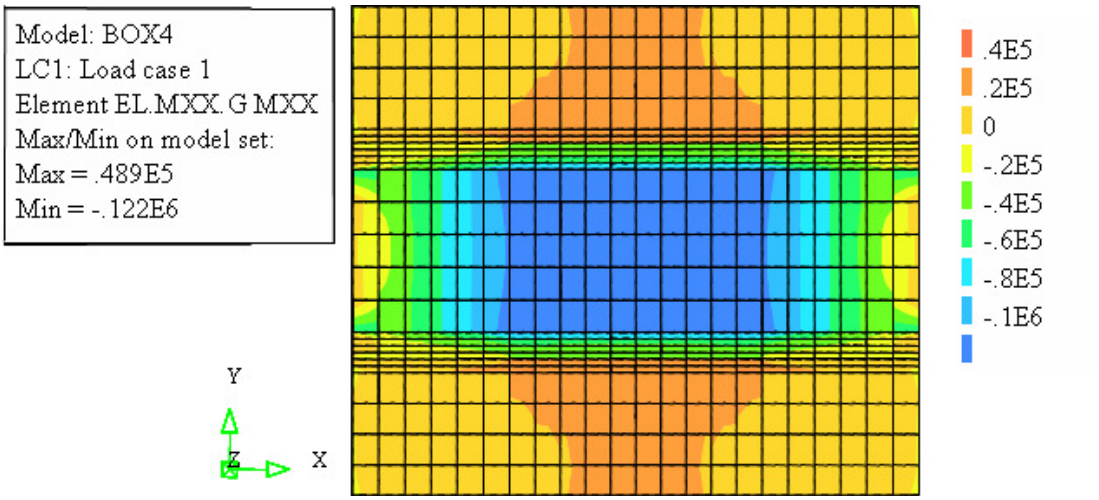

Figure 4.22 Top view of reference plane showing the distributed moment m_{xx}

Using the cross section in the middle of the box girder a check may be performed on this cross section plane, allowing the comparison of the total bending moment M_z, through an integration along the section, with the moment M_z that should be there on the basis of the load. The latter value is 0.108×10^{9} Nmm.

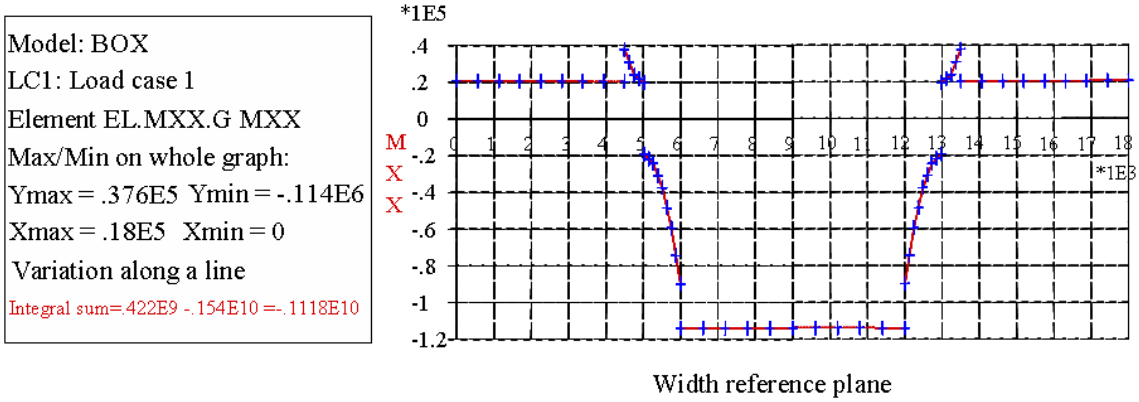

Figure 4.23 Distributed moment m_{xx} along the width of the reference plane

The integration along the width of the reference plane gives a value of 0.112×10^{10} Nmm for the bending moment M_z. This is a difference of 3% with the earlier given value 0.108×10^{10} Nmm, which is acceptable.

4.5 Achieved results

The examples presented in this chapter clearly show that the composed results of the higher model types in question, obtained from the usual results of elements, may be composed into shell or beam model results.
This applies to full 3D to 2½D and 1D, and also for 2D to 1D and even for a 3D structure to 2½D.
The results of all these composed results are also comparable to the results obtained through analysis, meaning that they are valid.

5 EVALUATION OF COMPOSED RESULTS AND THE ADDED VALUE FOR DESIGN PRACTICE

5.1 Evaluation

In Chapter 4 it was shown that results of a lower model type may be obtained through reference planes and reference lines with higher model types. The differences in absolute values are within the margins of the analysis. For the quadratic results the differences are often minimal, and for the linear results they are mostly below 3%.
Also, the higher analysis model types are seen as the most correct description of the geometry, because they allow the most realistic rendering of the variations in stresses, strains and displacements.
When using higher model types the overall processing time of the analysis will increase, but the present and future calculation power of the computer is ample reason to use these model types in future design practice.
This approach has also resulted in a certain degree of transparency between the various results of the different models. It is possible to continually generate the same results through the composed results from whichever calculation model.
This means the debate on the uncertainties surrounding the model facts may be limited, because the direct and composed results of the various analysis models types can now be compared to each other on a one on one basis.
Apart from these positive findings there is also one negative element. The tolerance of the normal axis on the reference plane or reference line plays an important role when projecting the results. This is important during the search process for elements that may be assigned to a reference plane or reference line. Once an element falls outside the scope, the results will not contribute to the result of a reference plane or reference line. The tolerance of the normal axis and the manner in which to address it with structured element distributions is shown in figure 5.1.

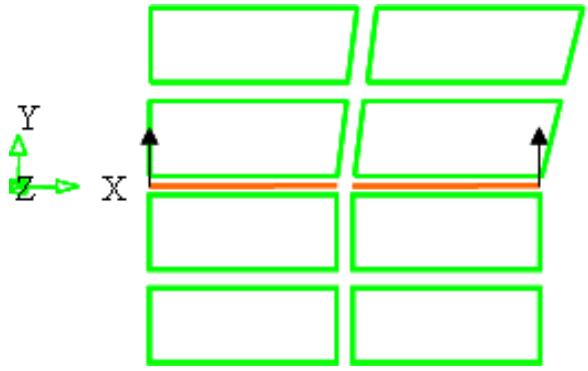

Figure 5.1 Normal axis tolerance back-substitution stresses

Figure 5.1 shows 8 elements with a single reference line and 2 matching normal axis lines. It is clear that the left normal axis will have no trouble finding the matching elements. The right normal axis, however, will have trouble finding these, due to the slant of the upper layer of elements. In modelling it is therefore advisable to give these upper 2 layers a rectangular shape as well. This is not something that applies to just a single direction, but also with connections or references in 2D or 3D in 2 directions. Coming from the beam and shell models, however, this approach is justified.

A second point of attention is the position of the reference line or the reference plane in the geometry model. Up till now no models have been analysed with variably positioned geometrical points of gravity that will occur when more than one type of material is used, e.g. a prefab beam and a compression layer. At cross section level this geometrical point of gravity can be calculated in advance using cross section programmes. If, however, this is done often, one may choose to include this option automatically into the computer programme.

5.2 Additional values in input and results of a higher model type

5.2.1 Increasingly realistic geometry of supports and loads

After the validation of the method to determine composed results through the projection of the direct results from an analysis model onto reference lines and reference planes, when modelling a structure the correct position of especially the supports and loads is an important aspect.
With the schematisation of a specific geometry to a beam model or a shell model, the point or surface of application of both the load and the support is often on the system line or system plane of the model that has been selected. With the schematisation of a beam to a plane stress model both the points and lines of application for the load and support are at the right altitude in relation to the geometry of the beam.
In the example addressing the beam in Chapter 4 the load was already on top of the beam, but the supports had not yet been attached in the middle of the beam. This is due to the evaluation of results with a beam model. In reality the supports are mostly at the lower side of the beam. By including the height of the beam in the analysis model, this will present a more correct image of the compression arc and the tension rod and, in turn, of the shear stresses.
A second observation in this respect is the possibility to assign a realistic length and width to the application surfaces of the loads within the geometry of the structure. In this manner, under load the maximum or minimum stresses at the points of application are distributed along the length and width of the lines and surfaces of the load, and reduced. This distribution and reduction of stresses also applies to including the lengths or surfaces with supports.
An even more advanced modelling is to include the interface behaviour between a load or support plate and the structure in question. Especially with experiments that naturally include validations of material behaviour or structural behaviour it makes sense to pay some attention to this, even if it is just to be able to exclude marginal phenomena connected with the behaviour that is being researched.
This may be illustrated by a simple model involving a half beam, modelled with plane elements.
Figure 5.2 shows the half beam from section 4.2 with the support on the left being positioned in a centric and eccentric manner, under load of the own weight and the nodal load indicated in figure 4.1.

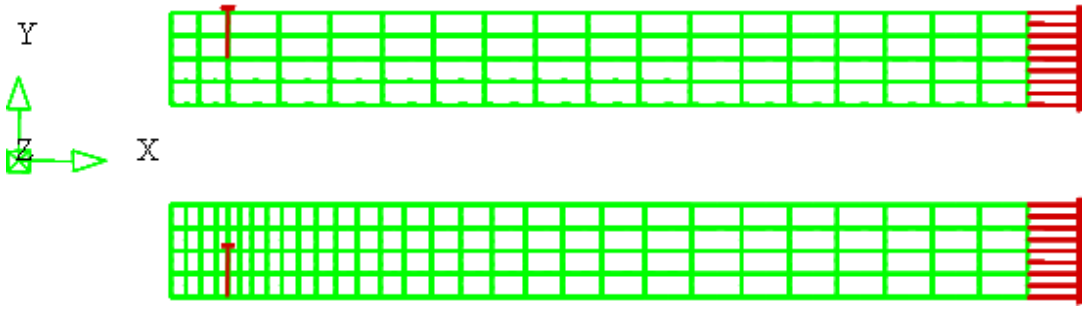

Figure 5.2 Supports shown in centric and eccentric manner

The top image of figure 5.2. shows a support in the heart of the beam located at half its height, in accordance with the first example addressed in Chapter 4. The lower image renders the schematisation of the support as it occurs in reality.

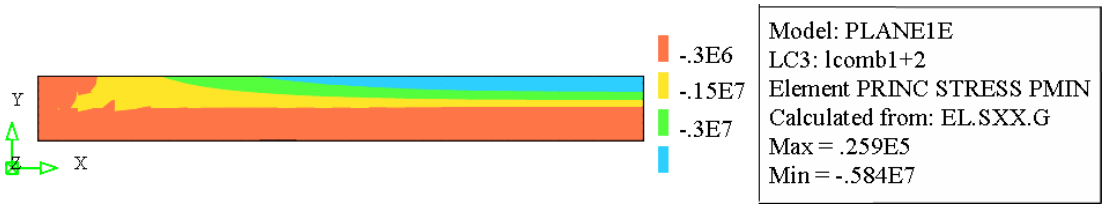

Figure 5.3 Compression arc of half beam with centric support

The compression arc in figure 5.3 with a centric support at half the height of the beam, is almost non-developed if one renders the principal compressive stresses of the beam.

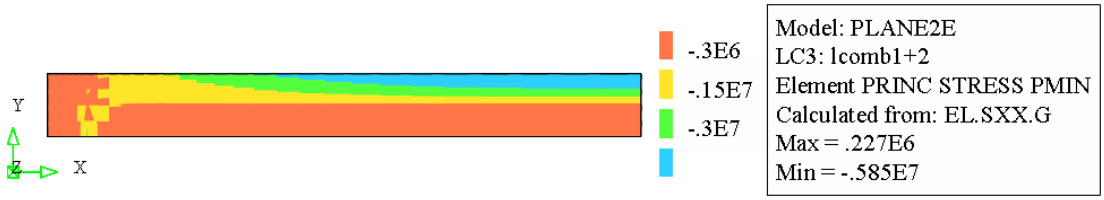

Figure 5.4 Compression arc of half beam with eccentric nodal support

When moving the support to the lower fibre of the beam, a much clearer compression arc becomes visible if the principal compressive stresses of the beam are shown, as in figure 5.5.

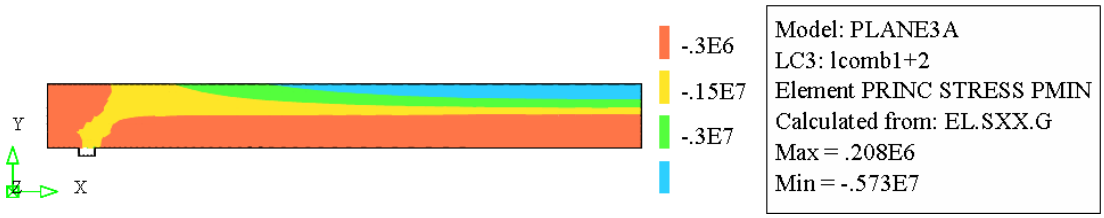

Fig. 5.5 Compression arc of half beam with eccentric line support

If the support force is distributed along the length the compression arc really becomes visible (figure 5.4). A numerical comparison of the absolute values of the various stress components in the three figures is possible. This is done in table 5.1.

Stress	Location	Centric support		Eccentric support			
		Nodal support		Nodal support		Line support	
		Max.	Min.	Max.	Min.	Max.	Min.
σ_{xx}	Upper fibre	.111E6	**-.584E7**	.127E5	**-.585E7**	.297E5	**-.573E7**
	Centre beam	.748E5	-.748E5	.117E6	-.350E5	.125E6	-.276E5
	Lower fibre	**.584E7**	-.112E6	**.585E7**	-.563E6	**.573E7**	-.731E6
σ_{xy}	Upper fibre	.148E6	-.150E6	.674E4	-.132E6	.148E6	-.152E6
	Centre beam	.396E6	**-.581E6**	.490E5	-.337E6	.231E5	-.322E6
	Lower fibre	.443E5	-.339E5	.352E6	**-.409E6**	.481E6	**-.505E6**

Table 5.1 Maximum and minimum values of stresses in upper, lower and centre fibre σ_{xx} and σ_{xy} with centric and eccentric supported beam model

The stresses σ_{xx} in the lower and upper fibre of the beam are, where the absolute maximum and minimum are concerned, approximately 0.584×10^7. With a line support the value decreases somewhat (0.573×10^7 instead of 0.584×10^7). But this is due to the shorter support length as a result of the width of the line support, that was introduced (= 0.2 m), which is in this case a reward of 2%. The maximum and minimum are viewed along the half length of the beam.
Naturally the shear stresses will increase especially at the lower side of the beam as a result of the repositioning of the support from the heart of the beam to the lower beam fibre. With the eccentric supported beam with nodal support already a shift of the absolute value to the lower fibre can be seen. When applying a line support the absolute value σ_{xy} is reduced to $.505\times10^5$, a reward of 15% compared to $.581\times10^6$.
This way the designer or analyst is rewarded for his additional effort when setting up the calculation model by rendering it more complete. Ultimately, this should lead to improved use of the material from which the structure is built.

5.2.2 Results at 3D level

The use of solid elements in the calculation model automatically means that the results are available at 3D level. It also means no prior parameters at result level are necessary.
In beam models it is customary to automatically calculate the shear stress from the transverse force divided by the cross section. If the surface cooperates only to a limited extent, the surface will have to be reduced, as is e.g. the case with a T-profile.
In shell models the transverse force is divided by the height of the shell element involved. By adding the option ‘shear factor’ with a specific value that results from a calculation of cross section quantities, it is possible to calculate the maximum or minimum shear stress. It is known that the shear stress along the height of a beam with a rectangular cross section shows a parabolic curve with a maximum value at half its height. In this case the corresponding factor is 1.5. The results from a 3D solid model automatically also provide this distribution of stress, meaning that no extra factors have to be determined in advance by the designer or the analyst.

5.2.3 Added value of results at 3D level

Since the results of the various models only show slightly different percentages the added value of the results at 3D level mainly concern the more realistic values of the shear stresses in a 3D solid model. The analyst is not obliged to enter a shear factor in advance, something that has to be done with the lower model types in order to get an idea of the maximum absolute value of the shear stress. When a specific load is transferred to a support node, the shear stress often indicates to which method the force transfer belongs. Both bending and distortion take care of force transfer, each in its own manner.
Bending is mainly related to the beam theory, whereas distortion is connected with a combination of bending and shear. These zones are therefore referred to as B- and D-zones, that mainly become visible in the Strut-and-Tie Method (STM). At a structural level one may think of consoles or high wall beams. In a more abstract sense one may say that with a height-length ratio of a beam that is smaller than 1:10, there will be a non-bending area. This area can now also be visualised using the presence of the shear stresses and a simple x-y figure. The horizontal axis is the local x-axis and the vertical axis indicates the shear stress. This may be illustrated with a figure that is composed of the simple example of the beam in section 4.2. The load that applies to this beam is a uniform distributed linear load in the Y-direction along half the length of the beam. There is also a nodal load at five meter from the beginning, also in the Y-direction. Figure 5.6 shows the stress in the X-direction and the shear stress as a result of the load on the left side of the beam along half the length of the beam.

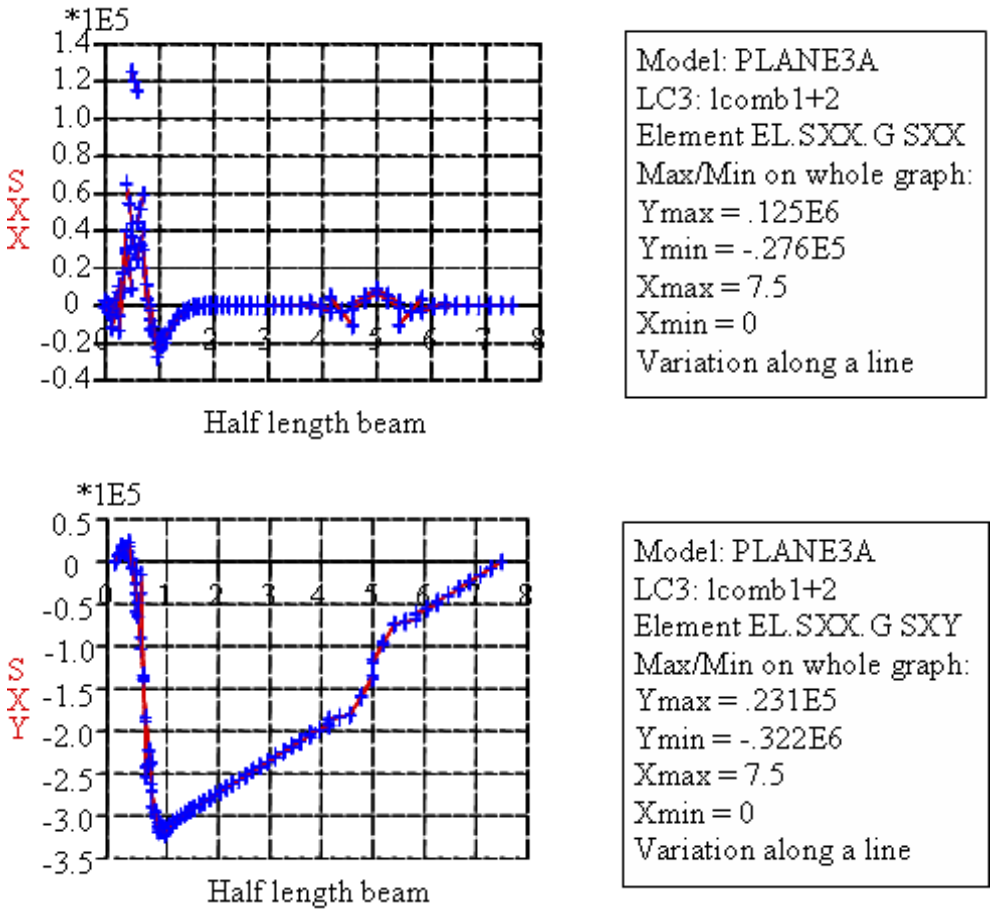

Figure 5.6 Variation of σ_{xx} and σ_{xy} along half beam at the longitudinal axis of the centre of the beam

In this case the σ_{xx} variation indicates that there is a disruption at approximately 0.5 m and 5.0 m. This indicates the so-called B- en D-areas of the beam, B standing for bending, D for disturbed.
The σ_{xy} variation shows that there is a transverse force transition between 0 and 1.0 m, another surge occurring at 5.0 m. The B-areas indicate that this is where bending takes place, whereas at the so-called D-areas there is a combination of bending and shear. These areas are important when it comes to the way in which the reinforcement is designed. In the case of beams this means one will have to look for additional reinforcing stirrups at the location of these disruptions. In practice this is where in the design process people resort to a Strut-and-Tie Method.

5.2.4 Determination of length of distribution of local nodal load

The beam in question has a span of 18 m and 2 small overhangs to the left and right of the support of 2 times 0.1 m. The cross section is 0.8 m high and 1.2 m wide and has a U-profile. The thickness of the flange and the webs is 0.2 m. Figure 5.7 shows a cross section with the dimensions and the mechanical diagram of the beam.

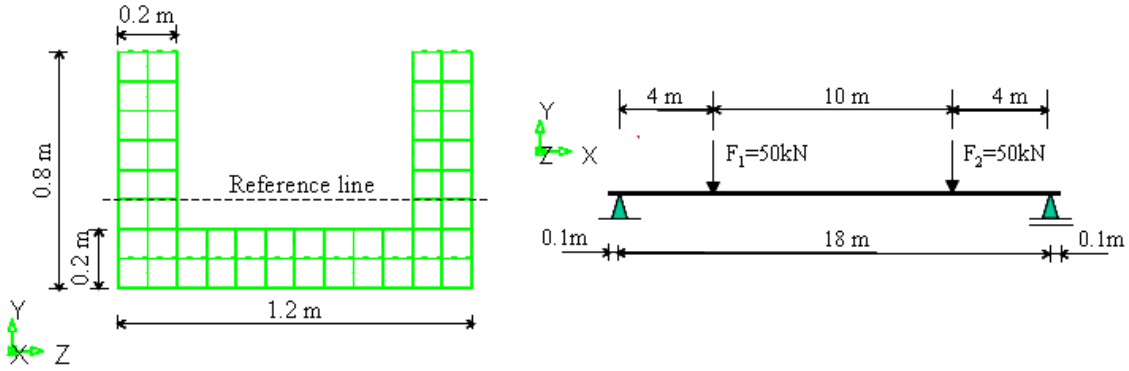

Figure 5.7 Cross section U-profile + mechanical diagram

The load consists of 2 nodal loads that apply at 4 m from both supports, amounting to 50 kN. The assumed load surface has a length of 0.2 m (2 element sides) and a width of 0.2 m, equalling the web width. With this load a distinction is made in two load cases. The first load case applies to the full cross section of the profile, the 50 kN being distributed over 24 element surfaces. The variant is the second load case that only applies to the edge of the U-profile, being distributed over 8 element surfaces.
The median of the cross section is at 0.1 m above the upper side of the lower flange. This is also the location of the desired reference plane, or the reference line. The elements have been selected within this profile in such a way, that all elements represent a surface of 0.1×0.1 m^2. This means the reference line coincides with a number of element sides. When discussing the result one is therefore at liberty to take the element side as the matching reference line. The support is entered as a line with a length of 1.2 m, equal to the width of the lower flange. For the material an Young's modulus of 30,000 N/m^2 and a Poisson ratio of 0.20 are assumed. Due to the symmetry in the cross section and the load a quarter of the beam will be modelled. The maximum bending moment M_z is:

$M_z = F_y \times l = 50 \times 4 = 200$ kNm

The resistance moments below and above are:

W_{zmax} = 0.544×10^{-1} m^3
W_{zmin} = 0.907×10^{-1} m^3

The corresponding stresses σ_{xx} in the lower and upper fibre then become:

σ_{xx} lower fibre = M_z / W_{zmin} = 220.6 kN/m^2
σ_{xx} upper fibre = M_z / W_{zmax} = 367.6 kN/m^2

The stress σ_{xx} at the reference line is shown in figure 5.8.

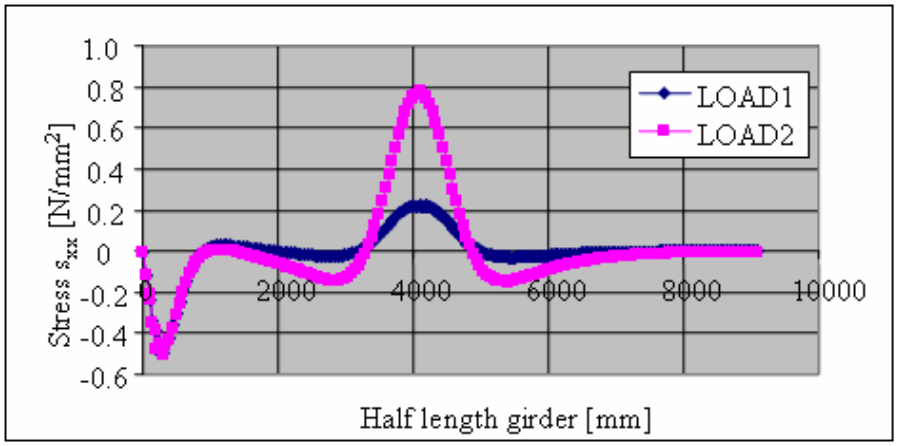

Figure 5.8 Stress σ_{xx} at the reference line in longitudinal direction of beam with U-profile

The stress σ_{xx} in figure 5.8 clearly shows disruptions at the support to the left and at the point of application of the nodal load at an x-value of 4.1 m. This is true for both load cases. The values of the stress σ_{xx} as a result of both load cases on the neutral line reach a maximum of 0.8 N/mm^2. It is still difficult to indicate which load case has the largest rate of distribution. This is better visible with the derivative to x of the stress σ_{xx} on the reference line, as is shown in figure 5.9. In the pure bending areas the value of the stress equals zero and also runs horizontally as a result of the load that was selected. The areas where the gradient is not zero are D-areas.

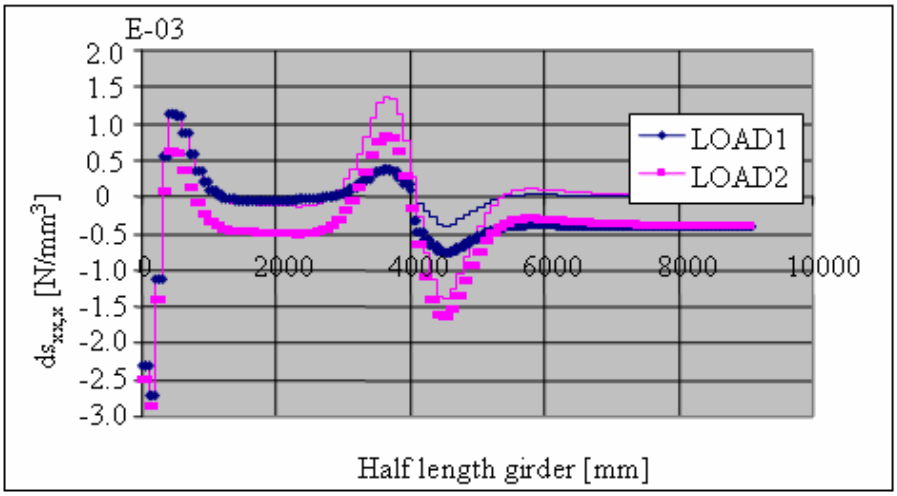

Figure 5.9 First derivative to x of the stress σ_{xx} on the reference line

Figure 5.9 shows that the rate of distribution around the nodal load is between a x-value of 2 and 6 m. A detail of this area is shown in figure 5.10 for an improved assessment of the rate of distribution.

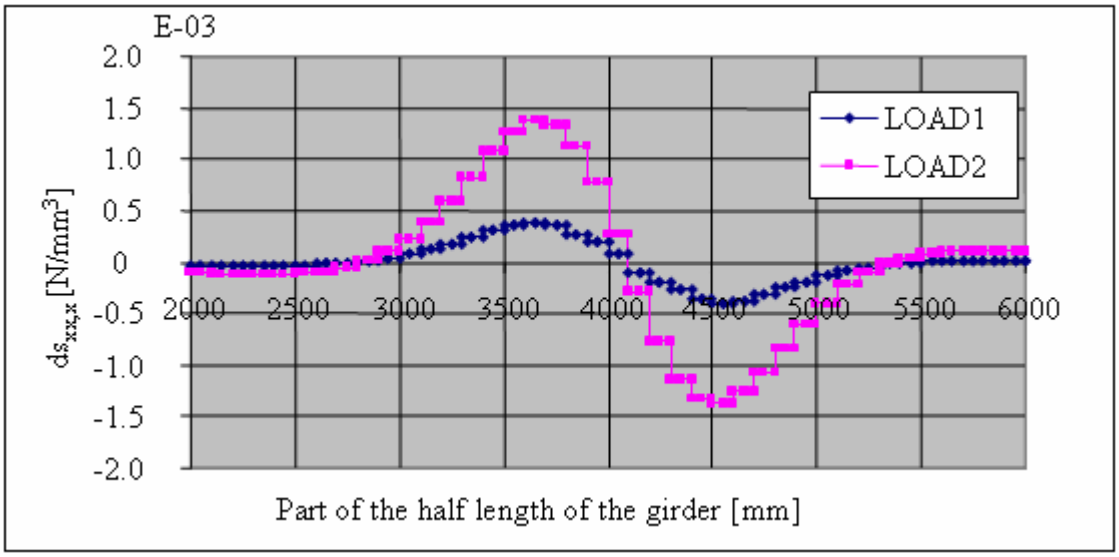

Figure 5.10 Detail of the first derivative to x of the tension σ_{xx} on the reference line

Figure 5.10 indicates that the rate of distribution as a result of both load cases is different. The area as a result of the nodal load uniformly distributed along the cross section has a distribution between x=2.7 m and x=5.5 m, whereas the distribution with the second load case falls in between x=2.4 m and x=5.8 m. This means that there is a longer area that may require stirrups, if the shear stress exceeds the allowed shear stress.
This rendering creates a visual insight into this mechanism, meaning that there is more control over the design.

5.2.5 Evaluation of calculated stresses in multi-axial stress condition

An increasing number of analysis packages allows users to save the strains and stresses of the various elements in a 3D manner. Naturally, this requires larger arrays inside the analysis package, especially with 1D elements. However, the unambiguousness when it comes to the storage of a wide range of available elements is ultimately profitable.
Also, this storage stimulates a simple link to any required post-processing programmes that may form the second stage after a linear analysis.
The storage furthermore allows users to evaluate strains and stresses not exclusively in a uni-axial way, but also bi-axial and/or tri-axial. Research in the bi- and tri-axial concrete domain has shown that this approach carries some advantages. In essence this means that an analysis package aiming to be of optimal use should be open to this 3D division in the storage of strains and stress.
In a 3D schematisation the various strain and stress components are each thoroughly analysed individually. This may certainly be seen as an advantage compared to the results from a 1D or 2D schematisation approach.

5.2.6 Better approach to limit states in optimisation and safety analysis

Up to the present the design environment of civil engineering structures does not include, apart from some exceptions, an optimisation and safety analysis process. The possibility

to create a closed chain within the design process also means that a better use may be made of the materials through optimisation.
The main lines of the design of structures are, of course, correct. However, with the introduction of 3D solid models the designer will obtain the best possible result in all directions. This possibility, in combination with the one on one transferability of the geometry of the structure, provides the opportunity to include the optimisation and safety analysis into the present design process.
This brings the closed design chain closer, and this will have a positive effect on the overall processing time and the manageability of the process.
Using the most realistic results from a full 3D analysis it is possible to come closer to the limit states that result from the actual regulations with which a design has to comply, by using optimisations. Also, based on these limit states a reliability index may be set up, showing which structural parameters have the most influence on the structural safety of a construction. The latter aspect will, in turn, again improve the insight into the behaviour of constructions, providing a link-up with the building and/or maintenance processes of the realised construction.

5.2.7 Transparency of embedded geometry components

The transparency of embedded geometry components, such as reinforcement bars embedded into the structural elements, will be better than with the underlying model types. After all, with schematisations of a structural component to a plane stress model the reinforcement bars will be grouped into a single reference line positioned in the element surface. This also applies to the 2D beam models. With 3D beam models and shell models the reinforcement bars maintain their own location, but it will of course cost the designer or analyst more time to enter the required data.

5.2.8 Reducing overlaps through model schematisations

By making a schematisation of a structure through a 3D geometry model the designer can make full use of the output of all stress components as available in the solid models, in order to get the most realistic impression of the true behaviour of the structure as a result of loads and supports. The connections of structural components no longer have to be schematised into system surfaces or system lines. Obvious problems in this respect are the connections between e.g. beams and columns and beams on floors in a 3D configuration. Below, some of these problems will be illustrated in diagrams. First, there is the connection between columns and beams in a schematisation into a 1D beam model. This is shown in figure 5.11.

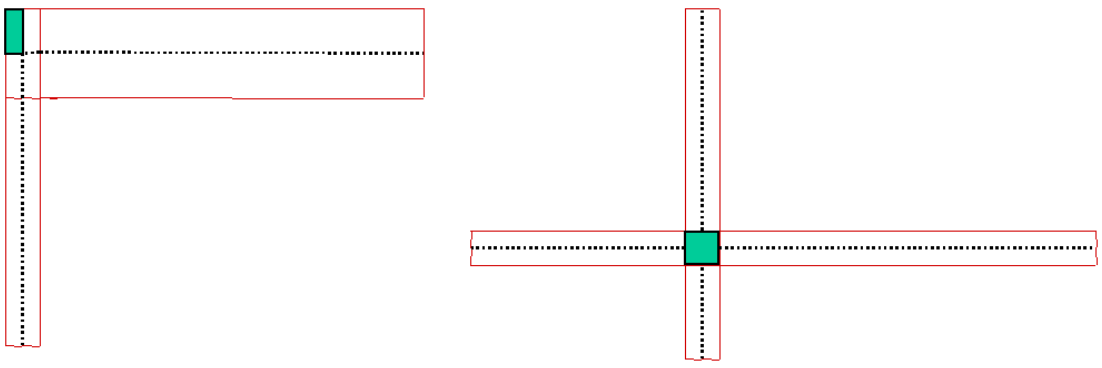

Figure 5.11 Schematisation 1D angle and connection

When a beam connects to a column there will be both overlap and exclusion of surface (volume), because with each beam and column with a rectangular cross section a height and width will be connected cross section-wise. If other types of cross sections are linked to the beam or column, there will also be overlaps and exclusions.
With an angular point the interior angle will have overlaps, whereas the exterior angle will show exclusion. In case of a clear crossing, as seen in the drawing on the right, the surface is doubled at the location of the crossing. This will play a small role as far as the total surface is concerned. However, when it comes to results such as strains and stresses, this connection will be stiffer than was envisaged in the design. This may have an effect on the stress distribution in the abutting structural parts.
With a 2D schematisation of these crossings in its plane these overlaps and exclusions are avoided. The geometry of possible local consoles may be locally included in the model, but in this case the consoles have to be positioned in a centric manner vis-à-vis the column-beam connection, each with its own thickness.
If the consoles are eccentric the only correct geometrical schematisation that remains is the 3D model. If the planes of e.g. a box girder are schematised to planes, there will also be overlap at the connections of the flanges and webs of the box. This is shown in figure 5.12.

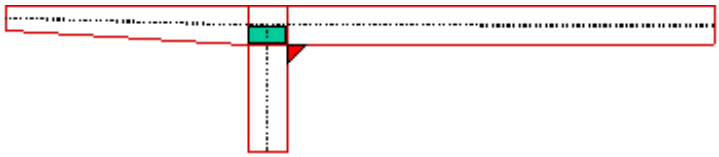

Figure 5.12 Schematisation of 2D type connection problem

The figure shows that if the dotted lines are the reference planes in a shell model, the green part is included twice. After all, the T-connection has a horizontal and a vertical system plane that requires the connection with the height of the wall or deck to achieve a description of the geometry that is as full as possible. Also, the reinforcement in the interior angle of the wall and deck connection is often not included due to its limited dimensions in relation to the entire model. However, these reinforcements are essential when it comes to the stiffness of the proposed connection, meaning the distribution of the stresses from wall to deck!
In short, the schematisations to 2D system planes or 1D system lines only occur with 3D models if the decision is made to project the results on these planes/lines, and not in advance when schematising the geometry into an acceptable analysis model. In this manner, it is left to the designer how he or she selects the reference planes in the 3D model. A wrong selection may of course generate a wrong result. On the positive side, the basic model does render the correct and most realistic results at stress and strain levels. This means the designer should become alarmed at an earlier stage in the process.

6 CHECKING THE STRUCTURAL CAPACITY IN THE DESIGN PROCESS THROUGH SEQUENTIAL STATIC ANALYSIS

6.1 Introduction

In the diagram in figure 2.1 it was shown how the design process of a concrete structure can be done. It is also indicated in what way the designer has to check the serviceability limit state and the ultimate limit state of a structure on the basis of the prevailing regulations. Up to the present, a number of cross sections of the structure, carefully selected by the designer are checked instead of the entire structure. This check is done on the basis of non-linear cross section analyses. Checking the entire structure, including the nonlinear material behaviour of both concrete and steel, still requires too much effort. A second argument to skip the nonlinear calculation process, is the knowledge that this calculation process is not always robust in view of the non-linear nature of concrete. Finally, the designer is not being 'rewarded' if a non-linear check analysis of the structure takes place, meaning that there is no motive to carry out such an analysis. The safety margins from the recommendations regarding the redistribution within the structure are such that in this sense the design should be safe enough.

6.2 Robustness of the current non-linear analyses

If there is a problem with the numerical robustness of a solid design this will be mainly found in the nonlinear material properties of the concrete and the corresponding calculation process.

6.2.1 Robustness of the material properties

The concrete material may crack in the tensile zone and be upset or become plastic in the compressive zone. The latter phenomenon, the plasticity of concrete, is not directly a problem for the analysis process, because in the compressive strain diagram there will either be a horizontal branch after exceeding the plasticity limit or a descending branch.

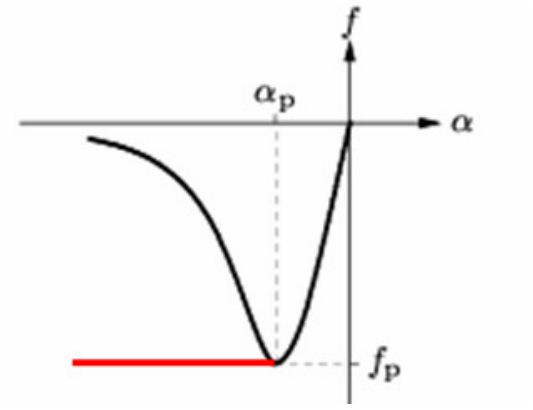

Figure 6.1 Uni-axial compressive strain diagram of concrete (Constant + Thorenfeldt)

It may, however, be said that the uni-axial compressive strain diagram with a constant branch after exceeding the maximum compressive stress is similar to the allowed compressive strain diagram in most regulations. Experiments have shown that the material

behaviour in the compression area in case of a further refinement is best described using the Thorenfeldt compressive strain diagram. Figure 6.1 shows both diagrams. When the tensile strength of concrete is exceeded, however, the cracking of the concrete may cause problems. If the load increases, a sudden crack may occur. This may then grow into the concrete volume, meaning that the embedded reinforcement material will simultaneously have to bear a greater load. The question is also whether the redistribution of the stresses to the embedded reinforcement bars can take place in a robust manner within the convergence requirements defined in advance of the calculation process. This redistribution of stresses may subsequently cause the crack pattern to occur in another direction than the original crack direction, which may become a rather complex issue.
If the concrete also shows brittle cracking behaviour, which is the least favourable situation one can imagine, the analysis process will only become even more fanciful than before. The brittle cracking behaviour is shown in the figure 6.2.

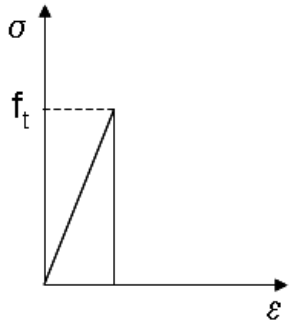

Figure 6.2 Brittle cracking behaviour of concrete

Figure 6.2 shows the stress against the strain in a uni-axial tensile strength test. When the tensile strength limit is exceeded, the allowed tensile stress falls back to the value zero.
A favourable variant is the addition of the softening behaviour of the concrete material to the explained tensile strength behaviour. This means another tensile stage is added in which the allowed tensile stress becomes less after exceeding the crack strain. This process may in principle be linear, multi-linear or in line with a specific (mostly exponential) curve, as is shown in figure 6.3.

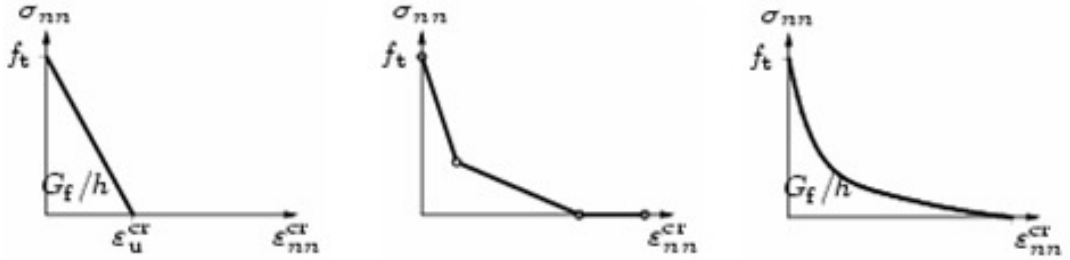

Figure 6.3 Various descriptions of concrete softening behaviour

All three subfigures in figure 6.3 show that when the tensile strength is exceeded, a residual stress occurs that decreases with the increasing strain, the so-called residual tensile strength. The first figure is referred to as a linear softening, the second being a multi-linear softening, whereas the third describes a continuous exponential softening. In view of the strongly descending branch after exceeding the tensile strength and the continuous development of the softening branch the latter description is preferred. The surface beneath this softening branch is called the crack energy. Experiments [Hillerborg1985; Hordijk1991] have shown that in normal concrete this crack energy G_f

lies between 60 kJ and 160 kJ. In two subfigures there is shown also an additional parameter called h. This bandwidth h renders the crack bandwidth, being directly connected with the calculated surface of the structural element, related to the underlying integration scheme of the structural element. This integration scheme reflects the method and the number of points of analysis of a structural element. The default is the Gauβ integration scheme as the method and a 2×2 scheme for a plane stress element and a 2×2×2 scheme for a solid element.
Apart from the default value, the bandwidth of the crack (=h) can also be indicated by the analyst in a non-linear analysis as an input parameter. This will be addressed in chapter 8 in the discussion of the fully non-linear simuation of experiments. The most current material models in connection with crack pattern are described in section 6.3.
The plasticity behaviour of the concrete material is, just like the plasticity behaviour of the reinforcing steel or prestressing steel, relatively robust in the fully non-linear analysis. Once the material has reached its plasticity limit, there remains a relation between the stress and the strain that occur. This means the force does not fall back into a material, but it stays at a single level, which is good news for the robustness of the analysis process.
In principle, the various model types may be linked to any material behaviour in terms of crack pattern or plasticity. It stands to reason that if there is a 3D model, this has to be linked to a 3D material model as well. However, the current regulations are limted to 1D or 2D material behaviour, so that it is reasonable to base the check in the design process on 1D or 2D behaviour. Due to the non-robustness of the concrete behaviour and the corresponding total processing time there is ample reason to look at other methods for checks in the design process of concrete structures. The sequential static analysis has come forward as an alternative. This will be addressed in section 6.4.

6.2.2 Robustness of the calculation process in a non-linear analysis

The iteration method most often used in non-linear analyses is the Newton-Raphson iteration method. This also allows a choice between the normal and the modified Newton-Raphson method. The robustness of this method in combination with the arc length method can be explained using a part of a load-deflection diagram, in which despite an indicated load increase this still automatically leads to an unloading stage. This is due to a certain amount of crack pattern that disturbs the balance in the structure in such a way that first an unloading loadstep will have to take place. This load-deflection diagram is shown in figure 6.4.

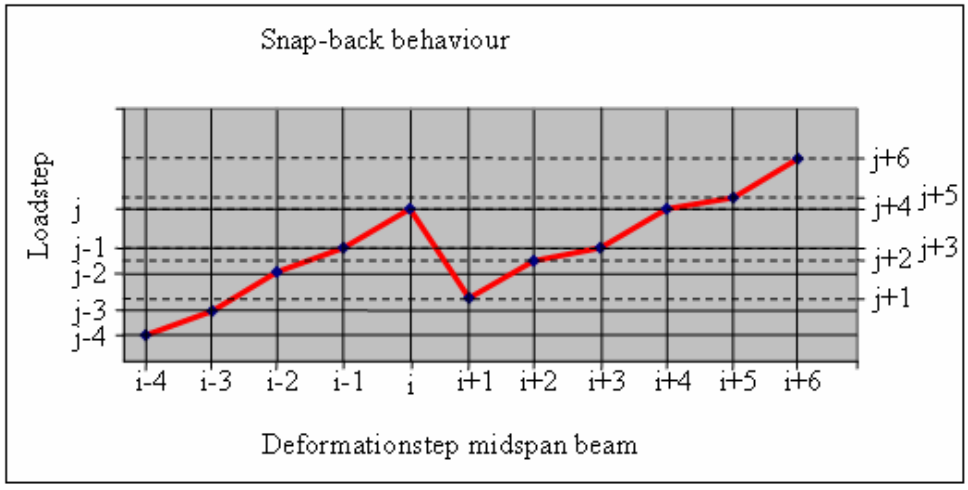

Figure 6.4 Detail of load deflection diagram with snap-back

What is remarkable in figure 6.4 is that the load increase till loadstep j is in line with the increase of the deflection in the middle of the beam. The next load step, however, provides an unbalance in the structure with an increase of the deflection and a decrease of the total load. Such discontinuities lead to an unstable iteration process, but the added use of a so-called arc length method in the calculation process may steer the entire process back to robustness. In this case the arc length method means unloading. Using the arc length in itself has a large effect on the processing elapse time of the analysis, as is shown in figure 6.5.

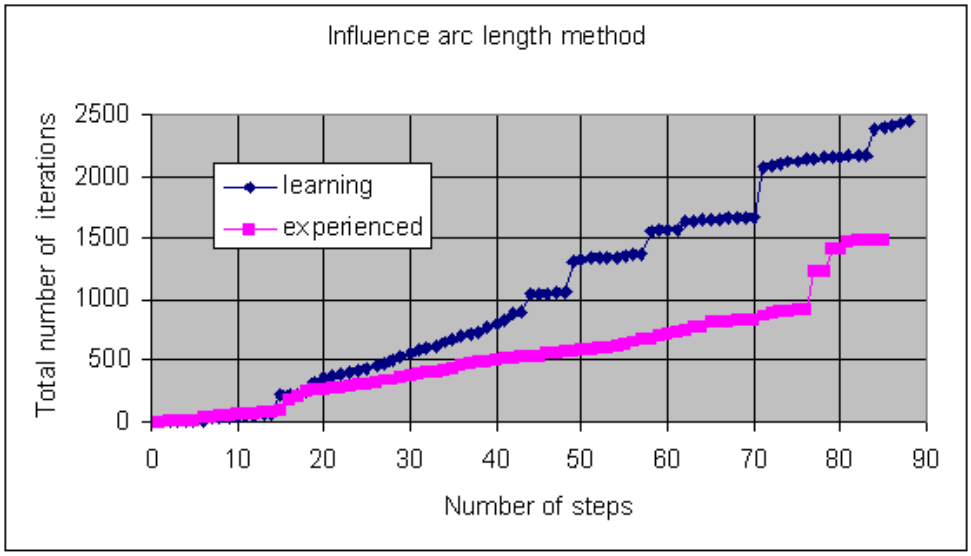

Figure 6.5 Influence arc length method and the non-linear analysis process

Figure 6.5 shows two cumulative lines. The dark blue line reflects a first attempt without prior knowledge of the analysis process, whereas at that particular moment the analyst does not really know how the crack pattern and the plasticity within the structure will develop. The purple line shows that when the nodal points that allow the application of the arc length method are adjusted, there is a considerable gain to be made regarding the processing time. According to figure 6.5 the total number of iterations is reduced from 2,500 to 1,500, which is a 40% reduction. This example also includes a reduction of the number of load steps in order to achieve the same load level. However, in the above example this reduction is limited to three load steps, so that the actual gain made, the saving of disk space with three steps, may be called low.

6.3 Available material models to handle crack pattern

6.3.1 The Mohr-Coulomb and the Drucker-Prager material crack model

Both the Mohr-Coulomb and the Drucker-Prager material model are based on a yield condition. The formulation of the yield function may be expressed in principal directions of strains or stresses ($\sigma 1 > \sigma 2 > \sigma 3$) as:

$$f(\sigma,\kappa) = 0{,}5\,(\sigma_1-\sigma_2) + 0{,}5\,(\sigma_1+\sigma_3)\sin\phi(\kappa) - c(\kappa)\cos\phi_0$$

in which:
$c(\kappa)$ = the cohesion as a function of the internal state variable κ and

ϕ = the angle of the internal friction that is also a function of the internal state variable κ.
The relation between the uni-axial stress $\sigma_3 = -f_c$ and the equivalent cohesion c is:

$c = f_c (1-\sin\phi_0) / (2\cos\phi_0)$

in which:
f_c = allowed tensile stress of concrete
ϕ_0 = angle of internal friction.

The Drucker-Prager yield criterion has been laid out as a more smooth approximation of the Mohr-Coulomb yield surface, which is a conical surface in the principal stress space. This yield criterion is shown in figure 6.6.

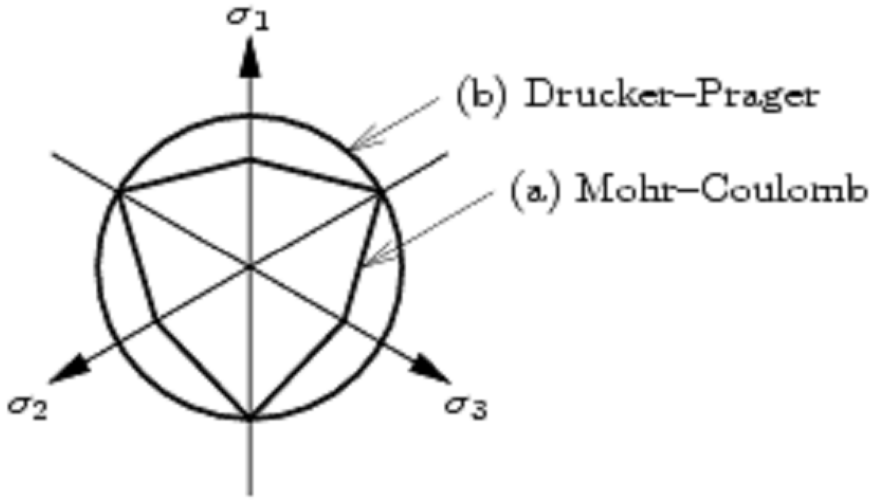

Figure 6.6 Mohr-Coulomb and Drucker-Prager yield criteria

Figure 6.6 clearly shows the difference between both yield criteria. In the space of the three principal stress directions, the Mohr-Coulomb criterion runs a straight course with blunt angles at the intersections with the principal stress directions and sharp transition angles at the bisector lines of the principal stress directions. These angles also explain the possible problems with this yield criterion. The analysis process may, in fact, become hold up in these corners. Just a slight change may cause the calculation process to move from one branch to the next, meaning that the number of iterations during the non-linear analysis in order to achieve convergence can rise considerably.
On the other hand, the Drucker-Prager criterion is a closed circle in the three principal directions of strains or stresses. This means that if this criterion is used there will often be a smooth non-linear iteration process.
As a result of the difficult iteration process in a non-linear analysis with the Mohr-Coulomb material model, a modifield Mohr-Coulomb material model was developed by Groen at Delft University of Technology [Groen2000]. This material model is highly suitable for sandy material. It is sometimes to be recommended for concrete material, because it is a mix of non-linear elasticity and a plasticity model.
If compared to the Mohr-Coulomb material model the Drucker-Prager material model is more extended, in the sense that it includes the dilatancy angle. This angle is important in connection with internal shear behaviour, as is seen in figure 6.7.

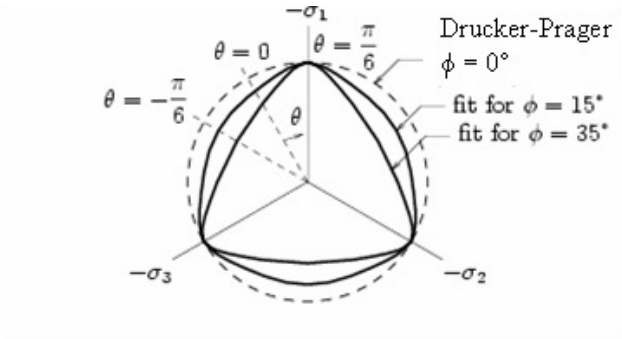

Figure 6.7 Rendering of the dilatancy angle in the Drucker-Prager yield criterion

Figure 6.7 shows that $\phi = 0$ and $\theta = 0$ produce an ideal circular yield criterion. If both ϕ and θ are increased the different branches of the yield criterion are levelled off, causing the non-linear process to become less robust, albeit that it does result in a better description of the material.

6.3.2. Rankine yield criterion

The Rankine yield criterion is also based on the principal stresses. It may be used as an autonomous material model, or in combination with the Von-Mises or Drucker-Prager yield criterion. It can handle both stresses and strains, giving it the reputation of a robust material model. One disadvantage is that this model can only be used in a 2D situation, usefull for plane stress models, plane strain models and axial symmetric models. In the past there have been attempts to extend this material model towards a 3D direction, but so far this option is not available in a software product version for the design environment.
The rendering of the yield criterion as well as the combinations are shown in figure 6.8.

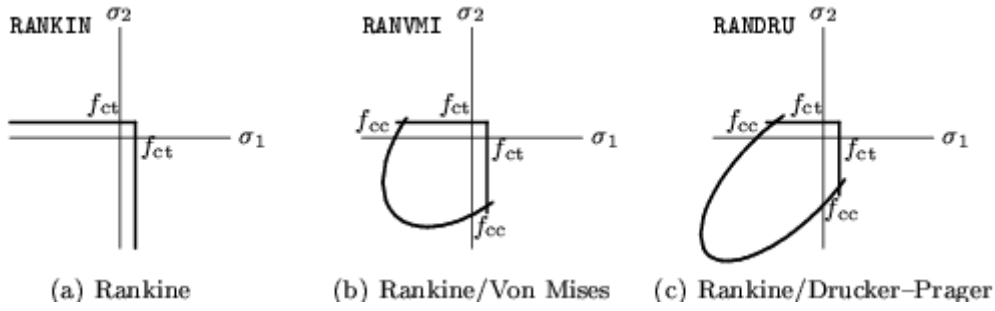

Figure 6.8 The Rankine plasticity model

Figure 6.8 shows a stress criterion in two directions, thus highlighting the 2D nature. Also, both the autonomous Rankine model and the combined models show discontinuity points between branches at the transition from the right branch with criterion f_{ct} to the bent branch of f_{cc}. In this respect, the combination of Rankine and Drucker-Prager provides more robust handling as a criterion in view of the blunt and, as a consequence softer transition between both criteria of f_{ct} and f_{cc} mentioned above. Within this yield criterion explicit values have to be entered for the tensile strength, the cohesion and both angles, the internal friction angle and dilatancy angle.

6.3.3 Total strain crack model

The total strain crack material model is, as is implied by its name, based on the total uni-axial stress-strain relation. This material model has gained popularity in recent years in the daily practice of the (research) design environment. This is due to the fact that the parameters of this material model enable a smooth connection between the material model and the regulations dealing with the check of structures on structural safety.
Various uni-axial formulations can be entered for both the compressive strain and tensile strain diagrams, to combine these with softening branches that were already used in the Drucker-Prager diagram. During the last few years both the compressive strain and tensile strain diagrams have also been made temperature-dependent, thus promoting the acceptance of this material model.
In the total strain crack model there are mostly two options available, the fixed crack option and the crack option free of rotation. In the fixed crack option the crack direction is fixed in relation to the subsequent load stages following the initiation of the first crack in an integration point of a structural element. During the next phase of the non-linear calculation process this crack direction can no longer be changed. After this, the shear component in the fixed model in this integration point can be made dependent on the value of the crack strain that occurs. One other possibility is to include the relation between the shear component and crack strain with a constant factor during the further stages of the calculation process. This constant possibility has to do with the easy use of input data rather than with physical reality. In most FE software programmes the decreasing resistance against shear can be entered using a factor β, that is somewhere between zero and one, and to multiply this by the sliding modulus. If use is made of the crack option free of rotation, the crack direction is free during the entire non-linear calculation process. There is no longer any question of shear in the plane of the crack. Using a value < 0.01 for the factor β enables the simulation of the rotated model with the fixed model. Further developments for both rotating and fixed cracks are found in the crack models that utilise more than one direction.

6.3.4 Maekawa non-orthogonal total strain crack model

Following this, Maekawa set up a combined material model starting from 2D and 3D experimental cyclic measuring data on the basis of the multi-axial damage plasticity model and the uni-axial total crack strain model for the compressive strain diagram of concrete. Out of these measuring data Maekawa then also distilled a hysteresis model based on the cyclic measuring data, including the renewed closing of the crack, which is an additional option in the material model mentioned earlier.
Finally, two shear crack models were added to the material model. The first model is based on the contact density, and in terms of physics this is equal to the previously indicated shear stiffness dependence of the crack strain that occurs at the integration point in question.
The second model is based on the addition of a softening parameter to the relation between the ultimate shear strain and the shear crack strain that occurs when the shear crack strain reaches a value that exceeds the ultimate shear strain.

6.4 The sequential method in the analysis process

It was seen in the Introduction that Beranek [Beranek1994] had already addressed the possibilities of a sequential analysis. In collaboration with Invernizzi and Belletti, Rots took this approach further [Rots2004, Rots2006a, b, c]. Their work does show some similarities to the so-called Lattice method by Van Mier, Vervuurt, Schlangen and Van Vliet [Vliet2000]. For this reason, this method will be addressed first, before presenting another type of sequential method.

6.4.1 The Lattice method

The Lattice method is based on structures being built using the simplest possible structural elements, namely bars. This is done with a element generator that will divide the structure in a geometrical sense into bars, in a regular or random manner. This provides each bar with its own length and own set of material properties. The material properties per bar are related to the fractions of materials that are present in a specific amount of concrete material. An example is shown in figure 6.9, coming from the thesis by Van Vliet in 2000 that was mentioned earlier.

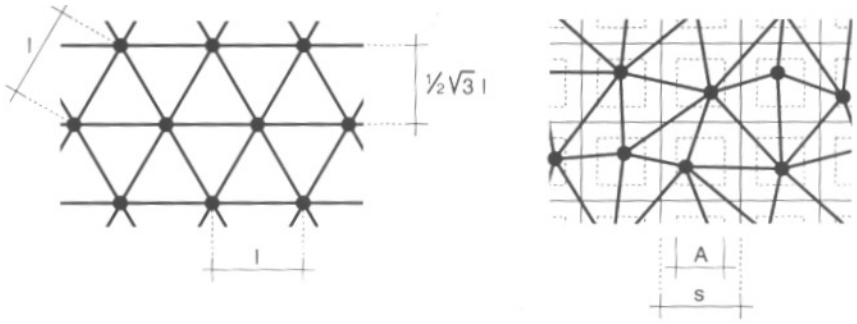

Fig. 6.9 Results mapped and random bar pattern

The first stage in the linear static calculation process in case of a specific load level on the structure in question is to look for the element where the tensile strength is exceeded the most. During the filtering stage or the evaluation stage of the tensile strength exceedance of all bars, this bar is removed from the calculation model. The next stage is a new linear static analysis with n-1 elements. This process is then repeated as often as is required, until the moment not a single allowed tensile strength in a bar is exceeded. Then there is balance. After this, the load is increased and the whole process is reiterated, using the results of the previous load level.
Ultimately, this results in a load-deflection diagram of the load and a deformation at a specific point of the structure.
The advantage of this approach is that it makes use of linear static analyses that are always numerically robust. A disadvantage is the processing elapse time to achieve a load-deflection diagram. For this reason, the Lattice method is mainly used in a research environment at the micro-meso level in order to gain a better insight into the behaviour of concrete. It allows researchers to distinguish between various parameters of concrete components, such as the various aggregate sizes of the additives and the interface behaviour between the grains and the cement paste. In her thesis, Lilliu [Lilliu2007] made the step towards a 3D geometry and to structures that allow practical application. The overall processing time on a single processor CPU was about one week. However, using a parallel version of the software on a multi-processor CPU (up to 256 processors) she

achieved an admissible processing time within the confines of her research. The calculation model in question was the simulation of the Brazilian (splitting) test. In view of the dimensions of the cylinder used, these dimensions are still far away from the dimensions of a structure in the infrastructure. Also, the multi-processor CPU type is mostly unavailable to the analysts in current engineering practice. A two-processor CPU is the most common in the current engineering practice. In short, the calculation process requires an acceleration in order to promote this approach.

6.4.2 Further plane stress model research

As was indicated before, together with a number of co-workers, Rots elaborated on this method by adding masonry and reinforced concrete structures. In various publicatons they demonstrated how to deal with softening, etc. As is common practice in engineering, a new approach has to be at least quicker and more complete than the current practice, if it wants to gain acceptance. The extension towards plane stress state elements instead of linear elements also means that the method moves towards the more common calculation models in engineering practice. This does not include the inclusion of shell models or solid models yet. Also, with Rots the focus is on separate aspects, and mainly on masonry mechanics originating from the fully non-linear analyses.
However, studies have demonstrated that one can resort to a shorter and consequently more acceptable overall processing time that is precise enough for current engineering practice.
Moreover, the focus can be placed on the load levels, the serviceability limit state and the ultimate limit state that require checking. In the serviceability limit state the check is on crack width, in the ultimate limit state it falls on the failure load. In this case the robust parts of the non-linear analysis process are applied as plasticity of both the reinforcement and the concrete. The combination of the use of physically interpretable material properties of concrete under tensile strain and the use of the reduction of the elasticity modulus of elements under tensile strain instead of removing elements means that larger steps may be taken to achieve the desired load-deflection diagram for the determination of the ultimate limit state. In this case it is also possible to determine the crack width that requires checking at the serviceability limit state. This method is treated in the following section.

6.5 Proposed sequential method

In the sequential static analysis method we split up both the material handling within the analysis process and the analysis process itself into two different parts.
The robustness of the concrete and reinforcing steel materials are maintained as far as plasticity is concerned, and will be processed in the existing non-linear analysis process using a Newton-Raphson iteration procedure. An additional Fortran programme has been written for handling the tensile stress of concrete in order to translate the isotropic material properties of concrete into orthotropic material properties if the tensile strength is exceeded.
For a plane stress element this means that in the principal direction in which the tensile strength is exceeded, a different Young's modulus and sliding modulus are calculated. For a solid element this means that in two directions we go from isotropy to orthotropy.
The Fortran programme mentioned above may also be used for beam, plate bending and shell models, albeit that not all internal stress components will be equal. After all, the

shear stress in these models is a quantity that originates from a generalised result, which is the transverse force Q_y. This is devided by the belonging cross-sectional area A_x, providing the analyst with a shear stress. In reality this is an average shear stress along the height of the structural part in question. In the plane stress and solid models mentioned, the shear stress may vary along the height or the width of the structural part, just like any other stress component.

As far as the splitting up of analysis processes is concerned, according to the current design norms, no plasticity is allowed to occur up to the serviceability limit state. This means that up to this serviceability limit state use may be made of the linear static analysis process, requiring only a few iteration procedures to produce the desired result. Time is gained here for the first time. Starting from a maximum of 15 load stages up to the ultimate limit state, this means there are approximately some eight load stages up to the serviceability limit state. For each load stage four to five iterations are needed to bring about the reduction of the eleasticity modulus of the concrete. This, in turn, means that about 35 linear static analyses will be required to arrive at the desired serviceability limit state. Already, figure 6.5 directly shows the gain in time when applying the linear static analysis process as opposed to the non-linear analysis module. In the experienced case 85 load stages were needed, meaning a total of 1,500 iterations, in order to arrive at the desired load level (in this case the SLS level). In the linear static analysis this load level is reached after a maximum of 35 analyses. This takes the processing time to 5% of the total non-linear analysis, something which will take about three hours on a 2008 desktop PC. With the current implementation of this sequential method the load level of the serviceability limit state is achieved after ten minutes. If we start using an integrated sequential method in an existing FE package, this will probably be less than five minutes. This processing time is highly acceptable if the desired crack width result, as a checking mechanism in the serviceability limit state can also be distilled from the analysis.

An elaboration of the above is found below with the test analyses of the experiments. For each load level in the sequential analysis that needs to be maintained the analysis is each time repeated four to five times in order to achieve convergence with these elements of which the tensile strength is exceeded. Each repetition means translating isotropic material behaviour to orthotropic material behaviour of ‘new’ structural elements, or an adaptation of the orthotropic material of ‘old’ structural elements that was already present. During analyses in the area of serviceability limit state to ultimate limit state, plasticity of both concrete and reinforcing steel will occur, requiring non-linear processing. This may be done through the robust processing in the non-linear analysis method that is already available. In the Fortran programme developed to simulate the exceeding of the tensile strength through orthotropic material behaviour, the stiffness of the concrete is adjusted after each analysis based on the uni-axial strain of the concrete material, as may be seen in the analysis diagram below. The diagram in figure 6.10 shows that at the start the average linear static material properties, as defined in the regulations, are attributed to each material. After the first linear static analysis it turns out that the tensile strength reaches level A. When the load is further increased, the tensile stress exceeds the value indicated with the letter B. This means that in this element a crack will occur, and that in the direction perpendicular to the crack use will be made of orthotropic material properties. The abovementioned Fortran programme calculates the adjusted allowed tensile strength for this element, the new Young’s modulus on the basis of the crack energy and the type of softening behaviour. The crack energy comes straight from the Model Code 1990, whereas the softening behaviour is selected by the analyst. In view of the fact that both the Hordijk curve and the Moelandts and Reinhardt curve are seen as the most realistic exponential softening curves, one of these will be used, namely the Hordijk curve.

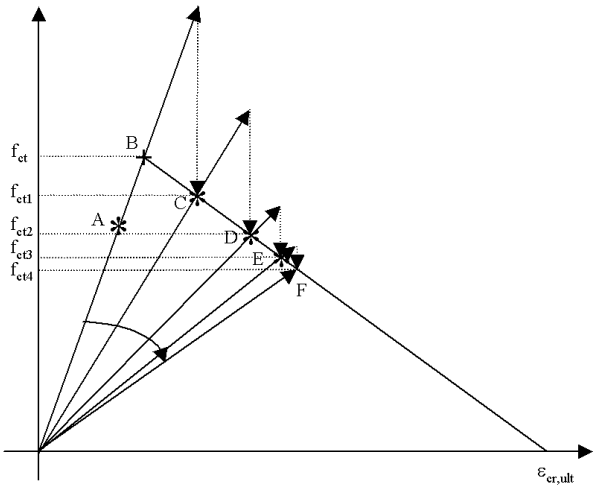

Figure 6.10 Analysis scheme of a sequential static analysis with linear softening

Because the principal tensile strain does not have to comply with one of the three global orientations of the coordinate system, the local principal direction of the tensile strain is added to the geometrical properties of the element. In the other two directions when using a solid element or the second direction when using the plane stress element, the original material properties and the corresponding static values are maintained. The new allowed tensile strength after adjustment of the orthotropic material behaviour can be read in the diagram as the value belonging to C, the Young's modulus being the angle of the straight line 0C. The shear stiffness is a function of the Young's modulus and this relation is maintained during the entire analysis process. In a subsequent analysis with the same value for the load level, the adjusted tensile strength of the element in question can be exceeded again, after which the procedure for the adjustment of the material properties may continue. In this manner point D up to and including point F are found. Again, there may also be new elements needing an adjustment of the material properties on the basis of the exceeding of the tensile strength. The increment of the tensile strength for each iteration may be designated as the local convergence criterion.
From a global point of view, it is also possible to select the vertical deflection in the middle of the beam. As was said before, after convergence a next load increase may occur. In this case a linear softening diagram was selected to explain the functioning of the sequential method in an easy manner. The same procedure applies to another type of softening diagram.
Contrary to what is maintained by previous researchers, in this method the material properties are adjusted in a single procedure for the entire structure for all elements in which the tensile strength is exceeded. It is therefore not limited to the element showing the most extreme tensile stress. If the load increments are selected correctly, the results so far present a reliable picture of the failure load that may be expected.
Taking all of the above into account, this approach does of course lead to a considerably shorter processing time, whereas it may still be termed robust because of the use of the linear static analysis in case of cracks in the concrete. The plasticity of both materials was already robust. In short, taken together this will be even stronger. When establishing the final design it is easy to continue the structure with a full non-linear method, using the same material properties coming straight from the regulations. It is expected that in that case this type of analysis process may be handled in a more or less robust manner. This sequential method can also be used as a checking method prior to a full non-linear analysis. The sequential method has already warned in advance if there is something

wrong with the reinforcement of the structure, requiring an adjustment. In view of the speed of this calculation process, one may say that engineering mistakes will come to the surface sooner, thus contributing to the quality of the entire structure. This also provides the foundation for the transition from a plate bending model or shell model to a full 3D geometry description of the structure, because it visualises the most realistic stress and/or strain components of the structure. This does lengthen the processing time of the analysis, but it remains sufficiently quick for engineering practice. Discussions around this subject have taken place at FIB and IABSE conferences [DeBoer2004a, DeBoer2004b, DeBoer2007, DeBoer2009]. The sequential approach could be used also to tackle the fatigue phenomena and is discussed on a Fatigue conference in the USA [DeBoer2006]. The advantages of the model have been listed above in chapter 5.

7 THE TORONTO BEAM EXPERIMENTS

7.1 Introduction

In order to be able to compare the results of the sequential method with the results of the available but not accepted non-linear method, the choice was made for a comparison with three beams that have been tested in experiments. Over the years a large number of beams has been tested in laboratories all over the world. The beam experiments carried out in the Toronto laboratory are adequately documented, which is why three of the Toronto experiments have been included here. These are classic experiments standing at the basis of the calibration of many material models. In fact, these experiments may be seen as the experiment benchmark.
The first experiment concerns a beam that fails under pure bending. In two other experiments the beams fail through shear force. In all, there is a series of 4×3 beams, in which the beams have been tested for the failure phenomena compression failure of diagonal tension and shear-compression failure. The shortest experiment A1 in the A-series was selected, the beam having collapsed through shear-compression failure, and also the longest experiment C3 in the C-series in which the beam collapses through flexure-compression failure. In the last example, experiment B2 from the B-series, the beam has failed through a combination of compression and shear force. The motivation behind all these experiments is that they are in line with the common design practice, which is not the case with the three beams from the fourth O-serie. These are beams without upper reinforcement. In infrastructural constructions these do not occur, other than in building structures, where these beams are being used. As such they have been included in the research done by Bresler. These experiments had been done before in 1963 by Scordelis and Bresler [Bresler1963]. In this case the focus was also on investigating the shear force. Following a state-of-the-art analysis by Willam and Tanabe in 2001 it was established that a similar research would be desirable for a more focused look at the failure phenomena involved. The idea was to maintain as many dimensions as possible of both concrete and reinforcement for an optimal comparison of results. These new experiments were done in Toronto by Vecchio and Shim, and published on a number of occasions [Vecchio 2004; Shim 2002]. All experiments are three-point bending tests.
The results of the new experiments nearly always match the results of the so-called old experiments, albeit that many more in between results of the tests are now known.
The new results of this series of tests also led to changes in the ACI code [ACI2005] and the CSA code [CSA2004] once again. In addition to this, Bentz (Toronto University) developed a cross section programme [Response-2000] using the results of these tests. The results of this research have been published in the dissertation by Bentz [Bentz2000]. The FE software code used has also been made available.

7.2 Description beam A1 experiment

Geometry

Beam A1 has a length of 4.10 m and a span of 3.66 m. The cross section of beam A1 is 305 mm in width and 552 mm in height. The effective depth d is 466 mm. The cross section includes an upper reinforcement (3×M10 bars), a double-layered lower

reinforcement (2×M30 and 2×M25) with additional stirrups (D5 at 210 mm head to head) at the bearing and support locations, the head to head distance being reduced to 105 mm. The distance between both layers of the lower reinforcement is 64 mm, whereas the distance from the lower side of the beam to the heart of the first lower reinforcement is also 64 mm. Figure 7.1 shows the beam configuration.

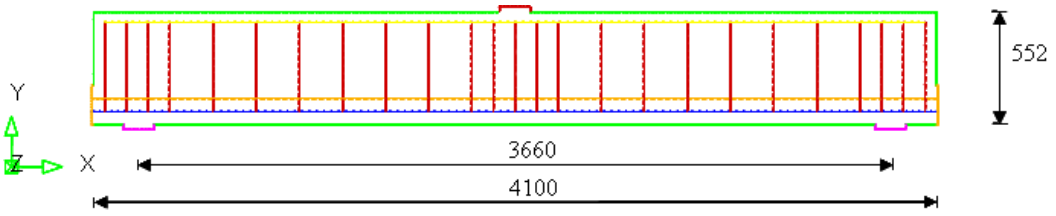

Figure 7.1 Configuration of beam A1

A cross section of beam A1 including the reinforcement is shown in figure 7.2.

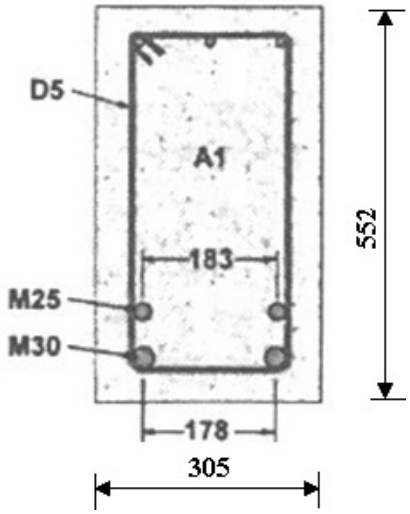

Figure 7.2 Cross section beam A1

The various reinforcement bars have their own cross section quantities, as is shown in table 7.1.

Bar type	Diameter mm]	Cross section [mm^2]
Stirrups D5	6.4	32.2
Upper reinforcement M10	11.3	100
Lower reinforcement #2 M25	25.2	500
Lower reinforcement #1 M30	29.9	700

Table 7.1 Geometrical quantities of beam A1 reinforcement bars

In order to gain a clear insight it is important to make a note of the reinforcement percentage of the various reinforcement bars. For the lower reinforcement this is 1.68%, for the upper reinforcement 0.2% and for the stirrups it amounts to 0.1%. The reinforcement bars in both lower layers are anchored at the start and end of the beam to the concrete using welded-on steel plates. This was done to prevent any slip between the reinforcement and the concrete at the ends of the beams. The reinforcement bars are at 64 and 128 mm from the lower fibre in all 3 beam configurations. The welded-on plate therefore has the same width as the beam, the height being 3×64=192 mm. For these plates the thickness dimensions and material quantities are the same as for the support

plates that are described with the supports. The thickness of the welded-on steel plate is therefore established at 25 mm.

Materials

The beam materials are, of course, concrete, reinforcing steel and steel for the support plates and bearing plates. The characteristic material values of the various parameters of steel and concrete are shown in table 7.2.

Material	$f_{ck\text{-}cylinder}$ [N/mm^2]	f_{sp} [N/mm^2]	ε_0 [-]	Young's modulus [N/mm^2]	f_y N/mm^2]	f_u [N/mm^2]
Concrete	22.6	2.37	0.0016	36,500	-	-
Stirrups bar D5	-	-	-	200,000	600	649
Upper reinforcement bar M10	-	-	-	200,000	315	460
Lower reinforcement #1 bar M25	-	-	-	210,000	440	615
Lower reinforcement #2 bar M30	-	-	-	200,000	436	700
Support plate	-	-	-	200,000	-	-

Table 7.2 Material characteristics beam A1

The maximum aggregate size of the concrete is 20 mm. Since ε_0 is not really a common material parameter in Europe, this is further exemplified in the figure below, being the yield point of the concrete where plasticity (crushing) starts to take place according to the Popovic-Vecchio concrete model, including softening under pressure. This model is very commonly used in Canada. It has been included here as a concrete material model.

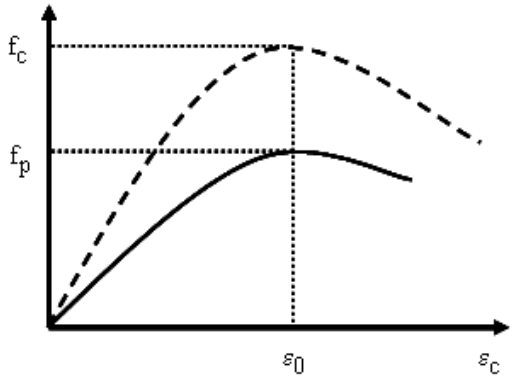

Figure 7.2 Compression diagram of concrete including softening under pressure

The table also shows a hardening branch of the reinforcement steel. From the point of view of simplifying the input data regarding the steel material, this has not been included in the full non-linear analysis yet. This branch has also not been included in the proposed sequential analyses that will be addressed afterwards. In the full non-linear analysis this material behaviour is seen as an additional reserve of the steel material. In order to achieve a realistic comparison with the experimental results this could still be added, provided the yield point of the reinforcement far exceeds ε_0.
However, the aim of this research is to elaborate the comparison between the sequential analysis and the fully non-linear analysis, requiring as little input and knowledge as

possible, yet leading to a simulation of realistic failure behaviour. Still, the section dealing with the results should indicate whether, and if so to what degree a specific yield limit is exceeded.

Loads
The load consists of a nodal load in the middle of the span on the bearing plate. In order to avoid crushing of the concrete at the bearing plate, the analyses of Bentz still use an increase of the reinforcement component in the first rows of elements directly beneath the bearing plate up to the location of the upper reinforcement with 5%. The reinforcement component in the following underlying row of elements plus the abutting elements 2 times wider than the bearing plate width is increased by 2.5%, as is shown in figure 7.3.

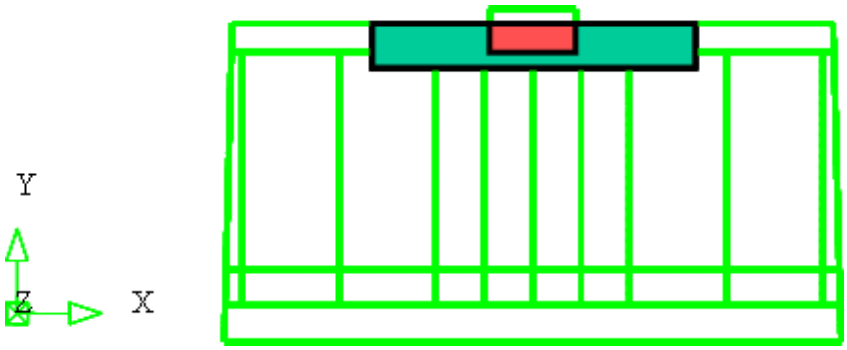

Figure 7.3 Increasing the reinforcement component at the bearing plate locally

In both the fully non-linear analyses and the sequential analyses this aspect has not been included, because reality must be simulated without resorting to tricks. The surface of the bearing plate is 150×300 mm^2, its thickness being 58 mm.

Supports
The supports consist of a left and right part, built from steel plates that have a thickness of 20 mm, while measuring 150×350 mm^2.

7.3 Results of beam A1 experiment

7.3.1 Result load-deflection diagram in middle of span

The most general result of an experiment is the load-deflection diagram of a design, in this case at the middle of the span. This will be compared to the result of the Bresler-Scordelis experiments in 1963. It is clear that the load-deflection diagram in figure 7.4 behaves slightly less stiff than the Bresler-Scordelis beam. Also, the diagram is able to continue longer. The failure load force in the Bresler-Scordelis experiment amounts to 467 kN, with a corresponding vertical deflection of 14.2 mm. The failure load force in the Toronto experiment was 459 kN, with a corresponding vertical deflection of 18.8 mm. The differences in the failure loads are not large, but the differences in deflection are significant. They may be explained by the slightly larger cross section of the concrete (307×561 mm^2 versus 305×552 mm^2), and the higher compression strength of the concrete (24.1 N/mm^2 versus 22.6 N/mm^2) with the Bresler-Scordelis experiments. Also, there is a difference in the cross sections of the upper reinforcement (300 mm^2 versus 254 mm^2), which is an increase of 18%.

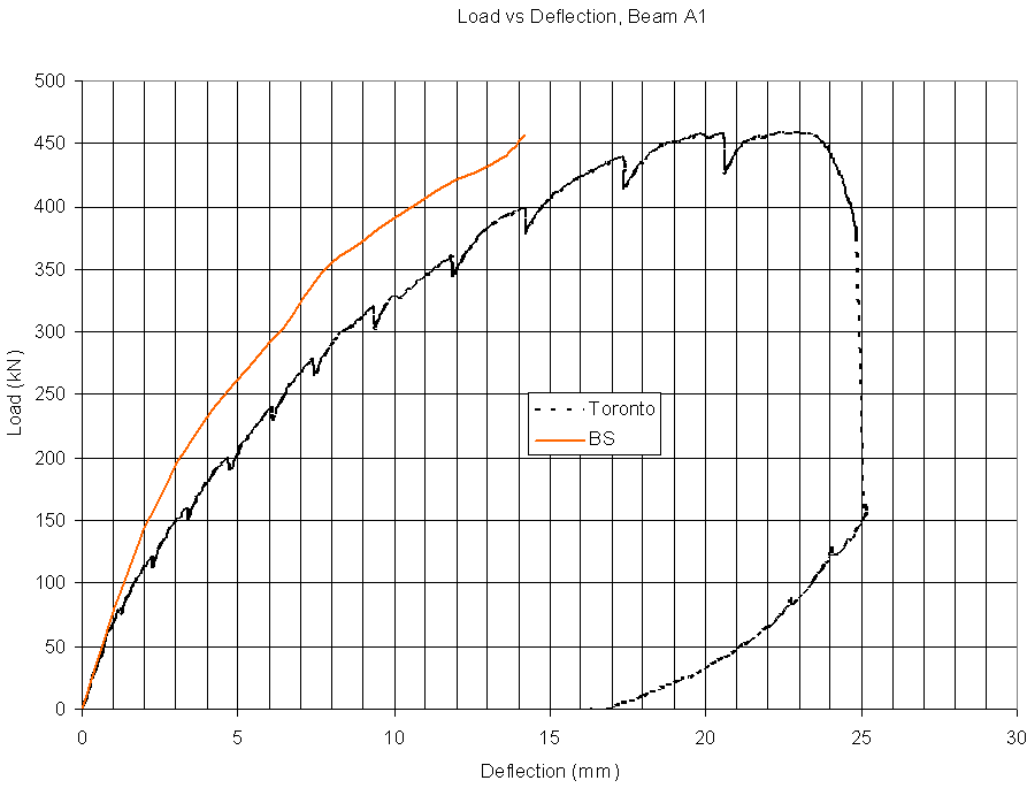

Fig. 7.4 Load-deflection diagram midspan of beam A1

Furthermore, the cross section of the lower reinforcement was reduced (2,400 mm^2 versus 2,580 mm^2), which is 7%. Especially the higher compressive stress of the concrete and the lower tensile reinforcement cross section will lead to increased deflection in the ultimate limit state. The unloading branch of Toronto beam A1 is still a stable reflection of the deflection.

7.3.2 Crack pattern

The crack pattern for the ultimate limit state is shown in figures 7.5 and 7.6.

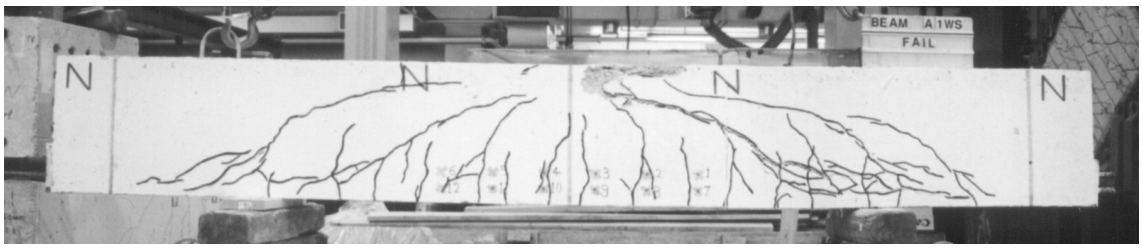

Figure 7.5 Crack pattern ultimate limit state on north face of beam A1

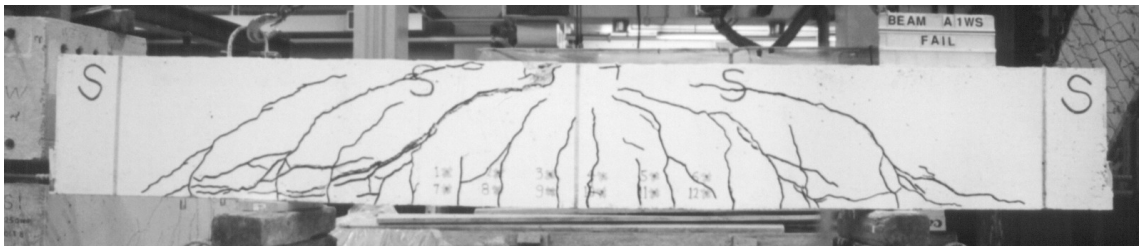

Figure 7.6 Crack pattern ultimate limit state on south face of beam A1

Both figures present a relatively similar picture. In the middle of the beam we see bending cracks, and there are clear shear force cracks to the left and right. These cracks continue into the compression zone. In the ultimate limit state the crack width of the bending crack was 0.5 mm and the width of the shear force crack 2.0 mm.

7.3.3 Strain in reinforcement bar at the bottom layer

The maximum strain in the reinforcement bar equals 1.17×10^{-3}. It occurs at the middle of the span at the location of the bottom layer of tensile reinforcement.

7.4 Description beam B2 experiment

Geometry

Beam B2 has a length of 5.01 m and a span of 4.57 m. The cross section of beam B2 has a width of 229 mm and a height of 552 mm. The effective depth d is 457 mm. Both latter dimensions are the same as with beam A1.
The cross section includes an upper reinforcement (3×M10 bars), a double-layered lower reinforcement (2×M30 in lower layer and 2×M25 in upper layer) with stirrups at the bearing and support locations, the head to head distance being reduced to 95 mm. The head to head distance between both lower layers of the reinforcement bars is 64 mm, whereas the distance from the lower side of the beam to the heart of the bottom reinforcement layer is also 64 mm. Figure 7.7 shows the B2 beam configuration.

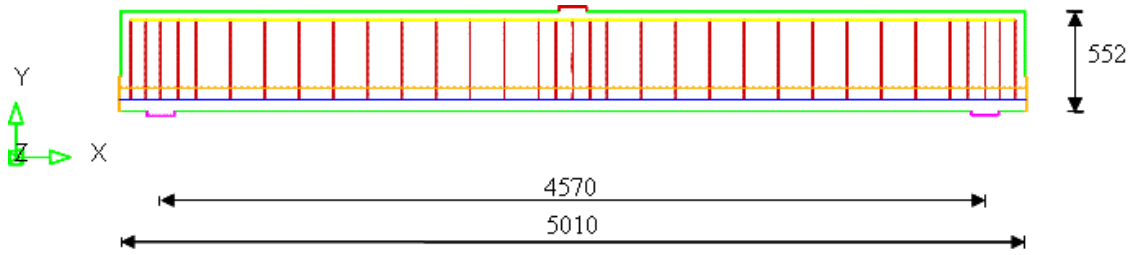

Figure 7.7 Configuration of beam B2

A cross section of beam B2 including the reinforcement is shown in figure 7.8.

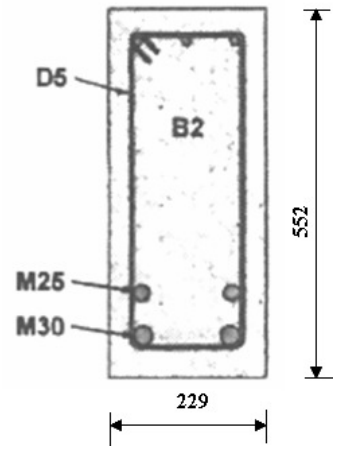

Figure 7.8 Cross section beam B2

The various reinforcement bars have their own cross section quantities, as is shown in table 7.3.

Bar type	Diameter [mm]	Cross section [mm^2]
Stirrups D5	6.4	32.2
Upper reinforcement bar M10	11.3	100
Lower reinforcement #1 bar M25	25.2	500
Lower reinforcement #2 bar M30	29.9	700

Table 7.3 Geometrical quantities of reinforcement bars in beam B2

In order to gain a clear insight it is important to make a note of the reinforcement percentage of the separate reinforcement bars. For the lower reinforcement this is 2.29%, for the upper reinforcement 0.29% and for the stirrups it amounts to 0.15%.
The reinforcement bars in both lower layers are anchored at the start and end of the beam to the concrete using welded-on steel plates. This was done to prevent any slip between the reinforcement bar and the concrete at the ends of the beams. The plate dimensions are 192×229 mm. For these plates the thickness dimensions and material quantities are the same as for the support plates that are described with the supports. The thickness of the welded-on steel plate is therefore established at 25 mm.

Materials

The beam materials are, of course, concrete, reinforcing steel and steel for the support plates and bearing plates. The characteristic material values of the various parameters of steel and concrete are shown in table 7.4.

Material	$f_{ck\text{-}cylinder}$ [N/mm^2]	f_{sp} [N/mm^2]	ε_0 [-]	E-modulus [N/mm^2]	f_y N/mm^2]	f_u [N/mm^2]
Concrete	25.9	3.37	0.0021	32,900	-	-
Stirrups bar D5	-	-	-	200,000	600	649
Upper reinforcement bar M10	-	-	-	200,000	315	460
Lower reinforcement #1 bar M25	-	-	-	220,000	445	680
Lower reinforcement #2 bar M30	-	-	-	200,000	436	700
Support plate	-	-	-	200,000	-	-

Table 7.4 Material characteristics of beam B2

For an explanation of the various material parameters, see the description of beam A1. Here, the maximum aggregate size of the concrete is also 20 mm.

Loads

The surface of the bearing plate is 150×300 mm^2, its thickness being 58 mm.

Supports

The beam supports consist of a left and right part, built from steel plates having a thickness of 20 mm, while measuring 150×350 mm^2.

7.5 Results of beam B2 experiment

7.5.1 Load-deflection diagram in middle of span

The load-deflection diagram of beam B2 is shown in figure 7.9, including the Bresler-Scordelis results from 1963.

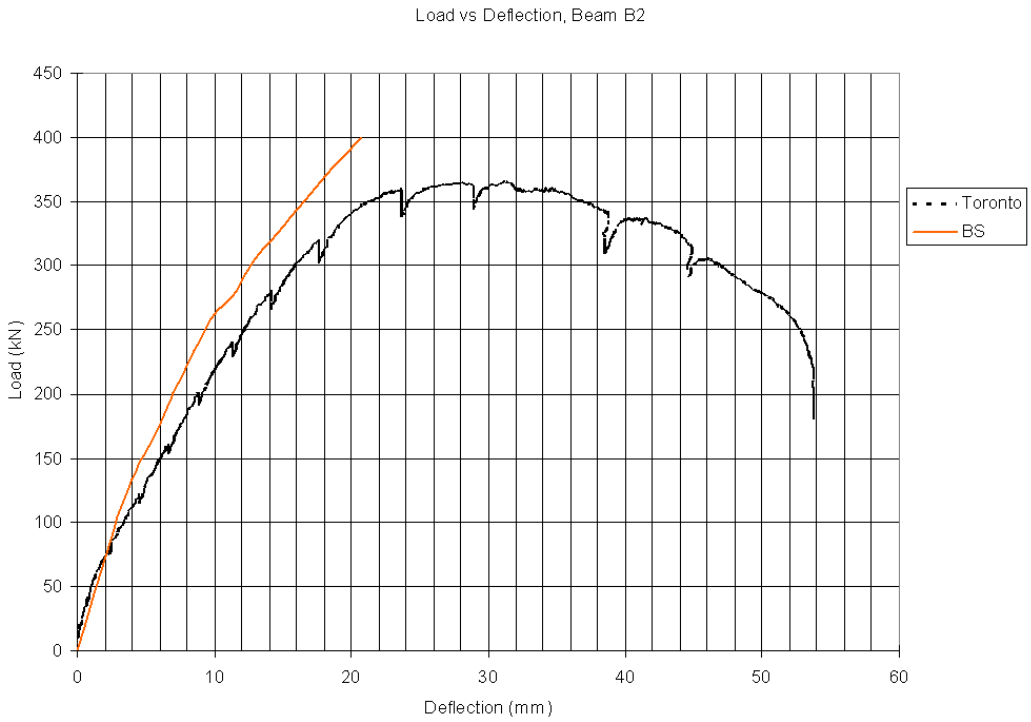

Figure 7.9 The load-deflection diagram of beam B2

In this load-deflection diagram there is also a reasonable harmony between the results of both experiments. The failure load through shear force with Bresler-Scordelis was 400 kN with a corresponding vertical deflection of 20.8 mm. In the Toronto experiment a failure load through shear force of 365 kN was found, with a corresponding vertical deflection of 31.6 mm. In this comparative experiment the Bresler-Scordelis experiment behaves slightly stiffer as well. The concrete compression strength is increased from 23.2 N/mm^2 to 25.9 N/mm^2, the upper reinforcement is increased from 254 mm^2 to 300 mm^2, whereas the tensile reinforcement is reduced from 2,580 mm^2 to 2,400 mm^2. The concrete cross section is exclusively reduced from 561 mm to 552 mm. Especially the reduction of the cross section of the tensile reinforcement will contribute to a larger vertical deflection in the ultimate limit state.

7.5.2 Beam B2 ULS crack pattern experiment

The crack pattern in this beam can be seen at both sides of the beam.

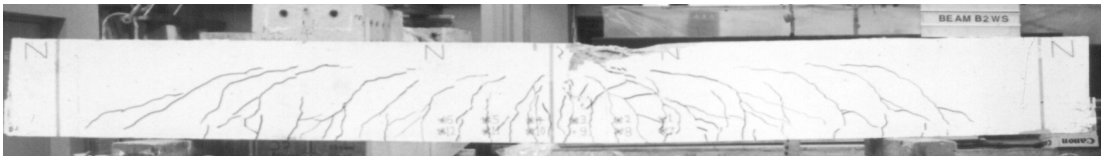

Figure 7.10 ULS crack pattern experiment B2 north face

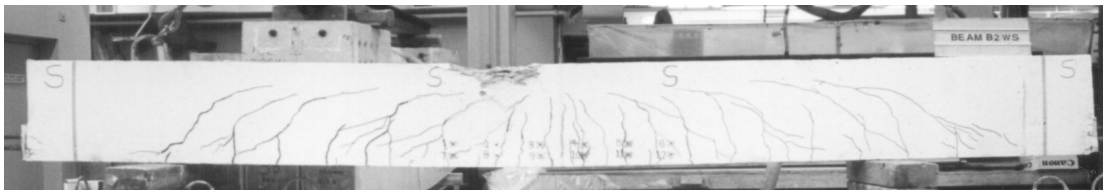

Figure 7.11 ULS crack pattern experiment B2 south face

The crack pattern that is visible on both sides of beam B2, showing a good mutual match. It can clearly be seen that the cracks run through till the compression zone, bending off just before reaching the compression zone to the bearing plate. The crack width due to the bending crack has a value 1.6 mm and the shear force crack is 0.5 mm.

7.5.3 Strain in reinforcement bars

The experiment leads to a maximum value for the strain in the reinforcement bar of 2.87×10^{-3}. This indicates the strain in the reinforcement bar in the bottom layer of the beam in the ultimate limit state. In view of the load-deflection diagram in figure 7.9 it is not really clear to which failure load the ultimate limit state applies. The horizontal branch of the diagram does have a considerable length at the loadlevel of 365 kN. For the time being the failure load with the corresponding vertical deflection of the experiment will be maintained.

7.6 Description beam C3 experiment

Geometry

Beam C3 has a length of 6.84 m and a span of 6.4 m. The cross section of beam C3 is 152 mm by 552 mm (height). The effective depth d is 457 mm.
The cross section includes an upper reinforcement (3×M10 bars), a double-layered bottom reinforcement (2×M30 in bottom layer and 2×M25 in upper layer) and stirrups (D4 at 168 mm head to head), with additional stirrups at the bearing and support locations, the head to head distance being reduced to 84 mm. The head to head distance between both lower layers of the reinforcement bars is 64 mm, whereas the distance from the lower side of the beam to the heart of the bottom reinforcement is also 64 mm. Figure 7.12 shows the beam configuration.

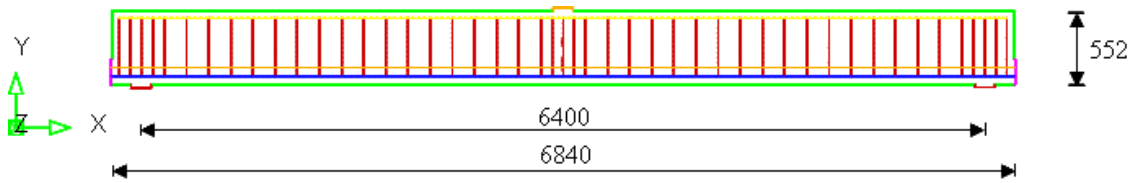

Figure 7.12 Beam C3 configuration

A cross section of beam C3 including the reinforcement is shown in figure 7.13.

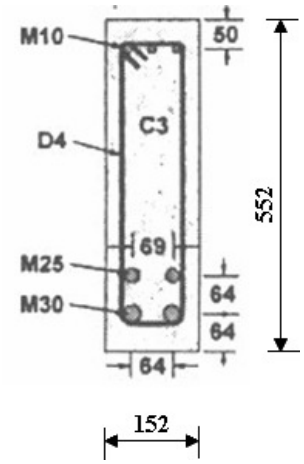

Figure 7.13 Cross section beam C3

The reinforcement bars have their own cross section quantities, as is shown in table 7.5.

Bar type	Diameter [mm]	Cross section [mm^2]
Stirrups D4	3.7	25.7
Upper reinforcement M10	11.3	100
Lower reinforcement #1 M25	25.2	500
Lower reinforcement #2 M30	29.9	700

Table 7.5 Geometrical quantities of reinforcement bars

In order to gain a clear insight it is important to make a note of the reinforcement percentage of beam C3. For the lower reinforcement this is 3.46%, for the upper reinforcement 0.43% and for the stirrups it amounts to 0.2%. The reinforcement bars in both lower layers are anchored at the start and end of the beam using welded-on steel plates, to prevent any slip between the reinforcement bar and the concrete at the ends of the beams. These steel plates are 192 mm high and have a width of 152 mm. For these plates the thickness dimensions and material quantities are the same as for the support plates that are described with the supports. The thickness of the welded-on steel plate is therefore established at 25 mm.

Materials

The beam materials are concrete, reinforcing steel and steel for the support plates and bearing plates. The characteristic material values of the various parameters of steel and concrete are shown in table 7.6.

Material	$f_{ck\text{-}cylinder}$ [N/mm^2]	f_{sp} [N/mm^2]	ε_0 [-]	E-modulus [N/mm^2]	f_y N/mm^2]	f_u [N/mm^2]
Concrete	43.5	3.13	0.0019	34,300	-	-
Stirrups bar D4	-	-	-	200,000	600	651
Upper reinforcement bar M10	-	-	-	200,000	315	460
Lower reinforcement #1 bar M25	-	-	-	210,000	440	615
Lower reinforcement #2 bar M30	-	-	-	200,000	436	700
Support plate	-	-	-	200,000	-	-

Table 7.6 Material characteristics beam C3

For an explanation of the various material parameters, see the description of beam A1. Here, the maximum aggregate size of the concrete is also 20 mm.

Load

The bearing plate is 150×300 mm^2 and has a thickness of 58 mm.

Supports

The beam supports consist of a left and a right part, built up with steel support plates of 150×350 mm^2, with a thickness of 20 mm.

7.7 Results of beam C3 experiment

7.7.1 Load-deflection diagram in middle of span

The load-deflection diagram of beam C3 is shown in figure 7.14, including the Bresler-Scordelis result from 1963.

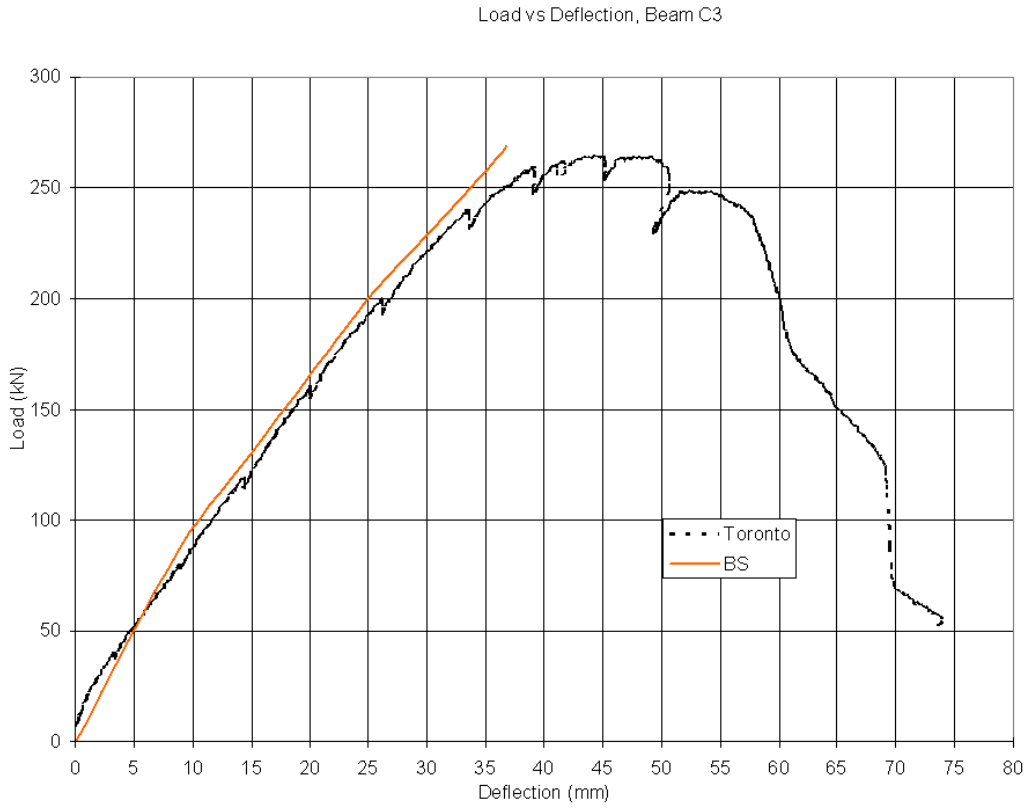

Figure 7.14 Load-deflection diagram at middle of C3 span

The load-deflection diagram shows a solid match between the Bresler-Scordelis experiment and the modified Toronto result. The Toronto experiment has been taken slightly further, also showing the decreasing load. However, this is of no relevance to the study of the full control over the design process of concrete structures. The failure load through bending at the ultimate limit state is fully achieved in both beams, namely 269 kN with Bresler-Scordelis and the corresponding vertical deflection of 36.8 mm (this is also

an abrupt failure load), against 265 kN in the Toronto experiment, including a matching vertical deflection of 44.3 mm.
The serviceability limit state is almost equal in both experiments as well, given that both load-deflection diagrams are almost identical.

7.7.2 Crack pattern

Unfortunately, nothing is known about the crack pattern in the Bresler-Scordelis beams, but there are photographs of the Toronto beams. Pictures were taken from both the north and south faces. These are shown in figure 7.15 and 7.16.

Figure 7.15 ULS crack pattern beam C3 north face

Figure 7.16 ULS crack pattern beam C3 south face

What is striking in both figures is the large number of cracks that bend off or stop when nearing the compression zone. The crack distance matches the distance between two stirrups. Wherever the stirrup distance has been reduced by a factor 2.0, the same happens to the crack distance, which is then also reduced by a factor 2.0. The crack width of the bending crack is 0.9 mm. In the shear force crack this is 0.25 mm.

7.7.3 Strain in reinforcement bar at the bottom layer

In this experiment at the midspan location the strain in the reinforcing bar in its ultimate limit state was established as well. It is 1.76×10^{-3}.

8 NON-LINEAR ANALYSES TORONTO EXPERIMENTS A1, B2 AND C3

8.1 Introduction

The experiments described in chapter 7, including the characteristic results of the experiments, are analysed in this chapter using the common physical non-linear FE method. For this purpose the DIANA FE code [DIANA 2005] is used. This means that on the basis of the indicated material quantities from the experiment, calculation quantities derived from the regulations are needed for the input on behalf of a physical non-linear analysis. This process will be treated in the following sections for each separate experiment A1, B2 and C3, after which the various results of the experiments will be described. In this case, the important results are divided into global and local results. The global results are the indicated failure load, the corresponding deflection of the beam in the middle of the span, the crack patterns in the concrete and the plasticity areas of both concrete and reinforcement. The local results are the crack width of the concrete in the bending area, the crack width in the shear force area and the strain in the bottom tensile reinforcement layer in the beam.

8.2 Beam A1 experiment non-linear analysis

8.2.1 Input non-linear material parameters

When discussing the experiment it was already seen that much value is placed on the Popovics compressive diagram of the concrete. This diagram has been entered as a multi-linear diagram within the Total Crack Strain Model Rotated (TCSM-R), with an alternation after reaching the maximum compressive stress. After reaching this maximum, the relation between the compressive stress and the strain is accepted as a constant compressive stress with an increasing strain. This relation is more in line with the prevailing regulations, instead of the descending branch. It is noted, however, that the 28 day cylinder compressive strength of 22.6 N/mm^2 shows a minimum compressive strength at a Young's modulus of 36,500 N/mm^2 (concrete class C40; $f_{ck\text{-}cylinder}$ = 40 N/mm^2). Figure 8.1 shows the compressive stress-strain diagram.

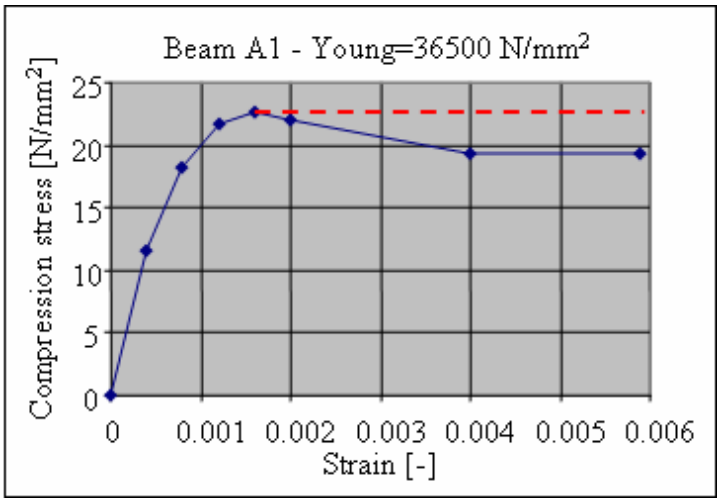

Figure 8.1 Compressive strength-strain diagram experiment A1

Apart from the compressive strength diagram in the TCSM-R model, a selection has also to be made regarding concrete softening. The splitting tensile strength of the concrete is given in the paper and measured in this experiment, having a value 2.37 N/mm^2. This value is similar to the mean tension strength value f_{ctm} = 2.4 N/mm^2, calculated from the compressive strength f_{cm}=22.6 N/mm^2.
Following this, the Hordijk softening diagram is selected [Hordijk 1991], because this includes strong crack pattern directly after exceeding the maximum tensile stress, whereas it also has a continuous branch deep into the tail of the diagram. This is important in view of the convergence behaviour with physical non-linear analyses. The principal stress-strain diagram is shown in figure 8.2.

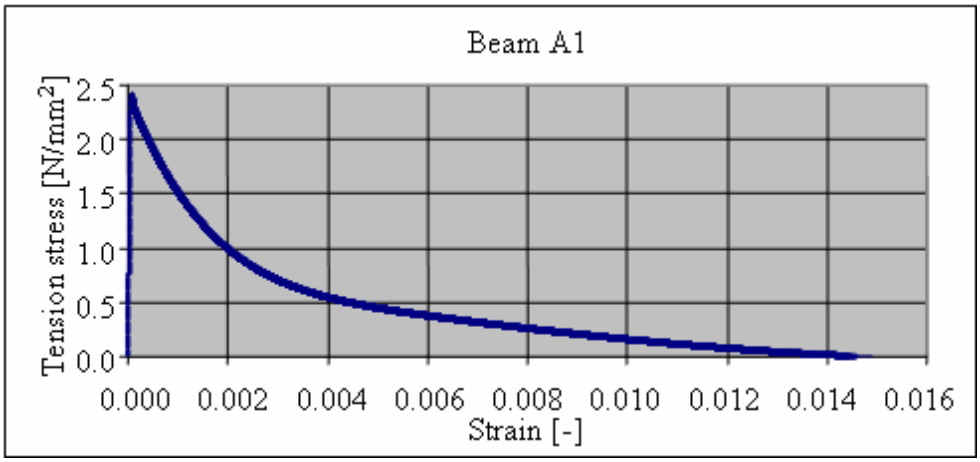

Figure 8.2 Principal tension strength-strain diagram experiment A1

Figure 8.2 shows the relation between the principal tensile stress that occurs and the corresponding principal tensile strain at an integration point of a structural element. Depending on the size of the element the crack bandwidth of a integration point is determined in a physical non-linear FE code. In order to remain independent of the FE code the crack bandwidth is indicated explicitly. For beam A1 a crack bandwidth of 8.75 mm is entered, being half the length of a structural element(=17.5 mm). The size of the crack energy that determines the surface beneath the softening curve is derived straight from the Model Code 1990. Using the indicated material parameter from the experiment (the largest aggregate size is 20 mm), the application of the formula surrounding G_F from the Model Code 1990 leads to the calculation of the crack energy. The formula is:

$$G_F=G_{F0} \times (f_{cm}/f_{cmo})^{0.7}$$

In which
G_{F0} = 0.037 Nmm/mm^2
f_{cm} = 22.6 MPa
f_{cmo}= 10 MPa

In this experiment A1 the crack energy is calculated as G_F = 0.063 Nmm/mm^2. Given the earlier indicated crack bandwidth of 8.75 mm, the surface beneath the indicated principal stress-strain diagram of figure 8.2 equals 0.063/8.75=0.0072, being the integral value of figure 8.2. This is also an important check on this input parameter.
The allowed tensile strength is derived directly from the given compressive strength.

A yield limit and a yield criterion are entered for the reinforcement steel. In this case the choice was made for the widely accepted Von Mises criterion with the corresponding values for the yield limit. After yielding the stress-strain diagram shows a horizontal branch similar to the compressive diagram of concrete (see figure 8.1) after reaching the yield point (plasticity, crushing). The yielding values for the upper, stirrup and lower reinforcement differ per experiment, as was indicated in chapter 7.
The various bearing, support and anchoring plates for the final anchoring of the tensile reinforcement have also been described in chapter 7. These will be included into the calculation model as linear elastic material.
The length of the side of the structural concrete element is set at ±20 mm, in agreement with the maximum aggregate diameter of 20 mm. As was mentioned earlier, the exact crack bandwidth is derived from the side of the concrete element and set at 8.75 mm.

8.2.2 Global results of A1 experiment simulation

The load-deflection diagram is shown in figure 8.3.

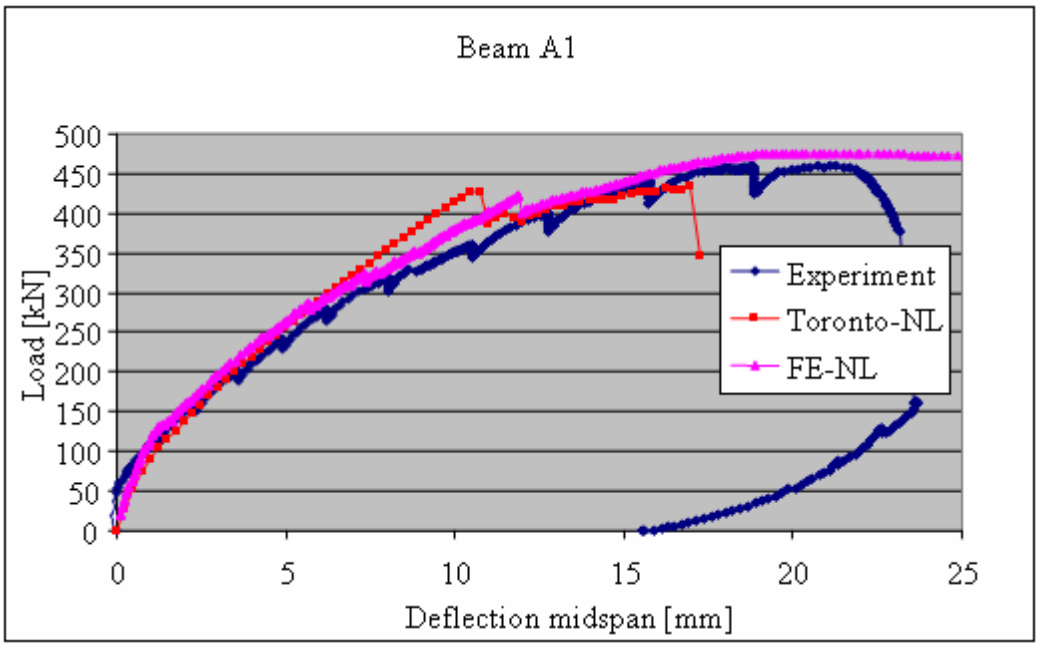

Figure 8.3 Load-deflection diagram experiment A1

This shows that the failure load (465 kN versus 473 kN) has been established correctly. At the beginning of the diagram the structure behaves in a slightly stiffer manner, whereas the latter track agrees well with the load-deflection diagram of the experiment.
The so-called tension stiffening effect as a result of the reinforcement present in the calculation model is clearly visible. The calculation process is terminated at a deflection of over 26 mm, which is slightly more than the maximum deflection in the experiment (=18.8 mm). The many discontinuities in the load-deflection diagram are remarkable. They mainly render the progress in the physical non-linear calculation process unstable.
In the publications by Vecchio and Shim [Vecchio 2004 and Shim 2002] mention is made of a corresponding deflection at the failure load of 18.8 mm. According to figure 8.3 in the experiment 20 mm as well as 23 mm could be valid. In this case it is not clear which criterion can be indicated as failure. Furtheron in this paragraph, the deflection of 18.8 mm will be noted as the deflection belonging to the ULS loadlevel.

A photo of the crack pattern of the beam at the moment of failure is available. This photo is shown in figure 8.4.

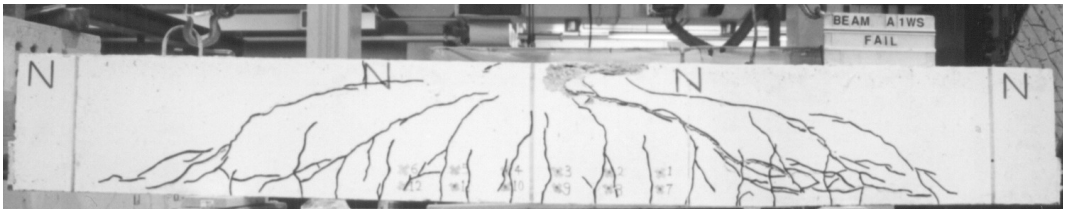

Figure 8.4 Crack pattern north side experiment when reaching failure load

This crack pattern indicates that there are mainly shear force cracks in the beam in the area to the left and right of the load. From the non-linear analysis a crack pattern can be generated as well, as is shown in figure 8.5.

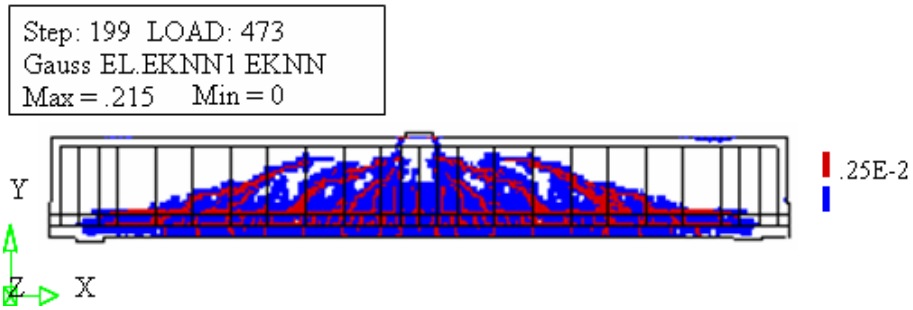

Figure 8.5 Crack pattern in non-linear analysis when reaching failure load

As far as their shapes are concerned, both crack patterns show many similarities. The red areas indicate the macrocracks, whereas the blue areas show the microcrack areas. The maximum crack strain has a value of 0.215, which means a crackwidth of 1.88 mm. Both the experiment and the numerical simulation clearly show three dominant cracks to the left and right of the load. The cracks are nearly all aimed at the point of application of the load, starting at the upper layer of the tensile reinforcement. What is important for the inspection process of structures, the cracks find their origin in a bending crack, starting in the lower fibre of the beam. It is also possible to make a distinction in the cracking behaviour surrounding both layers of the tensile reinforcement. At the middle of the beam there are small tensile bending cracks. The global behaviour of the beam is completed by two figures presenting the exceeding of the ultimate compressive strain of concrete as well as the plasticity of steel. According to figure 8.1. and table 7.2, the ultimate compressive strain of the concrete has a limit value of 0.0016.

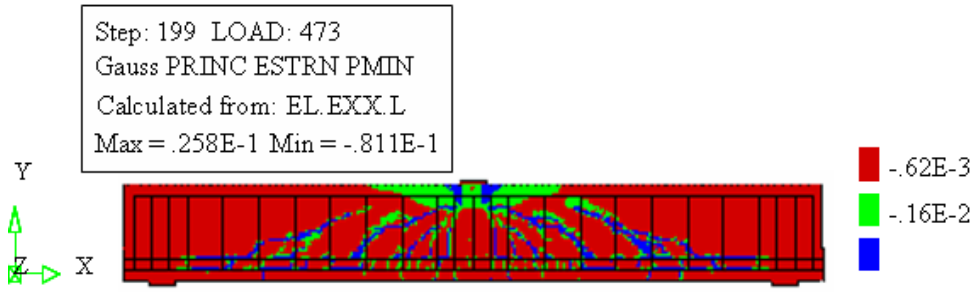

Figure 8.6 Compressive strain areas of concrete at failure load on beam A1

Figure 8.6 shows the different contour values at the right side of figure 8.6. The lower limit value of -0.81×10^{-1} is the value of the principal compressive strain. This value of the concrete doesn't still behave in an elastic manner. The figure 8.6 shows clearly that at the location of the macrocracks there is a limited area in which the principal compressive strain is exceeded. Near the bearing plate in the middle of the beam there is a larger area connected with the exceeding of the ultimate principal compressive strain of concrete. The width of these areas is confined to one or a few structural elements. This renders it a limited entity. In other words, there is no reason to extend the input data of the concrete material to a descending branch after reaching the compressive strain ε_0; see table 7.2 and figure 8.1. The same image type is shown in the plasticity areas of the reinforcement, indicated in red in figure 8.7.

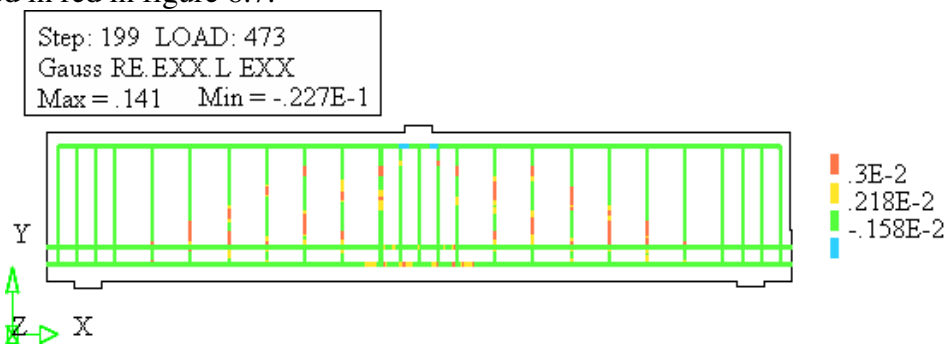

Figure 8.7 Plasticity areas of reinforcement at failure load on beam A1

The areas in red, yellow and blue are the areas involved, depending the type of reinforcement, where every type has its own yielding limit strain. These yielding areas are mainly found beneath the bearing plate(compression), and subsequently in the stirrups at both sides of the load(tension). These locations match the macrocracks in figure 8.5 and the areas where the compressive strain is exceeded in figure 8.6.

8.2.3 Local results of A1 experiment simulation

If the ultimate limit state of a structure needs to be established, it is important to address the strain in the tensile reinforcement.

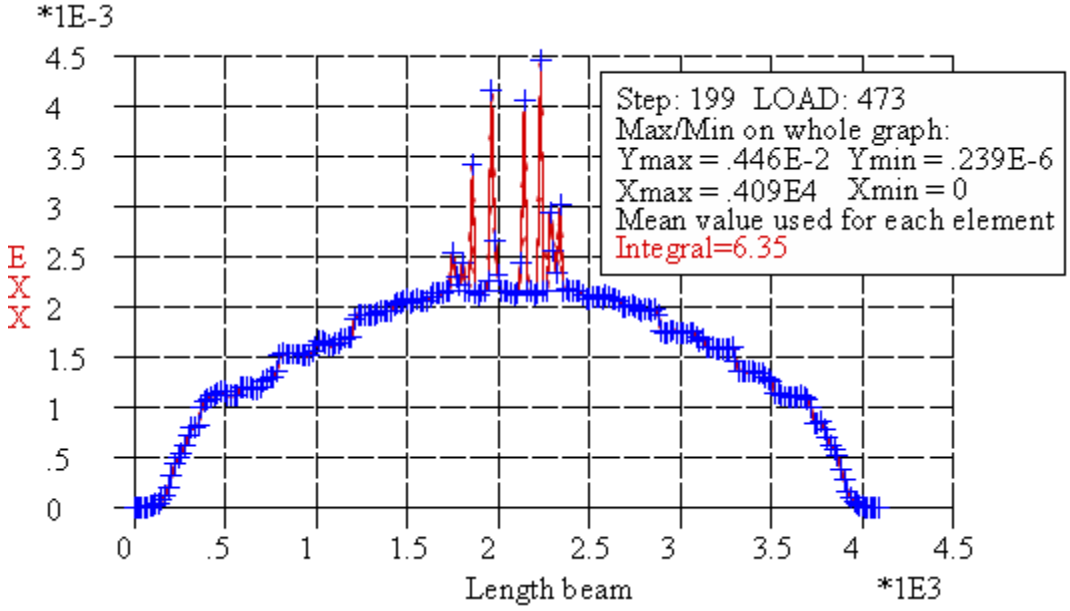

Figure 8.8 Strain in tensile reinforcement at ULS loadlevel

The strain in the tensile reinforcement at the moment of the experimental deflection of 18.8 mm is known, and has a maximum value of 4.46×10^{-3}. The overall graph of the strain of the lower reinforcement in the numerical simulation with the same deflection is shown in figure 8.8. The maximum strain in the tensile reinforcement according to figure 8.8, meaning that there is some considerable difference with the experiment. To give a better idea of this maximum only a midspan section with a length of one meter is given in figure 8.9.

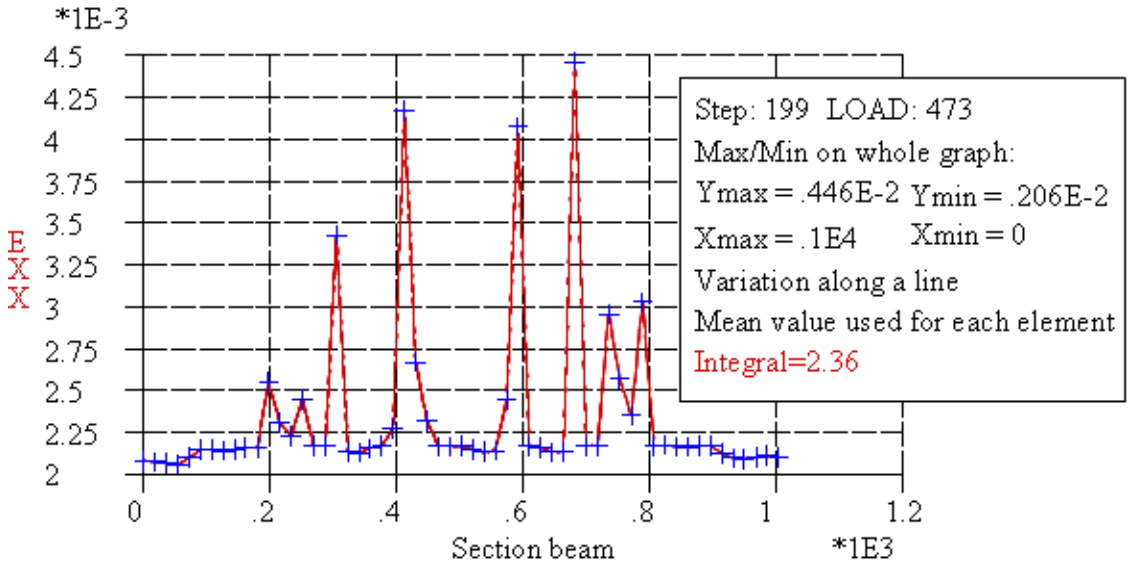

Figure 8.9 Strain in section lower tensile reinforcement ULS loadlevel

The mean value for the tensile reinforcement is calculated from the integral value over the section length in figure 8.9. This mean strain value is 2.36×10^{-3}, which value is closer to the given reinforcement value of the experiment, but still too high. It is important to know the development of this tensile strain in the reinforcement when the load was increased. The maximum is found at some distance from the middle of the span of the beam. The development of the strain is presented in figure 8.10.

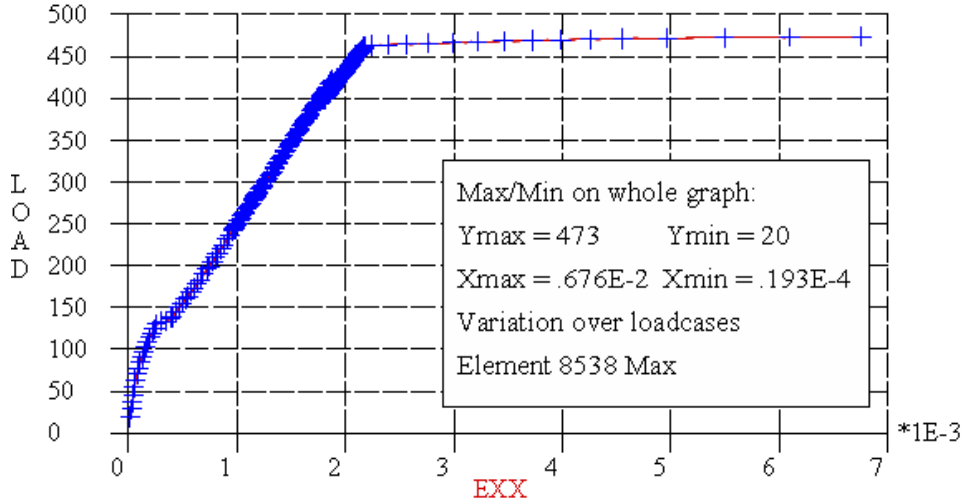

Figure 8.10 Development of the strain at an integration point with the maximum strain in the bottom layer of the tensile reinforcement at ULS loadlevel

Figure 8.10 shows a rather linear development of the reinforcement strain till almost the ULS load level. The value of the measured strain from the experiment in the tensile

reinforcement, amounting to 1.172×10^{-3}, is already reached in the numerical simulation with a load of approximately 260 kN. For the moment no conclusion can be drawn from this. One may say, however, that the maximum strain after reaching the value of 2.1‰ is above the yield limit. Ths strain value is reached at a loadlevel of 460 kN. Depending on what the hardening track of the reinforcement steel looks like, the tensile reinforcement has just reached the hardening limit or hasn't just reached the hardening limit. In this manner the input data still comply with the criterion that no hardening has to be modelled after reaching the yield limit of the bottom layer of the lower reinforcement. Other than in the bottom layers of the reinforcement, strains exceeding 0.002 are found in the stirrups (0.4) and the upper reinforcement (0.04). Hardening could therefore be entered here as well, provided that the decending track of the principal stress-strain diagram of the concrete is also added. Taken these aspects all together, this will not cause major changes in the calculated failure load.

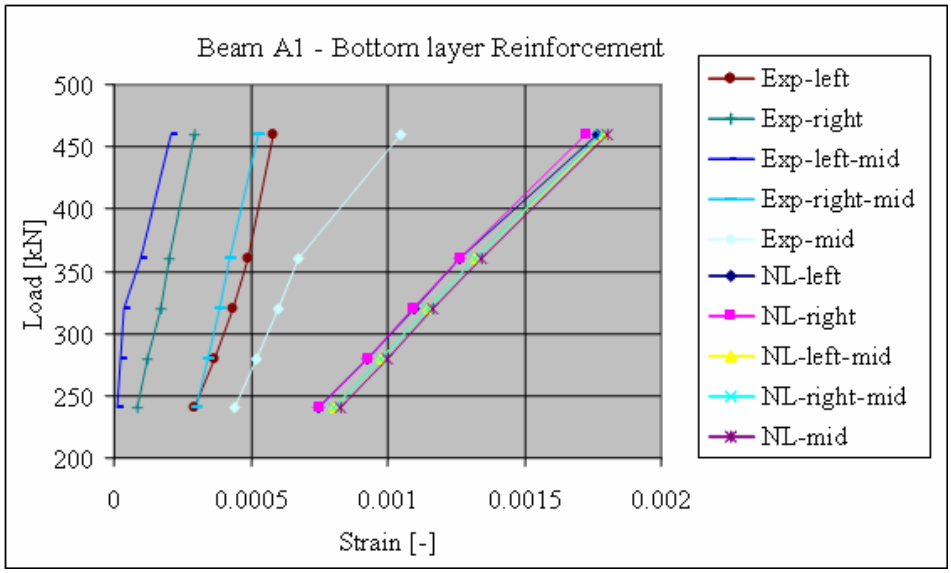

Figure 8.11 Comparison between strain development in bottom layer of tensile reinforcement in experiment and FE-NL analysis

Figure 8.11 shows that the calculated strains do not agree with the measured strains of the experiment. This applies to all load levels and all five sections with a length of 200 mm around the midspan of the beam at the lower reinforcement level. Because the global results do agree, this issue wil be treated further in the final evaluation.
The continuing crack pattern both in the bending area and in the shear force area causes this beam A1 to fail, at least as far as the horizontal branch in the load-deflection diagram is concerned, which is all the more reason to look at this in detail. The first result is the crack pattern at the lower side of the beam. In the experiment, the crack width is stated to have the value 0.5 mm, belonging to the failure load. Because the crack width is not a direct option in a Finite Element code, the crack strains of the lower edge will be addressed first. In order to obtain an idea of the crack pattern at the lower side a symbol figure plot of the crack strain is presented to visualise this local cracking behaviour. This is shown in figure 8.12.

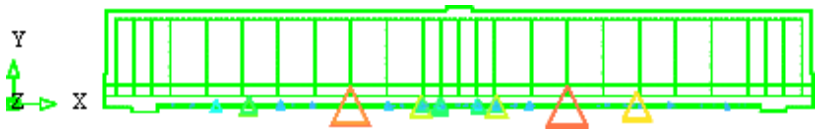

Figure 8.12 Crack strain lower fibre at the ULS load level of beam A1

Despite the concrete crack options entered, such as e.g. the inclusion of the crack energy, etc. in the calculation model, the lower fibre still shows local crack behaviour. The red triangle symbol illustrates in figure 8.12 the local behaviour. From this symbol pattern it is possible to calculate the head to head distance of the maximum cracks. Figure 8.12 shows a fairly regular pattern of areas (=crack strain > 0.001), the local crack strain peak values. Starting from this symmetrical picture of areas with maximum crack strains we find, at a length of half the beam, an average crack distance of 3660/19=192 mm. The stirrups that are present have a head to head distance of 210 mm. In short, this equation does agree well, and boosts confidence. The value of these specific crack strain areas can also be rendered along the length of the beam between the support plates.

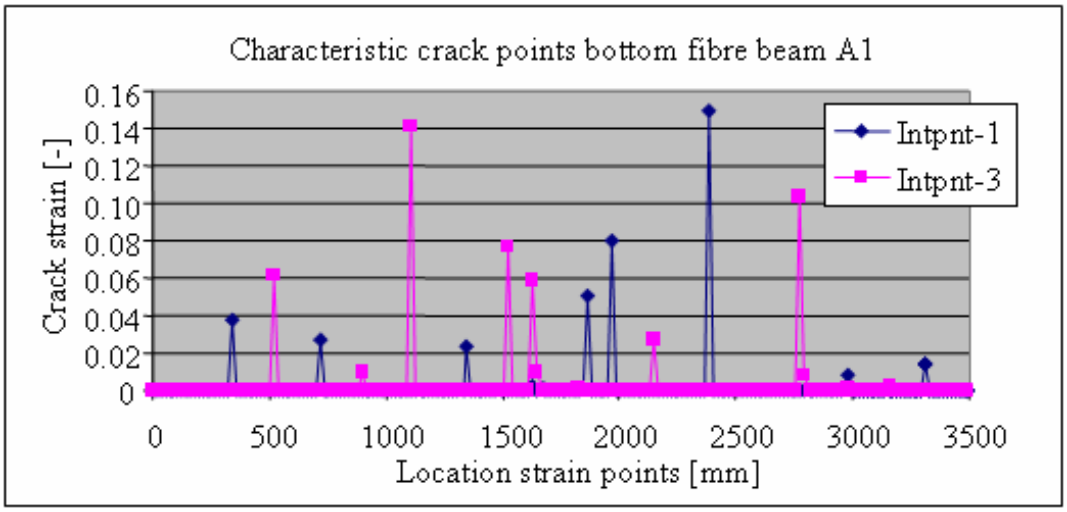

Figure 8.13 Crack strains in lower fibre of beam at ULS loadlevel

In figure 8.13 a distinction is made in the two different integration points per element, situated in the bottom side over half the length of the beam. In this way it is possible to give a more clear indication that the cracking behaviour is a purely local result, even within a single structural element. This figure also presents a clear pattern regarding the head to head distance of the cracks. The maximum crack strain does, however, not occur in the middle of the beam, where according to the publications the measurements were done, but rather in the area resulting from the development of the start of a shear crack. In the 'actual' bending area, the middle of the span, a maximum crack strain value of 0.059 is found. In view of the fact that only one integration point in the structural element has this maximum value, this value of the crack strain can be multiplied by the crack bandwidth that amounts to 8.75 mm. This produces a crack width of 0.53 mm, matching the crack width found in the experiment (= 0.5 mm) well. To gain an impression of the development of the crack strain in the specific maximum point, as starting point for the shear crack, see the development track in figure 8.14. In this figure 8.14 two developments of strains are added, one of the element (element 3796 in the legend; x=2400 mm) where the maximum shear crack is initiated and one element (element 592 in the legend; x = 1600mm in figure 8.13) at the mid span location of the beam.

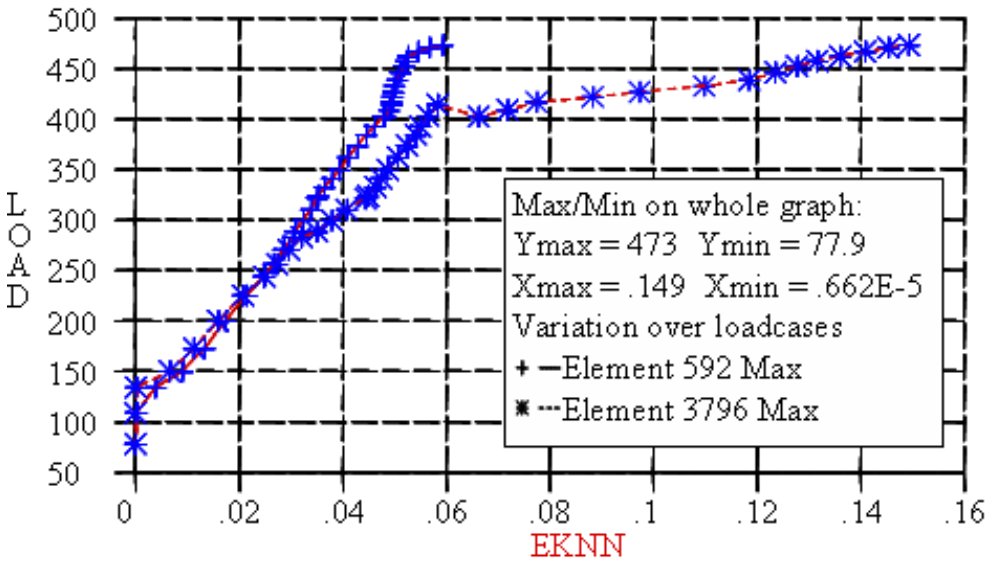

Figure 8.14 Development of maximum crack strain in lower fibre integration point

Figure 8.14 shows that the crack strain in the area surrounding 0.06 cannot be described in a uniform manner. The maximum bending crack strain is 0.06 at the ULS loadlevel, but the crack strain is much higher in this case at the shear area. The crack strain involved sometimes decreases due to crack pattern elsewhere in the beam, meaning that it is impossible to record the corresponding load in an unambiguous manner. This crack pattern elsewhere is most probably the crack pattern in the shear force area.
It is remarkable, however, that the crack strain at SLS level (± 286 kN) has a value 0.033, which amounts to a crack width of 0.28 mm. This is well above the allowed limit of 0.2 mm. The development of the calculated crack width is compared to the observations from the experiment, as may be seen in figure 8.15.

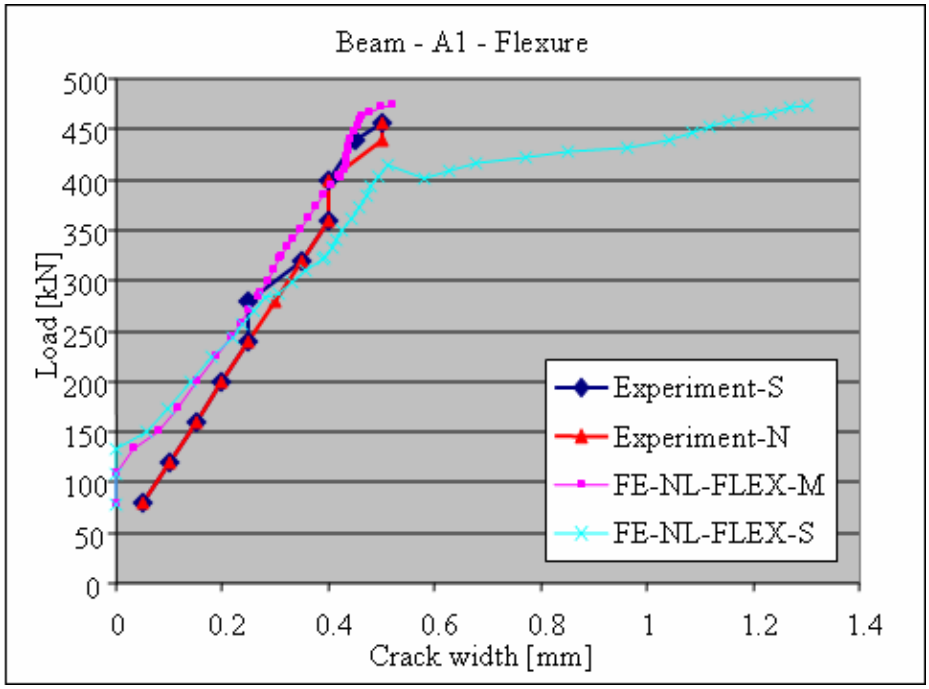

Figure 8.15 Development of crack width in beam A1 bending experiment and analysis

The maximum crack strain in the bending area of the calculation is 0.055. The measurements during the experiment went up to a crack width of 0.5 mm. This is therefore the final value of the crack width in figure 8.15. In the experiment, measurements took place on both sides of the beam. As with the load-deflection diagram we see a good match between the measured crack widths and the calculated crack widths in the upper part of the diagram till a load level of 425 kN. The bottom part is dominated by the stiffer behaviour, which is probably caused by tension-stiffening.
Apart from the crack strain in the middle of the beam there is also the crack strain in the shear force area, known from the experiment. The exact location and measuring method are missing, albeit that some impression may be given of the level of crack pattern. The area with the maximum crack strain is around the 1,200 mm measured from the support and in the direction of the middle of the span. A detail of the crack pattern in the shear force area with the maximum crack strain is shown in figure 8.16.

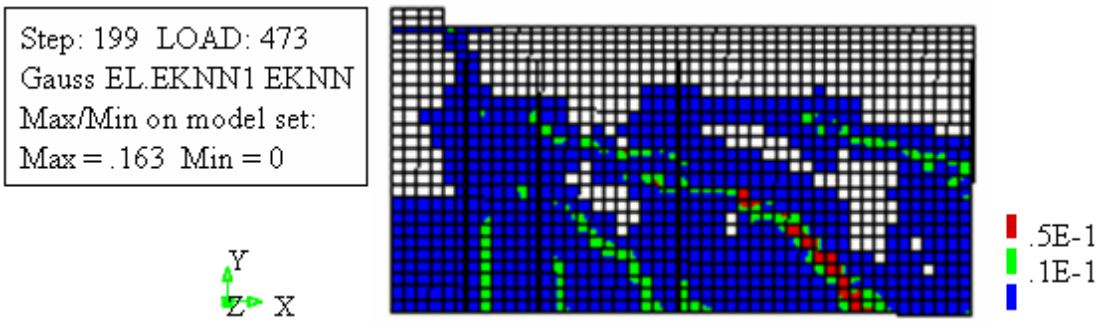

Figure 8.16 Crack pattern in beam A1 shear force area

Figure 8.16 shows that the dominant crack direction is at an angle of 45˚. The full cross section has cracked along three-quarters of its height. The maximum has a value 0.163, which taken together with a crack bandwidth of 8.75, multiplied by √2 because of the 45˚ crack angle results in a crack width of 2.02 mm. During the experiment, a crack width of 2 mm was measured. In short, this does boost confidence. The development of the crack strain in relation to the load increase gives more insight into this. It is shown in figure 8.17.

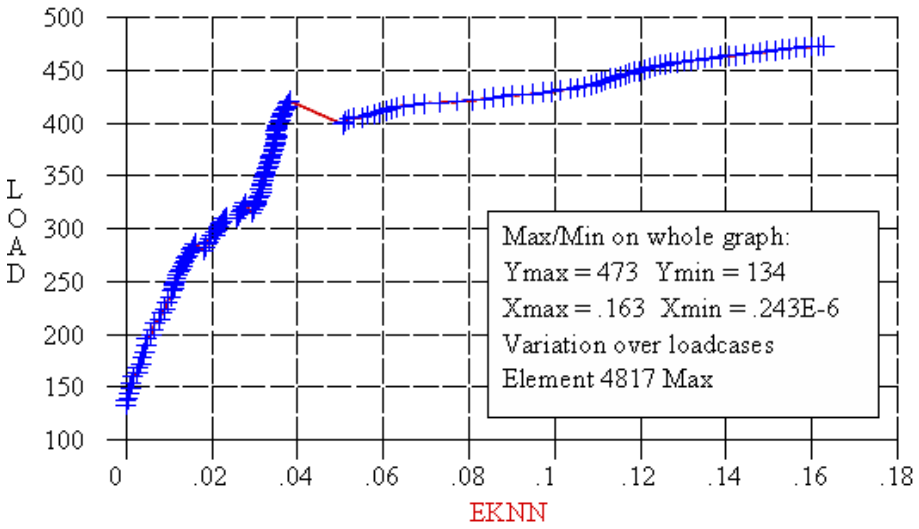

Figure 8.17 Crack strain development in the shear force area

Figure 8.17 shows that the crack strain in the shear force area develops in a rather discontinuous manner when the load is increased. At SLS level (=286 kN), however, there is already a shear force crack. The crack strain can also be seen, given its size of 0.016 which matches a crack width of 0.20 mm.
The maximum of the crack strain is 0.163, after which the development becomes totally unpredictable. With this maximum strain of 0.163 a maximum crack width of 2.02 mm is calculated at a load of 473 kN. Once again it is seen that it is difficult to obtain an exact match between the results of the experiment and a numerical simulation. A presentation of the development of the crack width in both the experiment and the analysis provides more clarity.

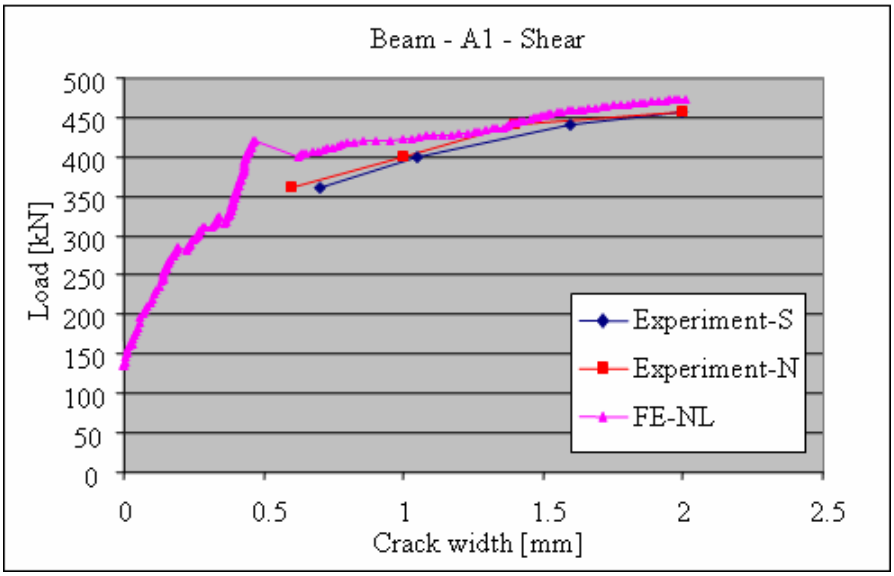

Figure 8.18 Development of shear force crack width in beam A1 experiment and analysis

Figure 8.18 shows that there is a good match between the crack widths of the experiment and those obtained during the analysis, especially starting from the 400 kN loadlevel.
In order to indicate that the crack strain is highly local within this area, a number of nine diagonal rows has been defined in an area of 5×5 elements, running across the available integration points of these elements. These lines, each containing six integration points, are shown in figure 8.19.

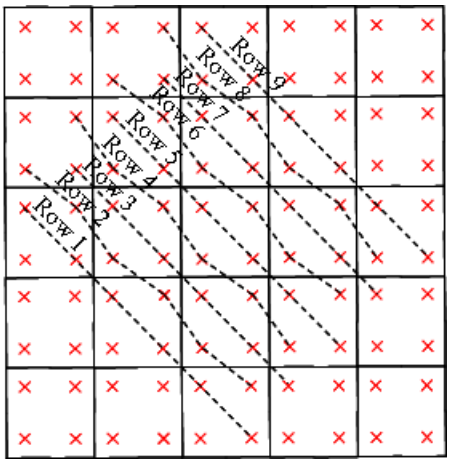

Figure 8.19 Layout of rows in detail of shear force area

Each row of integration points totals six integration points, that are not aligned entirely straight due to the element pattern. The fact that they are not in a straight line is in itself not relevant, however, because the issue at stake is the width of the maximum values of the crack strain in the integration points. The graph of the crack strains per row can now be plotted in a simple diagram, as is shown in figure 8.20. Figure 8.20 shows that the crack strain in most cases is limited to a single integration point, especially where there is a maximum crack strain. This means that the assumption of a crack bandwidth of 8.75, being half the length of the side of the element, can be maintained. Its physical meaning points at a narrow crack bandwidth.

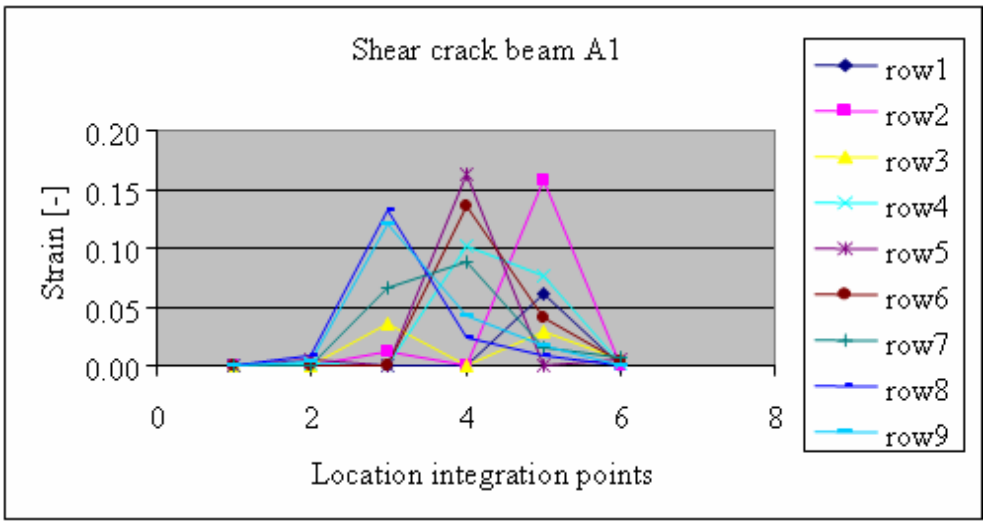

Figure 8.20 Crack strain in six integration points in direction of row in detail of shear force area

In general, one may therefore conclude that the calculated crack widths from the crack strains of the numerical simulation agree fairly well with the measured crack widths of the experiment. Both crack widths from the numerical simulation have a slightly lower value than in the experiment, but the mutual ratios do agree.

8.3 Beam B2 experiment non-linear analysis

8.3.1 Input non-linear material parameters

In the numerical simulation of beam B2 use is also made of the multi-linear compressive stress diagram in order to be able to simulate the Popovics model. The 28 day cylinder compressive strength in this experiment is 25.9 N/mm^2, whereas the corresponding Young's modulus is 32,900 N/mm^2. The pressure diagram is shown in figure 8.21.
Other than with the A1 experiment the compressive strength in the B2 experiment is higher, whereas the Young's modulus value is lower. The maximum aggregate size remains the same, namely 20 mm. The simulation of this experiment also makes use of the Hordijk softening diagram, but this time with an allowed tensile strength f_{ctm} = 2.62 N/mm^2, which is calculated directly from the admissible compressive strength.

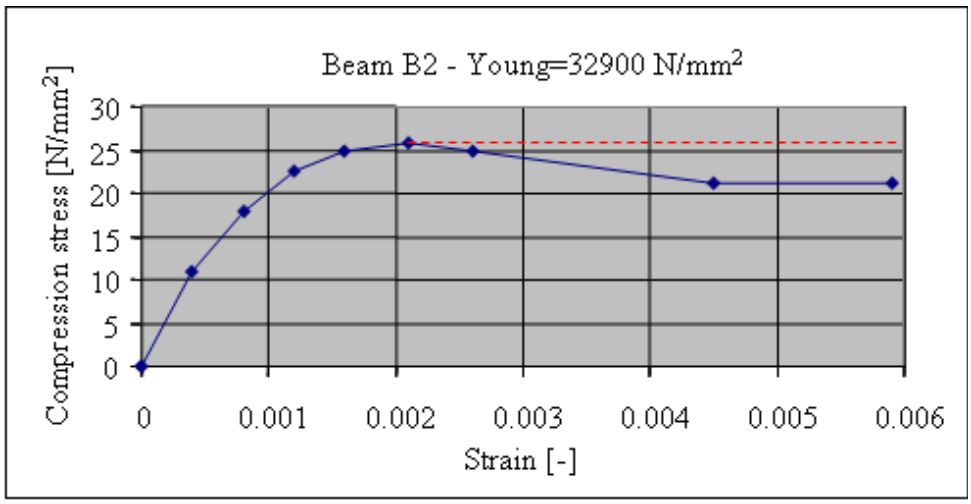

Figure 8.21 Principal compressive strength-strain diagram B2 experiment

The adjusted principal tension strength-strain diagram is shown in figure 8.22.

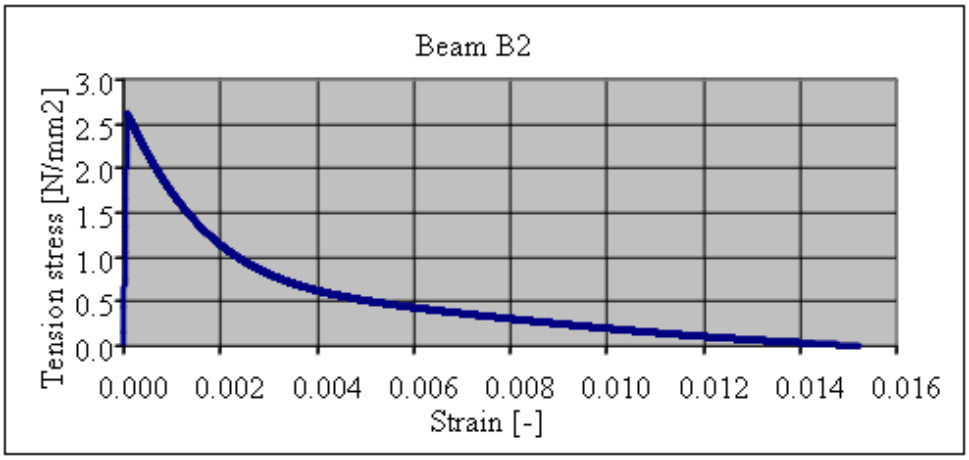

Figure 8.22 Principal tension strength-strain relation in FE simulation beam B2

The crack energy G_F with a maximum aggregate size of 20 mm again follows directly from the Model Code 1990, amounting to 0.072 N/mm/mm^2. With an assumed and entered crack bandwidth of 9.2 mm this produces a value for the area beneath the curve of figure 8.22 of 0.072/9.2=0.0078, thus providing a check once again. All other structural parts are included into this FE simulation model, in line with the experiment A1 procedure described earlier.

8.3.2 Global results of B2 experiment simulation

The load-deflection diagram for the middle of beam B2 is shown in figure 8.23. The experiment results in a failure load of 365 kN with a corresponding vertical deflection of 31.6 mm in the middle of the span. The corresponding failure load in the FE analysis is 354 kN. Figure 8.22 shows that the FE simulation is slightly higher with a failure load of 357 kN. The differences between both results are very slight. At a load of 352 kN it turns out all reinforcement components have started to yield, meaning that at that moment the beam has failed. However, the beam does have a residual capacity for a load of 5 kN.

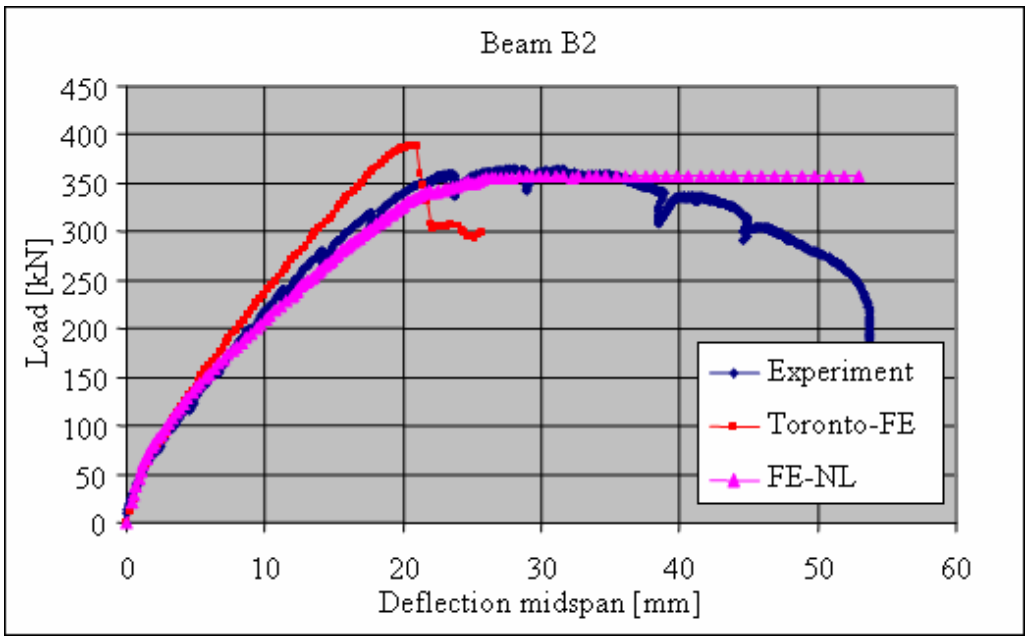

Figure 8.23 Load-deflection diagram of simulation of B2 experiment

The photo of the crack pattern at failure load in the experiment is shown in figure 8.24.

Figure 8.24 Crack pattern at failure load in experiment B2

This picture can also be generated from the numerical simulation of the experiment, as may be seen in figure 8.25.

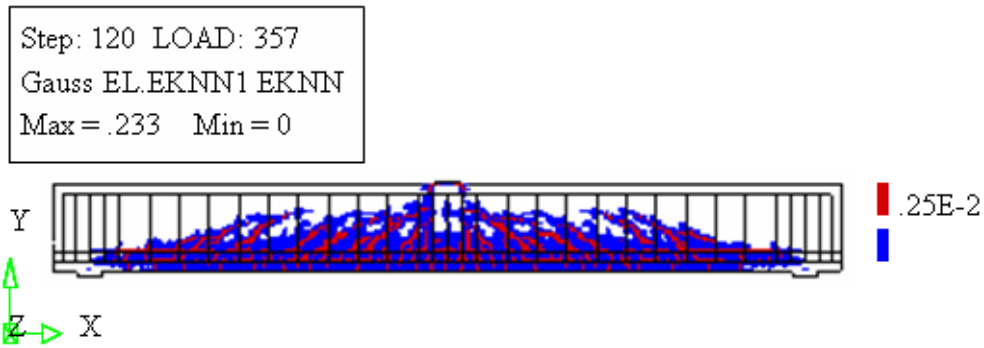

Figure 8.25 Crack pattern in simulation of B2 experiment

Figures 8.24 and 8.25 correspond well. In this case there are no three dominant shear force cracks as in the A1 experiment, but many more. The picture shows more distribution. At the locations in the lower part of the beam there is also crack pattern (=slip) around the tensile reinforcement. This renders comparison more difficult, because the calculation model does not include slip around the reinforcement and the abutting concrete. This will be treated further in chapter 10, addressing the evaluation of the various results. The global behaviour of the beam ends with the areas where the ultimate compressive strain of the concrete is exceeded, as well as with the rwsults of the reinforcement plasticity areas.

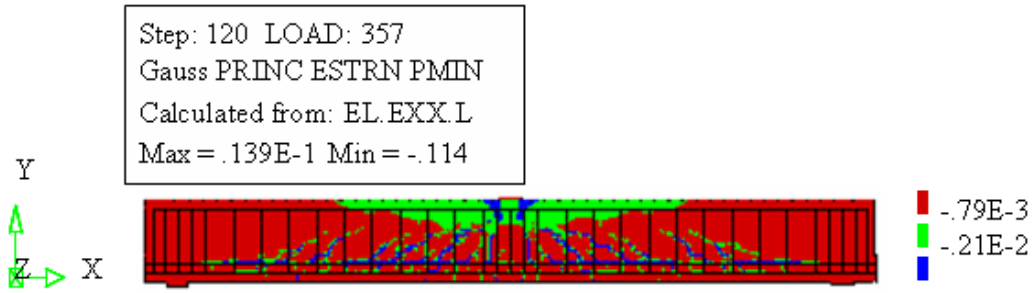

Figure 8.26 Areas where the ultimate compressive strain of the concrete is exceeded at beam B2 failure load

The areas in blue in figure 8.26, mainly at the location of the load bearing plate of the beam and the principal cracks, indicate where the principal compressive strain limit is exceeded. The areas have a width of one to some element sides and occur at those locations where crack pattern is found as well. This renders it plausible that the physical non-linear analysis of such a beam can be difficult for this area, even though this is not really expressed in the load-deflection diagram shown earlier in figure 8.23.

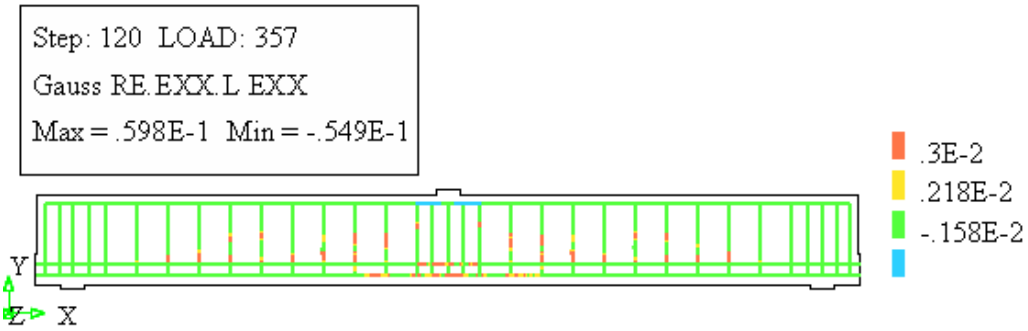

Figure 8.27 Plasticity areas in reinforcement at beam B2 failure load

The blue, yellow and red areas in figure 8.27 representing the plasticity areas of the reinforcement bars when reaching the beam failure ULS load level. All reinforcement components in this beam have to deal with plasticity areas, namely upper reinforcement, lower reinforcement and stirrups.

8.3.3 Local results B2 experiment simulation

The strain in the tensile reinforcement has an average value along one length of a element side of the reinforcement of 4.91×10^{-2} in the bottom layer of the tensile reinforcement. Figure 8.28 shows this maximum and the tensile strains along the full length of the beam. Other than with the A1 experiment, figure 8.28 of the numerical simulation of beam B2 shows an extreme maximum strain value of a section in the tensile reinforcement in the middle of the span.

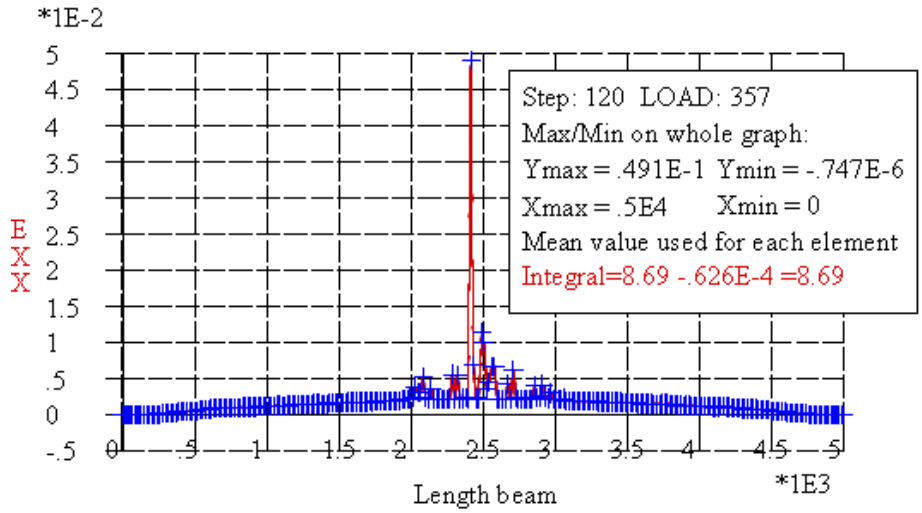

Figure 8.28 Strain reinforcement in tensile bottom layer at failure load

It may be that the measuring method in the experiment is of importance here, but maybe also the simulation of the experiment has been slightly too simplistic in this respect. This will be treated further in the section on the evaluation of the results.

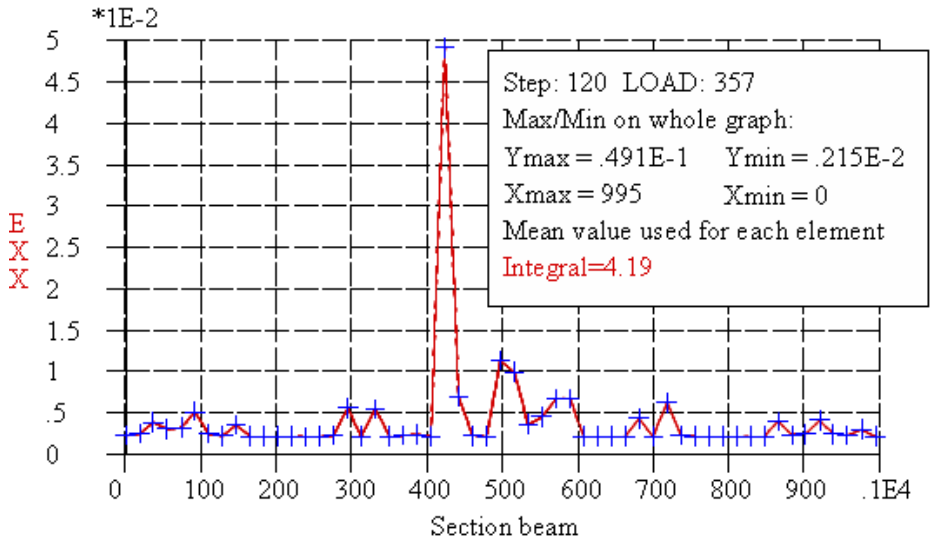

Figure 8.29 Strain in tensile reinforcement ε_{xx} along a section length of 1,000 mm

The reinforcement strain along the section with a length of 1,000 mm, located at the middle of the beam, shown in figure 8.29, presents a better picture of the actual strain values in the tensile reinforcement. It is clear that the value of the strain outside the peak values is 2.15×10^{-3} and that the average strain value along the entire section is 4.19×10^{-3}. The 1,000 mm length was selected on the basis of five adjoining measuring reinforcement lengths of 200 mm located around the middle of the beam. The measured strain value from the experiment is 2.87×10^{-3}. This lies in between the peak value of the tensile reinforcement and the lower limit of the section.
The development of the reinforcement strain in the tensile reinforcement is given in figure 8.30, where the maximum integration point is plotted instead of the mean value of the reinforcement element. The mean value of the same reinforcement element in figure 8.29 was 4.91×10^{-2}, where the maximum strain value is 5.98×10^{-2}.

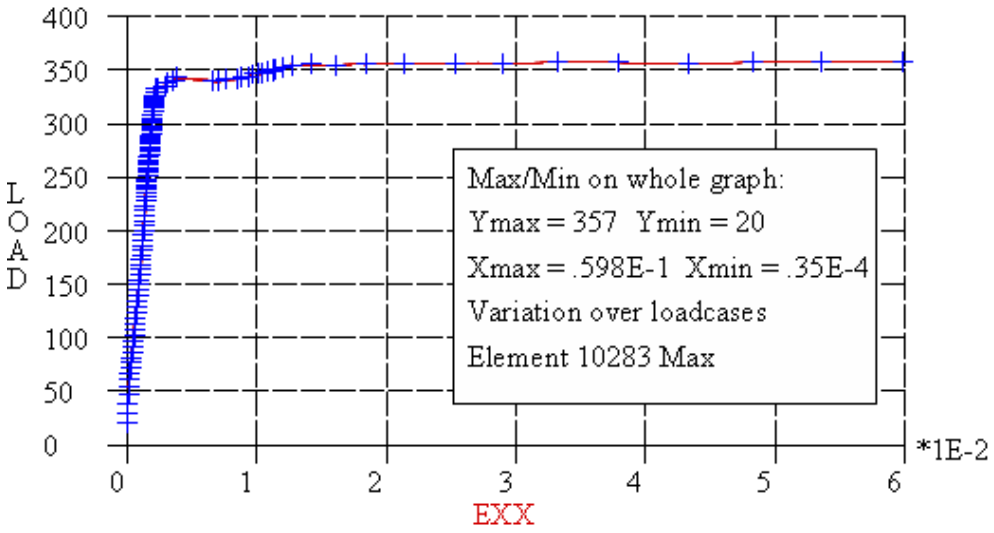

Figure 8.30 Development of the maximum tensile reinforcement strain

What is striking in figure 8.30 is that up to a 330 kN load the reinforcement strain still increases in a linear fashion, after which the reinforcement reaches the yielding stage. Just before a load of 350 kN the subsequent stage of the strain is still relatively admissible in terms of size. With hindsight one may say that at this point hardening would have to be added to the material quantities of the reinforcement. In the failure limit state also the maximum strain values for the stirrups are +0.06 and -0.055 for the upper reinforcement. The added value regarding the maximum failure load is, however, minimal in view of the horizontal branch of the strain in figure 8.30. These absolute maximum value for the reinforcement section is taken from the legend of figure 8.29. It is 4.91×10^{-2}, which is a factor 10 increase compared to the average reinforcement section of figure 8.28, being 4.19×10^{-3}.

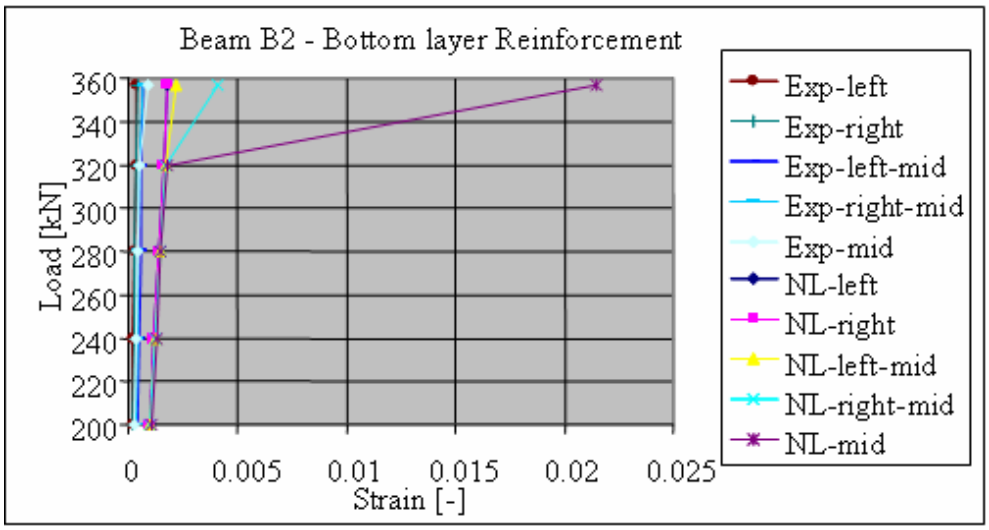

Figure 8.31: Comparison of strain development in bottom layer of tensile reinforcement in sections of the experiment and the FE-NL analysis

Also, in beam B2 the measured strains at the location of the tensile reinforcement do not agree with the strains calculated through the FE-NL analysis. The crack strain of the concrete is shown in figure 8.31 along half the length of the beam.

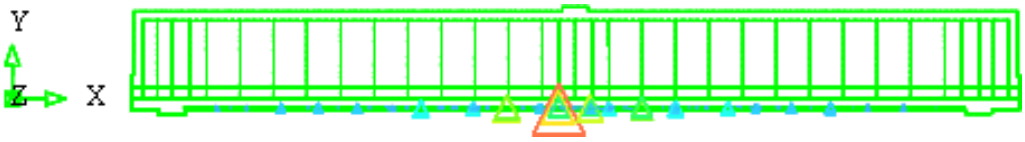

Figure 8.32 Crack strain concrete bottom fibre beam B2

Figure 8.32 shows that there is only one dominant crack strain at the bottom fibre in the beam near the location of the load plate at the midspan posisiton. Figure 8.33 shows these locations more in detail.

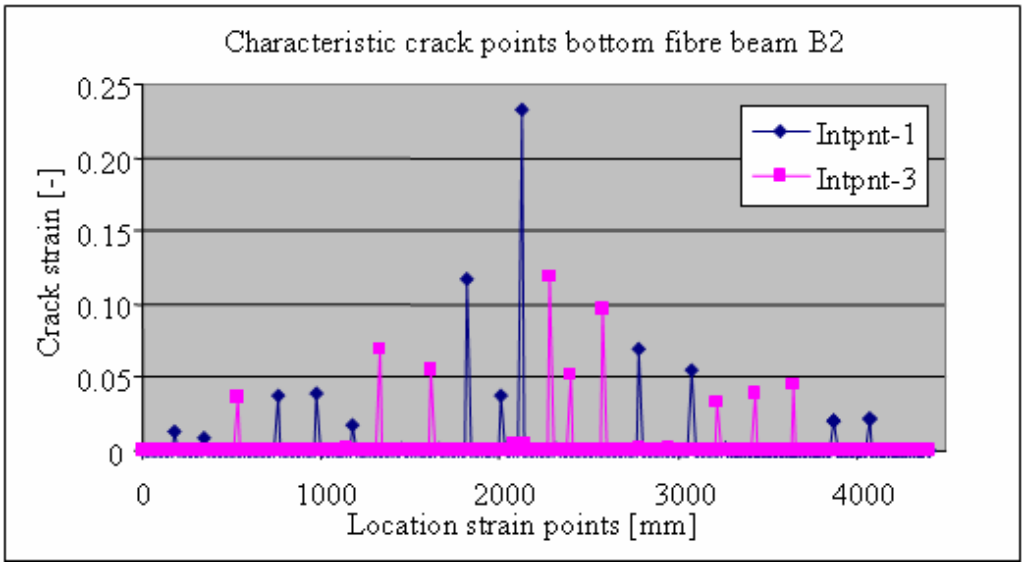

Figure 8.33 Crack strain at lower fibre of concrete at ULS load level along the length of B2 beam

Figure 8.33 shows a uniformly distributed pattern of the dominant crack distances mainly in the bending area of the beam. The crack distance is once again approximately 200 mm, which again agrees with the head to head stirrup distance.
Figure 8.33 clearly shows that the cracking behaviour is highly local, with only a single integration point cracking, whereas the second integration point at the same height in the lower fibre is not subjected to crack pattern yet. Therefore here the crack bandwidth is also limited to one length, belonging to one integration point.
The maximum value of the crack strain is 0.233, the second maximum value of the strain has a value of 0.122. Both values belong to bending cracks. Using an entered crack bandwidth of 9.2 mm this produces a maximum crack width of 2.14 mm. The measured crack width in the experiment was 1.6 mm in the bending area. Again this is a matter of choosing the right failure load limit. The development of the crack strain at this point gives a better view of comparing the crack width results, which is shown in figure 8.34. The development of the crack strain may be termed fairly linear till almost the ULS load level. Only at the last stage of the strain increase the strain growth becomes diffuse. In this case it is probable that the shear force crack will be the determining factor, the bending crack becoming smaller.

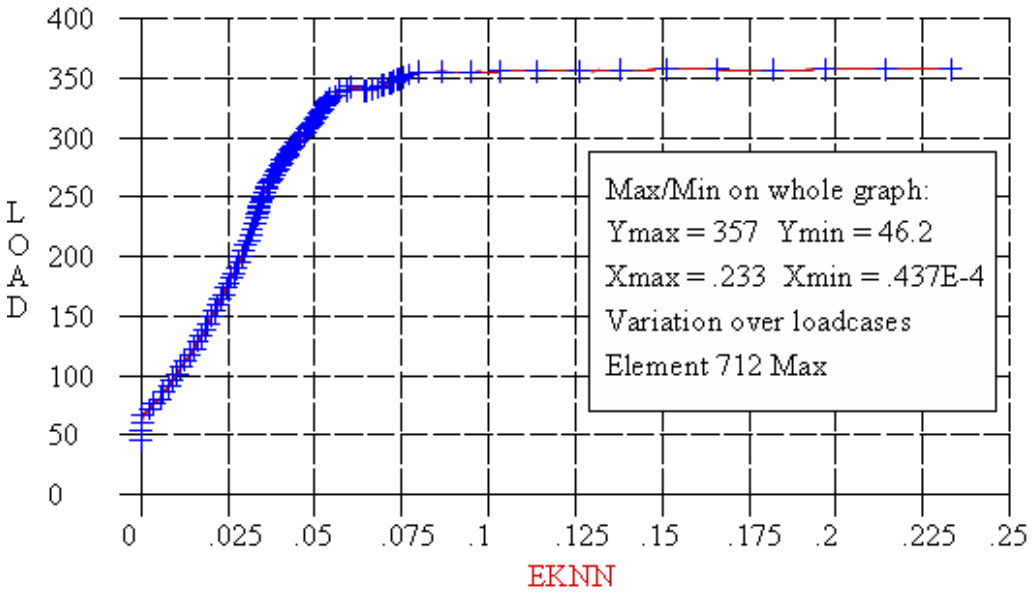

Figure 8.34 Development of crack strain in bending crack in lower fibre of B2 beam

The maximum value for the crack strain is 0.233, as was shown earlier in figure 8.33. The development of the width of the bending crack in the experiment can subsequently be compared to the development of the width of the same bending crack in the analysis, as is shown in figure 8.35.

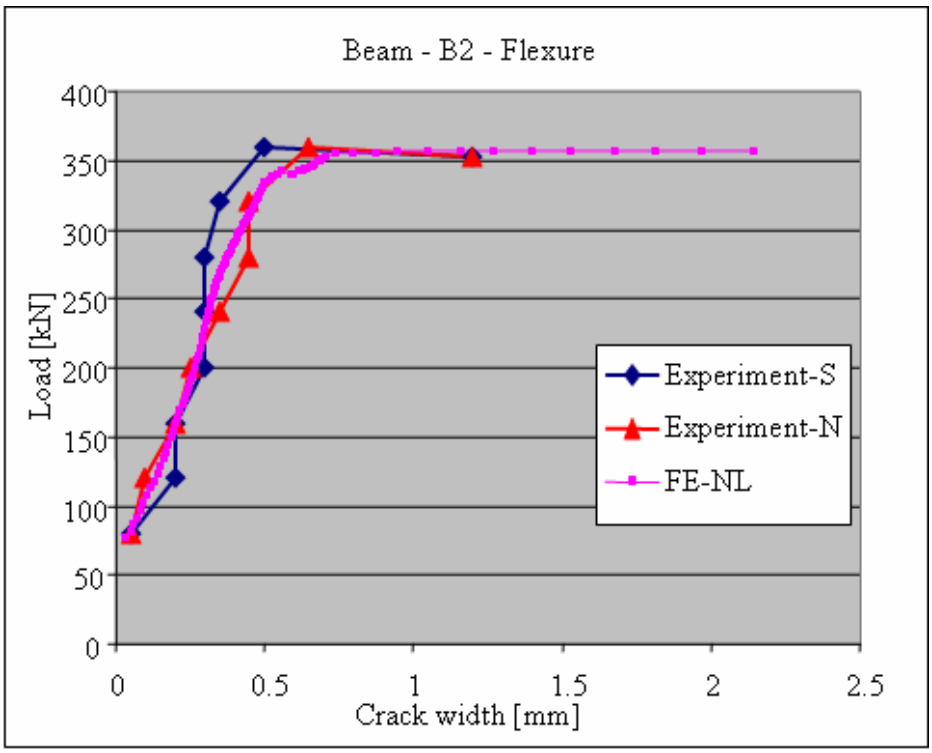

Figure 8.35 Development of crack width of bending crack in beam B2 experiment and analysis

One may take from figure 8.35 that the crack widths agree well with each other. In the ultimate limit state the values are even equal. The crack strain at a 228 kN load, the serviceability limit state, is 0.03. Again with a crack bandwidth of 9.2 mm (half the length

of the element) at SLS load level this already means a crack width of 0.28 mm, again larger than the admissible 0.2 mm at this load level. This crack width is therefore certainly too large!
The crack pattern in the shear force cracking area, to the left of the maximum crack strain in figure 8.33 with an X-coordinate of approximately 1,300 mm, is shown in figure 8.36.

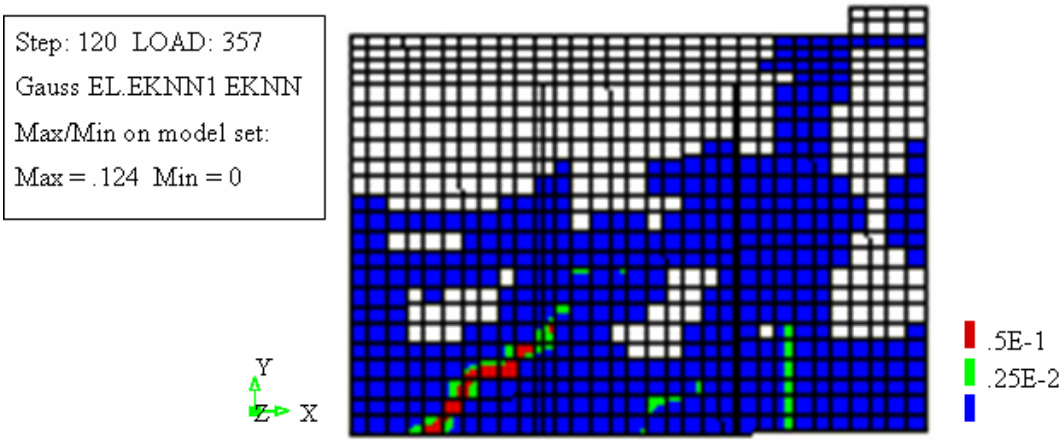

Figure 8.36 Cracking area of shear force crack in beam B2 at failure load

We see that in figure 8.36 the direction of the crack has also a 45˚ crack orientation, similar to the orientation of beam A1. Also, the height of the cracking area is as large as in beam A1. This means it clearly concerns a shear force crack in the tensile area of the beam. It also appears that the width of the distribution of the crack is slightly larger than with the shear force crack in beam A1. This is presented in a diagram showing the strains along the shear force area in a pattern of 5×5 elements, as was done in figure 8.19.

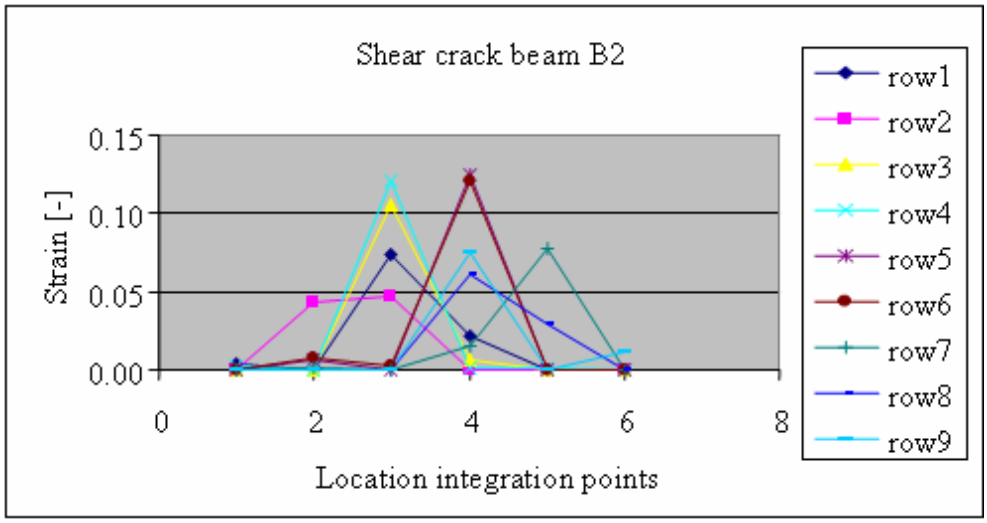

Figure 8.37 Crack strain in shear force area of beam B2

Figure 8.37 clearly shows that the crack strain is limited to the width of only one integration point within an element, meaning that the crack bandwidth may be set again at 9.2 mm, also for the shear force crack. This leads with a maximum crack strain value of 0.124 and a crack orientation angle of 45˚ to a maximum crack width of 1.66 mm. The measured value in the B2 experiment produced a value of 0.5 mm. Unfortunately, the publications on the experiments are silent on the location and the development, because they only give a value at failure load. However, the exact location of the measurements in

the experiment being of prime importance, if only because of the location of the shear force crack found through the numerical method. This is found just near the upper tensile reinforcement, which is not an obvious location to perform measurements! Finally, the development of the crack strain in the element with the maximum crack strain is shown in figure 8.38.

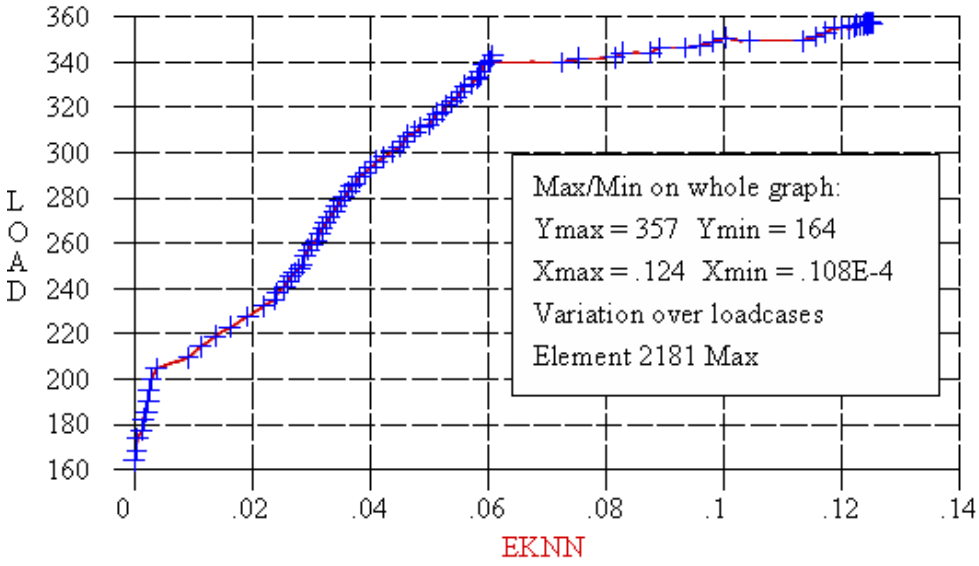

Figure 8.38 Development of crack strain in shear force area of beam B2

Also, figure 8.38 shows that at the SLS level (=228 kN) there could be still a small shear force crack pattern. At a loadlevel of 204 kN a transition point becomes visible. At the 340 kN load level the growth of the shear force crack is considerable, to be followed by a subsequent stage up to the failure load of 354 kN. The development of the crack width is shown in relation to the experiment in figure 8.39, albeit that the experiment only produced final values.

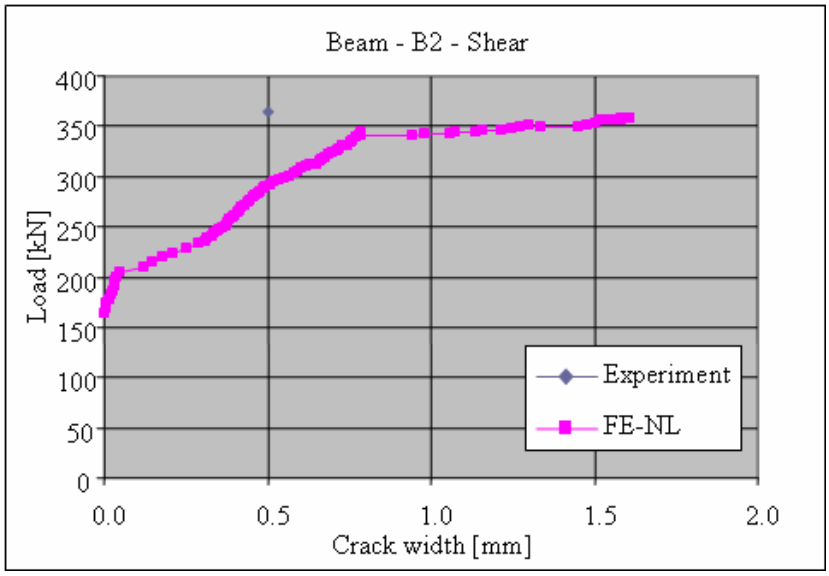

Figure 8.39 Development of the shear crack width till the ULS load level in beam B2 in FE analysis and experiment

Figure 8.39 demonstrates that the absolute value of the total failure load of the experiment is also achieved through the FE analysis, albeit at a much larger crack width.

8.4 Beam C3 experiment non-linear analysis

8.4.1. Input non-linear material parameters

In the numerical simulation of beam C3 use is made as well of the multi-linear compressive strength-strain diagram in order to be able to simulate the Popovics model. The 28 day cylinder compressive strength in this experiment is rather high compared to the other two experiments, namely 43.5 N/mm^2, with a corresponding Young's modulus of 34,300 N/mm^2. The compressive strength-strain diagram is shown in figure 8.40.

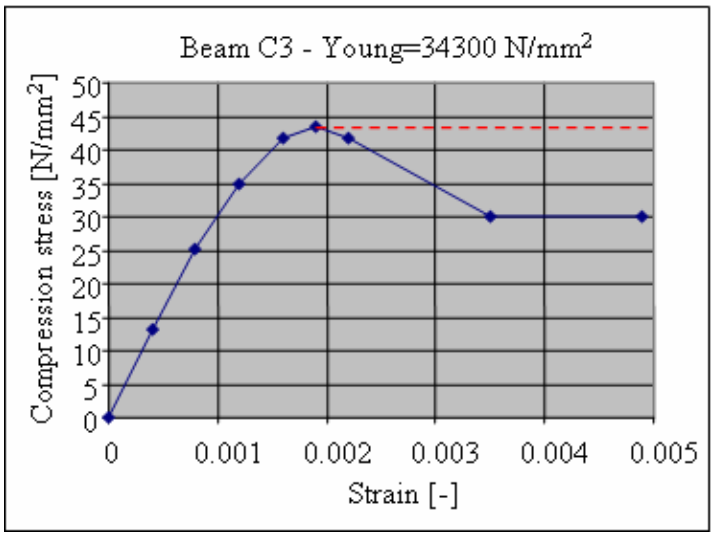

Figure 8.40 Compressive strength-strain diagram in beam C3

The maximum aggregate size is, once again, 20 mm. This simulation of the experiment also uses the Hordijk softening diagram, but this time with an admissible tensile strength of 3.7 N/mm^2, which is calculated directly from the admissible compressive strength. Because the dimensions of beam C3 are different, the element grid was also slightly adjusted. The new principal tension strength-strain diagram is shown in figure 8.41.

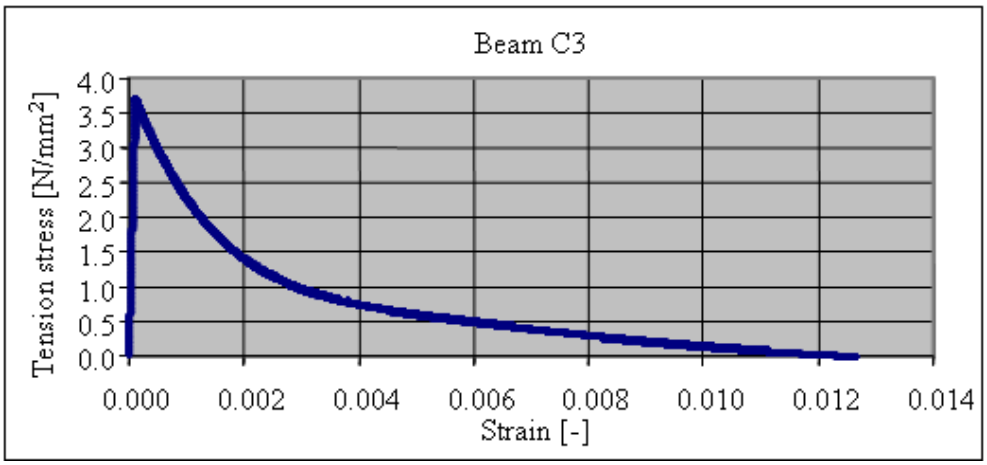

Figure 8.41 Principal tension strength-strain diagram in FE simulation beam C3

The crack energy is directly derived from the Model Code 1990, being 0.103 N/mm/mm^2. Assuming a crack bandwidth of 11.15 mm (half the length of the element), this produces a value for the surface below the curve of figure 8.41 of 0.103/11.5=0.0092. This value is almost equal to the calculated integral value of figure 8.41. This therefore provides a

check. All other structural parts are also included into this simulation model for the C3 experiment, in line with the procedure earlier described for experiments A1 and B2.

8.4.2 Global results of C3 experiment simulation

The load-deflection diagram for the middle of beam C3 is shown in figure 8.42.

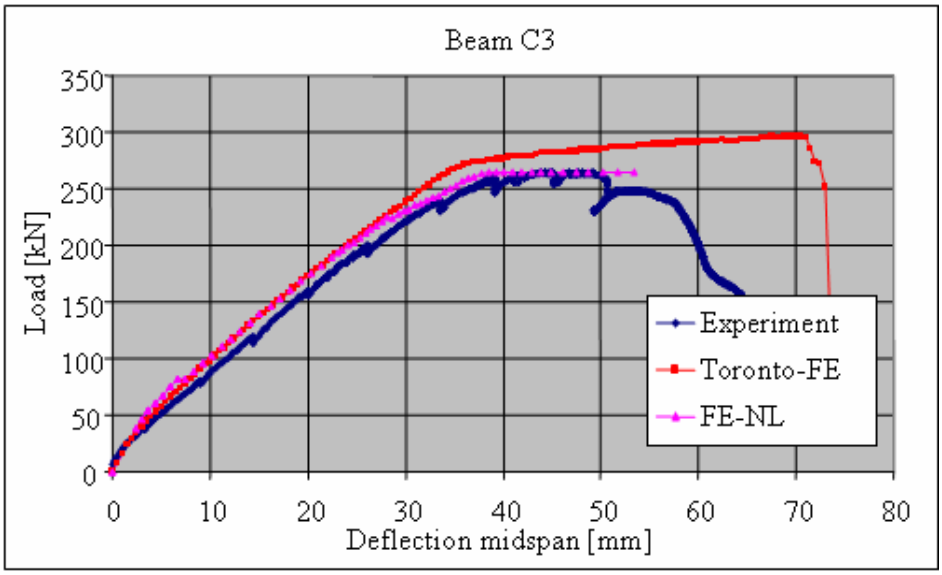

Figure 8.42 Load-deflection diagram of numerical simulation of midspan beam C3

Figure 8.42 demonstrates that the load-deflection diagram of the experiment matches the FE simulation well, and that there is nearly no tension stiffening. The FE analysis produces a maximum failure load of 264 kN, which equals the experiment. The experiment had a corresponding deflection of 45 mm. This load-deflection diagram shows discontinuities that hamper the progress of the non-linear calculation process. A comparison between the various crack patterns of the experiment and the FE-NL analysis is shown in figures 8.43 and 8.44.

Figure 8.43 Crack pattern at failure load in experiment

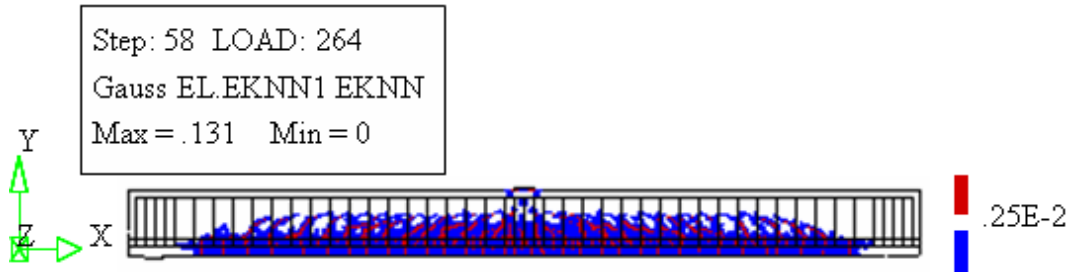

Figure 8.44 Crack pattern in FE analysis at failure load of 264 kN

Both figures correspond well. There is a myriad of cracks, veering off from the tensile bending cracks at the lower side of the beam through the bottom and at the upper layer of the tensile reinforcement towards the point of application of the load. Also in this beam there is slip between the tensile reinforcement in the bottom layer and the abutting concrete, in view of the high tensile stress around the tensile reinforcement bars. In order to enhance the global insight into the beam behaviour, two more figures are presented. Figure 8.45 shows the ultimate compressive strain of the concrete when the ULS load level limit is exceeded. Figure 8.46 gives an overview of the plasticity areas of the various reinforcement bars at the failure loadlevel.

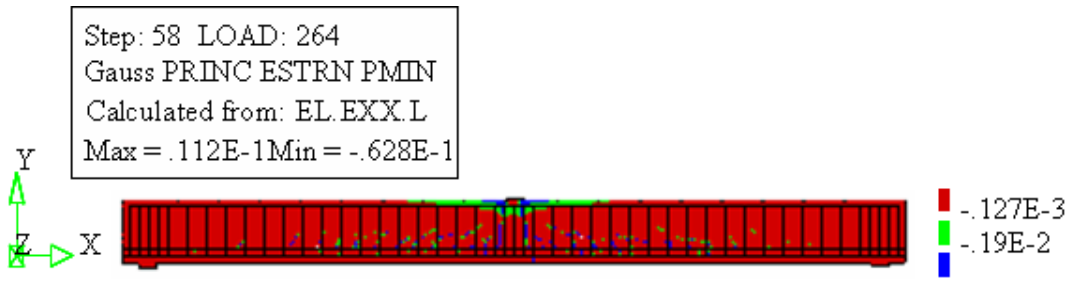

Figure 8.45 The ultimate compressive strain of concrete component at failure load of beam C3

Figure 8.45 shows that in a limited area around the bearing plate the ultimate compressive strain is exceeded. Also visible around the cracks are small areas in which the ultimate compressive strain of concrete is exceeded.

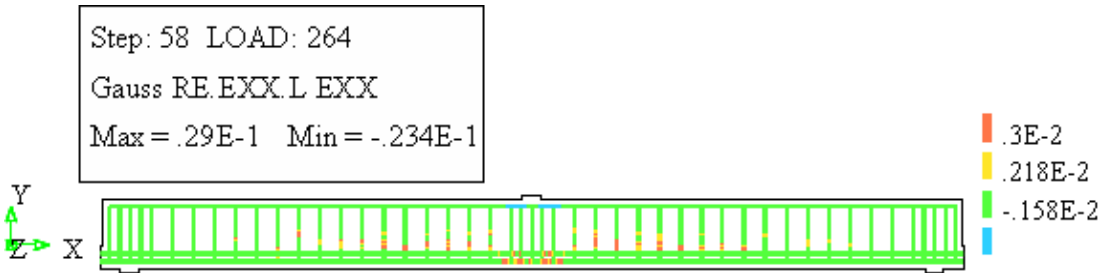

Figure 8.46 Plasticity areas in reinforcement at failure load of beam C3

Figure 8.46 shows that plasticity areas mainly occur in the stirrups in the bottom part of the beam near the cracks, as well as beneath the bearing plate at the location of the upper and lower reinforcements.

8.4.3 Local results of C3 experiment simulation

From a numerical point of view, we will compare the indicated strains in the reinforcement and the concrete in the publication of the experiments and the FE-NL analysis, starting with the strains in the tensile reinforcement.
The strain along the tensile bottom reinforcement in figure 8.47 shows a peak behaviour at the midspan location of beam C3. The absolute value at failure load is 0.28×10^{-1}, which is well above the yield limit of 2‰ and more then a factor ×10. For this local behaviour hardening would have to be entered, but it is still very local so that the effect will probably be marginal. The experiment has a strain in the tensile reinforcement of 1.76×10^{-3}. Comparison of both values also produces a factor more then ×10.

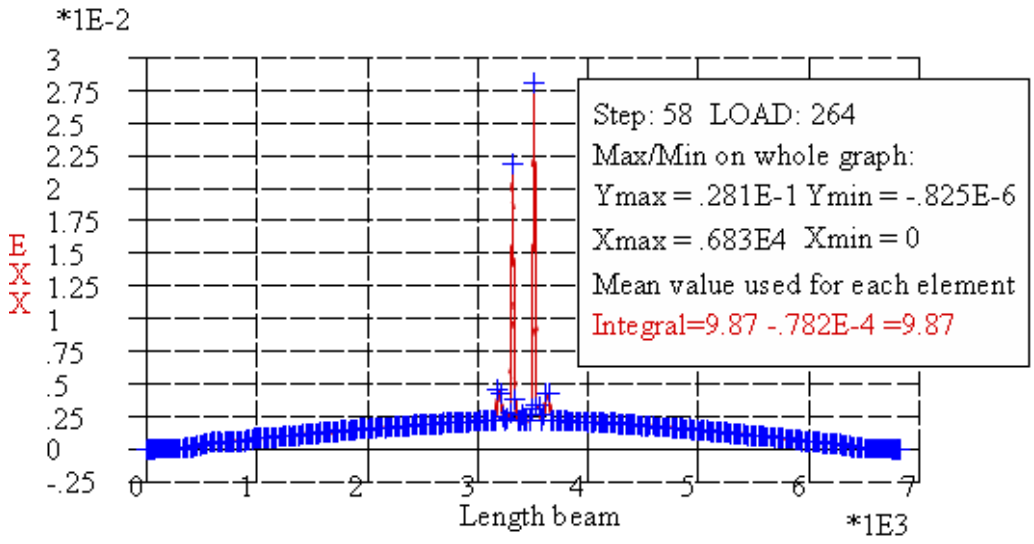

Figure 8.47 Strain in the bottom tensile reinforcement layer of beam C3

All the more reason to zoom in on the measuring area in the experiment with a length of 1,000 mm. The strain along the measuring reinforcement section is shown in figure 8.48.

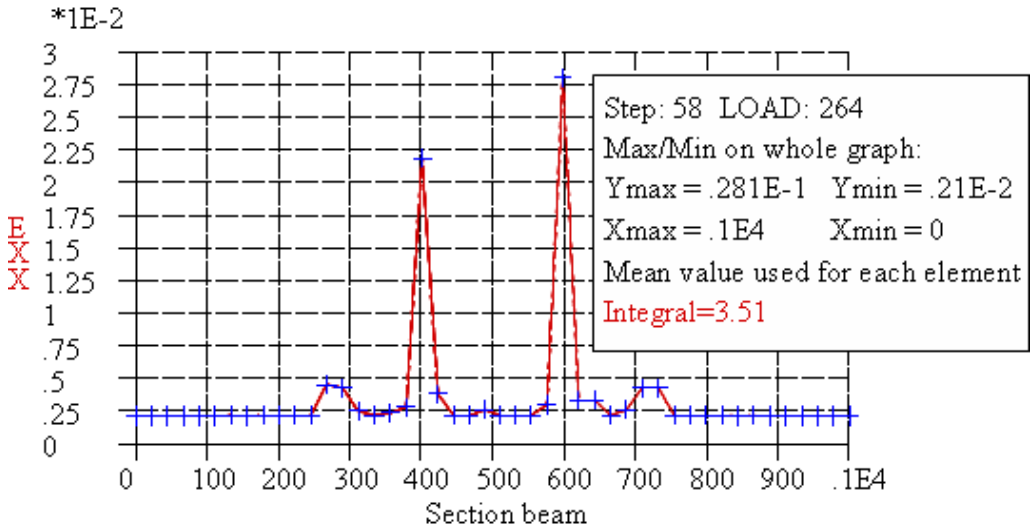

Figure 8.48 Strain over section length in the bottom tensile reinforcement layer of beam C3

The minimum value of the strain over the section length in the bottom tensile reinforcement layer has a value of 2.1‰, whereas the average value of the strain along the measuring area is still 3.5‰. The first value lies close to the published value of the strain in the tensile reinforcement(=1.76×10^{-3}), but the second value is well above it, by a factor 2. In this case it is also possible to show the development of the strain in the reinforcement element to the maximum value at ULS load level. This is done in figure 8.49. Up to a load of 255 kN the strain increases in a linear fashion. After this load level, yielding occurs with considerable values to a maximum of 2.9×10^{-2}.

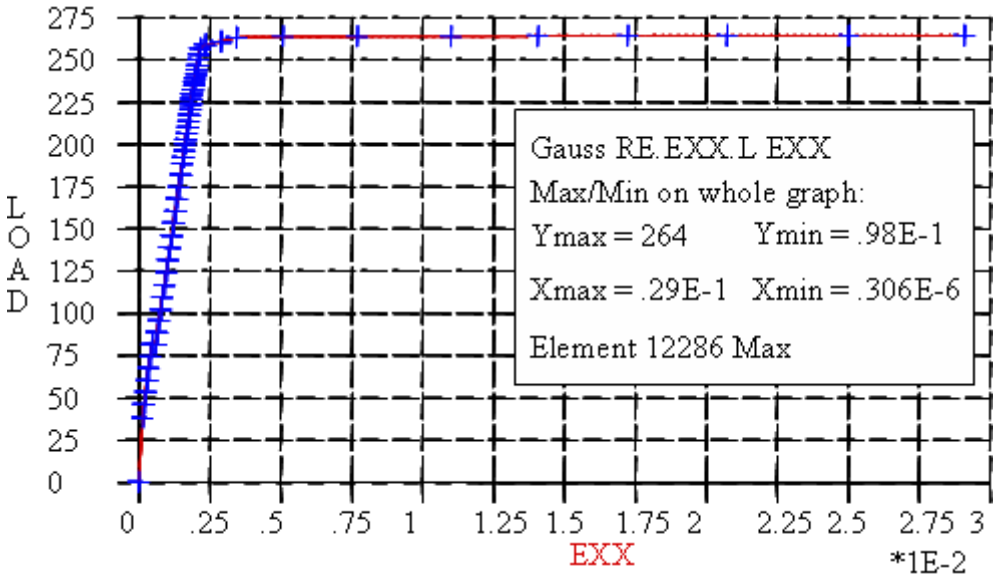

Figure 8.49 Development of the strain in the maximum reinforcement element of the tensile bottom reinforcement in beam C3

At the SLS load level(=165 kN) the tensile reinforcement shows a strain value, which is lower than 0.12%, so there is a lot of remaining capacity.

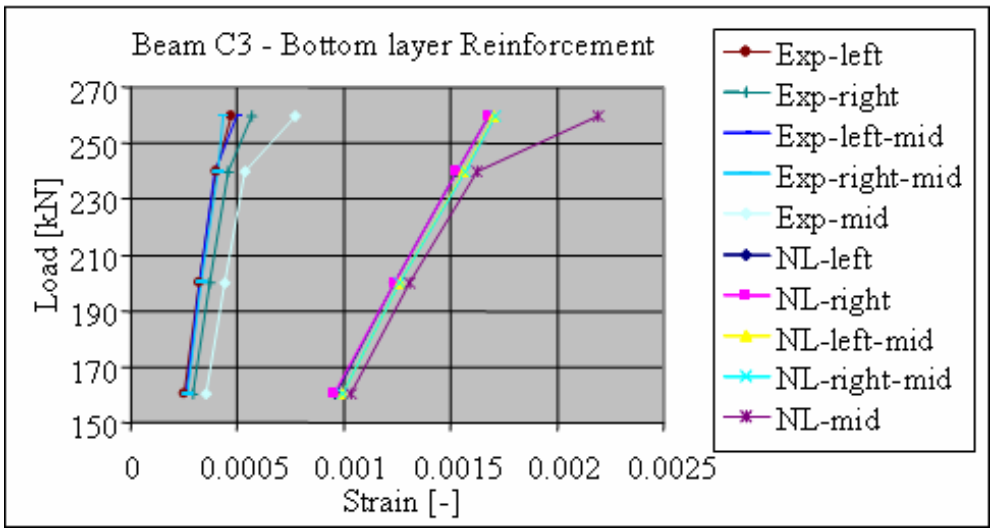

Figure 8.50 Comparison of development of strain in sections of bottom layer of tensile reinforcement in beam C3 experiment and FE-NL analysis

Figure 8.50 shows also in the case of beam C3, that the strains measured in the experiments do not agree with the calculated strains in the tensile reinforcement of the bottom layer.
Below, we will address the strain in the various concrete components, namely the bending area and the shear force area.

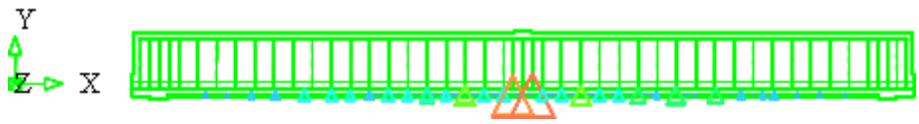

Figure 8.51 Crack strain concrete symbols at failure load level beam C3

Figure 8.51 shows again that there are two dominant bending cracks at the midspan location of the beam C3. For the bending area use is made once again of the lower fibre across the length of the beam, as is shown in figure 8.52.

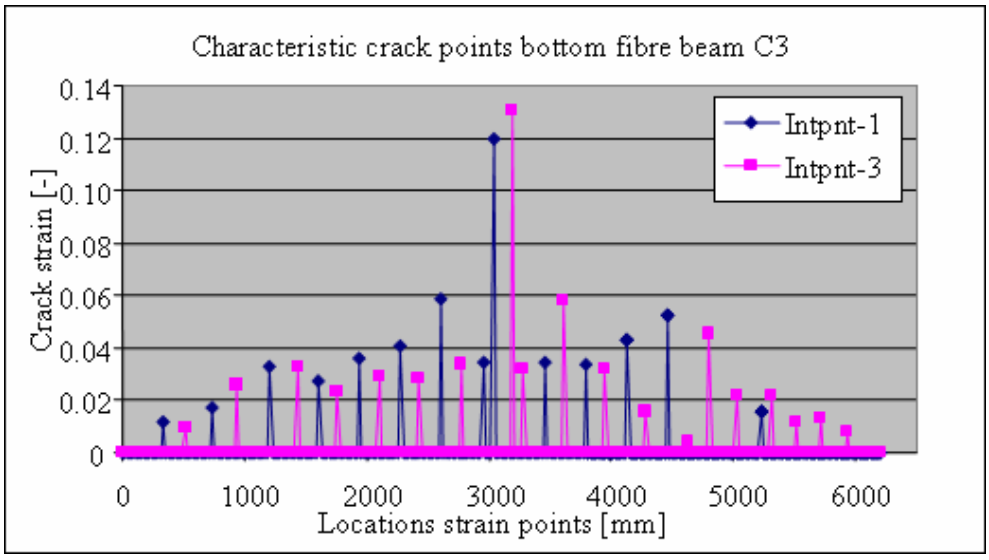

Figure 8.52 Crack strain in the bottom fibre of the concrete at the failure load level of beam C3

The first thing worth noting is the uniform pattern of the head to head distance between the dominant cracks in figure 8.46. Also remarkable is the crack along the length of the beam. The maximum crack strain has a value 0.13. On the other side of the beam a value of 0.12 is even seen, both agreeing with the locations of both ultimate strains in the tensile reinforcement in figures 8.47 and 8.48. On the basis of a crack bandwidth of 11.15 mm this leads to a maximum crack width of 1.46 mm. In the experiment a value 0.9 mm was found in the bending area. The development of the maximum crack strain in the element with the maximum value for the crack strain till failure load level is shown in figure 8.53.

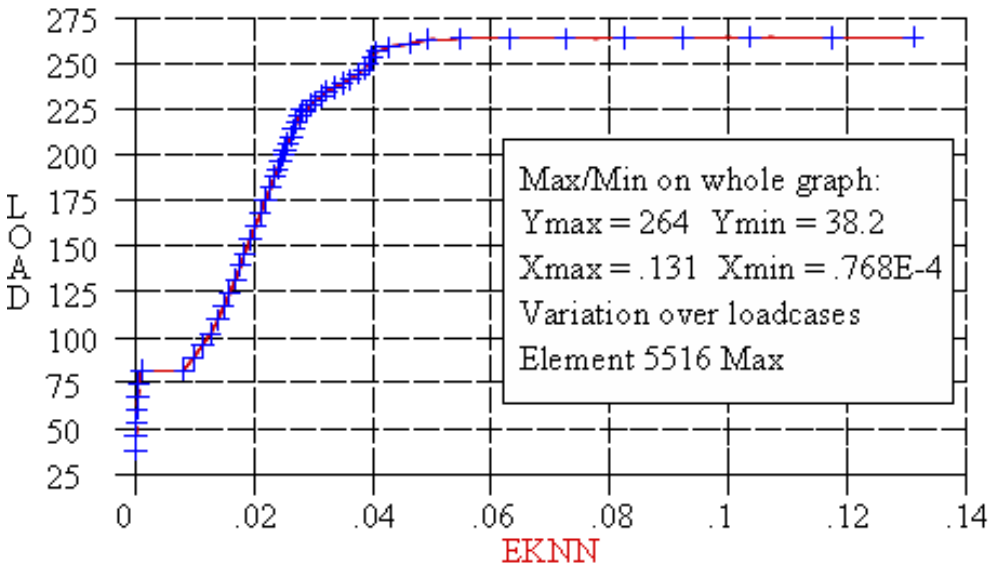

Figure 8.53 Development of maximum crack strain in the maximum element bending area of beam C3

The development of the crack strain in the lower fibre of beam C3 shows that this increases most after the load is increased above 255 kN. At this load level, the corresponding crack width is small with a value of 0.45 mm, but after this load level, the crack width value rises to the 1.46 mm mentioned earlier within a load increase of 10 kN. The development of the crack width is a good yardstick for a comparison with the experiment, as is shown in figure 8.54.

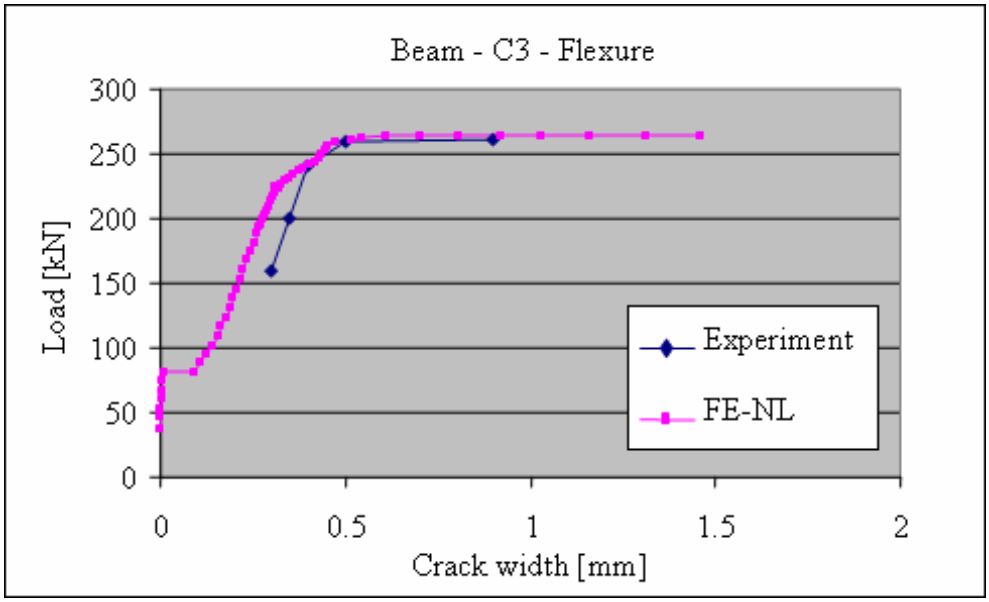

Figure 8.54 Development of crack width in bending crack experiment and analysis

In the experiment with this beam C3, no difference was made between observations on the north and south sides of the beam. There is a good match between the results of the experiment and the FE-NL analysis at failure level.
At the SLS load level of 165 kN the crack strain has a value of almost 0.03, leading to a calculated crack width of 0.3 mm. Figure 8.55 presents a contour plot of the area at the right side of the loading plate, where the maximum crack strain in the shear area occur.

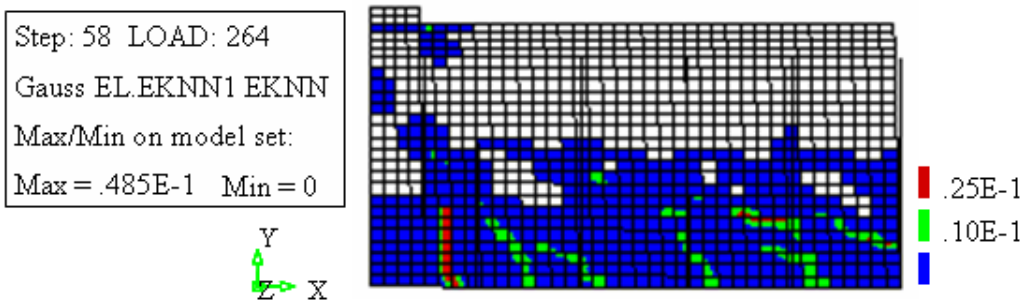

Figure 8.55 Contour plot of cracks in shear force area of beam C3

Figure 8.55 shows that the shear force crack area is close to the upper layer of the tensile reinforcement laying almost in a horizontal orientation on the right side of the figure. The maximum value for the crack strain in this area is 0.049, leading to a crack width of 0.55 mm. The experiment had a value of 0.25 mm, which is therefore exceeded by over 100%. For more reliability the crack strains are also shown along the rows in the 5×5 element pattern mentioned earlier. These strain patterns are shown in figure 8.56. In this figure 8.56 the limited width of the crack is striking as well, being the width of one integration

point of a structural element. This means that also in this case the assumed crack bandwidth in the FE analysis was processed correctly.

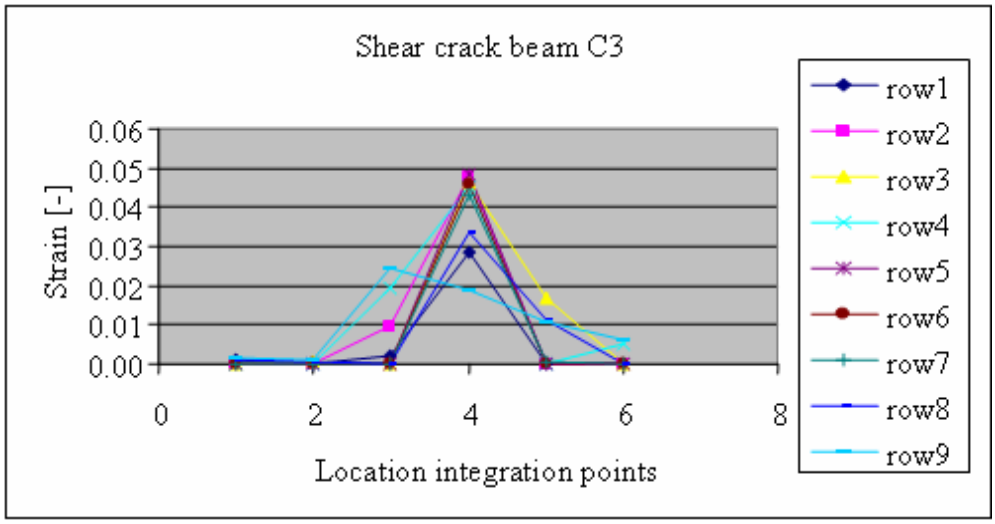

Figure 8.56 Development of the crack strain along the rows in the shear force crack area of beam C3

The development of the shear force crack in the element, where the maximum value of the crack strain occurs at the failure load, is shown in figure 8.57.

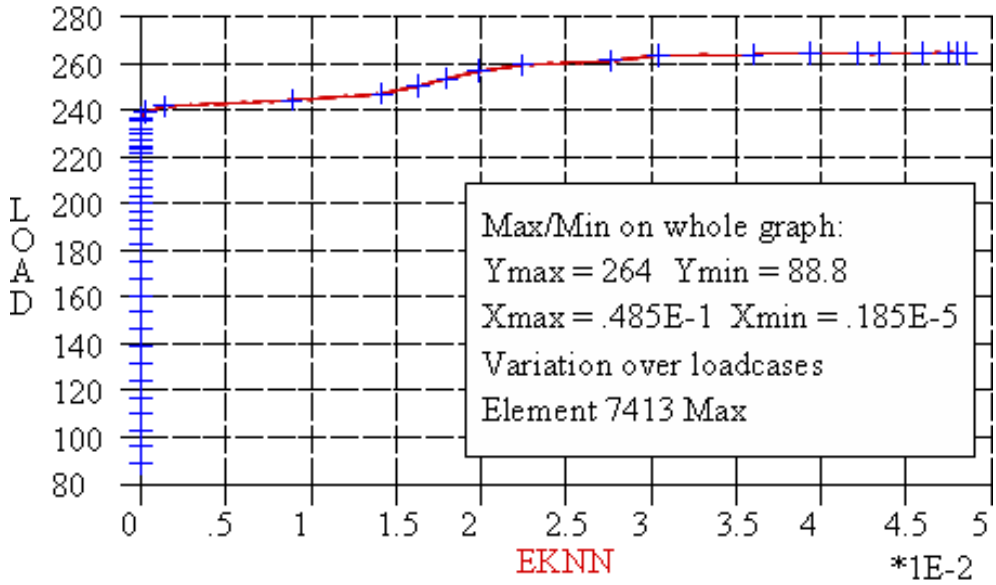

Figure 8.57 Development of crack strain in shear force area of beam C3

According to figure 8.57 the shear force crack starts developing far from the SLS level(=165 kN). At the 240 kN load level the strain grows quickly, from a crack width of 0.0 mm at a load of 240 kN to the value of 0.54 mm at 265 kN. In the experiment no shear force crack was measured according to the publication by Shim [Shim2000]. However, in the Vecchio and Shim paper [Vecchio2004] a value of 0.25 mm is mentioned for the crack width of the shear force crack at the ULS load level, albeit that it is unclear where this crack is located. Figure 8.58 shows the development of the experiment in relation to the FE-NL analysis regarding the shear force crack width. This figure 8.58 also demonstrates

that the one measured value is achieved and even exceeded by the calculated value, but that there are still major differences.

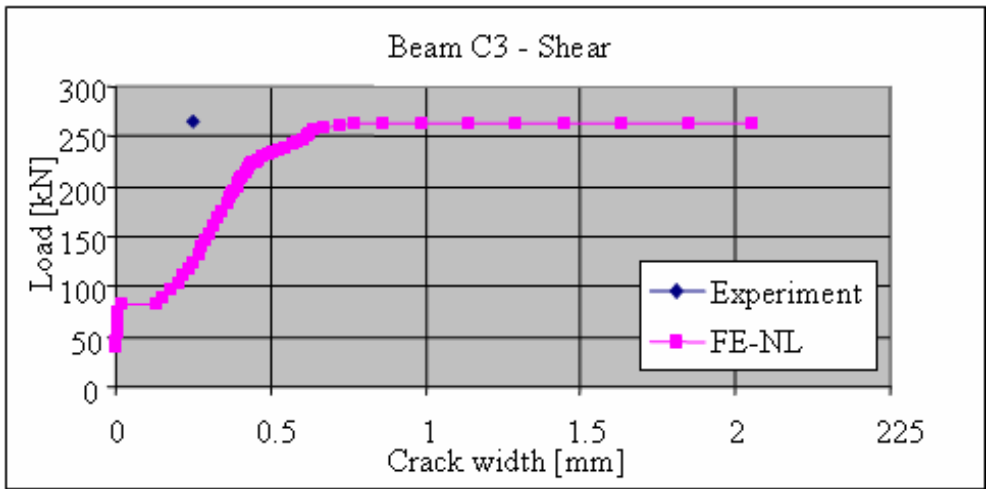

Figure 8.58 Development of crack width in shear force crack in experiment and FE analysis

8.5 Summary of and intermediate conclusions on global and local results of the three beams

For each beam the results fall apart into global and local results.

Global	A1		B2		C3	
	Exp.	FE-NL	Exp.	FE-NL	Exp.	FE-NL
Failure load [kN]	459	473	365	357	265	264
Corresponding vertical deflection [mm]	18.8	18.6	31.6	31.5	44.3	45.0
Crack pattern	Matching		Matching		Matching	
Local	**A1**		**B2**		**C3**	
	Exp.	FE-NL	Exp.	FE-NL	Exp.	FE-NL
Strain in tensile reinforcement [$\times 10^{-3}$]	1.17	2.06-4.46	2.87	2.15-49.1	1.76	2.1-28.1
Crack width bending ULS [mm]	0.50	0.53	1.60	2.14	0.90	1.46
Crack width shear force ULS [mm]	2.00	2.02	0.50	1.66	0.25	0.55
Crack width bending SLS [mm]	0.30	0.28	0.28	0.28	0.30	0.30
Crack width shear force SLS [mm]	-	0.20	-	0.28	-	0.0

Table 8.1 Summary of results of the three beam experiments and FE-NL analysis

Conclusions:

- The global results of the FE-NL analysis show a good match with the results of the experiment. Both the failure load and the corresponding vertical deflection in the middle of the beam correspond well.

- The global results for the crack patterns also show a good match.
- The local strain at the bottom layer of the tensile reinforcement also shows a considerable difference.
- The local results for the crack strains at ULS load level in the bending area show no good match. The horizontal branches of the development of the crack width at the ultimate load level underline the difficulties to get an exact value of the crack width at this load level.
- The local results for the crack strains at SLS load level in the bending area show a good match, except with experiment C3.
- The local results for the crack strains in the shear force cracking area do not always agree with each other, albeit that it is unclear where the measurements took place in the experiment.

9 RESULTS OF THE FE SEQUENTIAL ANALYSIS

9.1 Introduction

In chapter 8 we demonstrated that a full non-linear FE analysis produces global results that match the experimental results of chapter 7. For the local results there are some doubts. This time we will do the same for the presented sequential analysis of chapter 6. The presentation of the results is the same as in chapter 8, including a division into global and local results.

9.2 Sequential analysis simulation of the A1 experiment

9.2.1 Input non-linear material parameters for the sequential analysis

Just like in the FE-NL analysis, if set off against a linear static analysis, the sequential analysis also requires the addition of non-linear material parameters to the input data of beam A1.
For plasticity, use is made of robust material models such as Von Mises, as well as for reinforcement, and a simple uni-axial compressive-strain diagram for the design of a concrete structure. This plasticity normally occurs when the beam has passed the SLS load. This means that up to this load level use can be made of a linear static analysis, something that strongly accelerates the total processing time of the calculation process.
The cracking behaviour of the concrete will then be processed in an additional external executable, in which the material adjustment can be changed from isotropic to orthotropic.
Between the SLS and ULS load levels use will be made of the non-linear calculation module, including the non-linear material options for plasticity of both concrete and reinforcement.
The overall processing time will be addressed in the evaluation.

9.2.2 Global results of the sequential analysis of the A1 experiment simulation

For a determination of the failure load (ULS), the analysis of beam A1 requires 63 analyses, 35 of which may take place in a linear static manner. These first 35 analyses reach a load level that is supposedly the serviceability limit state (SLS). This is a supposition, because in principle these beams are meant to establish the failure load. In the simulation in advance a lower limit criterion has been determined for the material parameters entered, meaning that the SLS load can be calculated using a partial load factor (=1.6) in relation to the failure load. This means that with a ULS load of 459 kN, the SLS load value may be set at $459/1.6 \approx 286$ kN.
The 63 sequential analyses are subdivided into 16 load increments. Each load increment stage is between 25 and 33 kN, whereas for each load increment itself four analyses are in order. This was done to achieve a convergence criterion with a next increase of elements that change from isotropic to orthotropic.
As with the FE-NL analysis the sequential analysis also allows the set-up of a load-deflection diagram of the vertical deflection in the middle of the beam. This diagram is shown in figure 9.1.

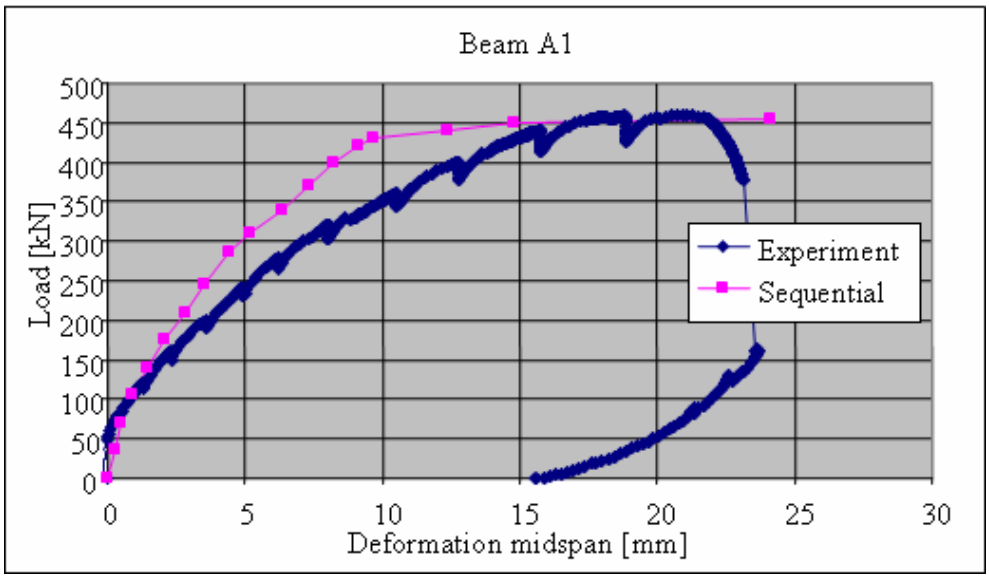

Figure 9.1 Load-deflection diagram at the midspan location of beam A1

The sequential analysis allows a robust determination of the failure load as well. As with the FE-NL analysis 'tension-stiffening' may be seen, but as the failure load is approached this aspect has disappeared from the load-deflection diagram.
The vertical deflection in figure 9.1 in this analysis is 17.9 mm, the value of the experiment being 18.8. This difference is negligible, because with a small load increase of 1 kN the 18.8 mm will be exceeded by far. The difference in the failure load of the experiment (459 kN) and the sequential analysis (450 kN) may also be neglected.
The vertical deflection with the FE-NL analysis was the break-down criterion to determine the failure load in this analysis and with the vertical deflection value of 17.9 mm from the sequential analysis that was found, is a good approximation. Figure 9.2 shows the crack pattern at the ULS load level.

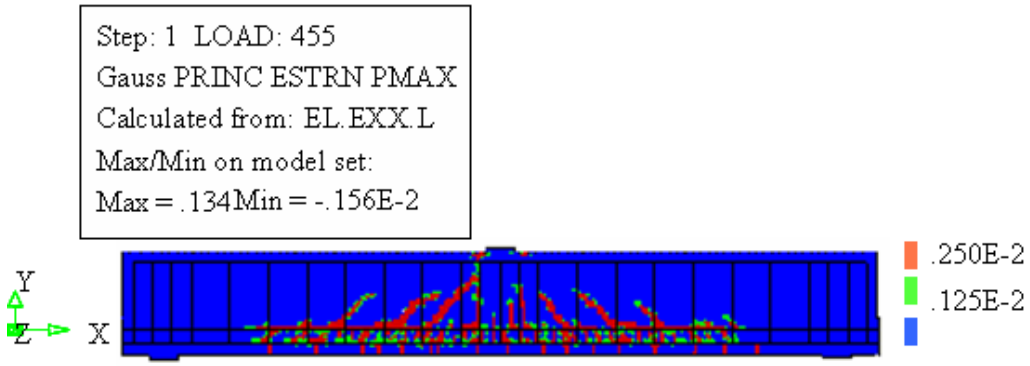

Figure 9.2 Crack pattern in concrete at failure load on beam A1

The crack pattern from figure 9.2 shows a clear shear force crack area near the load in the middle of the beam. Cracks also occur at the failure load around the tensile reinforcement at the lower layer of the beam. To the left and right of the bearing plates there is also some local crack pattern. The global behaviour of this analysis matches the experiment and the FE-NL analysis. The maximum size of the crack strain is 0.134, for which see the legend of figure 9.2. The location, however, is near the bearing plates.
Finally, the areas where the ultimate compressive strain of concrete and the plasticity of the reinforcement are exceeded at the ULS load are shown in figure 9.3 and 9.4.

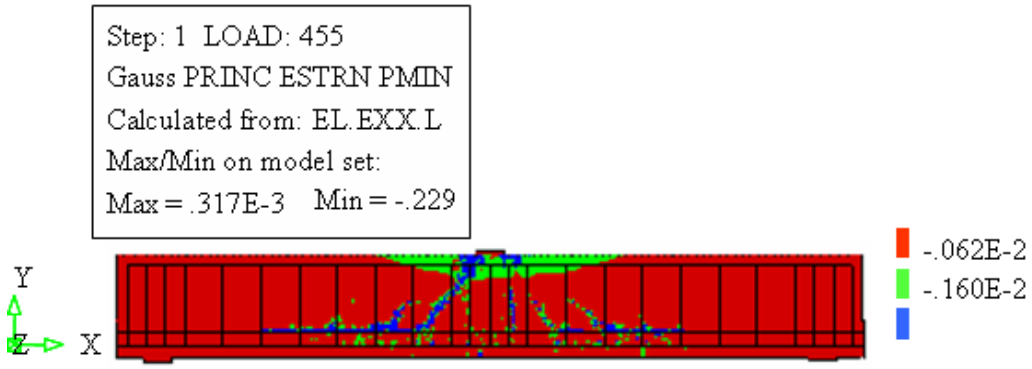

Figure 9.3 Areas where ultimate compressive strain of beam A1 is exceeded at failure load

In figure 9.3 we see that plasticity areas occur in the concrete near the dominant tensile cracks. Also remarkable is of course the local plasticity near the load bearing plate, with a minimum compressive strain of -0.23. The distance along which the ultimate compressive strain areas occur has a total length of 2×470 mm.

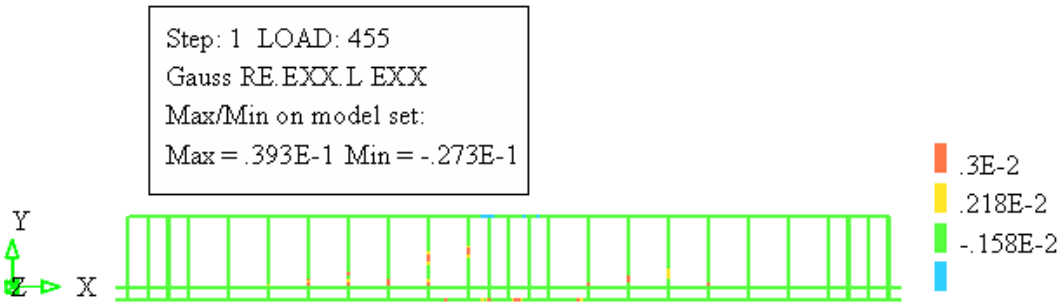

Figure 9.4 Plasticity areas of reinforcement bars at failure load of beam A1

In the sequential analysis plasticity does occur in the reinforcement at failure load as well. In beam A1 it all starts at the upper reinforcement near the bearing plates at a load of 370 kN. If the load is slightly increased, some stirrups start to yield, beginning with a load of 400 kN. The bottom tensile reinforcement layer starts to yield at a load level of 420-430 kN. At the 450 kN load level more sections of the reinforcement are yielding. So there is no longer any residual bearing capacity left in this beam.

9.2.3 Local results of the A1 experiment simulation

In order to obtain a local insight we will also look at the strain in the tensile reinforcement at the ULS load level. Remarkably so, the maximum tensile strain in the bottom tensile reinforcement has reached a maximum value of 1.97×10^{-2}, for which see figure 9.5. Figure 9.5 shows clear local behaviour of the tensile strain in the tensile reinforcement at the middle of the beam.

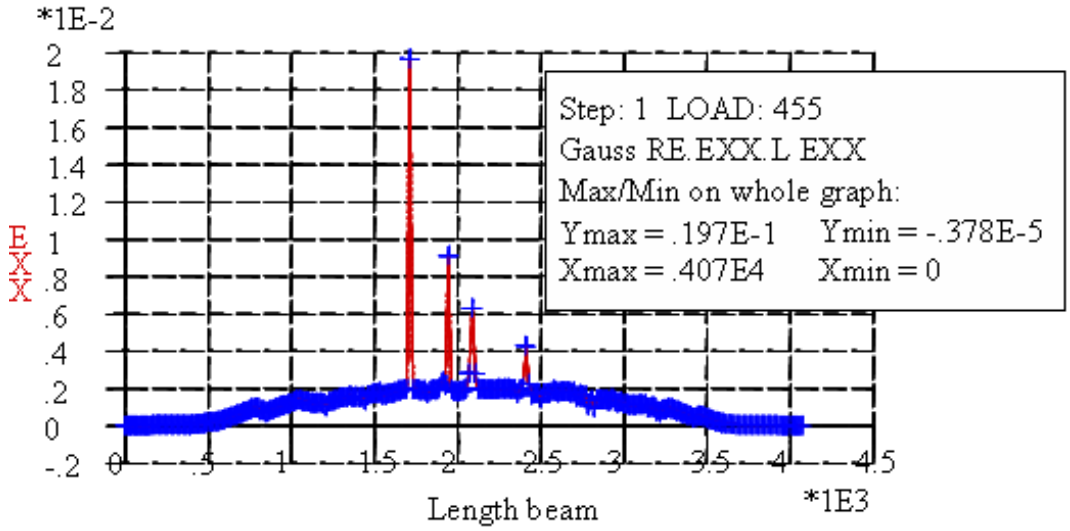

Figure 9.5 Strain distribution in bottom layer of tensile reinforcement of beam A1

A sectional layout with a length of 1000 mm of the tensile reinforcement is shown in figure 9.6. The heart of this section of the tensile bottom layer reinforcement is located in the middle of the beam.

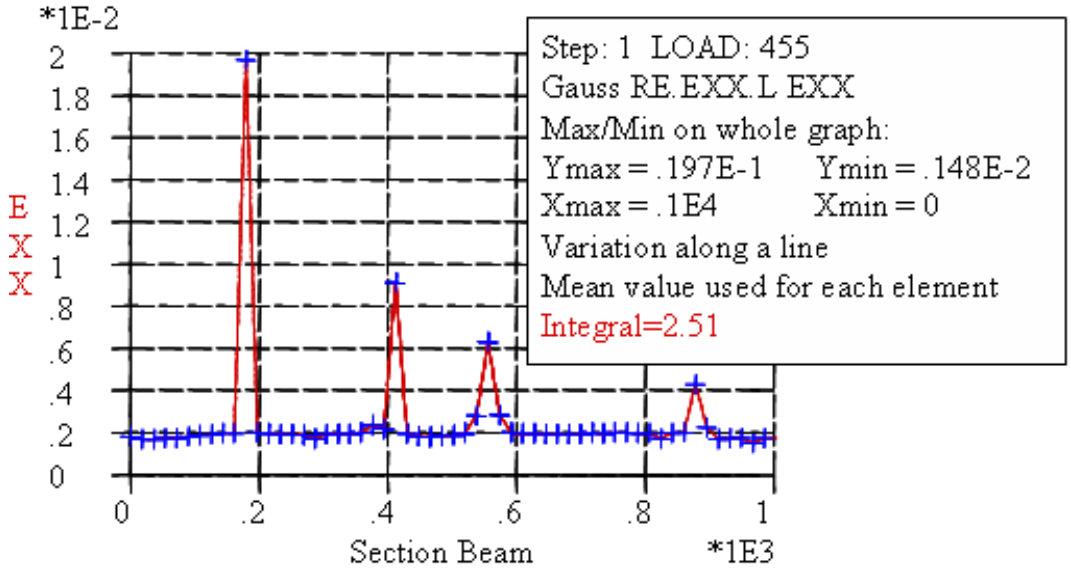

Figure 9.6 Strain distribution in bottom layer of tensile reinforcement along section of ≈1,000 mm of beam A1

In figure 9.6 we see that the average tensile strain in this part has a value of 2.51×10^{-3} and a maximum value of 1.97×10^{-2}. Neglecting the peak behaviour, the minimum strain value for this reinforcement layer would become 1.48×10^{-3}. This constitutes the range of results, being comparable to the values found in the FE-NL analysis. Now the crack strains in the flexure area of the beam.

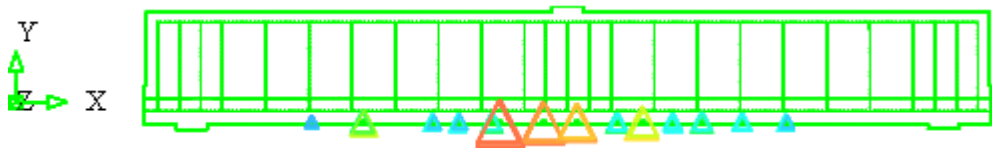

Figure 9.7 Crack strains in the flexure area of beam A1 at the ULS load level

Figure 9.7 shows that the maximum flexure cracks strains occur near the midpsan location of the beam, similar to the FE-NL analysis. The maximum value of the strain at midspan(X=1600 mm) is 0.42×10^{-1}. With a crack bandwidth of 8.75mm (=half the length of side of the structural element) this amounts to a crack width of 0.0.37 mm. This value has to be compared with the experimental value of 0.5 mm. However, in the sequential analysis the crack strain is distributed over both integration points. The band-width is not the half of the element side but has the length of the whole element side. The results of both integration points of the lower element side can be illustrated in figure 9.8.

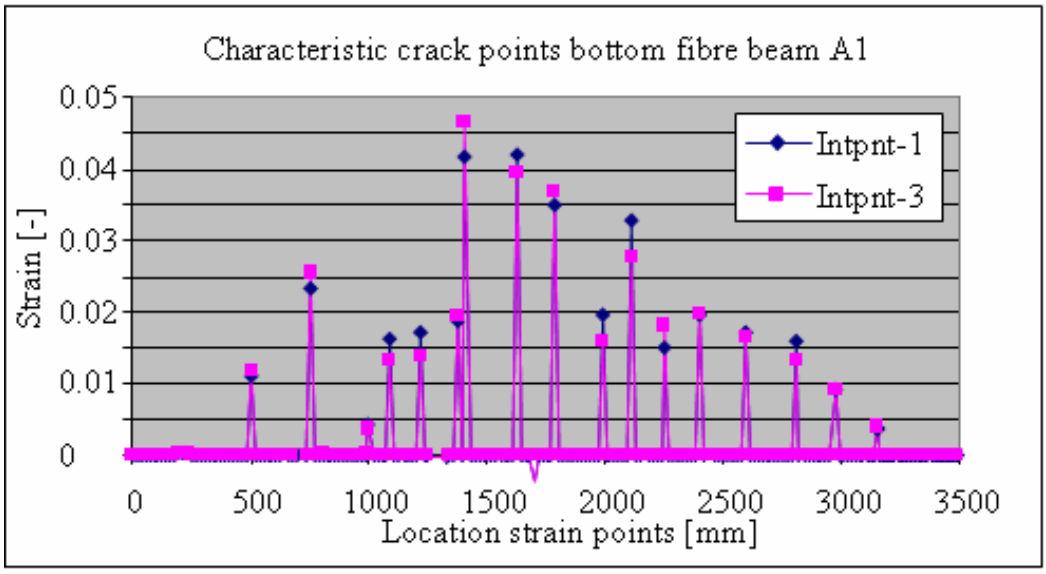

Figure 9.8 Cracking points in lower edge of concrete part at ULS load level along the length of beam A1

With the sequential method both the first and third integration points at the locations of the structural element show a crack strain, doubling the crack bandwidth. The crack width in the bending area is not 0.37 but 0.72 mm. The head to head crack spacing in figure 9.8 is ± 200 mm. This crack spacing is comparable to the head to head spacing of the stirrups used. So in this analysis type there is also one crack per stirrup head to head distance. Figure 9.9 shows the development of the crack width for both the experiment and the sequential analysis. We see that in figure 9.9 the absolute value of 0.72 mm for the crack width in the sequential analysis is higher than the value found in the experiment (0.5 mm). Still, the development of the crack width up to 0.53 at a load level of 435 kN is comparable to the experiment, while the different load level are almost similar to each other.
The SLS load level (=286 kN) counts a crack width of 0.22 mm. This value is a little bit lower than the 0.30 mm at the experiment.

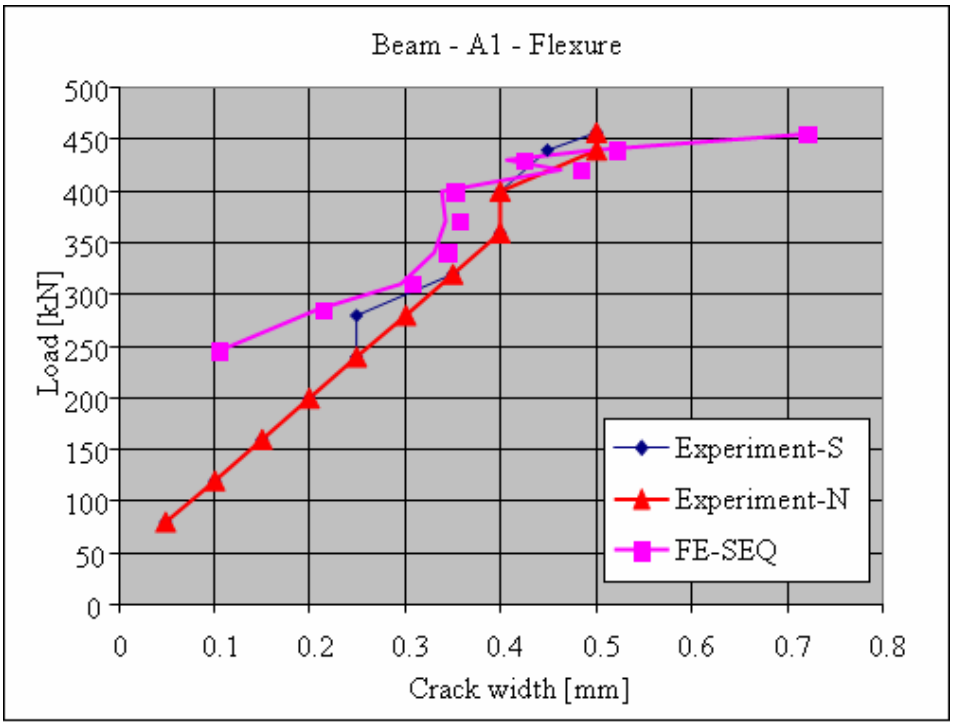

Figure 9.9 Crack width development in bending area experiment and sequential FE analysis

Below, we will address the crack strains in the shear force area in figure 9.10.

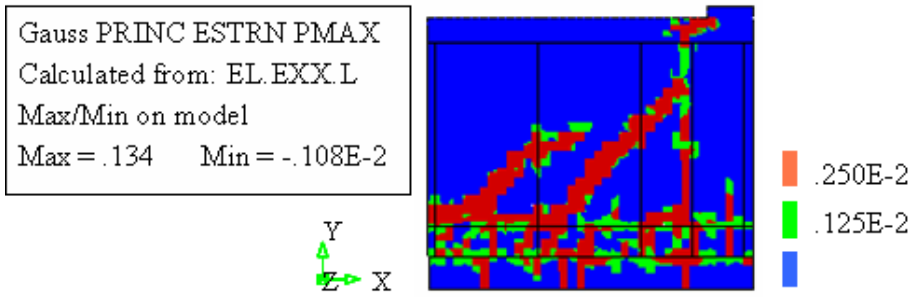

Figure 9.10 Strain distribution at ULS in the cracking area of the shear force area of beam A1

The maximum value of the crack strain is counted as 0.13, see the legend of figure 9.10. Hoewever this maximum value is located near the load bearing plate and not in the shear area. The shear area counts a maximum value of 0.10. The crack width can be calculated by multiplying this value by the crack bandwidth. The colours of figure 9.10 suggest that the crack bandwidth could contain a field of two to three element sides. However, looking at figure 9.11, where the total strain is given over the rows similar to the full FE analysis, the width is limited to only one single integration point of one structural element. For the shear force area the same may be done regarding the crack spacing, but presented along the diagonals of the elements. These cracks are more or less diagonally oriented. The row system of the presentation has been used before in chapter 8 in the discussion of the local results of the FE-NL analyses.

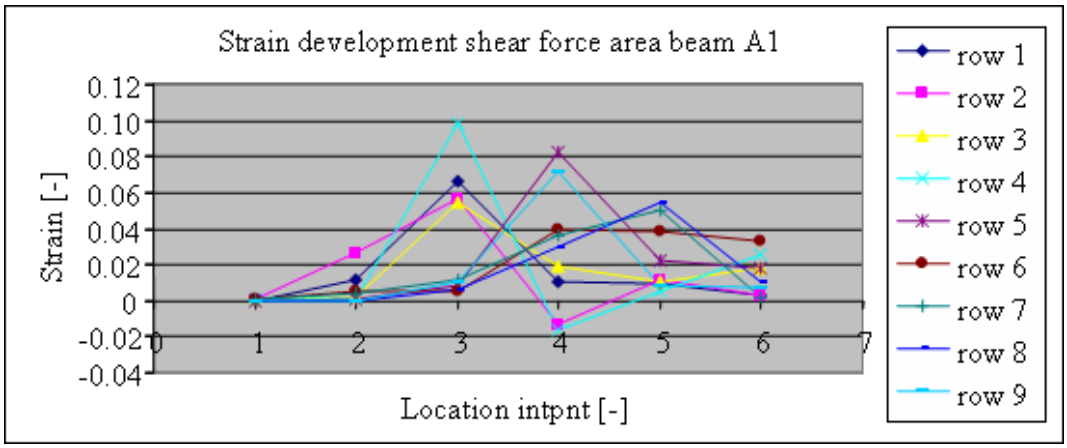

Figure 9.11 Crack strain over the rows in the shear force area at failure load on beam A1

Although there are rows of integration points in figure 9.11, in which the cracks are distributed along various integration points, it may be said that as a general rule the strain is limited to only one integration point. This means that for the shear force cracking area the crack bandwidth does not have to be doubled. Therefor the maximum crack width in the shear area with an orientation of 45˚ counts a value of 1.25 mm. Figure 9.12 compares the development of the crack width with the crack width development in the experiment.

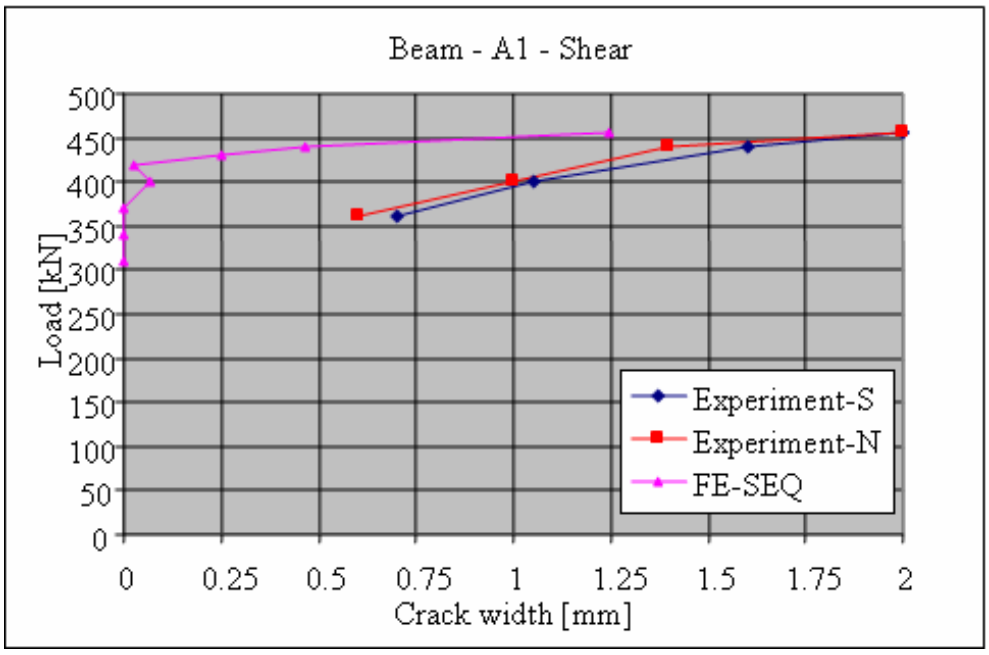

Figure 9.12 Development of crack width in the shear force area of beam A1

Figure 9.12 shows that the shear crackwidth coming form the sequential analysis differs from the results of the experiment, at least at the SLS load level. Here the crack width becomes 0.0 mm. The result at the ULS load level is rather lower then the experiment.

9.2.4 SLS load level results of the A1 experiment simulation

The most important result at the SLS load level is the crack width pattern and the yielding condition of the reinforcement.

Figure 9.13 shows the total crack strains at the SLS load level of beam A1.

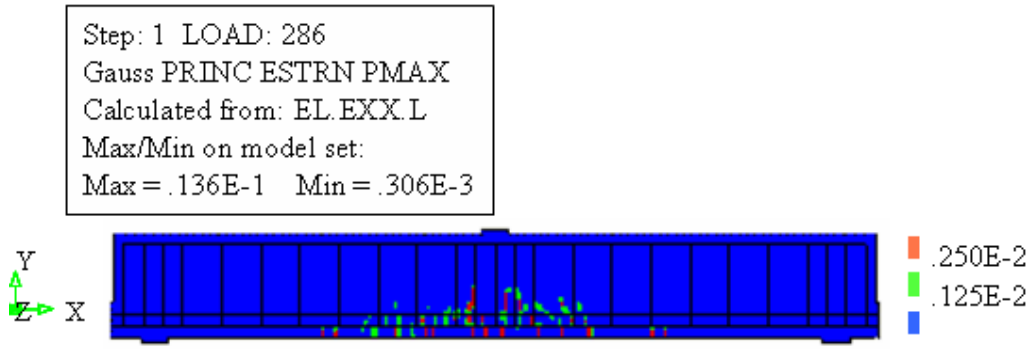

Figure 9.13 Crack pattern in concrete part at SLS load on beam A1

Figure 9.13 demonstrates that under the SLS load level the crack strains have increased to a maximum of 0.014. Here again a double crack width is seen, the maximum crack width being in this case 0.24 mm. At the SLS load level the reinforcement has not reached a yield limit yet, which is indicated by figure 9.14.

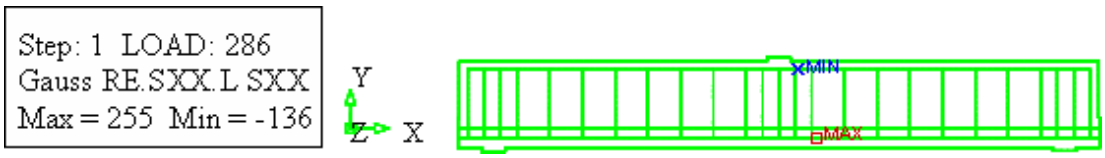

Figure 9.14 Stress reinforcement at SLS load level.

The lower reinforcement is under a maximum stress of 255 N/mm^2, and the upper reinforcement is under a minimum stress of -136 N/mm^2. The concluding remark is: both reinforcement parts have sufficient residual capacity, while the yield stress is 435 N/mm^2 for the lower reinforcement and -315 N/mm^2 for the upper reinforcement.

9.3 Sequential analysis simulation of the B2 experiment

9.3.1 Input non-linear material parameters for the sequential analysis

For the input data the reader is referred to the description of beam A1 of paragraph 9.2. The actual values of the various material parameters are found in chapter 7. In the sequential analysis the same material parameters play a role as in the FE-NL analysis. Only the analysis process differs.

9.3.2 Global results of the sequential analysis of the B2 experiment simulation

Figure 9.15 shows the load-deflection diagram of the midspan of beam B2.

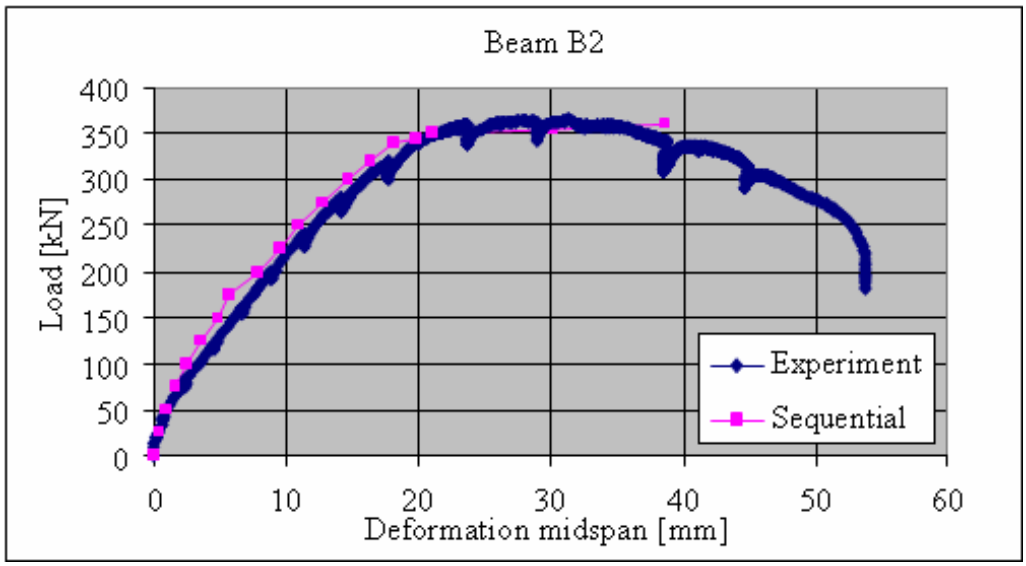

Figure 9.15 Load-deflection diagram of beam B2

The load-deflection diagram in the sequential analysis shows many similarities to the results of the experiment. The failure load of 365 kN is predicted adequately, and only a little tension-stiffening can be seen in the results of the analysis. The vertical deflection at failure load of 31.6 mm in the experiment is also nearly predicted. In the sequential analysis the vertical deflection is determined at 28.6 mm, including the yielding of all reinforcement components. The load level stages used were each time increased by 25 kN, with again four analyses for each load increment, in order to ensure a gradual transition from isotropic to orthotropic material behaviour. Figure 9.16 shows the crack pattern at failure load.

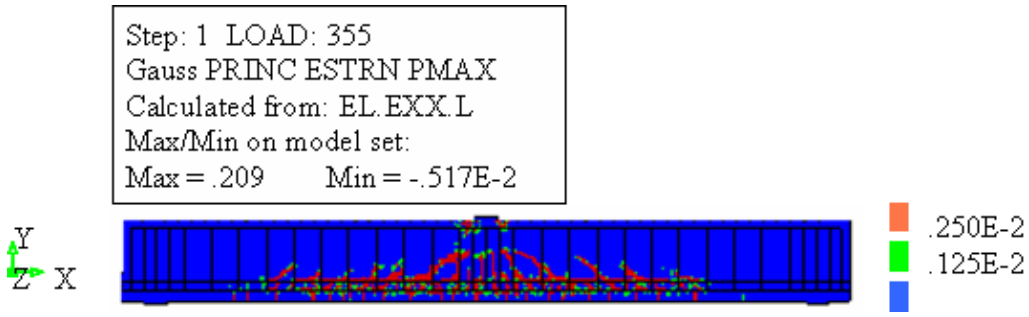

Figure 9.16 Crack pattern in concrete part at failure load on beam B2

Figure 9.16 shows that the crack pattern also matches the crack pattern of the experiment reasonably well. Various short shear force cracks can be distinguished till the compression zone. At failure load one crack continues to grow towards the bearing plate. To complement the global picture the ultimate compressive strain areas are shown for the concrete part and the plasticity areas of the reinforcement components of beam B2 in figures 9.17 en 9.18.

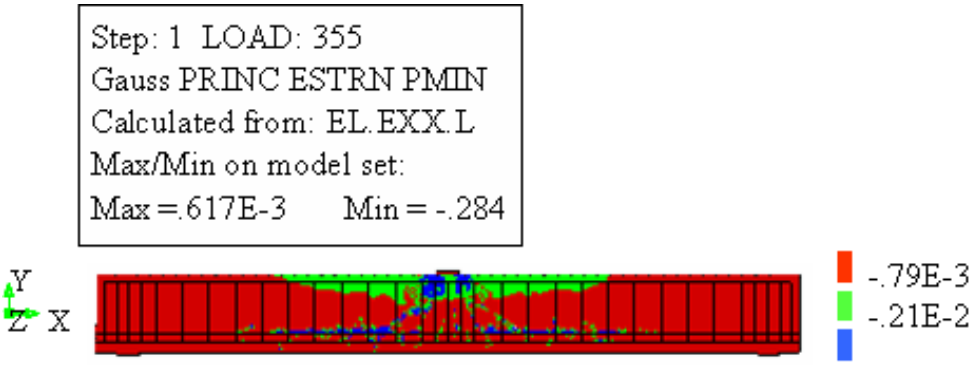

Figure 9.17 Principal compressive strain areas of concrete at failure load on beam B2

The exceeding of the ultimate principal compressive strain of concrete at failure load is concentrated at the bearing plates and the large shear force macro cracks. The minimum compressive strain is -0.284, which is well beyond the 2.1‰ compressive strain (see ε_0 in table 7.4). The length of the area where the compressive strain is exceeded is 540 mm at both sides of the middle of the beam.

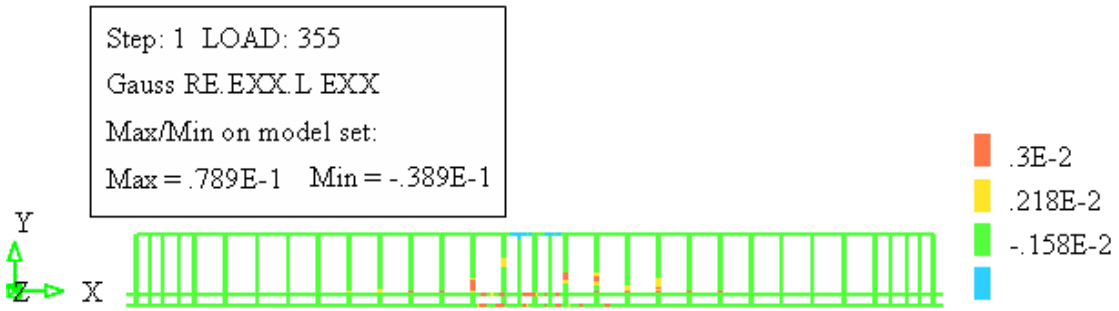

Figure 9.18 Plasticity areas of reinforcement component at failure load on beam B2

The reinforcement also shows plasticity areas in all reinforcement parts, starting at the upper reinforcement and subsequently at both layers of the tensile reinforcement and the stirrups. The maximum and minimum strains will be showed in detail in the next paragraph.

9.3.3 Local results of the B2 experiment simulation

Figure 9.19 shows the tensile strain in the bottom reinforcement layer over the length of the beam at failure load.

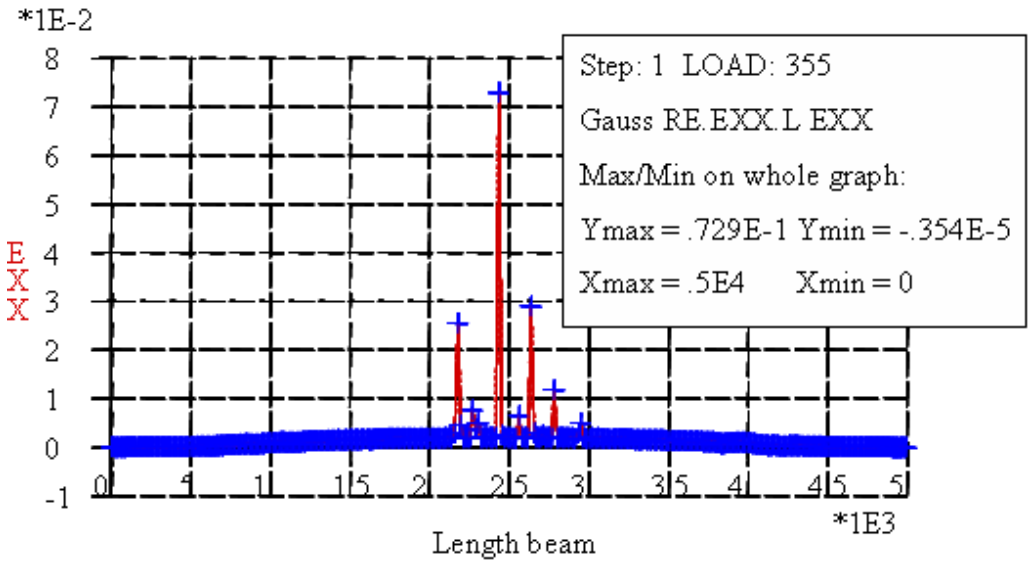

Figure 9.19 Strain in bottom reinforcement layer at failure load on beam B2

The maximum reinforcement strain in the bottom layer is 0.073, which is rather high for reinforcement. An overview of the strain, but this time for a limited section length of 995 mm at the midspan location is shown in figure 9.20.

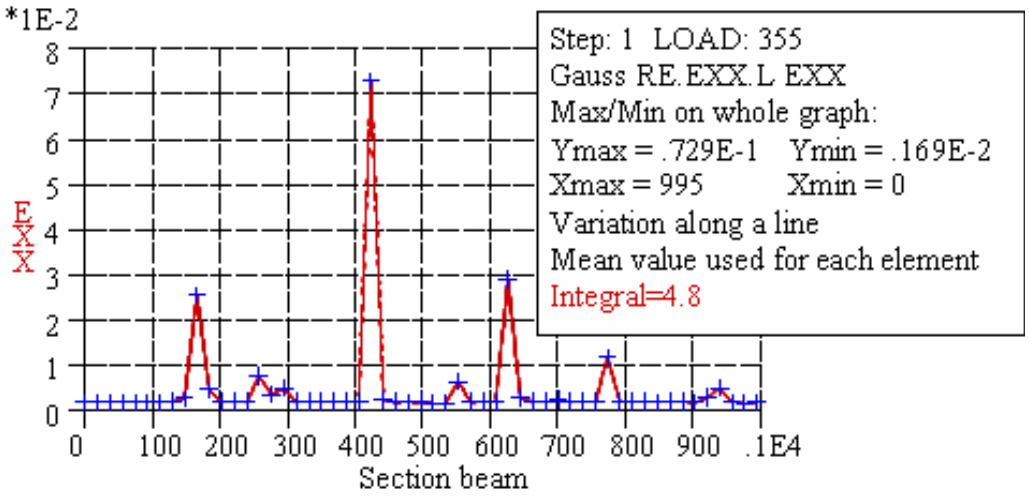

Figure 9.20 Strain in section of bottom reinforcement layer at failure load o beam B2

Again the maximum value of the strain is 0.073, which is too high.The minimum value is 1.69×10^{-3}, where the average value being 4.8×10^{-3}.
An overview of the crack strain in the bending area at the lower fibre of the concrete part of the beam is given in figure 9.21. The maximum strain has a value of 0.12. Also figure 9.21 demonstrates that the crack strain in one structural element has a maximum value at two integration points, this is similar to the behaviour in beam A1. This means that here as well we have a double bandwidth for the determination of the crack width. When determining the crack width, according to figure 9.20 a single crack strain of 0.121 should be taken into account.
When determining the crack width along two integration points, a total crack strain of 0.121+0.114=0.235 should be reckoned with. For beam B2 this means a maximum crack width in the bending area of 2.16 mm.

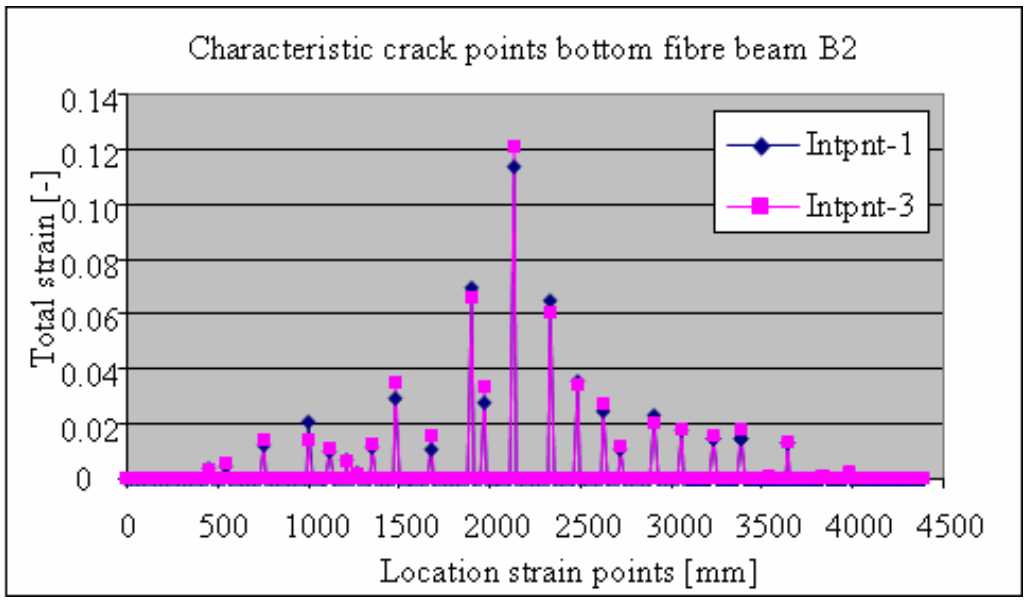

Figure 9.21 Crack strains at lower fibre at failure load along half of beam B2

Figure 9.21 shows also that the head to head spacing of the cracks is approximately 200 mm, almost the spacing between the stirrups of this beam.

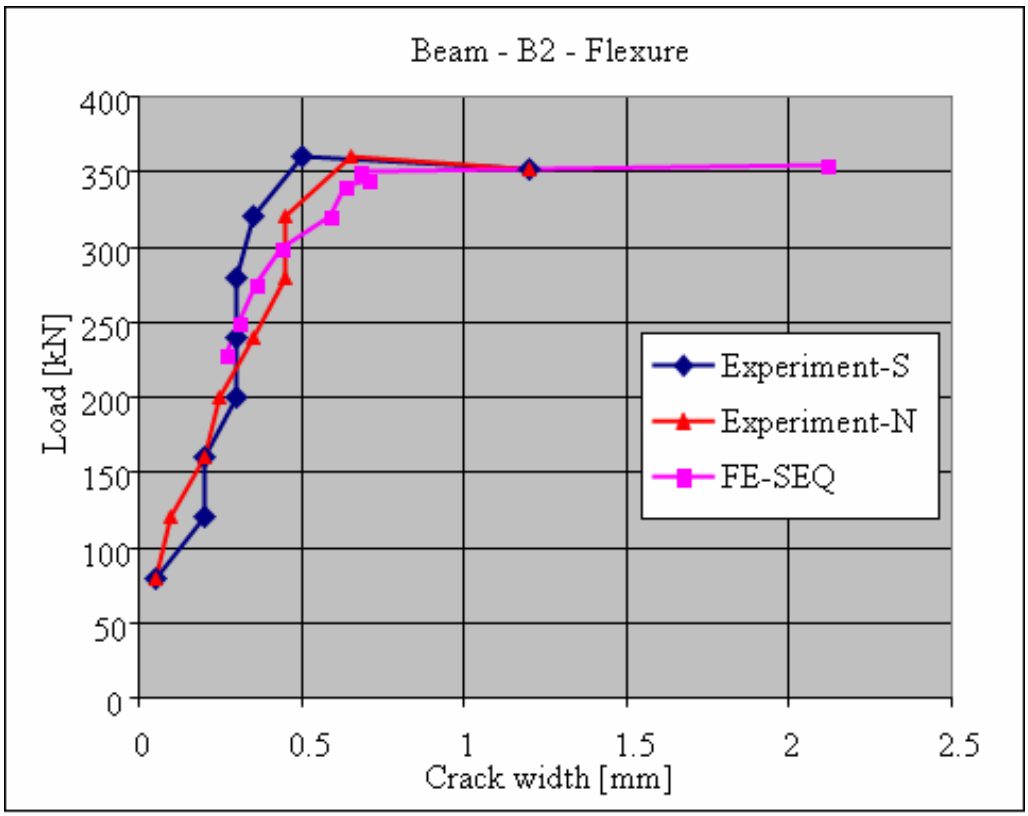

Figure 9.22 Development of crack width in the bending area of beam B2

The development of the crack width of the concrete shows a similar view of the development of the crack width in the experiment. Near the ULS load level the results differs in a range of 5 kN load increment. The crack width on the SLS load level seemes to be 0.24 mm, which is rather comparable with the experiment results.

The shear force crack strain reaches at the ULS load level a maximum value of 0.0875, where the legend of figure 9.23 shows the maximum of 0.121. This value is still the maximum value of the bending area.

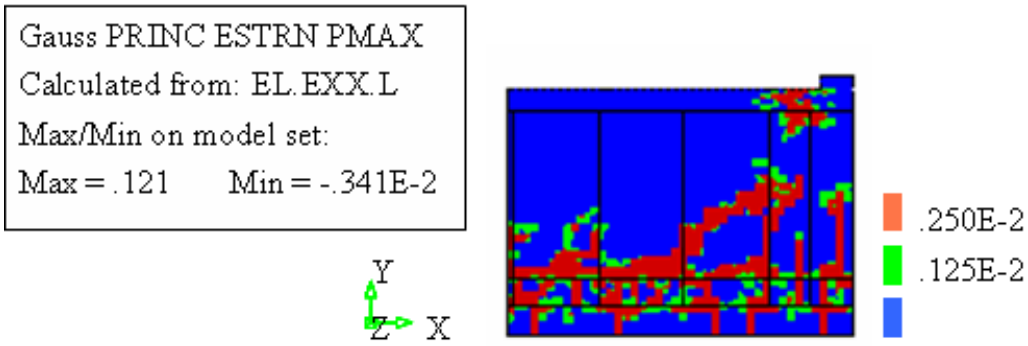

Figure 9.23 Development of the total strain in the shear force area at failure load on beam B2

In the legend of figure 9.23 a maximum strain of 0.12 is listed. Also this maximum value is located nearby the load bearing plate and not located in the resreached shear area. The maximum value of the strain in the shear area is counted as 0.091. In figure 9.23 it seems that the crack bandwidth in the shear force area takes on a crack width of two to three elements at failure load. Using the strain presentation based on rows shown in figure 9.24, it is possible to determine the crack bandwidth that actually occurs.

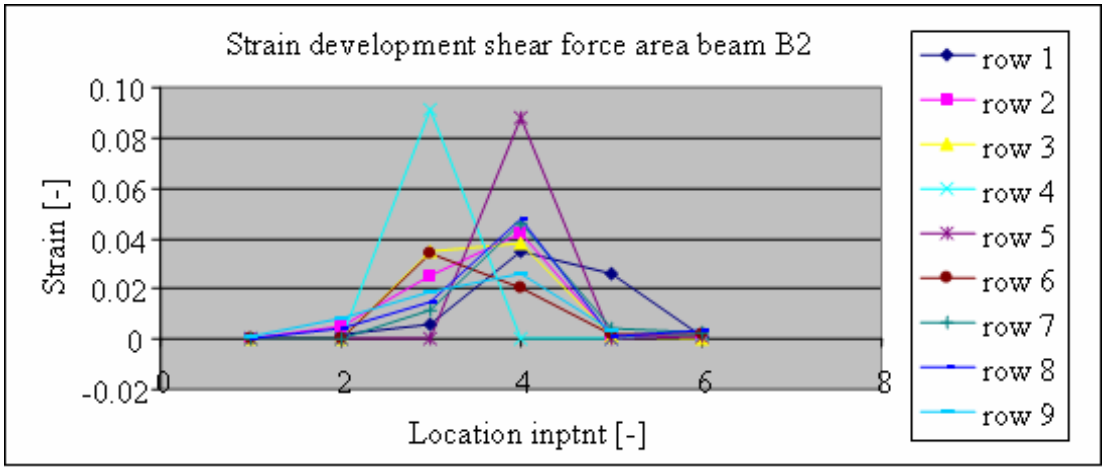

Figure 9.24 Overview of the principal tensile strain in the shear force area of beam B2

Figure 9.24 shows that the width of the crack encloses only one integration point. Wherever there is a distribution over two integration points, the value of the crack strain is limited. The width can therefore be maintained at the width belonging to a single integration point, being 9.2 mm. Including the crack orientation of 45° the total crack bandwidth has to be multiplied by √2. The corresponding crack width for the shear force area becomes 1.18 mm.

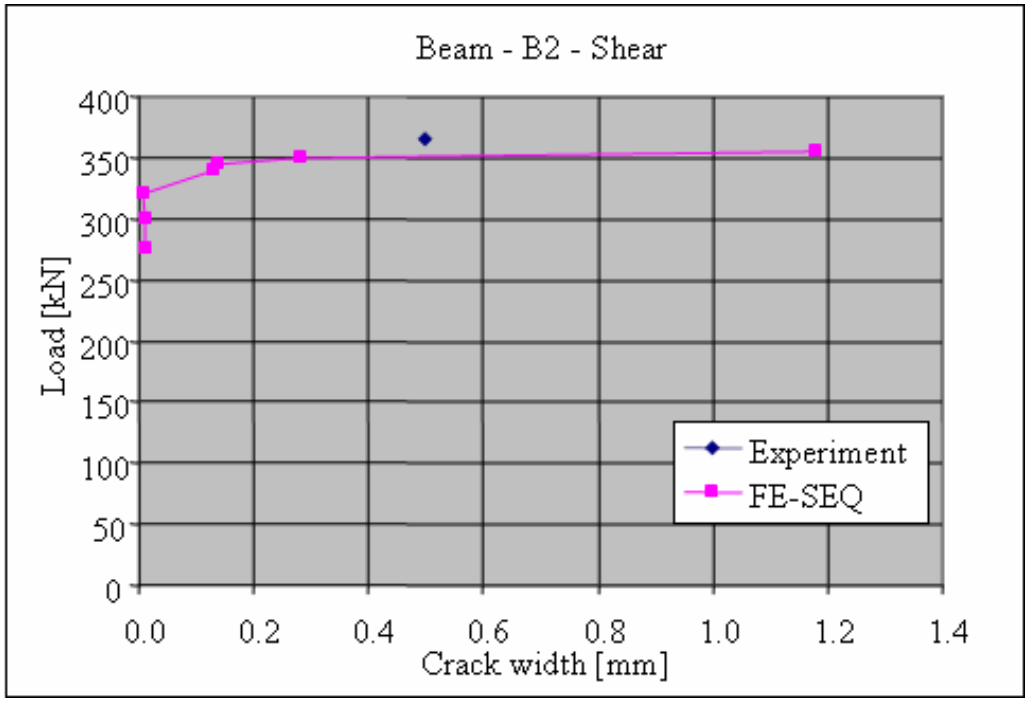

Figure 9.25 Development of crack width in shear force cracking area of beam B2

There is only one value of the crack width of the shear force area at ULS load level known from the experiment of beam B2, so a conclusion cannot be made from figure 9.25. However also this value is within the range of the calculated values from the sequential analysis of beam B2. At SLS load level the crack width in the shear force area seemed to be 0.0.

9.3.4. SLS load level results of the B2 experiment simulation

It is assumed that at the SLS load level, taken to be as the load level of 225 kN, no reinforcement will start to yield. This is shown in figure 9.26.

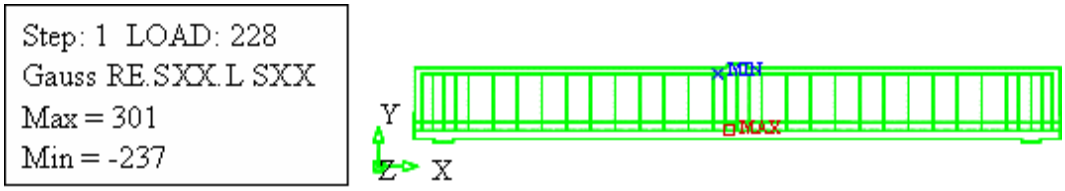

Figure 9.26 Maximum and minimum stresses in reinforcement components at SLS load level on beam B2

The maximum and minimum stress in the various reinforcement components are 301 N/mm^2 (tensile bottom layer reinforcement) and -237 N/mm^2 (upper reinforcement). For the upper reinforcement the residual capacity is still 315-237=78 N/mm^2, against 436-301=135 N/mm^2 for the lower reinforcement. The SLS crack pattern is shown in figure 9.27.

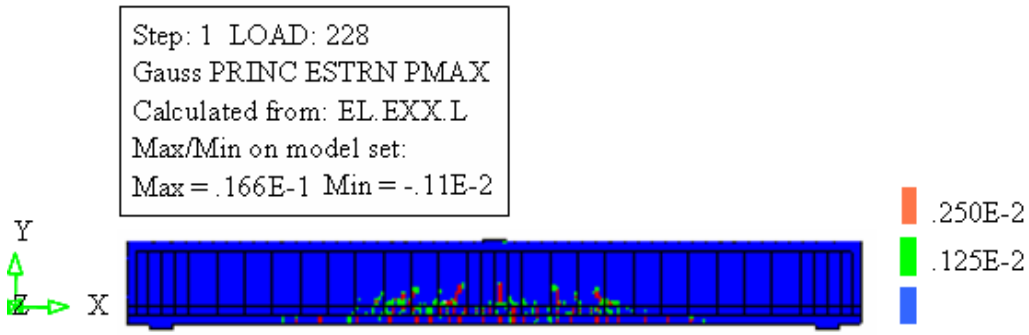

Figure 9.27 Crack strain in concrete part at SLS load level on beam B2

The maximum crack strain is 0.017, with an average over an element fibre of 0.013, which means a crack width of 0.24 mm at a crack bandwidth of 18.4 mm.

9.4 Sequential analysis simulation of the C3 experiment

9.4.1 Input non-linear material properties for the sequential analysis

The input data for beam C3 are equal to the data used for the FE-NL analysis, determined directly on the basis of the Model Code 1990.

9.4.2 Global results of the sequential analysis of the C3 experiment simulation

Figure 9.28 shows the load-deflection diagram of beam C3.

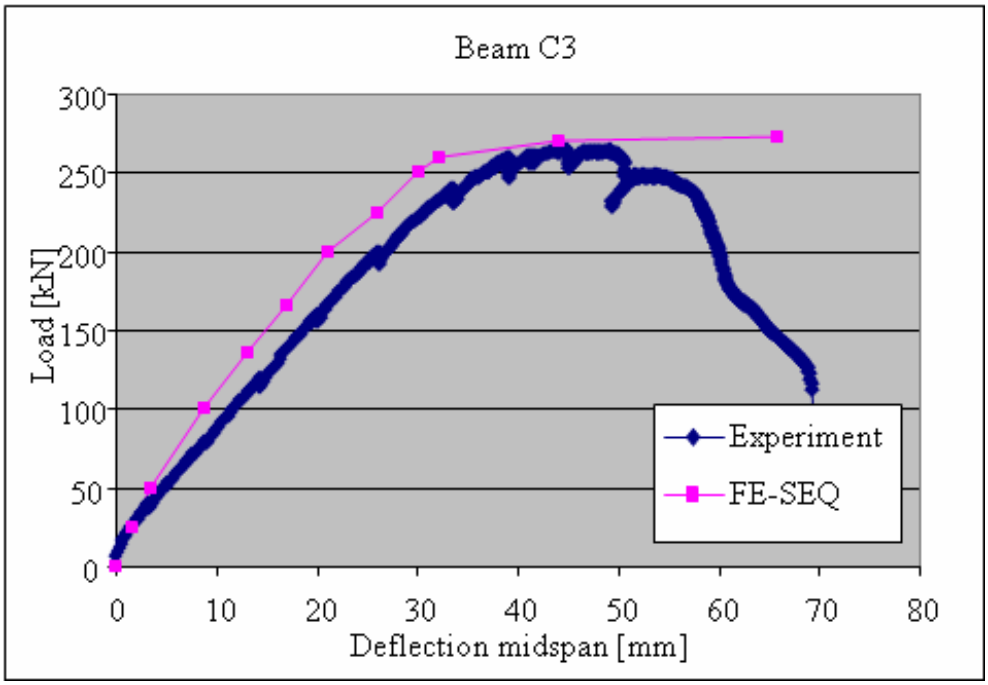

Figure 9.28 Load-deflection diagram of beam C3

There is much agreement between the results of the experiment and the results of the sequential analysis. Although the 'tension-stiffening' effect is more prominent than with

beam B2, it does not seem to be an influential determinant of the failure load of 270 kN. The corresponding maximum deflection of 44.3 mm is almost predicted by the sequential analysis as well. All reinforcement components yield at the ULS load lavel.
The separate load stages used at the sequential analysis of this beam again were between 25-33 kN. This turns out to be a good choice, because it produces a comparable load-deflection diagram using a total of 47 analyses. The beam C3 analysis also included approximately four analyses per load increment. This means that after 12 load increments the final failure ULS load level of 270 kN is reached. The corresponding crack pattern is shown in figure 9.29.

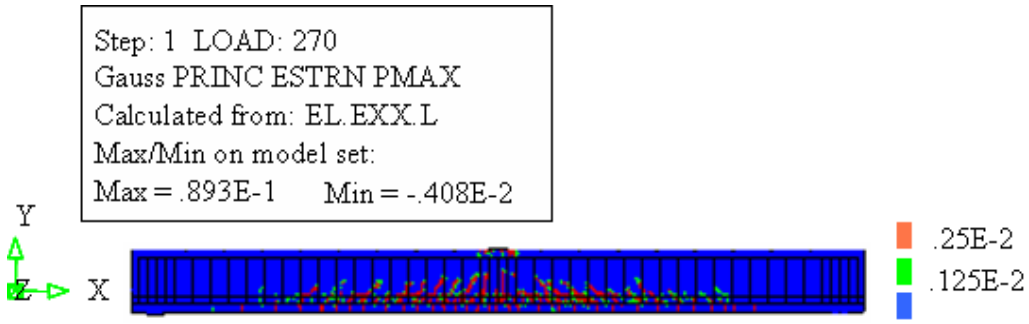

Figure 9.29 Crack pattern at failure load on beam C3

The crack pattern shows a multiplicity of small cracks distributed along a considerable length of the beam. In this case the maximum strain is 0.089. This is, however, at a location near the bearing plates, meaning that as such it is not relevant for the validation of the sequential analysis method. The local results will give more detailed information about the total strain divided in bending and shear areas. The global behaviour of beam C3 is followed through by showing the principal compressive strain areas for concrete and the plasticity areas of the various separate reinforcement components. Figure 9.30 shows the areas in which the principal compressive strain in the concrete part of the beam is exceeded.

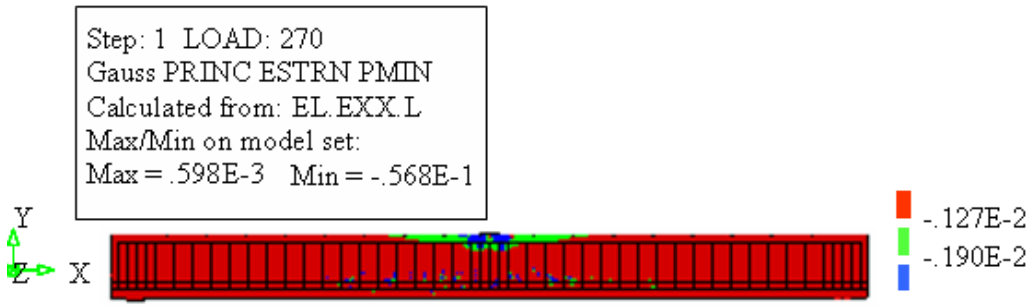

Figure 9.30 The principal compressive strain of concrete at failure load on beam C3

The areas where the principal compressive strain of concrete is exceeded in beam C3 are minimal, and mainly occur near the bearing plates. The minimum compressive strain is -0.057, which is a fairly high value for the concrete material. It is certain that concrete crushing will occur at the location of the bearing plates in this experiment as well. The length of this ultimate compressive strain area is 2×575 mm. The plasticity areas of the reinforcement in beam C3 are shown in figure 9.31.

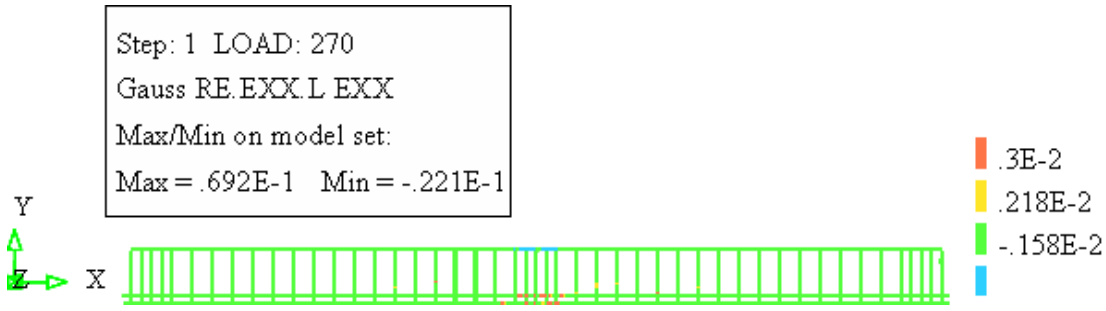

Figure 9.31 Plasticity areas in reinforcement bars at failure load on beam C3

Also in this beam the picture of figure 9.31 shows plasticity in all reinforcement components. There is a concentration of plasticity near the bearing plates in the upper reinforcement, but there is plasticity in the stirrups and lower reinforcement layers as well. The maximum value of the reinforcement strain is 0.069, which is far above the yielding strain limit. Hardening could be an option in a further analysis.

9.4.3. Local results of the C3 experiment simulation

Figure 9.32 shows an overview of the tensile strain in the lower bottom reinforcement.

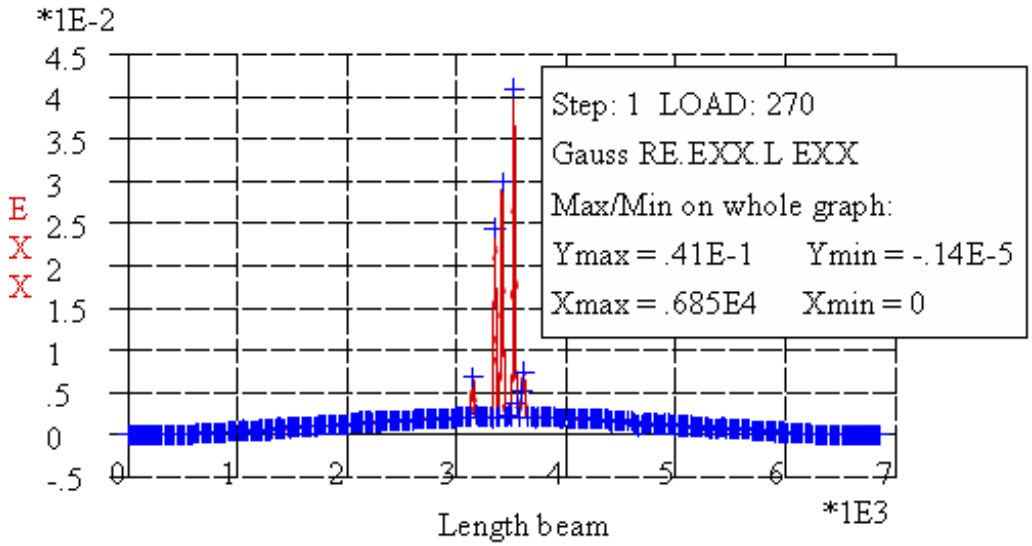

Figure 9.32 Overview of the bottom layer reinforcement strain at failure load on beam C3

The maximum tensile strain specifically occurs in one single integration point of the lowest reinforcement layer, being 0.041. A presentation of a section in figure 9.33 helps to slightly nuance this maximum reinforcement strain value.
Figure 9.33 shows a minimum tensile strain value of 0.19×10^{-2}. Along the 1,000 mm section an average value of 4.4×10^{-3} is found, with a maximum of 0.041, which means a scale factor of ×10.

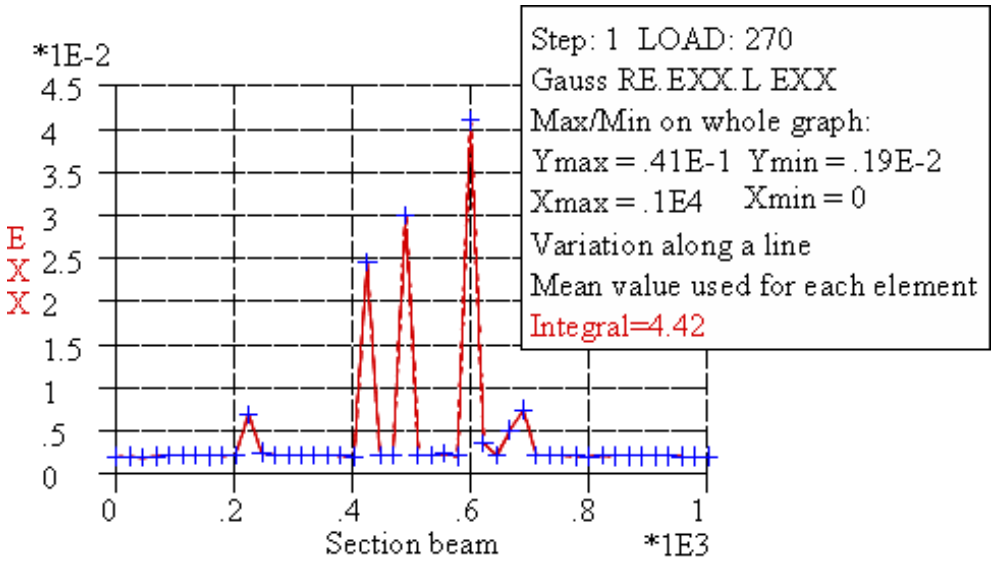

Figure 9.33 Overview of the strain in a section of the bottom layer reinforcement at failure load on beam C3

The figure with characteristic cracking points in the lower fibre indicates whether there is question of a single or a double crack spacing, as is shown in figure 9.34.

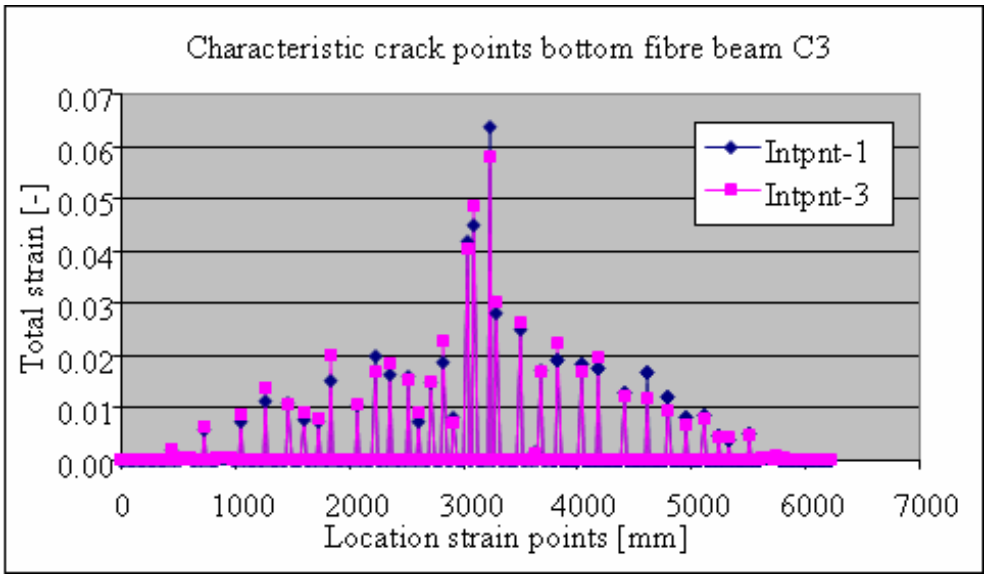

Figure 9.34 Total strain in lower fibre of concrete part at failure load along the length of beam C3

The overview of the total strain shown in figure 9.34 indicates that there is a double crack width spacing, because at both integration points crack strains occur that have a similar value. This means that in the bending area there is a crack bandwidth of 2×11.15=22.3 mm. The maximum total strain on the basis of two integration points is 0.061. The crack width in the lower fibre in the bending area at failure load with this type of beam is 1.36 mm. The development of this crack width will be given in figure 9.35.

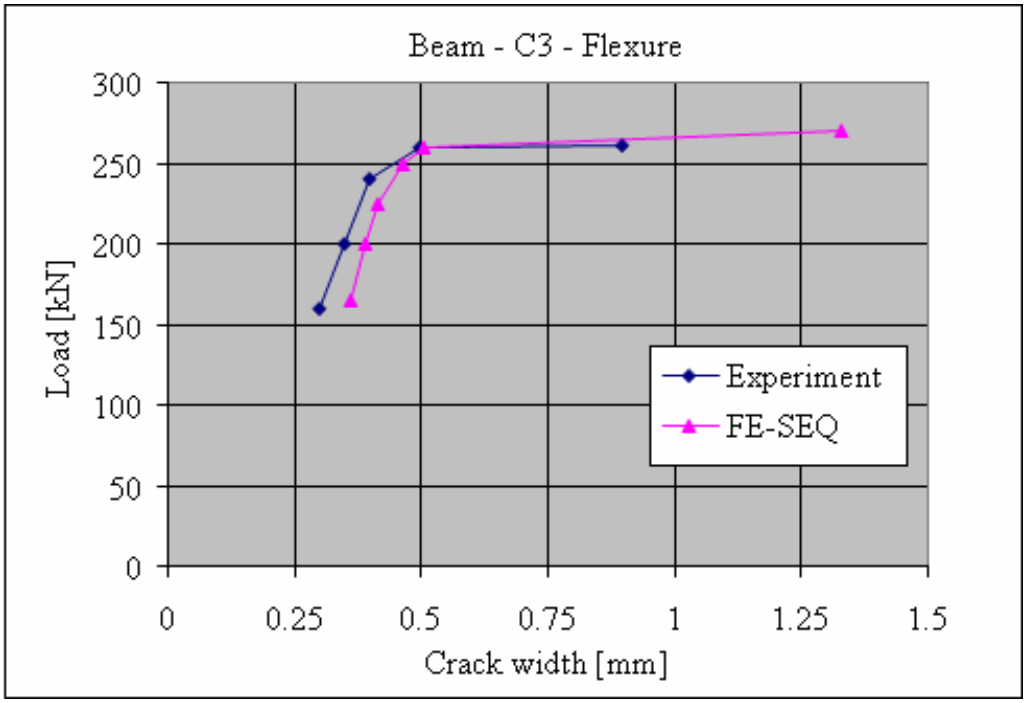

Figure 9.35 Development of crack width in bending area of beam C3

Again the development of the crack width of the sequential analysis is similar to the results of the experiment. At the SLS load level a crack width is counted of 0.36 mm. Further, figure 9.36 will zoom in on the crack strain in the shear force area.

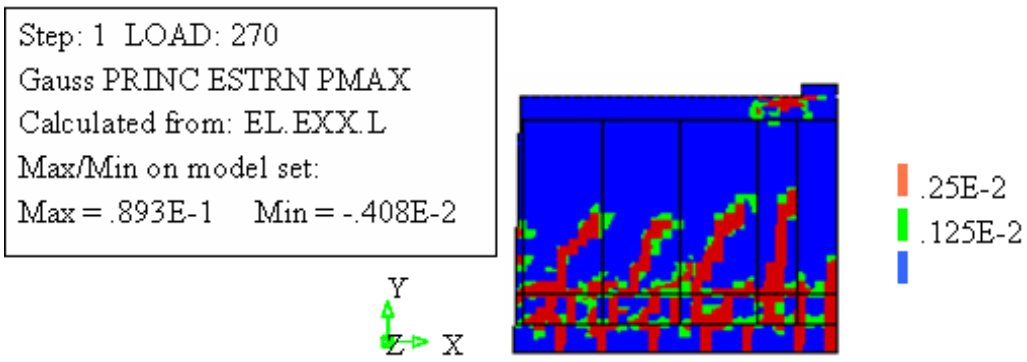

Figure 9.36 Crack strains in the shear force area at failure load on beam C3

The maximum value is listed in the legend of figure 9.36 and counts a value of 0.089. However, in the shear force area a value of 0.042 is counted. A single crack bandwidth with an orientation of 45˚ produces a crack width of 0.66 mm. The crack bandwidth was determined on the basis of the overview of the total strain along predetermined rows of integration points in the shear force area. This is shown in figure 9.37.

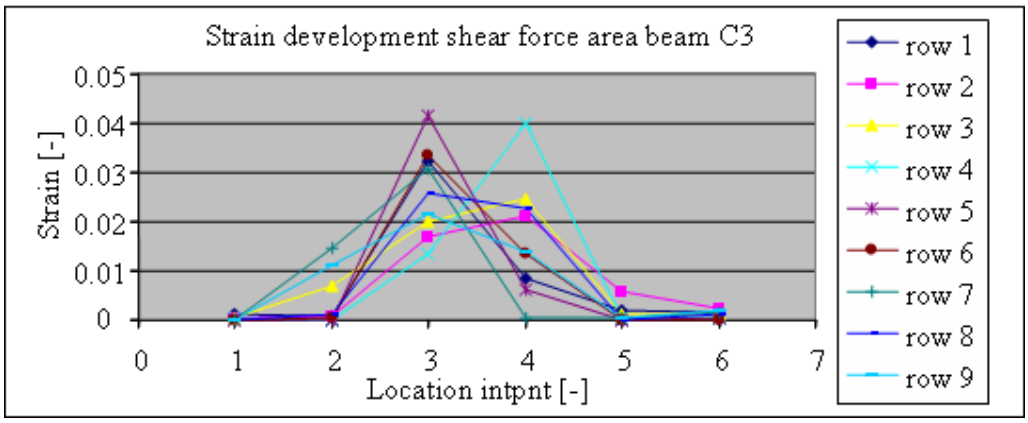

Figure 9.37 Overview of the total strain along the rows of the shear area at failure load on beam C3

We can see that in this shear force area the crack bandwidth is only one integration point. Even though the two values in the second row approach the maximum strain in one integration point, the maximum is reached in the fifth row with a strain behaviour belonging to a single integration point of a structural element. The development of the maximum shear crack width of the integration point in the shear area is given in figure 9.38.

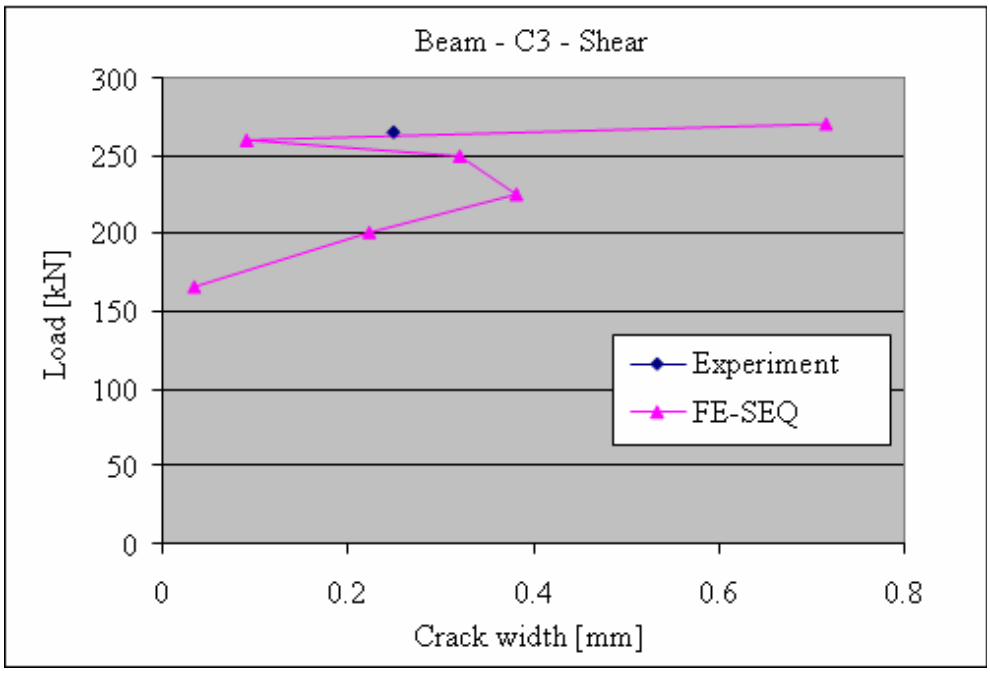

Figure 9.38 Development of crack width in shear force area of beam C3

Figure 9.38 demonstrates that up to a level of 250 kN the crack width is small, but that it exceeds the experimental value after adding just one load increment of 10 kN.

9.4.4 SLS load level results of the C3 experiment simulation

The cracking behaviour under SLS load level (=165 kN) also determines whether a beam is admissible according to current regulations. The corresponding crack pattern is shown in figure 9.39.

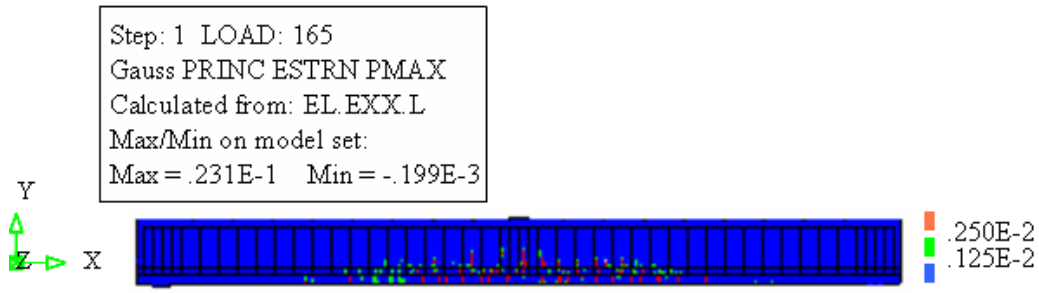

Figure 9.39 Crack patterns in concrete part at SLS load on beam C3

This crack pattern shows that there is a maximum crack strain of 0.023. The mean value of the fibre in this structural element has a value of 0.016. On the basis of a double crack bandwidth of 22.3 mm this produces a crack width of 0.36 mm for the SLS load level. Finally, the stress in the reinforment at the SLS load level is shown in figure 9.40.

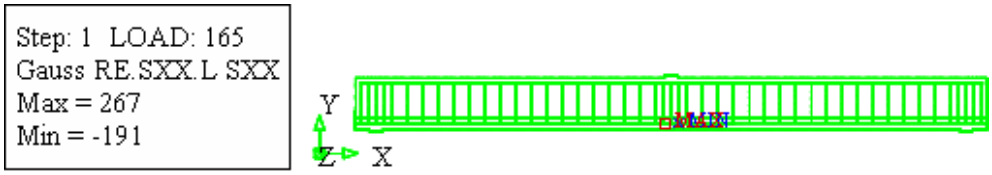

Figure 9.40 Maximum and minimum stress in reinforcement components at SLS load level on beam C3

Figure 9.40 shows that the minimum value of the stress is not in the upper reinforcement but in a stirrup conection to the lower reinforcement. The minimum value of the upper reinforcement is -189 N/mm^2 at the SLS load, which does not differ so much with the stirrup stress of -191 N/mm^2. The maximum stress in the lower reinforcement is 267 N/mm^2. This means both the upper and stirrup reinforcement still have sufficient residual capacity, regarding the yield stress of 436 or 315 N/mm^2. If both these reinforcement components start to yield, the tensile reinforcement could also yield.

9.5 Summary of and intermediate conclusions on global and local results of the three beams

For each beam global and local results can be distinguished.

Global	A1		B2		C3	
	Exp.	FE-SEQ	Exp.	FE-SEQ	Exp.	FE-SEQ
Failure load [kN]	459	455	365	355	265	265
Corresponding vertical deflection [mm]	18.8	17.9	31.6	28.6	44.3	38.2
Crack pattern	Matching		Matching		Matching	

Table 9.1 Summary of the global results of the experiment and the FE-SEQ

Conclusions on the global level:

- The global results of the FE-SEQ analysis show a good match with the results of the experiment. Both the failure load and the corresponding vertical deflection in the middle of the beam correspond well.
- The global results for the crack patterns also show a good match.

Local	A1		B2		C3	
	Exp.	FE-SEQ	Exp.	FE-SEQ	Exp.	FE-SEQ
Strain in tensile reinforcement [$\times 10^{-3}$]	1.17	1.48-19.7	2.87	1.69-72.9	1.76	1.90-41.
Crack width bending ULS [mm]	0.50	0.72	1.60	2.16	0.90	1.36
Crack width shear force ULS [mm]	2.00	1.25	0.50	1.18	0.25	0.66
Crack width bending SLS [mm]	0.3	0.24	0.28	0.24	0.3	0.36
Crack width shear force SLS [mm]	-	0.0	-	0.0	-	0.04

Table 9.2 Summary of the local results of the experiment and the FE-SEQ

Conclusions on the local level:

- The local strain at the bottom layer of the tensile reinforcement also shows a considerable difference.
- The local results for the crack strains in the bending area at SLS load level show a good match; on ULS load level it differs again like the FE-NL results
- The local results for the crack strains in the shear force cracking area do not agree with each other, albeit that it is unclear where the measurements took place in the experiment.

10 EVALUATION OF THE RESULTS AND SOME SENSITIVITY ANALYSES

10.1 Evaluation of the results

10.1.1 General results

The results of both methods, the fully non-linear method and the sequential method, have been discussed in chapters 8 and 9. The results of both analyses have been mainly compared to the results of the experiment. No explicit comparison between both methods has taken place. However, the similarities with the results of the various experiments have been such that one may conclude that both methods agree well with each other in advance. The global results from the simulations, like the load-deflection diagrams, the crack patterns, the exceedance patterns of the ultimate compressive strain and the plasticity areas of the reinforcement match well with each other in all three experiments.

10.1.2 Crack width

The local results show similarities as well. The development of the crack width in the bending areas, for instance, is similar to the results of the experiments in both analytical methods. The development of the crack width in shear force areas is not consistent in both methods, but not similar to the result of the experiment. Also, two experiments have not produced sufficient crack width data. Apart from no indication of the measuring location in the shear force area they also do not show the development. One may state that in both methods the crack widths in the concrete can be included in a more explicit manner into the design of a structure. Various analytical or empirical formulations for calculating crack widths, e.g. on the basis of the diameter of the reinforcement bar, do give an indication of the crack width in the current design process. A method for calculating the crack width in the Eurocode (art. 7.3.4) is explained by the fomula

$$w_k = s_{r,max} (\varepsilon_{sm} - \varepsilon_{cm})$$

in which:

w_k	- the maximum crack width
$s_{r,max}$	- the maximum crack width
ε_{sm}	- mean strain of the reinforcement bar
ε_{cm}	- mean concrete strain between the cracks

The maximum crack width can be expressed by the equation:

$$s_{r,max} = k_3\, c + k_1\, k_2\, k_4\, \phi_{eq} / \rho_{s,eff}$$

where:

k_1	- coefficient (=0.8) for bars with a high bond behaviour
k_2	- strain distribution coefficient =0.5 for bending and 1.0 for pure tension
k_3	- 3.4
k_4	- 0.425
c	- coverage longitudinal reinforcement
$\rho_{s,eff}$	- relation $A_s/(b \times h_{eff})$

The second term in the crack width equation is:

$$\varepsilon_{sm} - \varepsilon_{cm} = \frac{\sigma_s - k_t \frac{f_{ct,eff}}{\rho_{s,eff}}(1+\alpha_e \rho_{s,eff})}{E_s} \geq 0.6\frac{\sigma_s}{E_s}$$

in which:

σ_s - stress tension reinforcement
k_t - short term loading
α_e - relation E_s/E_c
$\rho_{s,eff}$ - relation $A_s/(b \times h_{eff})$
$f_{ct,eff}$ - average concrete tensile stress (f_{ct}) at the expected moment of first crack pattern
E_s - Young's modulus reinforcement steel

where:

h_{eff} - minimum of $2.5 \times (h-d)$ or $(h-x_e)/3$ or $h/2$
b - width of beam

in which:

x_e - height compression zone concrete
h - height of concrete cross section
d - effective depth of concrete cross section

The x_e formulation can be expressed by:

$$x_e = -\alpha_e \times \rho + \sqrt{[(\alpha_e \times \rho)^2 + 2 \times \alpha_e \times \rho]}$$

where:

ρ - reinforcement ratio related to the whole concrete cross section

This allows the drawing of a table showing first the minimum of the h_{eff} and afterwards the crack widths in the beams under discussion according to this method. Table 10.1 gives an impression of the h_{eff} calculation and table 10.3 the crack widths based on this formulation.

Beam	h	d	b	2.5×(h-d)	α_e	ρ	x_e	$(h-x_e)/3$	h/2
A1	552	457	305	237.5	5.48	0.0143	149	***134***	276
B2	552	457	229	237.5	6.08	0.0190	173	***126***	276
C3	552	457	152	237.5	5.83	0.0286	199	***117***	276

Table 10.1 Calculation of the effective height according to the Eurocode formulation

The bold italic indicated values in table 10.1 are the values for the h_{eff} in the continuation of the calculation of the crack width.

Beam	h	d	b	h_{eff}	$A_{c,eff}$	A_s	$\rho_{s,eff}$	f_{ct}
A1	552	457	305	134	40870	2400	0.059	2.41
B2	552	457	229	126	28854	2400	0.083	2.62
C3	552	457	152	117	17784	2400	0.135	3.70

Table 10.2 Calculated concrete parameters according to crack width formulation of the Eurocode

The reinforcement counts two bars of M30 en two bars of M25. This means an equivalent diameter must be calculated by the equation of art. 7.12 from the NEN-EN-1992-1-1.

$$\phi_{eq} = \frac{n_1\phi_1^2 + n_2\phi_2^2}{n_1\phi_1 + n_2\phi_2} = \frac{2\times 30^2 + 2\times 25^2}{2\times 30 + 2\times 25} = 27.7mm$$

All three beams have the same amount reinforcement bars, the equivalent diameter of the bars gets a value of 27.7 mm.
The above mentioned parameters are already explained in the earlier mentioned equations of this paragraph, except the parameter k_t, which becomes a value of 0.6, while it is a short duration loadfactor. Table 10.3 gives an impression of the different steps to come to crack widths corresponding with this calculation method.

Beam	k_3 c	$p_{s,eff}$	$k_1 k_2 k_4 \phi_{eq}$	$s_{r,max}$	$\frac{f_{ct,eff}}{\rho_{s,eff}}$	$1+a_e p_{s,eff}$	$\varepsilon_{sm} - \varepsilon_{cm}$	w_k [mm]	w_{kExp} [mm]
A1	160	0.059	4.71	240	41	1.32	0.0020	0.49	0.5
B2	160	0.083	4.71	217	32	1.50	0.0020	0.43	1.6
C3	160	0.135	4.71	195	27	1.79	0.0020	0.39	0.9

Table 10.3 Calculated parameters crack width method Eurocode

The crack width related to the Eurocode is far from the cracks width results of the experiment and the FE results. Only the crack width of beam A1 is similar to the experimental value. The calculated crack widths on the SLS load level will have the same ratio and are now similar to the crack widths of the experiment on the SLS load level.

10.1.3 Reinforcement results

Finally, one may state that the strains occurring in the tensile reinforcement in both methods deviate from the strain values that were measured in the experiment. In general, there is an overestimation of the strain in the tensile reinforcement of 50 to 80%. This picture applies to both the bottom layer of tensile reinforcement and the upper layer of tensile reinforcement. The abutting concrete elements show a strain that is similar to the strain in the tensile reinforcement. In engineering practice, the ULS load level is linked to the ultimate yield limit of the tensile reinforcement, meaning that the strain in the tensile reinforcement is important. However, because the strain is overestimated, this guarantees a structural design that is reliable enough. A request for further information on the Toronto experiments revealed that although the strains in the tensile reinforcement had been measured during the experiments, this could have been done in a more precise manner. In conclusion, it may be said that the target has been achieved for the most part, namely to devise a reliable design process that may be checked at various levels.

10.1.4 Processing time results

As was seen in chapter 8, the FE-NL analysis method is also very suitable as a tool for checking. However, the overall processing time is not acceptable. An indication in relation to the sequential methods is shown in figure 10.1. The periods of time that are being compared are the sum of the net CPU time and the net IO time. The clocked times in between the start and the ending of the analysis are, in fact, incomparable, because there are always other processes running on the computer at the same time.

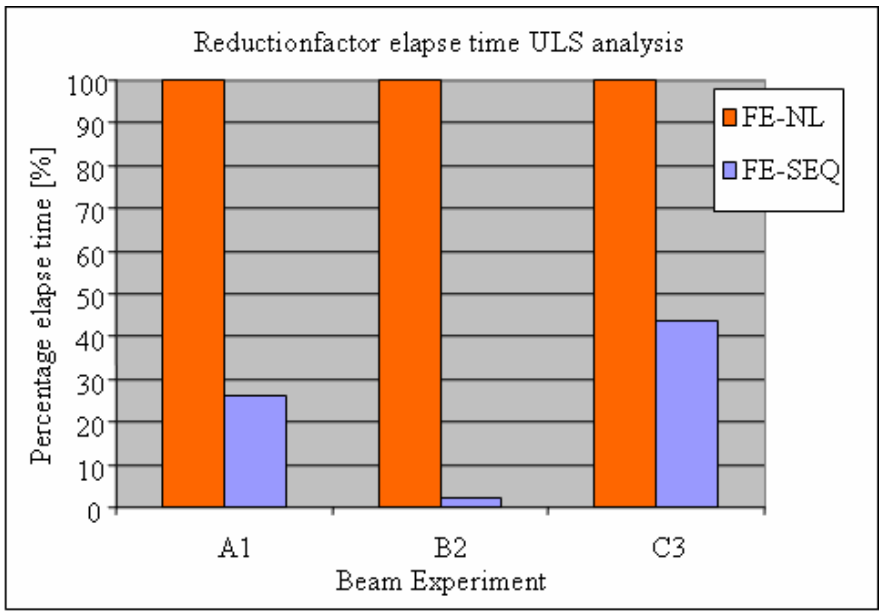

Figure 10.1 Comparing processing times of FE-NL and FE-SEQ analyses at ULS load level

Figure 10.1 shows that the overall gain in time at the ULS load level is minimally a factor 2, showing a maximum of a factor 40. From an absolute point of view, these times depend very much on the type of computer. However, if we start from the use of a desktop PC-CPU (Intel Duo Core CPU, E4500@2.2 GHz), common in current engineering practice, the ULS analysis can be done in a robust manner between 1.5 and 3 hours. If software providers decide to incorporate the sequential method into their software, the gain factor may perhaps be again 2. In the future, a more robust and extended check on the design is conceivable. In we look at the gain factor at the SLS load level, the figures improve somewhat, although one should keep in mind that the total processing time will be much shorter. These gain factors are shown in figure 10.2.

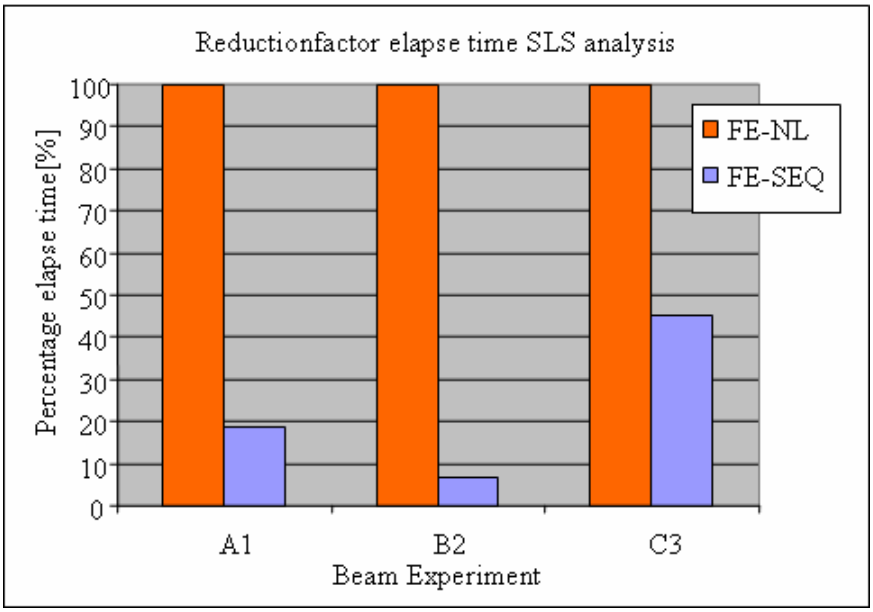

Figure 10.2 Comparing processing times of FE-NL and FE-SEQ analyses at SLS load level

The gain factors shown in figure 10.2 demonstrate that there is a gain factor of 2 to 13. From an absolute point of view, the processing times are mutually related within the range of 13 to 37 minutes. Given the expected gain from a more direct implementation of the software mentioned earlier, the maximum time can be reduced to at least 15 minutes. This means engineering practice will be provided with a crack width checking tool that enables rapid checking of the concrete and reinforcement design of a structure at the SLS load level.
In chapter 9 it was seen that 35 analysis steps are needed to arrive at the SLS load level. The sequential analysis process including the required processing time is shown below for all three analyses.

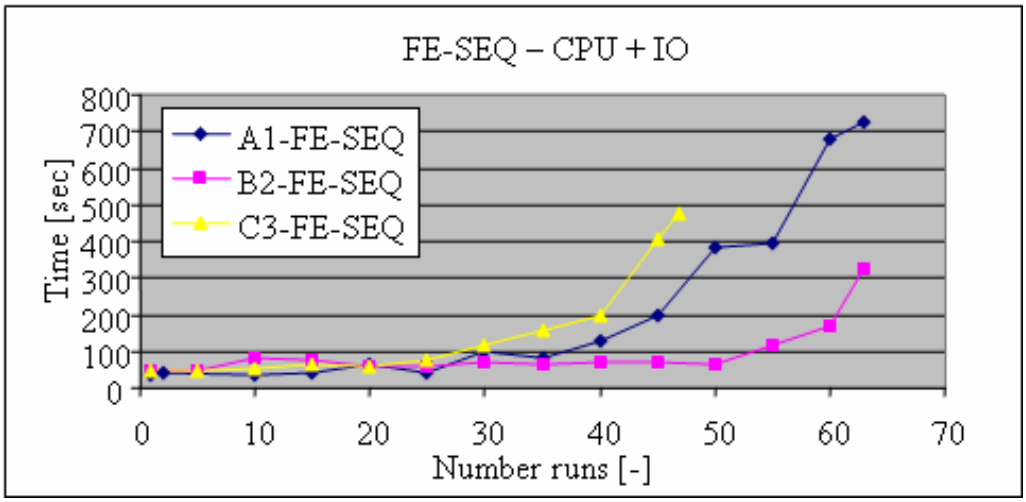

Figure 10.3 Comparison of processing time of sequential analyses of three experiments

Up to the SLS load level the periods of time per analysis are limited, after which at various spots in the structure the reinforcement will start to yield. At that moment the total elapse runtime goes up to a maximum of 10 minutes per analysis. It is also important that once the Eurocode standards are introduced, there will be a reduction of partial safety factors in relation to the ULS load level. Up to the present, the amount of reinforcement was primarily designed for the ULS level. After this, the SLS load level is looked at to see how much more reinforcement will have to be added in order to comply with the crack width requirement. Due to the reduction of the partial safety factor at the load level from 1.5 to 1.35, the SLS load level becomes more important. Complying with the SLS load level can in many cases also mean complying with the ULS load level.

10.2 Some sensitivity analyses

10.2.1 Dependency on element dimensions

Chapters 8 and 9 did not address the dimensions of the elements, albeit that in the analysis the crack bandwidth was derived from these as a parameter for the crack pattern. A prior investigation of the element dimensions did take place, but has not been included into this study. The failure load was similar for all models, as were the crack patterns at the SLS load level, whereas those at the ULS load level did show increasing deviations. In view of the internal integration schemes also being different as far as the various types of elements are concerned (linear, square, triangular and quadrilateral), this could become a separate

study of its own. In this case, the most common element was selected, the quadrilateral rectangular structural element with the 2×2 Gauss integration scheme. Various models were set up, from coarse meshes to finer meshes. Here we also find a form of convergence when it comes to a selected element distribution. The basis for the convergence is that the reinforcement, and especially the stirrup reinforcement, is supposed to yield at equal load levels. The three selected experiments come from a Canadian-US research on shear force. It is important whether there is stirrup reinforcement in structures present or not. The chance of yielding of the upper and lower reinforcement is not a point of debate within the current coarse or fine meshes. The calling on the stirrups in the case of a redistribution of stresses after the occurrence of a crack pattern in the concrete has led to the element distributions as used in chapters 8 and 9. It is, however, remarkable that the maximum aggregate size of the concrete almost matches the length of the side of the element. In order to give an impression of what happens if the stirrups have to answer a force formation, the figure shows the development of the strain in a stirrup in a coarse and a fine mesh.

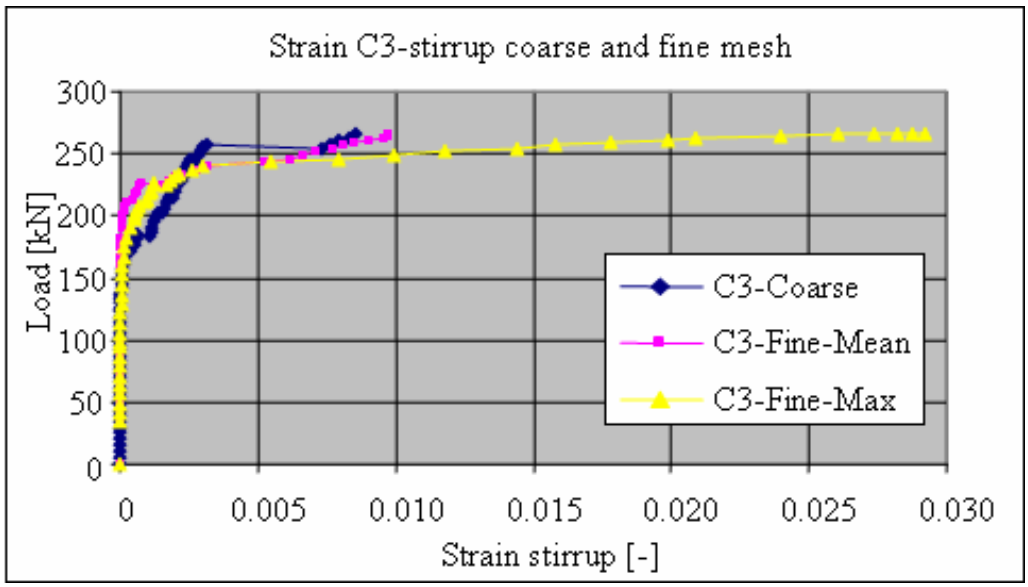

Figure 10.4 Development of strain in stirrup on the same location with coarse and fine mesh

Figure 10.4 clearly shows that if a single stirrup section is split up into two stirrup sections, the maximum strain with a fine mesh is three times as large as with the coarse mesh. Even the second section in the finer mesh shows a slightly higher strain value than in the coarse mesh. Still, all sections will commence yielding at a strain of 0.003, albeit that the corresponding load levels differ. For the coarse mesh this yield point is at a load level of 258 kN, whereas for the finer mesh this happens at 240 kN. For both element distributions the ultimate failure load is 265 kN. The residual capacity is influenced by the element distribution during the last 10% of the load.

10.2.2 Effect of the characteristic tensile strength and the corresponding reduction of the crack energy

The value of the tensile strength that needs to be entered into the simulation of experiments has been a subject of debate for years. Likewise, the form and the size of the value of the crack energy has been an important aspect in non-linear concrete mechanics.

After years of research, the form has now become relatively stable, being an exponential function. Although the linear softening curve is the easiest curve, the exponential softening curve is applied increasingly to the simulation of experiments, so also in current engineering practice. In chapters 8 and 9 the Hordijk curve was used in view of the strongly descending branch of the allowed tensile stress after reaching the allowed tensile stress value. In the material parameters then a minimum tensile strength formulation was used that is seen as the characteristic lower limit in the Model Code 1990. This was used for the analysis because of the most unfavourable situation for the concrete material regarding the crack pattern. The average value for the concrete tensile strength is more common, but in some analyses it was seen that the estimation is slightly (too) favourable when it comes to the determination of the failure load. The calculation of the crack energy is derived directly from the Model Code 1990. This is based on the average tensile strength, not on the characteristic tensile strength of concrete. This means a reduction factor for the calculated crack energy is in order to comply with the selected minimum characteristic value for the tensile strength. It stands to reason that this reduction factor is selected on the basis of the measured tensile strength and the characteristic tensile strength. The effect on the load-deflection diagram of beams A1 and C3 is shown in figures 10.5 and 10.6.

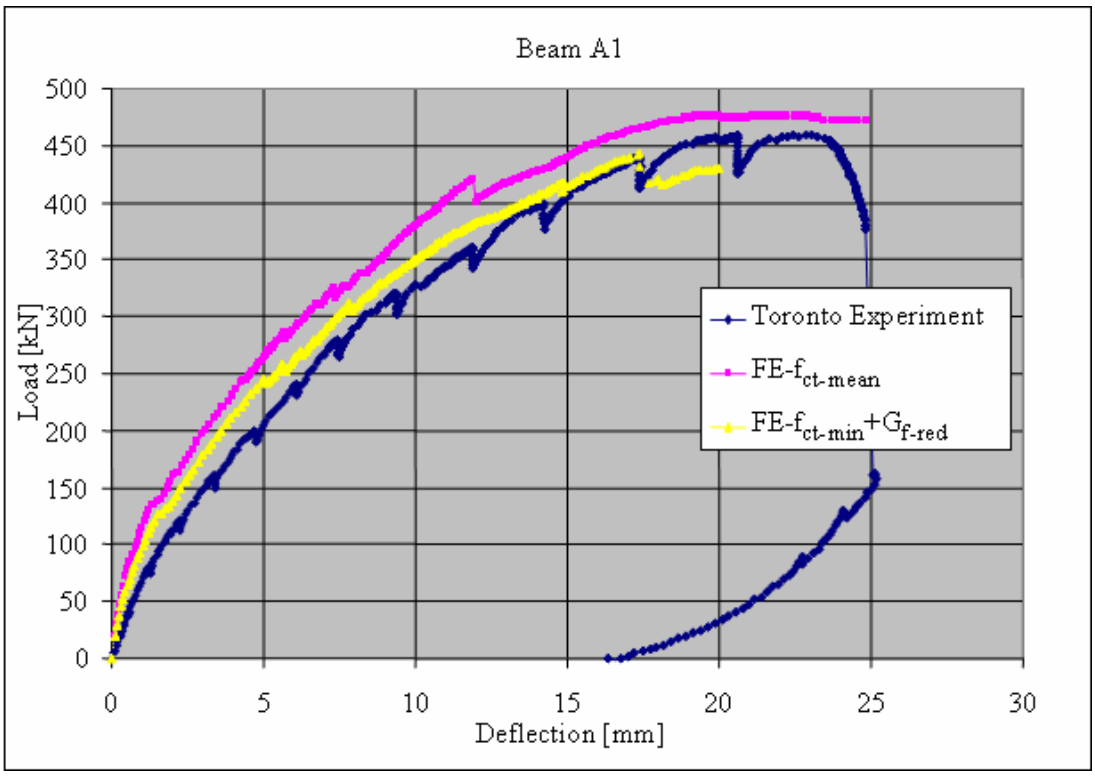

Figure 10.5 Load-deflection diagram of beam A1 at reduced tensile strength f_{ct} and reduced crack energy G_f

In figure 10.5 it is seen that as a result of the reduction of the crack energy G_f the load-deflection diagram moves up closer to the experimental curve. Also, in this analysis the failure load is slightly lower, which is very logical and in line with expectations. The corresponding 20 mm deflection is achieved. In short, in this beam the effect is minimal.

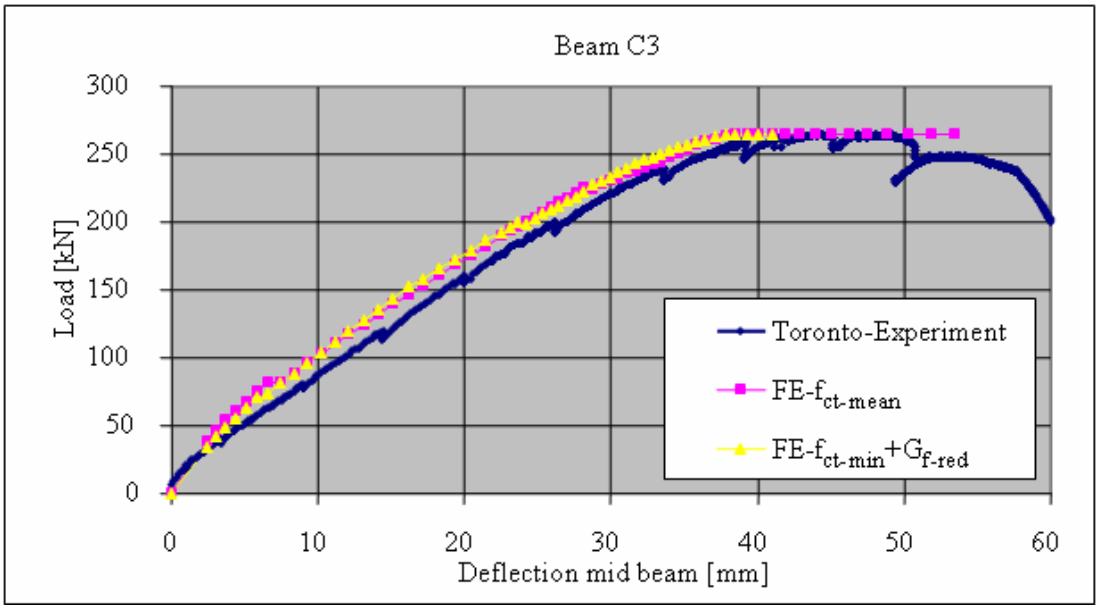

Figure 10.6 Load-deflection diagram of beam C3 at reduced tensile strength f_{ct} and reduced crack energy G_f

The load-deflection diagram of beam C3 in figure 10.6 also shows a curve that is closer to the load-deflection diagram of the experiment, albeit that the difference is minimal. Here, the failure load and the corresponding vertical deflection of the middle of the beam are achieved as well. The general conclusion is that the reduction has some effect, in the sense that the match with the results from the experiment becomes better, but that the effect in a global sense is minimal.

10.2.3 Hardening stage of reinforcement components

It was already seen in chapter 8 that no hardening was added to the material parameters of the various reinforcement components. The material was entered in the simplest possible manner. Still, some of the figures presenting the development of the strains in the various reinforcement components show that they haven't exclusively reached the yielding stage. In order to enable the purest possible comparison, especially where the determination of the ULS load level is concerned, the hardening stage of the reinforcement still should be added. In view of the results of section 10.2.2 the characteristic tensile strength of concrete was selected for comparison. With this value the result of the simulation matches the result of the experiment the most. Figure 10.7 shows the effect of the addition of hardening to all reinforcement components in experiment A1, as described in chapter 7 of the experiments.
Figure 10.7 demonstrates that the effect of the addition of hardening to the reinforcement steel is minimal. The reversion at various load levels in the load-deflection diagram is maintained, which is bad news for the robustness of the non-linear analysis process. The failure load is achieved including the corresponding vertical deflection if compared to the full FE analysis without adding hardening to the reinforcement steel.

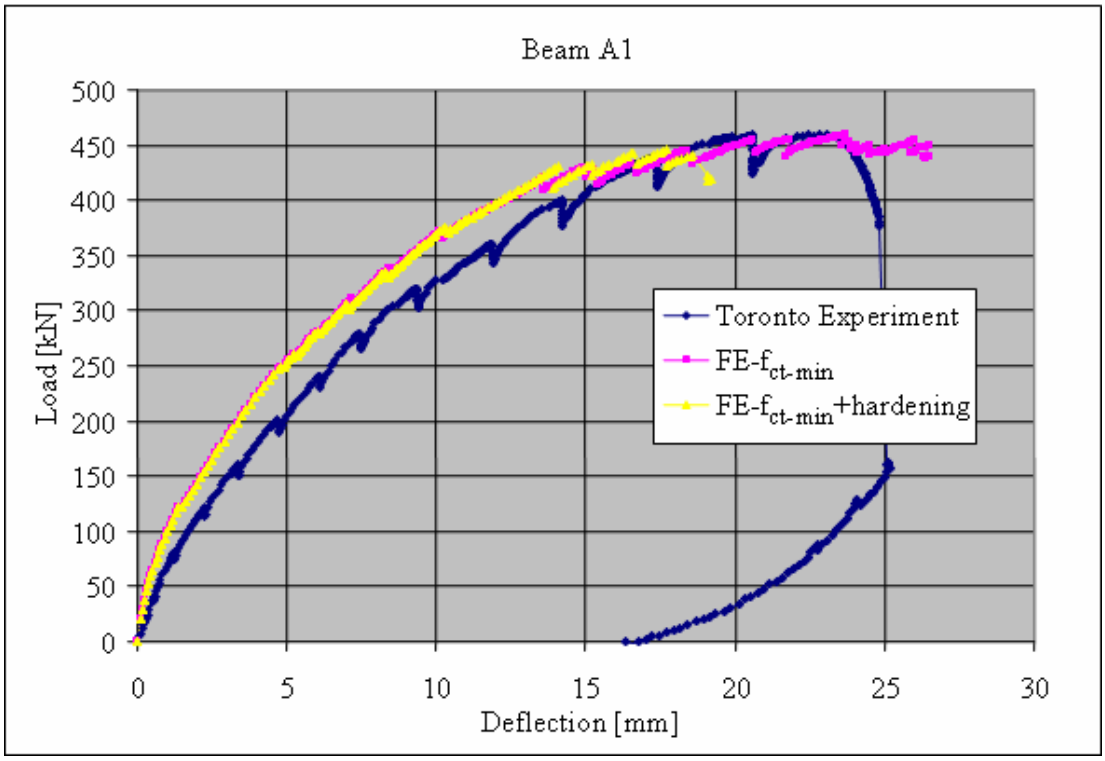

Figure 10.7 Effect of the addition of hardening to reinforcement steel in beam A1

Figure 10.8 shows the effect of adding hardening to all reinforcement components in experiment C3, as described in the publication of the experiment. In this analysis, use was made of the characteristic tensile strength of concrete as well.

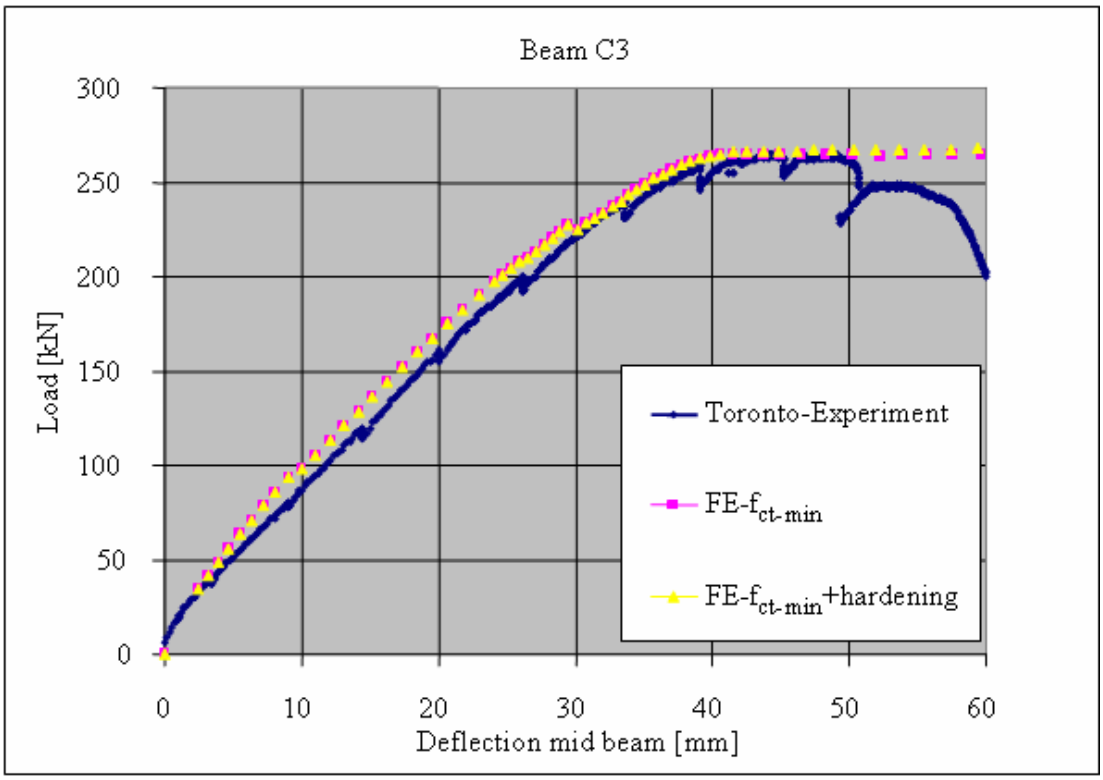

Figure 10.8 Effect of the addition of hardening to reinforcement steel in beam C3

Figure 10.8 shows that the hardening has some effect on the failure behaviour of beam C3 only after reaching the failure load level. Before that, little or no effect can be seen.
Based on both analyses of both beam A1 and C3, the conclusion is that the effect of hardening is minimal.

10.2.4 Slip behaviour of reinforcement in relation to concrete cover

What is remarkable about the various contour figures in chapters 8 and 9 is that especially at the ULS load level a large amount of the crack pattern occurs around the reinforcement bars. This applies mainly to the two layers of tensile reinforcement at the bottom of the beams. This could result in an adjustment of the calculation model, meaning that this behaviour is also incorporated into the model. However, for the time being this aspect is mostly not included in the analysis, apart of course from the fact that the non-linear analysis is not a generally accepted tool in current engineering practice yet. To clarify the issue at stake here, figure 10.9 show some crack patterns at different load levels proving that this aspect can actually play a role if the load increases. The upper part of figure 10.9 shows the crack pattern belonging to the load level of 310 kN, just above the SLS load level in beam A1, followed by the load level of 370 and 420 kN.

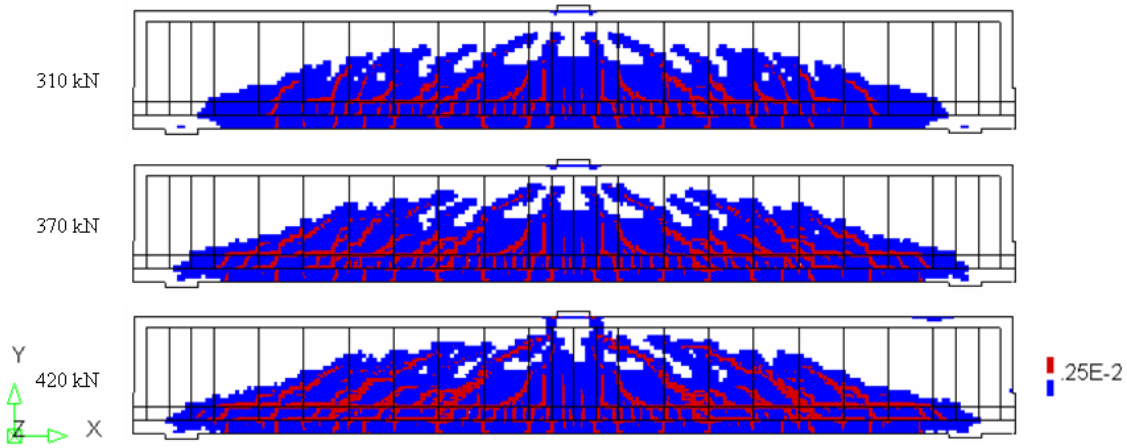

Figure 10.9 Crack patterns at load levels of 310, 370 and 420 kN in beam A1

Figure 10.9 demonstrates that just above the SLS load level(=286 kN), there is no crack pattern that also includes slip between the reinforcement and the concrete. At the 370 kN load level there seems to be slip formation, even though this only really materialises at the subsequent 420 kN load level. Chapter 8 already demonstrated that at the ULS load level there is in fact slip between the reinforcement and the concrete.
In view of the fact that up to the SLS load level there is no serious slip formation, a calculation model was selected without slip aspects. In case of a deeper examination of the load-deflection stage between the SLS and ULS load levels it would be advisable to include this behaviour in the examination, meaning in the model. The most obvious material model is the addition on the basis of the shear stress-strain diagram between the reinforcement and the concrete in order to simulate slip behaviour. From the point of view of modelling this would include an automatic link to the concrete for each reinforcement component. This has already led to a pilot implementation in a 3D solid model, and this in turn could of course be implemented further into another model type during a next stage.

10.2.5 Break-down criterion for the ultimate tensile strength of concrete

The current break-down criterion for the uni-axial tensile stress-strain diagram was addressed in chapter 6. It was also stated that there are various possibilities to limit the tensile stress. The most important aspect is whether the break-down criterion is based on the average tensile stress along the four integration points in a single element, or on the maximum tensile stress of a single integration point within an element of four integration points. Normally, the designer has no access to internal programming on the basis of examinations per integration point. The adjustment of isotropic material behaviour to orthotropic material behaviour is in designing limited to only the adjustment of material behaviour of the element. In this study, the effect of the basic criterion of the average tensile stress or maximum tensile stress takes place outside the FE software. The effect of the selected basic criterion can be visualised. This effect has been investigated for beam C3, as is shown in figure 10.10.

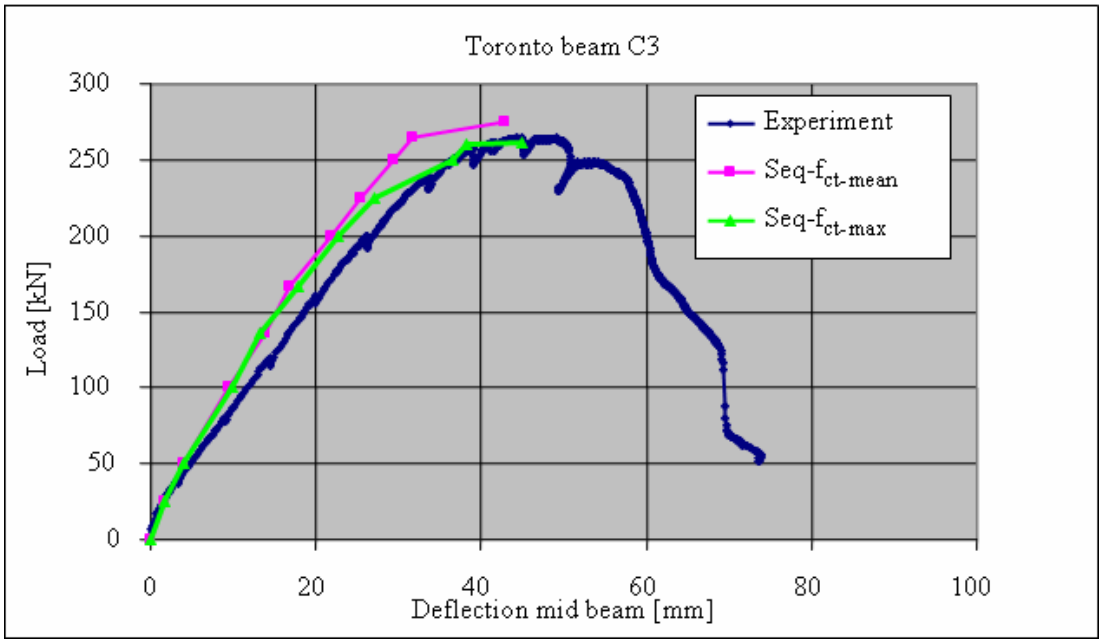

Figure 10.10 Effect of the break-down criterion on the ultimate tensile strength

Figure 10.10 tells us that if a break-down criterion is assumed that is based on the average of a structural element, the failure load will be slightly higher than with a break-down criterion based on only the maximum value of a single integration point of an element. In an absolute sense this is a difference of 275 kN as opposed to 261 kN. Since the ambition is to design structures in the safest possible manner, it is preferable to select just one integration point. Possibly, if in due time this implementation is included in an FE software package, this issue could be addressed in more detail.

11 CONCLUSIONS

The research described in the previous chapters allows the following conclusions:

Transparent output of models

1) When using the additional output option of the composed results in the solid models, the results are equal to those of the lower order model types, the beam, plane stress and shell models.
2) The values of the various composed results are comparable to the results of lower order models.
3) On the basis of the above, the reinforcement forces and moments can also be calculated from a higher order model, which includes the calculation of the amount of reinforcement from the higher order model.
4) Using both 2D and 3D models, it is possible to visualise the difference between bending and distortion areas, which also means that the reinforcement process of the structure may be improved.

Fully non-linear analysis

5) As far as the behaviour is concerned, the experiments can be simulated through a fully non-linear analysis. The influence arc length method is required within the Newton-Raphson iteration method in order to achieve convergence for the redistribution of stresses in crack patterns.
6) The global results of a fully non-linear analysis lead to reliable failure loads and corresponding crack patterns of the concrete, as well as plasticity of reinforcement steel, if compared to the experiments discussed above.
7) It is possible to provide an insight into the crack width development as a result of bending, providing a reliable development in accordance with the development of the crack widths from the experiments.
8) Shear force cracks start as bending cracks, following through as shear force cracks above the upper layer of the tensile reinforcement.
9) A first indication was given for the development of crack widths in shear force areas. This will require working out in more detail through simulation in the future.

Sequential analysis

10) The sequential analysis method is a quick, robust and attractive alternative to the current non-linear analysis techniques used in engineering practice to check the ULS and SLS load levels.
11) The overall processing time of the sequential analysis method has stimulated acceptance as a checking tool for future structural designs and for old existing structures.
12) The robust sequential analysis method can be used to determine the condition of existing civil engineering constructions, once the geometry and reinforcement data are known.

Acceptance

13) Because there are no obstacles standing in the way of the use of the sequential analysis method in full 3D models, providing the most realistic stress image, an extension towards a probabilistic approach as well as an optimisation technique within the design process will become a definite possibility, now more than ever before.
14) The sequential analysis method will render possible mistakes in the design process visible already during the design phase instead of the construction or management phase of a structure. It will therefore improve the quality of the structure.

REFERENCES

ACI2005 ACI Committee 318 Building Code Requirements for Structural Concrete (318-05) and Commentary ((318R-05). American Concrete Institute, Farmington Hills, USA, 2005, 391 pp.

Asin1999 Asin, M., The behaviour of reinforced concrete continuous deep beams, PhD Thesis, Delft University Press, December 1999, ISBN 90-407-2012-6, 168 pp.

Bentz2000 Bentz, E.C., 2000, Sectional Design of Concrete Structures, PhD thesis, Department of Civil Engineering, University of Toronto, Canada, 310 pp.

Beranek1994 Beranek, W.J. and Hobbelman, G.J., Constitutive modelling of structural concrete as an assemblage of spheres, Proceedings EURO-C 1994 International Conference, editors Mang e.o., Volume I, Innsbruck, Austria, 1994, pg. 37-51

Blaauwendraad1994 Blaauwendraad, J., Design of concrete structures with the Stringer-Panel model, Cement, 46^{e} Jrg., 1994, No. 5, (Dutch) pg. 48-55

DeBoer2002 Boer, A. de, Veen, C. van der, Future trends in FE-modelling of prestressed concrete structures, 1st FIB World Congress, 13-18 October 2002, Osaka, Japan, CD

DeBoer2004a Boer, A. de, Veen, C. van der, Safety aspects during construction steps in the design of concrete structures, FIB 2004 symposium Concrete Structures: the Challenge of Creativity, 26-28 April 2004, Avignon, France, CD

DeBoer2004b Boer, A. de, Comparing sequential LE analysis and full NL analysis in 3D structural concrete design, 5th Int. PhD symposium in Civil Engineering, PhDCE5, 17-19 June 2004, Delft, The Netherlands, pg. 607-614

DeBoer2006 Boer, A. de, Lu, L.H., Realistic deckplate crack growth approach of bridge decks by probabilistic analyses, 9th Int. Fatigue Congress, 14-19 May 2006, Atlanta, Georgia, USA, CD

DeBoer2007 Boer, A. de, Veen, C. van der, Reliability at all stages of the design of Structures", IABSE Symposium, 19-21 September 2007, Weimar, Germany, CD

DeBoer2009 Boer, A. de, Veen, C. van der, Full control in designing of RC structures, FIB 2009 Symposium, Concrete: 21st Century Superhero, 22-24 June 2009, London, United Kingdom, CD

Böhms1995 — Böhms, H.M., Rousset, M., Miles, C. Leal, D., Helpenstein, H.J., The GEM Modelling Methodology, Esprit CIME 8894 - Generic Engineering analysis Model, jan. 1995

Böhms1997 — Böhms, H.M., Willems, P.H., Hendriks, M.A.N., Bakkeren, W.J.C., Boer, A. de, Korwasser, H., GEM Civil Engineering Internal TNO Demonstration, Esprit CIME 8894 - Generic Engineering analysis Model, June 1997

Braam1990 — Braam, C.R., Control of crack width in deep reinforced concrete beams, PhD Thesis, Delft University of Technology, 1990, ISBN 90-900-3853-1, 109 pp.

Braam1993 — Braam, C.R. en De Haas, F.G., Reinforcement based to in and out of plane loads, Cement, 45e Jrg., 1993, No. 12, (Dutch), pg. 54-59

Bresler1963 — Bresler, B. and Scordelis, A.C., Shear strength of reinforced concrete beams, Journal American Concrete Institute, Volume 60, No. 1, pg. 51-72

Breugel1996 — Breugel, K. van, Veen, C. van der, Walraven, J.C., Braam, C.R, Concrete structures under temperature- and shrinkage deformation, Theory and Practise, Concrete practise Serie 2, Betonprisma, 's Hertogenbosch, 1996, (Dutch), pg. 31-34

Cornelissen1986 — Cornelissen, H.A.W., Hordijk, D.A. and Reinhardt, H.W., Experimental determination of crack softening characteristics of normal weight and lightweight concrete, Heron 31, No. 2, 1986, pg. 45-56

CSA2004 — Canadian Standards Association, 2004. A23.3 Design of Concrete Structures, CSA, Mississauga, Ontario, Canada, 214 pp.

CUR1994 — Naaktgeboren N.M., and Gijsbers F.B.J., Analysis of a box-girder bridge: Case-study in the framework of "Concrete mechanics for engineering practice" TNO Building and Construction Research, 1994, (Dutch)

CUR2006 — CUR-report 218, Future of the construction process- A 3D object approach, CUR, Gouda, 2006, ISBN 90-376-0502-8/978-90-376-0502-0, (Dutch), 38 pp.

Denton2001 — Denton S.R., The strength of reinforced concrete slabs and the implications of limited ductility, PhD Thesis, 2001, Cambridge, United Kingdom, 332 pp.

DIANA2005 — DIANA User's Manual, Release 9.1, TNO DIANA BV, Delft, The Netherlands, July 2005, www.tnodiana.com

EU2005 Monitoring industrial research : the 2005 EU industrial R&D investments Scoreboard, Directorate General Joint Research Centre, Technical Report EUR 21851 EN, European Union 2005

Feenstra1993 Feenstra, P.H., Computational aspects of biaxial stress in plain and reinforced concrete, PhD Thesis, Delft University of Technology, Delft, The Netherlands, ISBN 90-6275-935-1 / CIP, 1993, 151 pp.

FIB2008 FIB bulletin 45, Practitioners'guide to finite element modelling of reinforced concrete structures, Chapter 2.4 3D solid modelling, FIB, ISBN 1562-3610, 2008, pg. 70-78

Foster2003 Foster, S.J., Marti, P. and Mojsilovic, N., Design of Reinforced Concrete Solids Using Stress Analysis, ACI Structural Journal, Vol. 100, No.6, Nov-Dec 2003, pg. 758-764

Frissen2000 Frissen, C.M., Numerical analysis box-girder viaduct, TNO Building and Construction Research, TNO-report 1999-MIT-NM-R0013, Rijswijk, The Netherlands, 2000, (Dutch), 79 pp.

Groen1995 Groen A.E., Three dimensional elasto-plastic analysis for soil, PhD Thesis, Delft University of Technology, Delft, The Netherlands, 1995, ISBN 90-407-1450-9,128 pp.

Gupta1986 Gupta, A.K., Combined membrane and flexural reinforcement in plates and shells, ASCE, Journal of Structural Engineering, Vol. 112, No. 3, March 1986, pg. 550-557

Hillerborg1985 Hillerborg, A., Results of three comparitive test series for determining the fracture energy Gf of concrete, RILEM Materials and Structures, 18(107), 1985, pg. 407-413

Hoiseth1996 Hoiseth K.V., Case study : Nonlinear behaviour skew plate viaduct Burgerveen, TNO report 96-NM-R1033, TNO Building Construction Research, Rijswijk, The Netherlands,1996, 79 pp.

Holtzhauer2006 Holtzhauer, E. und Saal, H., Durchganges Datenmanagement im Stahlbau, Proc. 10th Industrietag der IAI–Hochschulsymposium, Munchen, Germany, 2006

Hoogenboom1993 Hoogenboom, P.C.J., The Stringer-Panel model, MSc Thesis, Delft University of Technology, Delft, The Netherlands, 1993, (Dutch)

Hoogenboom1998 Hoogenboom, P.C.J., Discrete Elements and Nonlinearity in Design of Structural Concrete Walls, PhD Thesis, Delft University of Technology, July 1998, ISBN 90-9011843-8, 184 pp.

Hoogenboom2008 Hoogenboom, P.C.J. and DeBoer, A., Computation of reinforcement for solid concrete, Heron 53, 2008, No. 4, pg. 247-271

Hordijk1991 — Hordijk, D.A., Local approach to fatigue of concrete, PhD Thesis Delft University of Technology, Delft, The Netherlands, 1991, 210 pp.

IFC — Website www.buildingsmart.com

Jong2002 — Jong, T.M. and Voordt D.J.M. van der, Criteria for scientific study and design in: T.M. Jong and D.J.M. van der Voordt, Ways to research and study urban, architectural and technical design, Delft, Delft University Press Science, 2002

Juwet2001 — Juwet, M., en Kenis, K., Efficient use of FE – Guideline for the efficient use of FE in machinery and product development, KaHo Sint-Lieven, Gent, 2001 ISBN 90-806182-2-5, (Dutch)

Kennedy2003 — Kennedy, G., Goodchild, C., Practical yield line design, British Cement Industry, Berkshire, 2003, ISBN 0 7210-1581-9

Klerks1989 — Klerks, L., Failure load cable stayed bridge of Heusden, MSc Thesis, Delft University of Technology, Dec. 1989, (Dutch)

Lilliu2007 — Lilliu, G., 3D Analysis of fracture processes in concrete, PhD thesis, Delft University of Technology, Delft, The Netherlands, ISBN 978-90-5972-184-5, Eburon, 151 pp.

Lourenco1995 — Lourenco, P.B., Blaauwendraad, J., First step to a consistency in reinforcing panels, plates and slabs(I), Cement, 47^{e} Jrg. 1995, No 2, pp. 44-51, (Dutch)

Lourenco1995 — Lourenco, P.B., Blaauwendraad, J., First step to a consistency in reinforcing panels, plates and slabs(II), Cement, 47^{e} Jrg., 1995, No 3, pp. 21-26, (Dutch)

Lourenco1993 — Lourenco, P.B., Figueiras, J.A., Automatic design of reinforcement in concrete plates and shells, Engineering Computations, Vol. 10(6), 1993, pg. 519-541

Maekawa2003 — Maekawa, K., Nonlinear Mechanics of Reinforced Concrete, Spon Press, 2003.

Maekawa1993 — Maekawa, K., Takemura, J., Irawan, P. and Irie, M., Continuum fracture in concrete nonlinearity under tri-axial confinement, Proc. of JSCE 18, 460 (February 1993), pg. 113-122.

Maekawa1993a — Maekawa, K., Takemura, J., Irawan, P. and Irie, M, Plasticity in concrete nonlinearity under tri-axial confinement, Proc. of JSCE 18, 460 (February 1993), pg. 123-130.

Maekawa1993b — Maekawa, K., Takemura, J., Irawan, P. and Irie, M., Tri-axial elastoplastic and fracture model for concrete, Proc. of JSCE 18, 460 (February 1993), pg. 131-138.

Marti1991 — Marti, P., Dimensioning and Detailing, IABSE Conference Structural Concrete, Stuttgart, 1991, pg. 411-443

McFarlane2006 — McFarlane, B., Building Services Modelling using Industry Foundation Classes (IFC), Proc. 10th Industrietag der IAI–Hochschulsymposium, Munchen, Germany, 2006

ModelCode90 — CEB-FIB Model Code 1990, Design Code, ISBN: 0-7277-1696-4, 1993, Lausanne, Switzerland

Nielsen1999 — Nielsen, M.P., Limit Analysis and Concrete Plasticity, The Technical University of Denmark, CRC Press LLC, Boca Raton, Florida, USA, 1999, ISBN 0-8493-9126-1, 908 pp.

Otaredian1993 — Otaredian, N., Force distribution in skew slabs, Part I, II and Appendix, MSc thesis, Delft University of Technology, Delft, The Netherlands, September, 1993, (Dutch), All parts 197 pp.

Palácio2004 — Palácio, K., Lourenco, P.B., Barros, A.O., Design of RC thin surface Structures, Report 04-DEC/E-06, University of Minho, Departemento de Engenharia Civil, Azurem, Guimares, Portugal, 2004, 65 pp.

Popovics1973 — Popovics, S., A numerical approach to the complete stress-strain curve of concrete, Cement and Concrete Research, Vol. 3, No. 5, 1973, pg. 583-599

Reinhardt1984 — Reinhardt, H.W., Fracture mechanics of an elastic softening material like concrete, Heron 29, No. 2, 1984, 42 pp.

Richter2006 — Richter, S., Structural timber model, Proc. 10th Industrietag der IAI–Hochschulsymposium, Munchen, Germany, 2006

ROBK6 — Recommendations designing concrete infrastructures 2006, Rijkswaterstaat - Centre for Public Works, Utrecht, 2006, (Dutch)

Roelfstra2002 — Website www.femmasse.nl

Rots1988 — Rots, J.G., Computational modelling of concrete fracture, PhD Thesis, Delft University of Technology, Delft, The Netherlands, 1988, 132 pp.

Rots2004 — Rots, J.G., Saw tooth softening/Stiffening Model, Proceedings FramCoS, editors Li e.o., Vail, Colorado, USA, 2004, pg. 375-382

Rots2006a — Rots, J.G., Invernizzi, S. and Belletti, B., Event by event strategies for modelling concrete structures, Proceedings EURO-C 2006, editors Meschke e.o., Mayrhofen, Austria, 2006, pg. 667-678

Rots2006b — Rots, J.G., Invernizzi, S. and Belletti, B., A sequentially linear saw-tooth model for interface elements, Proceedings EURO-C 2006, editors Meschke e.o., Mayrhofen, Austria, 2006, pg. 203-212

Rots2006c — Rots, J.G., Invernizzi, S. and Belletti, B., On the shape of the saw-tooth softening curves for sequentially linear analysis, Proceedings EURO-C 2006, editors Meschke e.o., , Mayrhofen, Austria, 2006, pg. 431-442

Schlangen1993 — Schlangen, E., Experimental and numerical analysis of fracture processes in concrete, PhD thesis, Delft University of Technology, Delft, The Netherlands, ISBN 90-9006167-3, 121 pp.

Sherwood2008 — Sherwood, E.G., One-way shear behaviour of large, lightly-reinforced concrete beams and slabs, PhD thesis, University of Toronto, Canada, 2008, ISBN 9780494397909, 547 pp.

Sherwood2007 — Sherwood, E.G., Bentz, E.C., and Collins, M.P., Effect of aggregate size on Beam-Shear strength of thick slabs, ACI Structural Journal, 104(2), 2007, pp. 180-191

Shim2002 — Shim, W., Analysis of beams with low shear reinforcement, MSc Thesis, Department of Civil Engineering, University of Toronto, Canada, 2002, 383 pp.

Skinner2005 — Skinner, B. and Geeves, D., Advanced bridge analysis and design methods simplified, Proceedings Bridge design, construction and maintenance, CD ICE, Kuala Lumpur, Malaysia, 2005

SpanCad1999 — Website www.mechanics.citg.tudelft.nl/spancad

TEKLA2006 — Website www.tekla.com

Thorenfeldt1987 — Thorenfeldt, E., Tomaszewicz, A., and Jenssen, J.J. Mechanical properties of High-strength concrete and applications in design. In Proc. Symp. Utilization of High-Strength Concrete (Stavanger, Norway) (Trondheim, 1987), Tapir

VanMier1997 — Mier, J.G.M. van, Fracture processes of Concrete, CRC Press, Inc., Florida, USA, 1997, ISBN 0-8493-9123-7, 448 pp.

VanVliet2000 — Vliet, M.R.A. van, Size effects in Tensile Fracture of Concrete and Rock, PhD Thesis, Delft University of Technology, Delft University Press, Delft, The Netherlands, 2000, ISBN 90-407-1994-2, 192 pp.

VBC95 Voorschriften Beton TGB 1990, Constructieve eisen en rekenmethoden, NEN6720, NEN Institute, Delft, The Netherlands, 1995, (Dutch)

Vecchio2004 Vecchio, F.J., Shim, W., Experimental and analytical re-examination of classic concrete beam tests, Journal of structural engineering, ASCE, March 2004, pg. 460-469

Vervuurt1997 Vervuurt, A.H.J.M., Interface fracture in Concrete, PhD thesis, Delft University of Technology, Delft, The Netherlands, ISBN 90-9010440-2, 164 pp.

Vulpen2002 Vulpen, R. van, Strip method to reinforce skew plates, MSc Thesis, Delft University of Technology, Delft, The Netherlands, 2002, (Dutch)

CURRICULUM VITAE

Name:
Ane de Boer

Born:
4 December 1951, Warga, The Netherlands

Education:
ULO Nylân, Leeuwarden 1968
Hogere Technische School, Leeuwarden, 1973
Delft University of Technology, Faculty of Civil Engineering, 1988

Courses:
Basics of Finite Elements, 1976
Word-Perfect 5.0, 1990
Non-linear Finite Element Analysis, 1991
Dynamics Finite Element Analysis, 1991
Computational Geotechnics, 1992
Technical Advising Specialists, 1992
Infomod, 1993
Probabilistic Methods in Civil Engineering, 1995
Quality of software products, 1996

Work:
Soldier, Dutch Military Service, 1973
Technical employer, Delft Univervity of Technology, 1975
Scientific employer, Delft University of Technology, 1988
Scientific employer, Rijkswaterstaat, 1991
Senior scientific employer, Rijkswaterstaat, 1993
Senior Advisor/Specialist, Rijkswaterstaat, 2006

Contributions:
A lot of contributions can be seen in different committees on the level of Rijkswaterstaat, national and international organisations. The national Dutch organisations are CIAD, CUR, COB, Concrete Society, Stufib, DOV. The international organisations are IABSE, fib, COBRAE and NAFEMS.